Photoaffinity Probes to Label Formyl Peptide Receptor 1

Devon Helen Legge

Submitted in accordance with the requirements for the degree of Doctor of Philosophy

The University of Leeds

School of Chemistry

August 2021

The candidate confirms that the work submitted is her own and that appropriate credit has been given where reference has been made to the work of others.

Acknowledgements

Firstly I would like to thank my wonderful supervisor Megan, I could not have asked for a better mentor to guide me through my PhD. Megan has been supportive and encouraging, and I have learnt a lot from her. A big thank you to my co-supervisor Stuart for his help and endless supply of crazy ideas. Megan and Stuart have made my PhD journey enjoyable and I always left our monthly meetings feeling better than when I entered.

I would like to thank Martin Huscroft and Jeanine Williams for running all of my analytical HPLC samples and for their huge amount of help with HPLC and biotage purification. Thank you to Jo Sier for welcoming me into food science and providing many helpful tips for cell culture. Thank you to Sally Boxall and Ruth Hughes for teaching me flow cytometry analysis and fighting to get me remote access to flow software during COVID. Thank you Mark Howard for the upkeep of and advice with NMR. I am very grateful for the work done by Rachel George on the digestion and mass spectrometry. Many thanks to James Ross for his help and support with PyMol.

I am extremely grateful to Martin Walko and Mehreen Khan for their input in this project. Martin was a friendly face when starting my PhD and taught me so much about diazirine formations and peptide purification. On top of this he has also provided two compounds for this project and helped to supervise Mehreen whilst I was away during my internship. Mehreen was a hard-working masters student who I enjoyed supervising and getting to know. Mehreen was successful in making two peptidic probes for use in this project, for that I am very thankful.

Lab1.49 has been my home for the last 4 years and I am so lucky to have been a part of this family. To my two desk neighbors, Jack and Holly, thank you for the support. Even in the depths of writing his thesis, Jack was always up for a laugh and a well needed cup of tea. The chats, eye-rolls and many Nero trips with Holly are what got me through the last months of my PhD. Thank you to Jack White for his many dramatic life stories and constant up-beat energy. Thank you Zoe, Sophie and Holly for hair-therapy and way-too-long lunches out in the sun. Thank

you to Ryan who answered all of my million questions when I started in the chem lab and provided epic playlists to get me through yet another column. I am very grateful to all Lab1.49 members, past and present, for providing a friendly and supportive working atmosphere.

Finally, I would not be where I am today without the help and support of my friends and family. Thank you Mum and Dad for believing in me and providing me with the tools I needed to be who I am today. To my husband Zac, thank you for always being there.

Abstract

The recognition of bacterial cells by the human immune system is crucial in the protection of the body from infection. Formyl peptide receptors (FPRs) are present on nearly all types of immune cells in the human body. They detect and bind formyl peptides passively released by invading bacterial cells and alert the innate immune system that bacteria are present.

FPR1 is the most active FPR towards formyl peptides and to date there is no crystal structure present of the receptor. Affinity-based protein profiling has become a useful technique for studying ligand-protein interactions and binding site structure. This thesis describes the use of photoaffinity labelling to label FPR1 via the formyl peptide binding site. This work includes the design and synthesis of photoreactive formylated peptidic probes, including the preparation of the photoreactive diazirines. These probes are employed to target FPR1, with analysis by combination of gel-based methods, flow cytometry, confocal microscopy and mass spectrometry. Optimised conditions have been established for FPR1 expression in mammalian cells and the photoaffinity labelling work-flow.

FPRs are important in our first line of defence against bacteria and in addition to this have been shown to be linked to multiple diseases associated with inflammation. Despite this, research into the structure of these receptors, their binding sites and the mechanism of ligand binding has been limited. The labelling of FPR1 is performed, aiming to improve our knowledge of the formyl peptide binding site.

Abbreviations

A*f*BPP	Affinity-based protein profiling
Boc	tert-Butyloxycarbonyl
cAMP	Cyclic adenosine monophosphate
CHS	Cholesterol hemisuccinate
CuAAC	CuI-catalysed azide/alkyne cycloaddition
Da	Dalton
DBU	1,8-Diazabicyclo[5.4.0]undec-7-ene
DCC	N,N′-Dicyclohexylcarbodiimide
DCM	Dichloromethane
DCU	Dicyclohexylurea
Dde	1-(4,4-dimethyl-2,6-dioxocyclohex-1-ylidene)ethyl
DDM	*n*-Dodecyl β-D-Maltoside
DIC	N,N′-Diisopropylcarbodiimide
DIPEA	N,N-Diisopropylethylamine
DMAP	4-Dimethylaminopyridine
DMF	Dimethylformamide
DTT	Dithiothreitol
EC_{50}	Half maximal effective concentration
EDT	Ethanedithiol
EDTA	Ethylenediaminetetraacetic acid
Em	Emission

ESI	Electrospray ionisation
Ex	Excitation
f	Formyl group
FG	Functional group
FITC	Fluorescein isothiocyanate
FLAG	DYKDDDDK
Fmoc	Fluorenylmethyloxycarbonyl
FPR	Formyl peptide receptor
GFP	Green fluorescent protein
GPCR	G-protein coupled receptor
HCS	High-content screening
HPLC	High-performance liquid chromatography
HRMS	High-resolution mass spectrometry
HRP	Horseradish peroxidase
HTS	High-throughput screening
IC_{50}	Half-maximal inhibitory concentration
IR	Infrared
K_d	Equilibrium dissociation constant
LC-MS	Liquid chromatography mass spectrometry
LED	Light-emitting diode
LPS	Lipopolysaccharide
MALDI	Matrix-assisted laser desorption/ionisation
MAMP	Microorganism-associated molecular pattern
MS/MS	Tandem mass spectrometry

MS/MS	Mass spectrometry
Mtb	*Mycobacterium tuberculosis*
NHS	*N*-Hydroxysuccinimide
NMR	Nuclear magnetic resonance
PAL	Photoaffinity labelling
PBS	Phosphate buffered saline
PG	Protecting group
PRR	Pattern recognition receptor
SDS	Sodium dodecyl sulphate
SDS-PAGE	Sodium dodecyl sulphate–polyacrylamide gel electrophoresis
SPPS	Solid-phase peptide synthesis
TAMRA	5-(and-6)-Carboxytetramethylrhodamine
TB	Tuberculosis
TBS	Tris buffered saline
t-Bu	Tert-Butyl
TFA	Trifluoroacetic acid
TIS	Triisopropyl silane
TMSCl	Trimethylsilyl chloride
UV	Ultra-violet
WB	Western Blot

Contents

Chapter 1 Background 1

1.1 Host Recognition of Microbes 1

1.1.1 Production of Microorganism-Associated Molecular Patterns and Their Detection by the Host 2

1.2 Bacterial Peptides 3

1.3 Formyl Peptide Receptors 3

1.3.1 G-Protein Coupled Receptors 4

1.3.2 Human FPR Family Members 5

1.4 Methods to Detect and Analyse Ligand-GPCR Interactions 13

1.4.1 GPCR Pharmacology 14

1.4.2 Receptor Binding Assay 14

1.4.3 G-Protein Dependent Assays 15

1.4.4 Generic G-Protein Independent Assays 16

1.4.5 Flow Cytometry 17

1.5 Affinity-based Protein Profiling 20

1.5.1 Photoaffinity Labelling 21

1.5.2 Click Chemistry 31

1.5.3 Mass Spectrometry for Proteomics 34

1.6 Photoaffinity Probes for GPCRs 36

1.6.1 Photoaffinity Labelling to Target the Formyl Peptide Receptor 36

1.6.2 Recent Literature Reports of Diazirine Probes to Target GPCRs 41

1.6.3 Conclusion 45

1.7 Project Aims 45

Chapter 2 Synthesis of Photoreactive Diazirines 47

2.1 Introduction 47

2.2 Photoreactive Unnatural Amino Acids 47

2.3 Synthesis of Photoreactive Groups 48

2.3.1 Synthesis of 4,4-Azo-pentanoic Acid 48

2.3.2 Synthesis of Fmoc-photo-Met 49

2.3.3 Synthesis of Fmoc-photo-Leu 52

2.4 Conclusion....55

Chapter 3 Preparation and Use of First-Generation Photoreactive Probes 56

3.1 Photoreactive Chemical Probe Design....56

3.2 Optimisation of *N*-formylation Reaction....58

3.2.1 Formic Acid and Isobutyl Chloroformate....58

3.2.2 Formic Acid and DCC....59

3.2.3 *p*-Nitrophenyl Formate....59

3.3 Synthesis of Photoreactive Chemical Probes....60

3.3.1 Photoreactive Probe Incorporating 4,4-Azo-pentanoic Acid..62

3.3.2 Photoreactive Probes Incorporating photo-Met and photo-Leu 63

3.4 Establishing the HEK293T Cell Line....66

3.4.1 Transient Transfection of HEK293T Cells....66

3.5 Binding, Crosslinking and Click Reaction of Photoreactive Probes 69

3.5.1 Binding and Crosslinking of Probe1.0Met to FPR1....69

3.5.2 Investigation of CuAAC Reaction Conditions....70

3.5.3 Cold Incubation of Probe1.0Met....71

3.5.4 Testing Probe Binding with Flow Cytometry....71

3.6 Conclusion....75

Chapter 4 Preparation and Use of Photoreactive Probes Containing Detectable Tags....76

4.1 Generation 2.0 Probe Design and Synthesis....76

4.2 Flow Cytometry Experiments to Analyse Probe2.0TAMRA Binding to FPR1....79

4.2.1 Specific Binding of Probe2.0TAMRA....79

4.2.2 Concentration Range of Probe2.0TAMRA....80

4.2.3 Competitive Binding Between TracerFITC and Probe2.0TAMRA....81

4.2.4 Competitive Binding Between Probe2.0TAMRA and Known Agonist fMLF and Antagonist Boc-MLF....84

4.2.5 Binding of Probe2.0TAMRA to Endogenously Expressed FPR1 86

4.3 Confocal Microscopy to Image the Internalisation of FPR1....87

4.4 Binding and Crosslinking of Probe2.0TAMRA to FPR1....90

4.4.1 Experimentation of Repeated Crosslinking....93

4.5 Generation 2.1 95
4.5.1 Generation 2.1 Probe Design and Synthesis 95
4.5.2 Flow Cytometry to Test the Binding of Probe2.1Desthio 96
4.5.3 Binding and Crosslinking of Probe2.1Desthio 97
4.6 Generation 2.2 Probes 99
4.6.1 Generation 2.2 Probe Design and Synthesis 100
4.6.2 Flow Cytometry to Test the Binding of Probe2.2SDi and Probe2.2SDiAlk 102
4.6.3 Binding and Crosslinking of Probe2.2SDi/SDiAlk 106
4.7 Conclusion 109
4.7.1 Structure of Second-Generation Probes 109
4.7.2 Probe2.0TAMRA 111
4.7.3 Probe2.1Desthio 112
4.7.4 Probe2.2SDi and Probe2.2SDiAlk 112
Chapter 5 Immunoprecipitation and Proteomics 114
5.1 Anti-FLAG Pull-Down of Probe2.0TAMRA-FPR1 Complex 114
5.1.1 GPCR-Specific Anti-FLAG Pull-Down 117
5.2 First Proteomics Experiment 120
5.3 Anti-FLAG Pull-Down with Deglycosylation of FPR1 122
5.4 Proteomics with Deglycosylated FPR1 124
5.5 Anti-FLAG Pull-Down of FPR1-Probe2.2SDi 125
5.6 Proteomics with FPR1-Probe2.2SDi 126
5.7 Conclusion 128
Chapter 6 Conclusions and Future Work 133
6.1 Synthesis of Photoreactive Diazirines 133
6.2 First-Generation Probes 133
6.3 Second-Generation Probes 134
6.4 Anti-FLAG Pull-Down and Proteomics of FPR1-Probe Complexes 135
6.5 Work-Flow Establishment for Binding and Crosslinking Studies ..136
6.6 Future Work 136
6.6.1 Bottom-Up Proteomic Experiments on FPR1 136
6.6.2 A New Generation of Probes 137
6.6.3 The Labelling of Endogenous FPR1 with Probe2.0TAMRA 138
6.6.4 Photoaffinity Labelling to FPR2 139

Chapter 7 Experimental....140
7.1 Synthesis of small molecules....140
7.1.1 General experimental....140
7.1.2 Synthesis and characterisation....141
7.2 Solid Phase Peptide Synthesis....159
7.2.1 General Reagents and Equipment....159
7.2.2 General Methods for Solid Phase Peptide Synthesis....159
7.2.3 Synthesised Peptides....162
7.3 Biochemical Methods....169
7.3.1 General Methods and Equipment....169
7.3.2 Media and buffers....169
7.3.3 Bacterial Transformation of FPR1 gene cDNA ORF....170
7.3.4 Mammalian Cell Culture....172
7.3.5 Probe Crosslinking in HEK293T Cells and cell lysis....172
7.3.6 Gel-Based Fluorescent Imaging....173
7.3.7 Western Blot Analysis....174
7.3.8 Deglycosylation of FPR1....175
7.3.9 Flow Cytometry....175
7.3.10 Confocal Microscopy....176
7.3.11 Anti-FLAG Pull-Down....176
7.3.12 Proteomics....177
Chapter 8 References....180
Chapter 9 Appendix....192
9.1 Analysis of Synthesised Peptides....192
9.1.1 Mass Spectrometry....192
9.1.2 Analytical HPLC....193
9.2 Protein Sequences....199
9.2.1 FPR1....199

Chapter 1 Background

The following background topics relevant to this project will be discussed: host recognition of invading microbes, including the detection of N-formylated peptides released from bacteria; the role of the formyl peptide receptors in host defence; the analysis of GPCR-ligand interactions; and finally affinity-based protein profiling.

1.1 Host Recognition of Microbes

A major cause of disease and mortality throughout the world is bacterial infections.[1] Successful and early suppression of an infection depends on fast detection of invading pathogens and is vital for the survival of multicellular organisms.[2] The human immune system has two different responses: the non-specific and rapid innate immune system, and the slower and more specific adaptive immune system.[1-5] The innate immune response relies upon pattern recognition receptors (PRRs) which recognise molecules expressed by microorganisms, known as microorganism-associated molecular patterns (MAMPs).[1] There are three types of PRRs, nucleotide-binding and oligomerization domain receptors which recognise bacteria, Toll-like receptors recognising bacteria, viruses, fungi and protozoa, and retinoic acid-inducible gene I receptors that recognise viruses.[5] MAMPs include parts of the bacterial cell envelope such as lipopolysaccharide (LPS), flagellin and bacterial DNA. Recognition of these molecules activates the innate response and provides signals for the development of the adaptive immunity. PRRs are present in almost all cell types throughout the human body.[1, 5]

1.1.1 Production of Microorganism-Associated Molecular Patterns and Their Detection by the Host

During growth and cell division, bacteria must engage with their environment whilst maintaining their structural integrity.[4] A key structural component of a bacterial cell is its envelope - the bacterial cell surface arranged as a series of tightly packed layers of the cell wall and membrane. Bacterial envelopes are unique to each species of bacteria and therefore metabolic pathways which involve the envelopes can be used as antibiotic targets.[4]

Muropeptides are an example of a MAMP. Muropeptides are the collective of structures produced from enzymatic digestion of the peptidoglycan polymer of the bacterial cell wall. They therefore accumulate during synthesis of the bacteria cell wall and during infection of a host, because the immune system breaks down the bacterial cell walls.[4] The involuntary release of these muropeptides provides messenger molecules which tell bacteria that cell wall targeting antibiotics are present, and host cells that a bacterial infection has begun.[4] Studies into the recognition of muropeptides by the host immune system have only recently begun, despite the advanced knowledge of muropeptides.[4] Nucleotide-binding and oligomerization domain receptors recognise and bind muropeptides from bacterial peptidoglycan.

Toll-like receptors were the first identified PRR and as such are the best characterised. Toll-like receptors recognise and bind lipids, lipoproteins, and proteins from bacterial membranes.[6] Upon binding of these MAMPs, Toll-like receptors recruit adapter-proteins which subsequently recruit kinases to the intracellular toll-like receptor domain. Different Toll-like receptors cause different downstream signalling pathways, but all include at least one of the two main signalling pathways:[6]

- Myeloid differentiation primary-response protein 88 recruited as the adapter protein, leading to inflammatory cytokine production.
- Intracellular domain-containing adaptor protein inducing type I interferon-β recruited, leading to stimulation of type I interferon.

For most Toll-like receptors, activation ends in the release of pro-inflammatory cytokines, protecting the host from infection.

1.2 Bacterial Peptides

Bacterial signal peptides are another type of MAMP. The biosynthesis of peptides and proteins within bacteria is different to the process within humans. During ribosomal protein synthesis, a formylated methionine (fMet) is added to the N-terminus, creating *N*-formylated polypeptides.[3] For many bacterial proteins, a short N-terminal sequence is cleaved off post-translationally to create the native form of the protein and to release the signal peptide.[3, 7, 8] Some proteins remain formylated and their degradation also produces shorter formyl peptides. Formyl-methionine-leucine-phenylalanine (fMLF **1.01**, also referred to as fMLP) (Figure 1.1) is the smallest formyl peptide to exhibit agonistic activity in PRRs. The involuntary release of these formyl peptides from bacteria occurs continually, including during infection of the host, when the pathogen destroys host-tissue.[9] As well as the release of formyl peptides from the bacterial cells, host-derived mitochondrial formyl peptides are passively released from dying host-cells. Bacterial formyl peptides are essential for the initial detection and elimination of bacterial infections.[3] Formyl peptides produced from dying host cells alert macrophages to engulf the dead cells.[9]

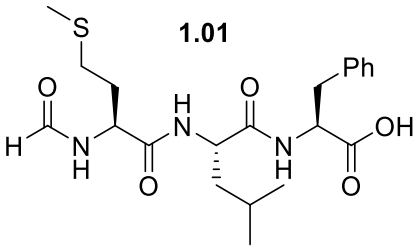

Figure 1.1: Structure of fMLF.

1.3 Formyl Peptide Receptors

The human formyl peptide receptor (FPR) was defined biochemically in 1976 as a high affinity binding site on the surface of neutrophils for the prototypic *N*-formyl peptide fMLF.[10] The FPRs act as an alert for the immune system and are involved

in the innate immune response. FPRs are found on a variety of cell types, including neutrophils, macrophages, epithelial cells and astrocytes.[11]

1.3.1 G-Protein Coupled Receptors

FPRs belong to the G(guanine nucleotide-binding)-protein coupled receptor (GPCR) superfamily and the rhodopsin-like subfamily.[12, 13] GPCRs are transmembrane receptors typically containing seven transmembrane helical segments, an extracellular N-terminus and an intracellular C-terminus.[14]

GPCRs are found in eukaryotic cells and interact with intracellular G-proteins in a signal transduction pathway. In the inactive state of a GPCR, the membrane associated G-proteins $G_\alpha G_\beta G_\gamma$ are bound together with GDP. Upon binding of a ligand, the GPCR will undergo a conformational change.[3] Following this, the G-protein complex dissociates into G_α and $G_\beta G_\gamma$, and GDP is exchanged for GTP. G_α and $G_\beta G_\gamma$ are now activated and can regulate many effector molecules depending on the GPCR (**Figure 1.2**). For example, there are many signalling pathways involved in the polarisation of a chemotaxing neutrophil. Secondary messenger molecules from phosphoinositide 3-kinase (P13K) such as PIP_3, a phospholipid, generate at the leading edge of neutrophil early in cell polarisation.[15] Leukocyte specific PIP_3 has been shown to regulate chemotaxis and adhesion in neutrophils, and also increases proinflammatory cytokines. The small GTPase Rac also plays an important role in the directionality of the cell and actin assembly, and is also localised at the leading edge of the cell.[15]

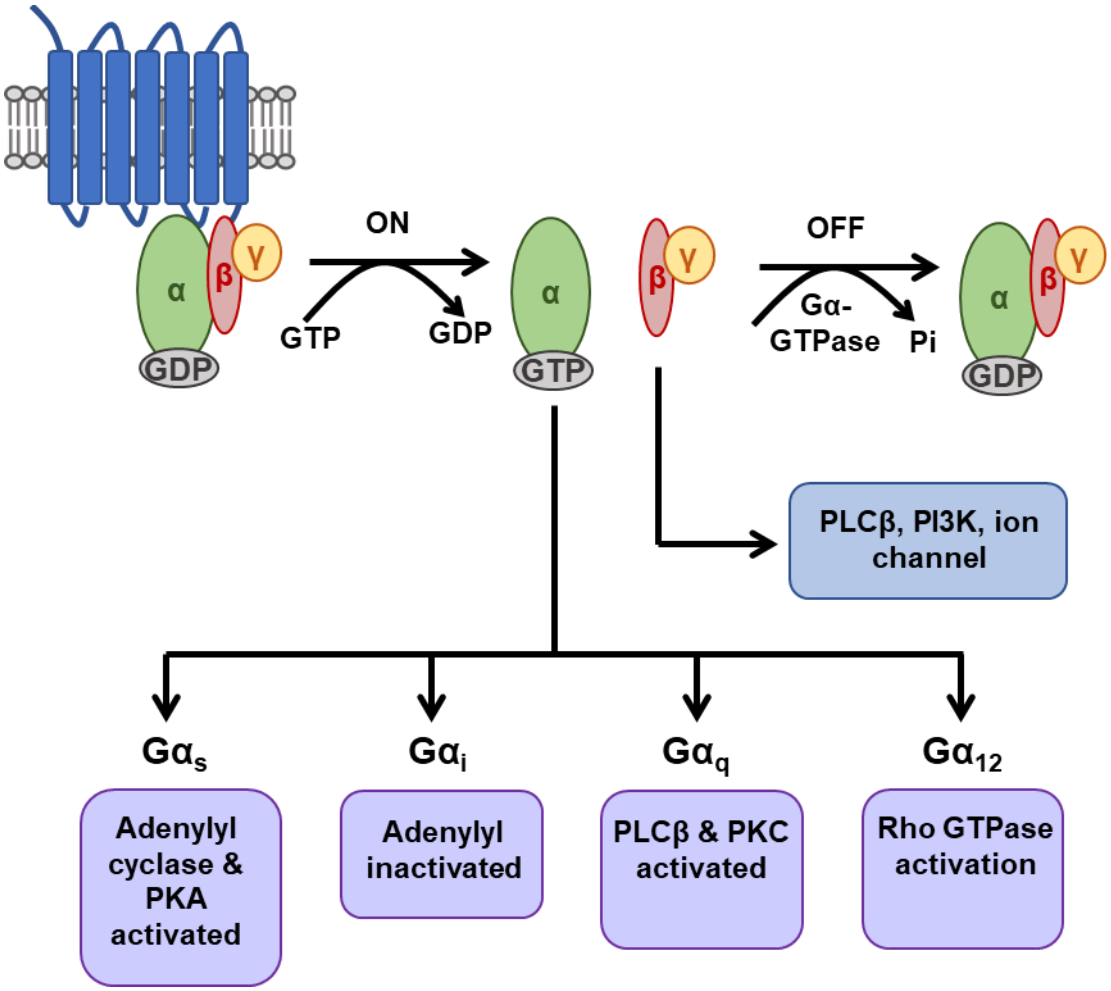

Figure 1.2: Activation of GPCRs upon ligand binding

1.3.2 Human FPR Family Members

There are three members in the human FPR family, FPR1 (previously called FPR), FPR2 (previously called FPRL1) and FPR3 (previously called FPRL2); and all play a role in the initiation, propagation and resolution of inflammation.[9, 11]

1.3.2.1 FPR1

FPR1 is a 350-residue protein with seven hydrophobic segments (Figure 1.3).[9] Its up-regulation has been observed in the neutrophils of patients with emphysema, Crohn's disease and sepsis.[9] The synthesis of FPR1 appears to occur late in the neutrophil maturation, with neutrophil activation increasing the

rate of synthesis. Expression of FPR1 is rapidly up-regulated in response to inflammatory stimuli such as LPS.[9]

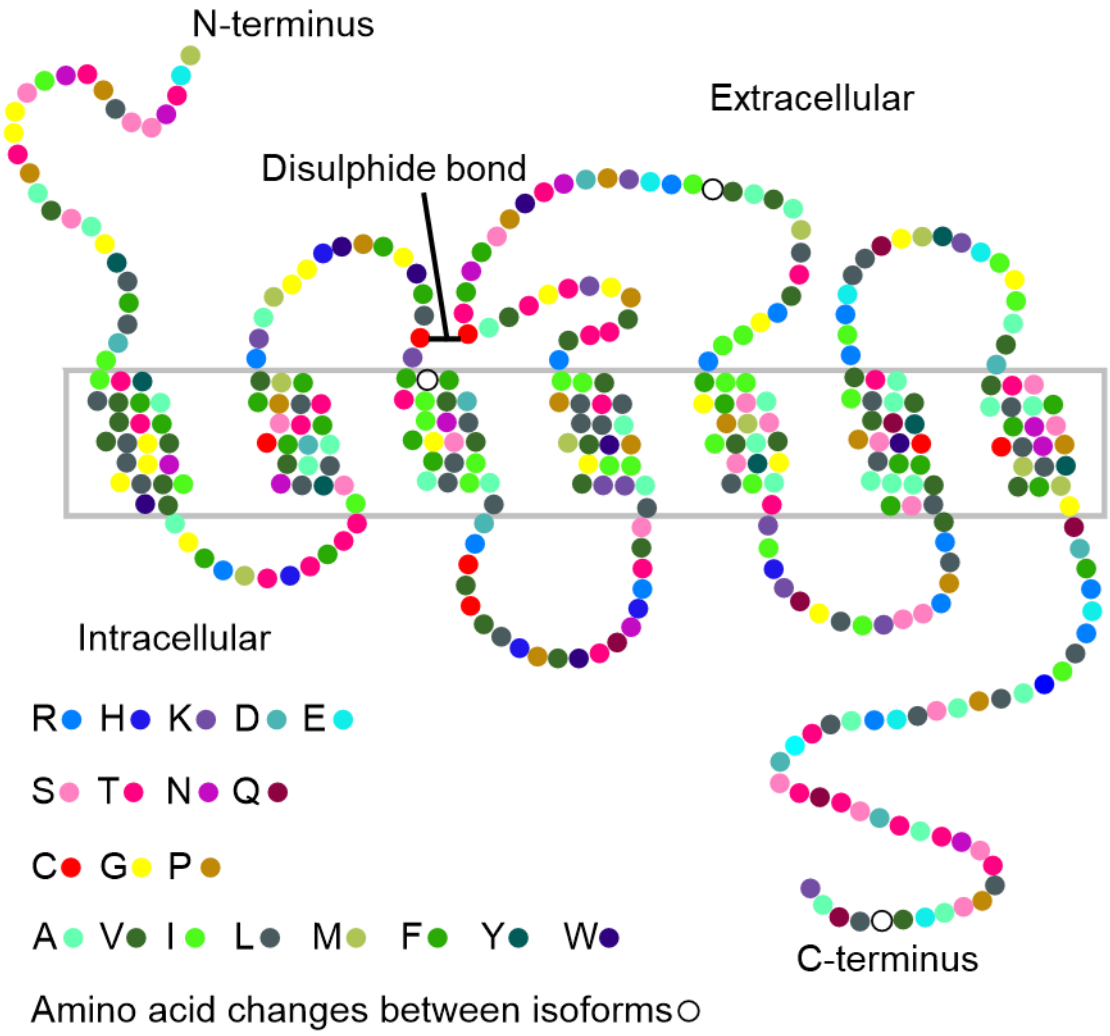

Figure 1.3: Amino acid sequence of FPR1 with predicted folding from a hydropathy plot[13, 15].

There are three isoforms of FPR1; FPR-26, FPR-98 and FPR-G6 formed from mRNA alternative splicing,[12] which have different amino acids at positions 101, 192 and 346.[9, 12, 13, 16] FPR-26 has a higher activity compared to FPR-98 and FPR-G6, measured using a GTP binding assay.[15] It has also been shown to be more efficient with coupling to G_i-proteins. It has been proposed that FPR-98 and FPR-G6 possess a folding defect, which leads to the formation of inactive aggregates (dimers and tetramers have been detected), and defective G_i-protein coupling.[16]

FPR1 ligand binding to formyl-peptides triggers chemotaxis, degranulation, ROS production and phagocytosis.[9] Its best characterised ligands are *N*-formylated peptides, with fMLF having an IC_{50} in the nanomolar range.[10, 17-19] Although the formyl group is not essential for binding to FPR1, the *N*-formylated copy of any peptide containing a methionine residue at the N-terminus is still >100 fold more potent than the non-formylated version.[9] Following binding, fMLF is internalised in under one minute and stimulates intracellular signalling cascades which lead to cellular responses such as chemotaxis.[9] Despite not providing any evidence to back up this information, Dorward *et al.* state that much is known about the interaction between FPR1 and fMLF.[9] They explain the binding mechanism of a formyl peptide with FPR1 but do not state how this was discovered or measured. Conversely, in two recent papers discussing the structure (crystal and cryo-EM) of FPR2, a FPR2-based homology model of FPR1 was created and used to model the binding of fMLF.[20, 21] The docking shows the formyl group of the peptide pointing down into the binding site and reveals that the C-terminal carboxylate forms ionic interactions to a lysine and arginine residue in the 2nd helix of FPR1 (**Figure 1.4**). This interaction is not possible in FPR2, which has a negative binding surface, and is believed to contribute to the stronger binding of fMLF to FPR1.[20-22] For interaction in FPR2, the C-terminal carboxylate faces the opposite way to interact with arginine residues on the 5th helix of FPR2 (**Figure 1.4**).[20, 21]

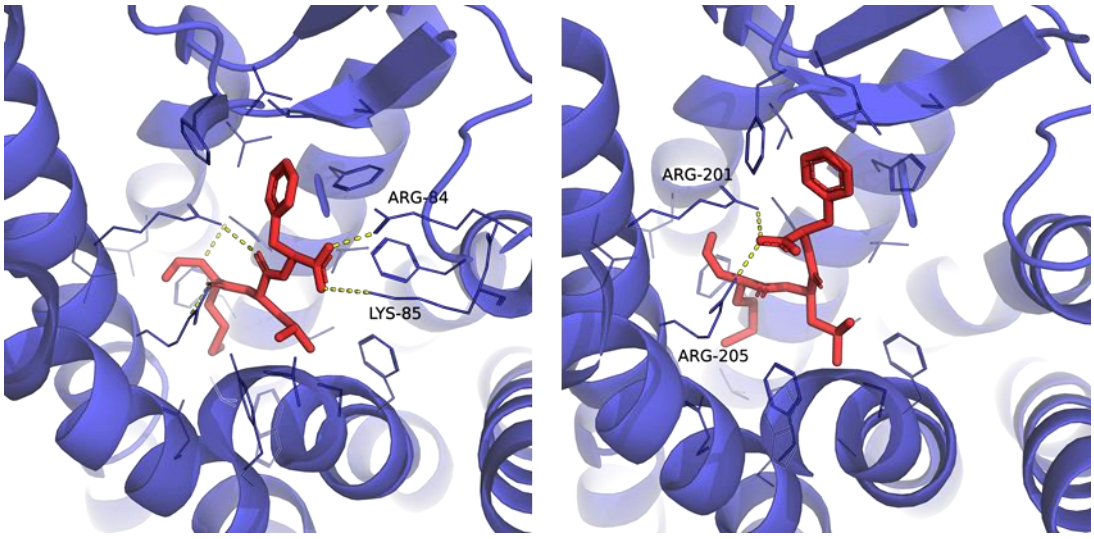

Figure 1.4: Docking model of FPR1-fMLF (left) and FPR2-fMLF (right); highlighting interaction between C-terminal carboxylate group and FPR1/2 residues; FPR1/2 in blue, fMLF in red, interactions in yellow.[20, 21]

1.3.2.1.1 FPR1 Ligands

Formyl peptides act as agonists towards FPR1 and are the most studied and characterised of its ligands. Most bacterial and mitochondrial derived formyl peptides show higher potency towards FPR1 than FPR2/3.[23] Although FPR2 shows higher ligand diversity, formyl peptides are not the only FPR1 ligands. FPR1 has been shown to bind to non-formylated host-derived peptides, and agonistic peptides and small molecules from libraries.[8, 23]

In addition to bacterial peptides, FPR1 binds other exogenous ligands, for example, two peptide domains from an HIV-1 envelope protein show agonistic activity towards FPR1.[10, 24-26] The T20/DP178 and T21/DP107 peptides from the C-terminal of HIV-1 gp41 bind to FPR1 and FPR1/2 respectively, causing activation of monocytes.[25]

Annexin 1, and some of its N-terminal derived peptides, were the first endogenous FPR1 agonists described.[24] Annexin 1 is a glucocorticoid regulated protein and is abundant in the cytoplasm of neutrophils. It is often secreted from the cells, where 75% of the protein is cleaved in the N-terminal domain giving rise to various peptides. Annexin 1 has been shown to produce anti- and pro-inflammatory responses in the cell.[26] At low concentrations, it triggers calcium flux but does not fully activate the downstream signalling pathway. This causes receptor desensitisation and inhibits cell migration.[10, 24, 26] At high concentrations, Annexin 1 fully activates FPR1 initiating chemotaxis and cell engulfment.[10, 24, 26]

Synthetic peptide ligands have also been studied for FPR1. W-peptides (Trp-Lys-Tyr-Met-Val-Met and Trp-Lys-Tyr-Met-Val-D-Met) have shown agonistic activity towards FPR1, though display higher activity towards FPR2.[10, 24-26]

A range of antagonists have been characterised for FPR1, including Boc peptides such as Boc-MLF and Boc-FLFLF. Boc-MLF and Boc-FLFLF have been shown to block fMLF (10 nM) binding to FPR1 with an inhibition efficiency of almost 100%.[27] Cyclosporin H (CsH) is a cyclic peptide that fungi produce and is also antagonistic towards FPR1.[27, 28] CsH inhibits fMLF activity at 100% efficiency[27] with an IC_{50} of 0.7 µM (14-fold higher than for Boc-FLFLF) calculated with a

scintillation assay using radiolabelled fMLF.[28] CsH and BocFLFLF have also been shown to block fMLF induced Ca^{2+} influx.[26, 28]

There have also been small molecule ligands reported for FPR1. Benzimidazole derivatives and the pyridazinone-based compounds show high specificity to FPR1, but exhibit EC_{50} above 1.5 μM.[23] In 2020, Ahmet *et al.* reported the use of the pyrazole small molecule antagonist ICT12035 **1.02** (**Figure 1.5**) for FPR1, as a potential cancer treatment.[29] **1.02** is potent (IC_{50} = 30 nM in a calcium mobilisation assay) and selective, and has been shown to reduce proliferation of U87 glioblastoma cells. The authors also showed that **1.02** slowed the rate of tumour growth in mice.

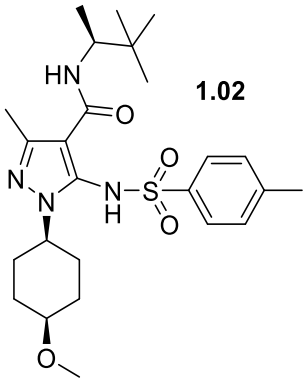

Figure 1.5: Structure of FPR1 small molecule antagonist ICT12035

1.3.2.2 FPR2

Like FPR1, FPR2 can also detect bacterial microorganism-associated molecular patterns and has a crucial role in the innate immune response to bacterial infections. FPR2 is expressed in many white blood cell types, including neutrophils, but only responds to formyl peptides at a very high concentration (several magnitudes higher than needed for FPR1).[3] It has a lower affinity for fMLF than FPR1, with an IC_{50} of 10 μM,[10] and the binding to FPR2 is determined by the charge of the peptide C-terminal.[9] FPR2 is a versatile receptor and can be activated by protein and lipid ligands.[30]

The crystal structure of FPR2 and the cryo-EM structure of the FPR2-G_i signalling complex were published in 2020 by Chen *et al.* and Zhuang *et al.*

respectively (**Figure 1.6**); becoming the first reported structures of the human FPRs.[20, 21] Both papers use WKYMVm, one of the most potent peptide agonists of FPR2, to achieve their structures. Chen *et al.* achieve the structure of FPR2 to a resolution of 2.8 Å,[20] whereas the cryo-EM structure determined by Zhuang *et al.* has a resolution of 3.17 Å.[21] This binding of WKYMVm (and also fMLF) to FPR2 is modelled using the calculated structures. Both papers show that the C-terminus of WKYMVm reaches deep into the binding pocket of FPR2, further than other known ligands, and interacts with a cluster of hydrophobic residues.[20, 21] The N-terminal tryptophan and tyrosine residues of the peptide interact with a second hydrophobic cluster, made mainly from residues on the second and third extracellular loop of FPR2. Mutations in these hydrophobic clusters completely disrupt WKYMVm binding to FPR2.[20, 21] The negatively charged surface to the binding pocket of FPR2 also plays a role in the binding of WKYMVm. Salt bridges are formed between the N-terminus of WKYMVm and an aspartic acid residue at the extracellular surface of transmembrane helix 7; and the lysine residue in WKYMVm with a glutamic acid residue in the first extracellular loop.[20, 21]

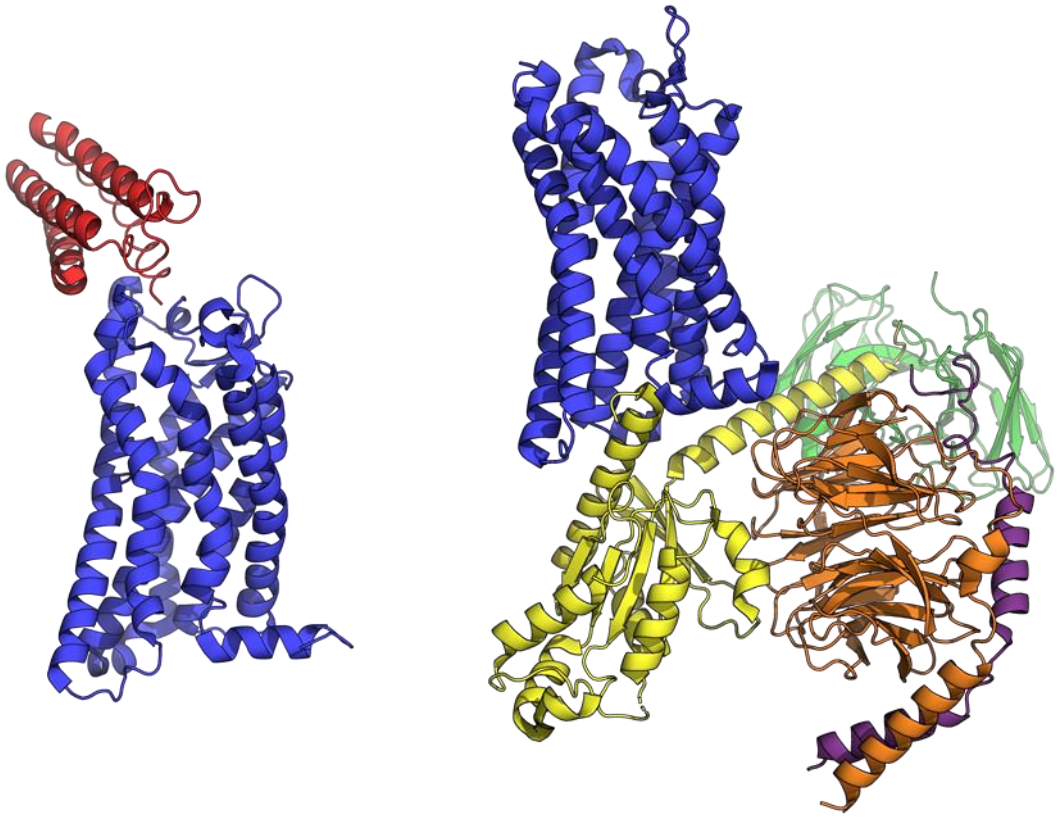

Figure 1.6: Crystal Structure of FPR2 with soluble cytochrome b562 (left); cryo-EM structure of FPR2-G_i complex (right); FPR2 (blue), soluble cytochrome b562 (red), $G\alpha_i$ (yellow), Gß (orange), Gγ (purple), scFv16 (green).[20, 21]

1.3.2.2.1 FPR2 Ligands

All Staphylococci bacteria secrete phenol-soluble modulins and these are strong contributing factors to virulence.[30] Although FPR1 shows higher binding affinity to most bacterial formyl peptides, phenol-soluble modulins show potent agonistic activity towards FPR2 (nanomolar concentrations) with only weak activity towards FPR1.[3] Phenol-soluble modulins are a type of MAMP and therefore their binding to FPR2 helps to initiate the innate immune system. Phenol-soluble modulins are peptides, ranging from 20-45 amino acids long, that form an amphipathic α-helix. They do not have a formylated N-terminus.

Like FPR1, two peptide domains from an HIV-1 envelope protein show agonistic binding to FPR2. In addition to the T21/DP107 peptide that activates both FPR1 and FPR2, the N36 peptide specifically activates FPR2.[24-26, 30]

FPR2 reacts with a greater variety of host-derived ligands than FPR1.[24] Most of these are chemotactic agonists, such as mitochondrial peptides, that cause a proinflammatory response.[24] Lipoxins are generated at inflammation sites and are lipid mediators.[30] Lipoxin A4 is a metabolite of arachidonate – a fatty acid essential for human bodily function – that possesses anti-inflammatory and immunoregulatory functions. Lipoxin A4 acts as an antagonist to FPR2, blocking proinflammatory responses induced by FPR2 agonists.[24] It has a high affinity for FPR2 and its binding stimulates the release of arachidonate.[30]

1.3.2.3 FPR3

Despite the 83% sequence similarity between FPR2 and FPR3, the function of FPR3 is poorly understood and this receptor is not expressed on neutrophils.[3, 9] FPR3 is expressed by macrophages, monocytes and dendritic cells.[9] FPR3 is insensitive to formylated peptides[9] and it is thought that it plays a role in the pathogenesis of allergic diseases.[9]

Several low affinity ligands have been described for FPR3, most being agonists for FPR2 (including the mitochondrial peptide fMMYALF and W-peptides).[10, 25] However, most of these occur in addition to FPR2 binding or only when FPR2 is desensitised. The only endogenous FPR3 ligand described is F2L (Ac-MLGMIRNSLFGSVETWPWQVL), a peptide from the N-terminus of a heme-binding protein. F2L shows high affinity and specificity for FPR3, inducing intracellular calcium release.[25]

The true role and relevance of FPR3 remains to be discovered.

1.3.2.4 Disease Relevance of FPRs

5-15% of healthy adults who are infected with *Mycobacterium tuberculosis* (*Mtb*) will develop active tuberculosis (TB) within two years of the infection.[31] Macrophage polarisation is important for restricting *Mtb* early growth and advanced inflammation later on. M1 monocytes promote small areas of inflammation around *Mtb* and help to eliminate it, whereas M2 monocytes inhibit inflammation and aid in the growth of *Mtb*.[31] At present there are no biomarkers

to differentiate between a slow progressing latent TB infection and active TB. FPR1 expression in M1 monocytes could be an indicator for active TB. Chen *et al.* have shown that in response to *Mtb*-specific antigens, FPR1 is activated on M1 monocytes whilst FPR2 is inactivated to maintain M1 polarisation.[31]

In addition to their role in host defence from invading microorganisms, FPRs have also been associated with human diseases. Many ligands have been shown to bind to FPR1 and have been associated with HIV, amyloidosis, Alzheimer's Disease and prion disease.[10] The binding of these ligands causes inflammation and is thought to be involved in disease onset.[10] Therefore it is possible that FPRs could be used as drug targets in the future for these diseases.

FPRs have also been linked to the development of cancer.[10, 32, 33] It was found by Zhou *et al.* that FPRs are expressed in glioma cells – an unexpected discovery.[33] Glioblastoma makes up 65% of malignant gliomas and has a post-surgery median survival rate of 12-15 months.[34] The FPRs were found to mediate self-mobility, growth and the development of new blood vessels of glioblastoma through the interaction of human agonists.[33] Hu *et al.* found that the expression of FPR1 triggers specific anti-tumour host immune responses in mice and resulted in their resistance to tumour cells.[32] More recently, Boer *et al.* have shown that the FPR1 expression in glioma cells is stimulated by the microenvironment. Glioblastoma is characterised by areas of necrosis and Boer *et al.* found that supernatant from the necrosis activated FPR1 on U87 cells this is likely due to the presence of mitochondrial formyl peptides.[34] The authors showed that calcium flux and migration of U87 cells were inhibited with the chemotaxis inhibitory protein of *Staphylococcus aureus* (CHIPS).[34] They proposed further investigation into CHIPS a potential drug for glioblastoma.

It is evident that FPRs are becoming a very attractive pharmacological target.

1.4 Methods to Detect and Analyse Ligand-GPCR Interactions

GPCRs are the largest family of druggable targets and therefore GPCR ligand screening for binding is very important.[35] Over the past few decades there has

been investigation into the development of accurate assays for the targeting of GPCRs. The ideal assay would be non-radioactive, simple and easily adapted for automation.[35]

1.4.1 GPCR Pharmacology

There are several types of ligands that bind to GPCRs and these belong to three categories: agonists, allosteric modulators and antagonists. Agonists activate the GPCR either with high affinity or with low affinity, and can exhibit a full or partial response. Inverse agonists elicit an alternative response to agonists, and can be competitive or non-competitive by binding to the same or alternative binding site respectively. Allosteric modulators bind to an alternative site to the agonist binding site and cause a conformational change in the GPCR. This change either increases (positive allosteric modulator) or decreases (negative allosteric modulator) the affinity for ligands. An antagonist stops agonist activity, binding to the same site (competitive) or a different site (non-competitive). The binding of some antagonists is irreversible.

1.4.2 Receptor Binding Assay

Receptor binding assays are a cell-free method for the screening of GPCRs. They are suitable for any type of GPCR, but do not give information about the downstream signalling.[35] Although this method can be used to detect agonists and antagonists in one experiment, it cannot distinguish between the two types of ligand. This method is limited by the availability of labelled ligands, and can't be used for the discovery of ligands for GPCRs with no known ligands.[35] Lefkowitz and Roth performed the first radioligand binding assay in 1970,[36] using it to determine the binding affinity of adrenocorticotropic hormone to its receptor. ^{3}H- or ^{125}I-labelled ligands are commonly used in receptor binding assays.[35] The binding affinity is calculated by competing the radioligand with a non-labelled ligand. Lefkowitz and Roth utilised a ^{125}I-labelled ligand.[36] For the automation of high-throughput screening (HTS) applications, homogenous scintillation proximity assays have been developed.[35] The scintillation proximity assays was

originally established for antibody-antigen binding,[37] but was developed for membrane receptors by Nelson in 1987.[37, 38] The receptor is bound to the scintillation bead as the purified protein or expressed in membranes (**Figure 1.7**). The ^{125}I-labelled ligand emits Auger electrons, which have a short path length in water. When the ligand binds to the receptor, the Auger electrons stimulate the scintillation beads to emit light.[37] scintillation proximity assays allows the binding of ligands to be measured without the need for washing and filtration.[37] However, radioligands are expensive and hard to dispose of. As an alternative, new assays based on time-resolved fluorescence energy transfer have been established.[35]

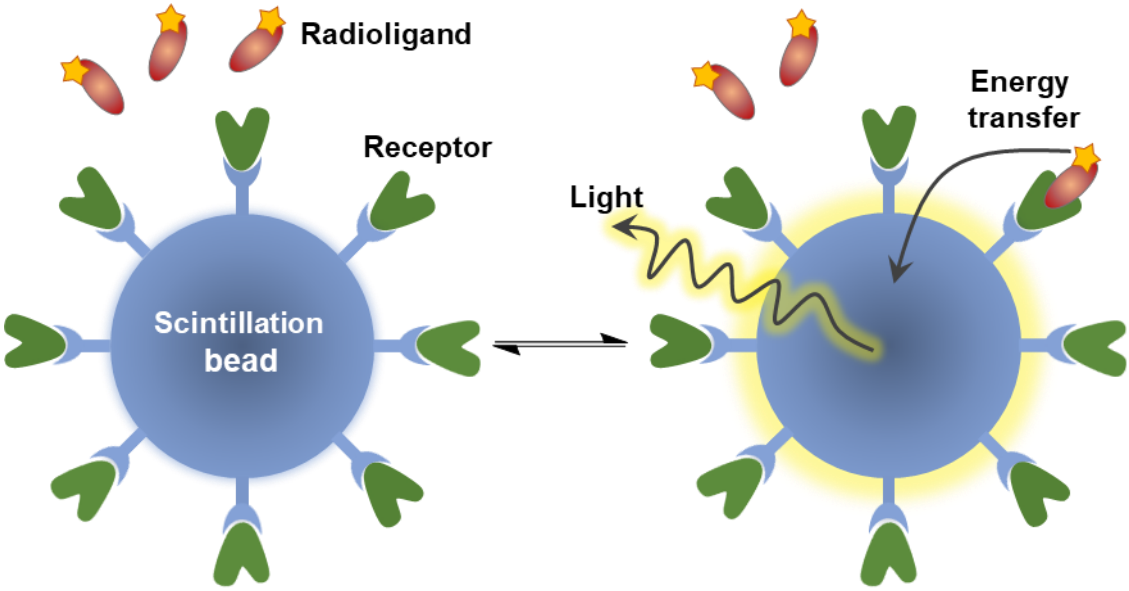

Figure 1.7: Scintillation proximity assay.

1.4.3 G-Protein Dependent Assays

G-protein dependent functional assays are useful for the discovery of new ligands targeting GPCRs and help to analyse the biological response after binding.[35]

1.4.3.1 GTPγS Binding Assays

Guanine nucleotide exchange of G-proteins occurs quickly after GPCR activation, GTPγS binding assays directly measure this exchange.[35, 39] The build-up of GTP analogues stable to hydrolysis, such as [35]S-GTPγS, on the plasma

membrane of GPCR-expressing cells is measured after stimulation by an agonist.[35, 39] This method allows ligands to be identified as full or partial agonists, inverse agonists or allosteric modulators. A problem with GTPγS binding assays is that a filtration through a glass fibre is required to separate free and bound [35]S-GTPγS; this limits the throughput of the assay.[35] However, scintillation proximity assays can also be used for this type of assay, removing the need for the filtration. Unfortunately, the assay is also limited by its poor signal to background due to the low expression levels of GPCRs.[39] Isolation of the target GPCR can improve the signal to background. The activation of adenylyl cyclase can be measured in a similar way by measuring the levels of cyclic adenosine monophosphate using an enzyme immunoassay.

1.4.3.2 Ca^{2+} Assays

The release of Ca^{2+} intracellularly is agonist-dependent. Due to the availability of cell-permeable Ca^{2+} sensitive fluorescent dyes and automated real-time fluorescence plate readers, Ca^{2+} assays are very popular for GPCR screening.[35] Biosensors can also be employed for the detection of Ca^{2+}. The photoprotein present in jellyfish, aequorin, provides a strong luminescence signal in response to raised intracellular Ca^{2+}.[35, 40] Aequorin has been used in biological systems and has shown very little toxicity issues.[40] This has been developed for GPCR screening and is widely used for finding new ligands.[35] The Ca^{2+} assays are suitable for HTS. However, this assay cannot detect inverse agonists, is not suitable to detect slow binding and false positives are a recurring issue.[35]

1.4.4 Generic G-Protein Independent Assays

1.4.4.1 Receptor Internalisation Assay

Receptor internalisation assays are based on the desensitisation of GPCRs. GPCRs activated by agonists are phosphorylated by GPCR kinases (GRKs) causing cytosolic β-arrestins to be recruited to the cell membrane. This uncouples the GPCR from its G-proteins, and encloses the GPCR in a vacuole.[35] The

internalisation of the formyl peptide receptor (does not state which FPR is studied, as the three individual FPRs were not referred to at this point) has been studied using a rhodamine peptide ligand.[41] GPCR internalisation is now quantifiable in conjunction with high-content screening (HCS). HCS combines high-resolution fluorescence microscopy and automatic image analysis,[35] allowing the monitoring of biomolecules with the use of different fluorophores. HCS requires no previous knowledge of the GPCR signalling pathway, therefore it is a useful method for de-orphaning GPCRs.[35]

1.4.4.2 β-Arrestin Recruitment Assays

The binding of β-arrestin to ligand-activated GPCRs has been demonstrated for almost all types of GPCR.[35, 42] β-Arrestin recruitment assays provide a novel, universal and G-protein independent way for the screening of GPCRs. These are useful assays for the de-orphaning of GPCRs.[35] Using GFP-tagged β-arrestin, Transfluor was the first commercially available β-arrestin recruitment assay and provided HTS screening for compounds targeting GPCRs. This type of assay is beneficial as no fluorescent dyes or secondary substrates are needed.[35] The β-arrestin recruitment assays also allow cell imaging.

1.4.5 Flow Cytometry

Flow cytometry began in the 1960s for the analysis and sorting of cells. Since then it has been used to study ligand-receptor interactions and aid drug discovery research. In flow cytometry a suspension of particles/cells is analysed with measurements of light scattering and fluorescence performed for each particle (**Figure 1.8**).[43, 44] The population of particles is characterised and subpopulations created. The light scatter measures the size and density of the particle, and the fluorescence detects probes associated with an individual particle. Thousands of particles are evaluated per second. The light scatter analysis is given as a dot plot of the side-scatter (SSC) against the forward-scatter (FSC) (**Figure 1.9**). Fluorescence intensity is given as histograms (**Figure 1.9**).

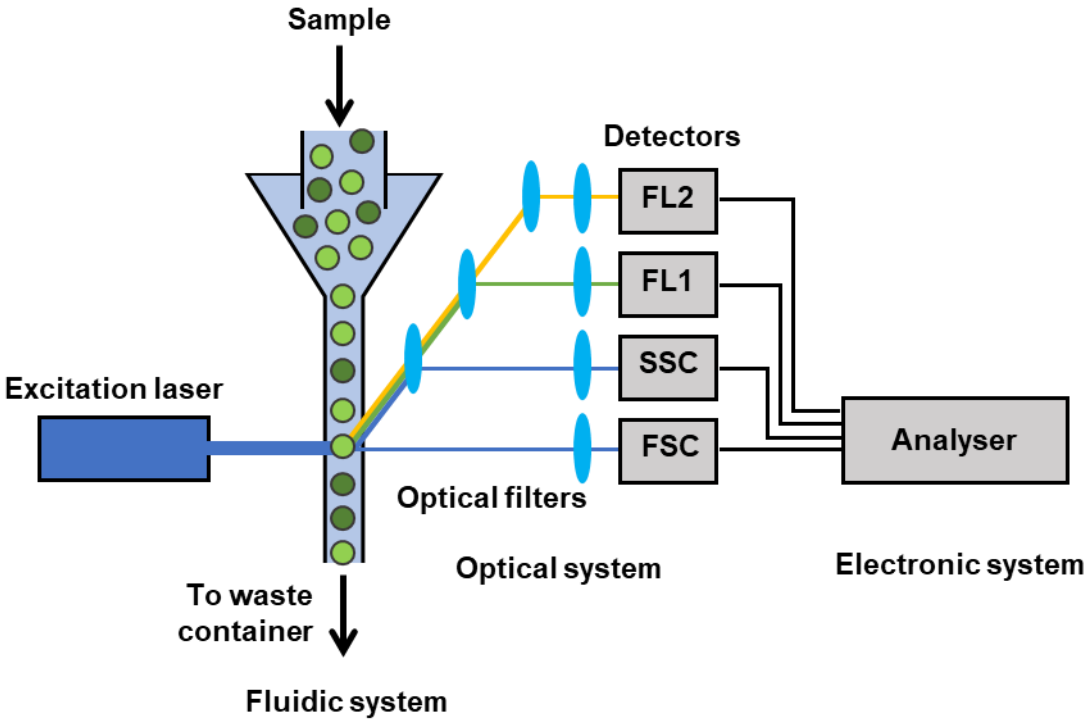

Figure 1.8: Flow cytometry. Sample of particles/cells (green circles) is focused into a laminar stream from the pressurised sheath fluid. The line of particles passes through the excitation laser and emitted light at a specific wavelength is directed through a series of mirrors and filters to detectors (FSC and SSC for light scatter, and FL1 and FL2 for fluorescence emission).[43, 44]

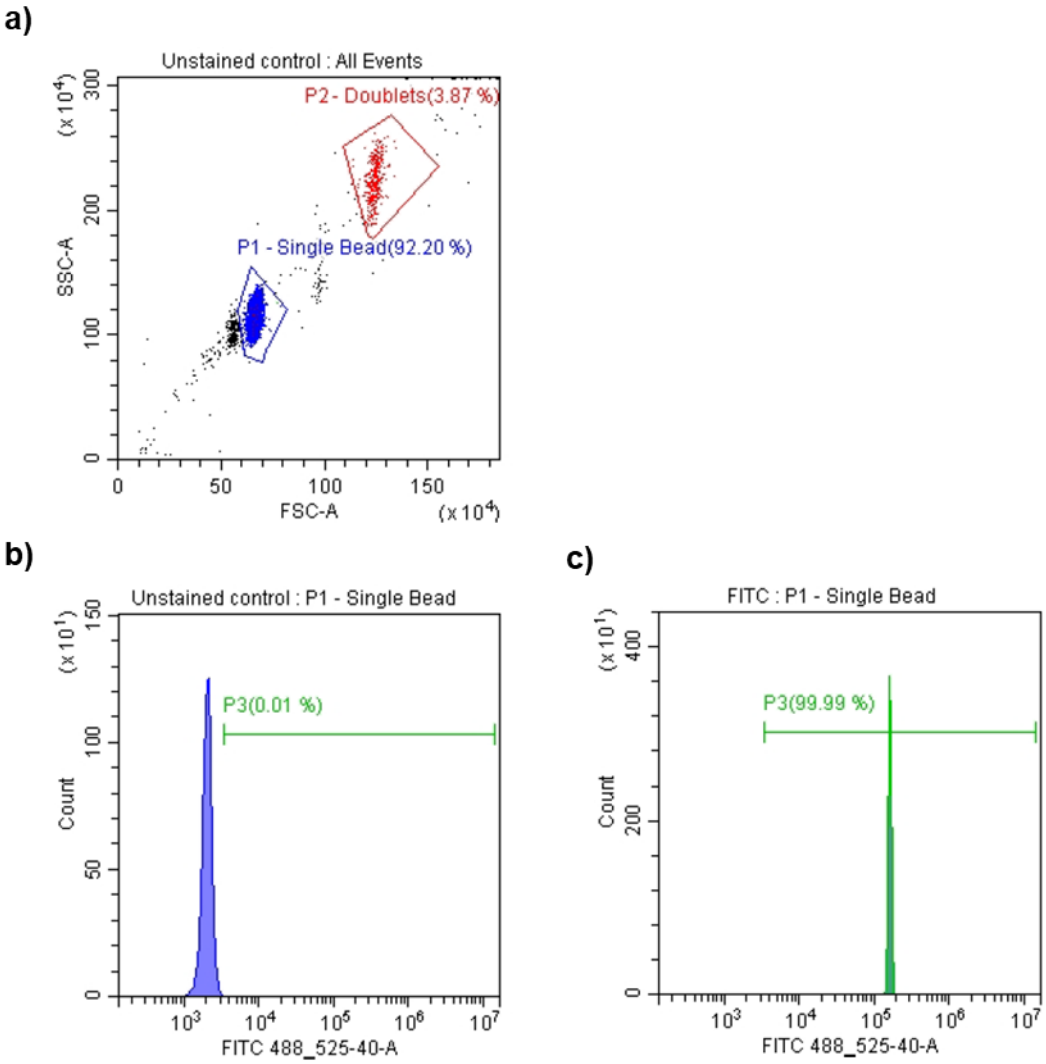

Figure 1.9: Real-time flow cytometry analysis of stained and unstained beads; a) dot plot of SSC versus FSC for a sample containing two populations of beads; b) histogram of fluorescence intensity at 488 nm (525/40 filter) for the subpopulation of single beads (P1 blue) for the unstained bead sample, this is the control sample and a gate is drawn (P3 green) to define staining; c) histogram of fluorescence intensity at 488 nm (525/40 filter) for the subpopulation of single beads for the stained bead sample, >99% shown in the gated area. Data obtained by Ruth Hughes at University of Leeds.

Techniques for attaching pure components onto beads have been developed and two main platforms are used: ligand-beads and G-protein-beads.[43] Ligand-beads are ligands conjugated to a bead and binding is viewed by using a GPCR–GFP fusion protein.[43] G-protein-beads are beads displaying chelated Ni^{2+} or antibodies to couple to the GPCR.[43, 44] Fluorescent ligands are then employed to observe binding. This approach has been used to observe the binding of fMLFK-FITC to

C-His FPR1 coupled to Ni^{2+}-nitriloacetic acid silica particles by Sklar *et al.*[45] Of course flow cytometry can also be used to study ligand-receptor interactions on the surface of mammalian cells. The binding of ligands to FPR1 expressed on the surface of cells has also been previously published.[22, 46-48] During flow cytometry analysis, gating is involved, which is a refinement of the cell population. Unfortunately, this can lead to bias and human error in data sets as the scientist sets the gate parameters and chooses which cells to analyse in the population.

1.5 Affinity-based Protein Profiling

Affinity-based protein profiling (A*f*BPP) couples photoaffinity labelling with proteomics allowing the investigation of ligand-molecule interactions and binding site structure (**Figure 1.10**). A*f*BPP can be a two-step or one-step method.[49] Two-step A*f*BPP utilises an affinity-based probe containing a tag to allow addition of a detectable group (fluorophore/biotin); and a reactive group (commonly a photoreactive group) to form a covalent link between the probe and molecule. One-step A*f*BPP has the detectable group attached directly to the probe. The fluorophore/biotin tag allow detection, purification and analysis of the hits of the probe. Digestion of the labelled protein paired with tandem mass spectrometry is a popular analytical method.

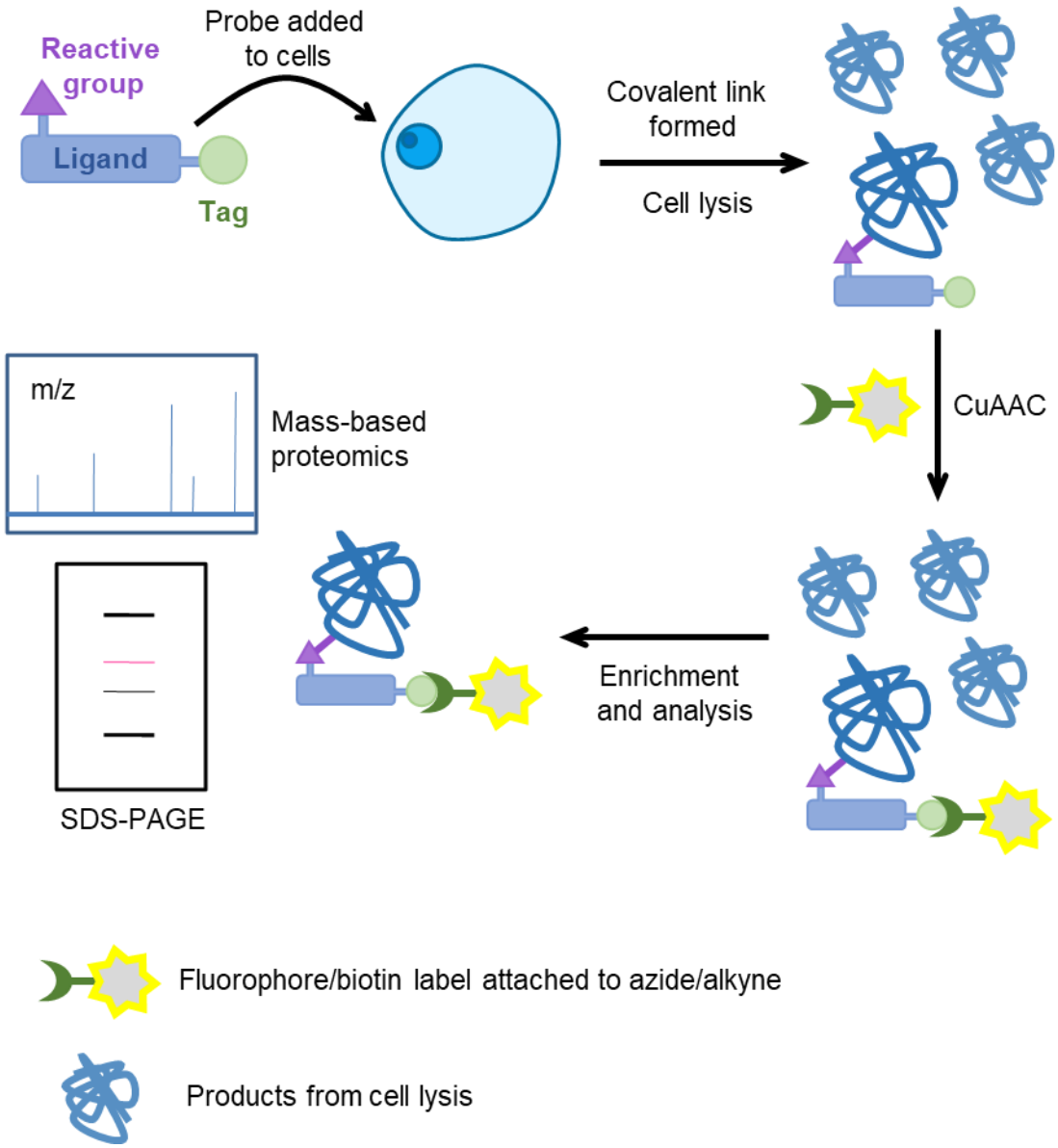

Figure 1.10: Two-step affinity-based protein profiling, probe is designed based on a known ligand of the target protein; probe covalently reacts via the reactive group; cells are lysed and the CuAAC is performed on the lysis products to attach a fluorophore/biotin to the bound probe for proteomic analysis.[49]

1.5.1 Photoaffinity Labelling

Knowledge of protein-ligand binding interactions is important for the understanding of biology, and for the development of drugs to target these interactions. Therefore methods that reveal insight into these binding mechanisms are crucial. In the early 1960's Westheimer introduced photoaffinity

labelling (PAL).[50-55] This technique is used for the study of receptor-ligand interactions, where a chemically synthesised probe binds covalently to its target through activation by light. This can be achieved by the addition of a photoreactive group on the probe, which would otherwise bind to the receptor reversibly. A particular wavelength of light will cause the photoreactive group to form a highly reactive intermediate that will react with the target receptor. This method allows the isolation of many receptor-ligand complexes, even those formed from weak interactions.[51] The ideal photoprobe should possess the following qualities; 1. stability in the dark across a broad pH range, 2. close similarity to its parent molecule with comparable affinity, 3. activation at wavelengths that will do minimal/no damage to the biological system, 4. generation of highly reactive intermediates at this wavelength, 5. ability to react with any bond/residue with no bias (but not react intramolecularly), to form a stable covalent bond to the target receptor.[56]

1.5.1.1 Photoreactive Groups

Diazocarbonyl derivatives were the first group to be used as photoaffinity labelling reagents.[51, 52, 54, 55] Currently, there are three main photoreactive groups used for PAL: phenylazides **1.03**, diazirines **1.06** and benzophenones **1.09**.[50, 51, 53, 54] Upon activation of ultra-violet (UV) light, these groups form a nitrene **1.04**, carbene **1.07** and diradical **1.10** respectively (**Scheme 1.1**). The half-lives of these reactive intermediates are often shorter than the dissociation of the ligand from the receptor, allowing the formation of the covalent bond. In addition to these three main groups, tetrazoles **1.12** are also beginning to be employed as photoreactive groups.[57] Upon irradiation with UV light tetrazoles form a nitrile imine dipole **1.13** that reacts with an alkene in a 1,3-dipolar cycloaddition.[57] However, due to the absence of alkenes in proteins, the alkene would need to first be installed in the protein. More recently, it has been shown that tetrazoles react with carboxylic acids (**Scheme 1.1**),[58-62] a promising discovery for photoaffinity labelling given the high frequency of aspartic acid and glutamic acid residues in proteins (10% combined).[59]

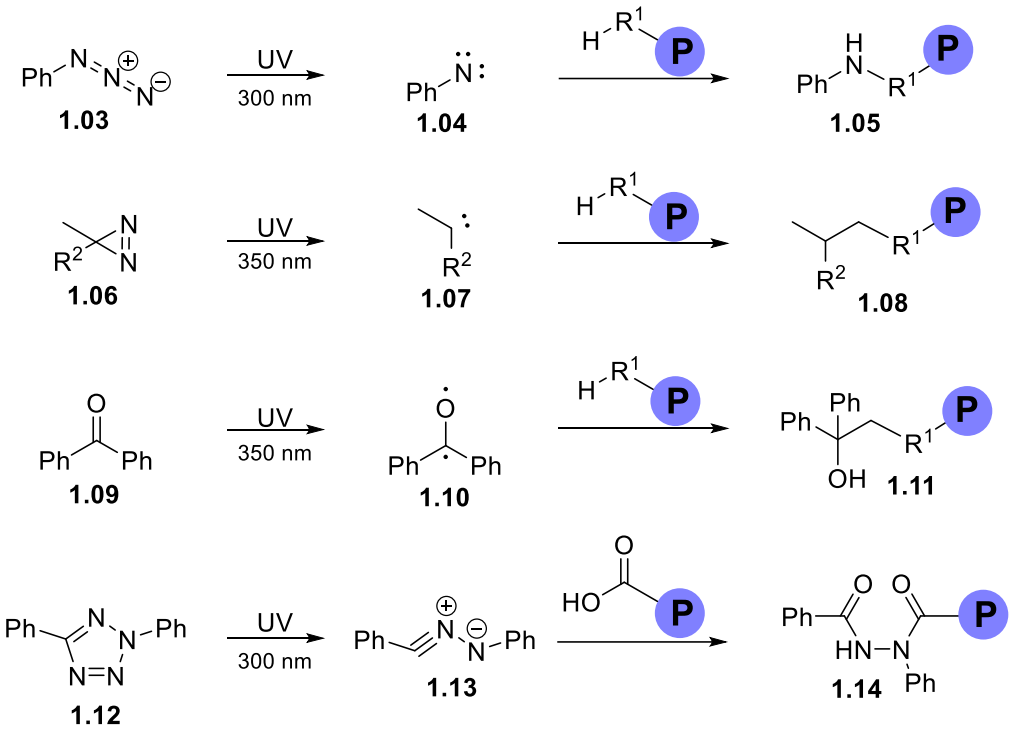

Scheme 1.1: Activation of photoreactive groups and formation of covalent bond to protein.

1.5.1.1.1 Phenylazides

Phenylazides were first reported for the use of photoaffinity labelling in 1969 by Knowles, Porter and Fleet.[63] The small size of this photoreactive group means that it causes the least change in structure to the ligand among all the photoreactive groups, when introduced into an existing aromatic ring.[51, 54] Due to this, and the ease of synthesis, phenylazides are frequently used for photoaffinity labelling.[50, 51, 53, 54] A synthetic method using triflyl azide allowing the one step conversion of an amine **1.15** to its corresponding azide **1.03** with high yields has been reported (Scheme 1.2).[54] In addition to this, many phenylazides are commercially available.

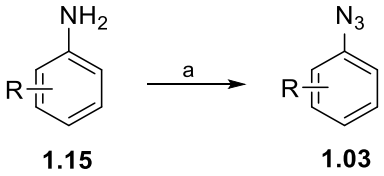

Reagents and conditions: (a) TfN_3, $CuSO_4$, Et_3N, 88%.

Scheme 1.2: Formation of azide from amine[54].

Excitation of a phenylazide requires irradiation of UV light at 300 nm which can cause damage to biological molecules.[51, 53, 54] Upon irradiation, the reactive nitrene intermediate **1.04** is formed via photolysis of the phenylazide and nitrogen gas is expelled.[51, 54] Phenylazides have shown decreased photoaffinity yields compared with diazirines due to the nitrene intermediate being less reactive than the carbene[64] and the rearrangement of nitrenes to form benzazirines **1.16** and ketenimines **1.17** as undesired side products (**Scheme 1.3**).[50] The ketenimines produced are very reactive towards nucleophiles, such as amine groups present on proteins. To prevent the rearrangement of nitrenes to ketenimines, substituted phenyl azides can be used, for example tetrafluorophenylazide.[50, 51, 65] The nitrene intermediate can also be reduced to an amine by thiols; however this is unlikely to occur at physiological pH.[14] Nitrenes insert into C-H, O-H and N-H bonds and show a preference to react with cysteine or aromatic amino acids.[65]

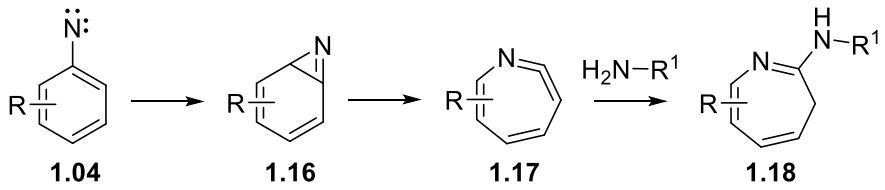

Scheme 1.3: Formation of side products from nitrene.

As a result of low reactivity and these side reactions, phenylazides often have a low crosslinking yield.[14] It is evident that the phenylazide is used frequently because of its ease of preparation and often commercial availability, and not its photoaffinity labelling properties.

1.5.1.1.2 Benzophenones

Benzophenones were first reported for the use of photoaffinity labelling in 1973 by Galardy, Craig and Printz,[66] and are commonly used due to their commercial availability.[53, 54] Unlike phenylazides which require a lower wavelength of UV light for excitation, benzophenones require 350-360 nm for the formation of a benzhydril triplet diradical **1.10**. At this wavelength of UV light biological molecules are not likely to be damaged. However prolonged irradiation is

necessary to achieve a high crosslink efficiency, and this can lead to unwanted sample heating.[50, 54] The diradical reactive intermediate has the advantage of being more reactive than a nitrene and it is less susceptible to intramolecular rearrangements than carbenes. The diradical preferentially inserts into C-H bonds, particularly those adjacent to a sulphur or nitrogen.[65] In the absence of a suitable C-H bond to react with, the diradical relaxes to its ground state and can be re-excited to improve crosslinking yield.[51] In addition to this, reaction with water generates the hydrate **1.19** which immediately dehydrates to the original ketone which can be excited again (**Scheme 1.4**).[54] A possible side reaction is the homodimerisation of the formed ketyl **1.20** to furnish benzopinacols **1.21**; however these are only produced in small yields.[54]

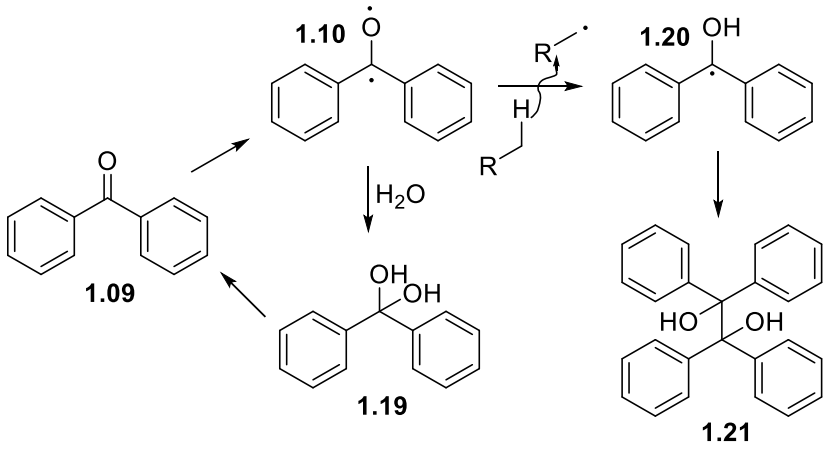

Scheme 1.4: Side product formation from benzhydril diradical.

Despite having a high crosslink efficiency, there are some drawbacks to the benzophenone as a photoreactive group. It is bulky in comparison to the small azides and diazirines, which can lead to undesirable interactions between the receptor and ligand.[50, 53, 54] Resulting steric hindrance from the benzophenone can cause discrimination between reactive sites leading to nonspecific labelling.[50, 54] It has also been suggested that benzophenones preferentially react with methionine residues.[67] Wittelsberger *et al.* explored this suggestion and found that benzophenone always cross-linked to a methionine residue, they termed this the “magnet effect”.[67] However, this study was only performed on one GPCR (with several methionine modifications) and one photoaffinity ligand; therefore this “magnet effect” needs to be explored further. Benzophenones are

still a common choice of photoreactive group for their ease of production and inertness to many reaction conditions.

1.5.1.1.3 Diazirines

Diazirines **1.06** were first reported for the use of photoaffinity labelling in 1973 by Knowles and Smith.[68] Like benzophenones, diazirines absorb UV light of 350-380 nm, ensuring there is little damage to biological systems.[50, 51, 54] Upon irradiation, nitrogen gas is expelled and a singlet carbene **1.07** is produced (**Scheme 1.5**). However, over 30% of diazirines will not be converted into carbenes but will form long-lived diazoisomers that slowly convert into carbenes under UV light. These diazoisomers can lead to acidic residue labelling (**Scheme 1.6**). The successfully formed singlet carbene are short-lived and quickly transform into triplet carbenes **1.23**.[54] Singlet carbenes give fast insertion reactions with almost no bias between reaction sites. With the addition of a trifluoromethyl group, insertion into primary or secondary N-H bonds can lead to the production of hydrofluoric acid and form an enamine **1.26** in equilibrium with its corresponding imine **1.27**. In physiological environments, these are hydrolysed to the ketone **1.28**. Triplet carbenes react in an analogous way to triplet nitrenes. Oxidation can occur of the triplet carbene to give the equivalent ketone. The carbene inserts into C-C, C-H, N-H, O-H and S-H bonds.[65]

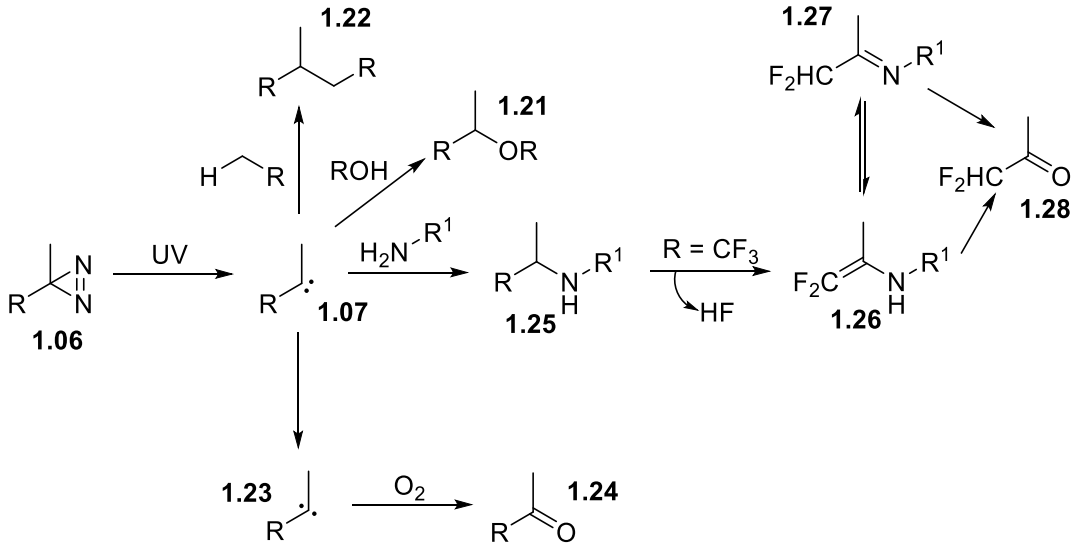

Scheme 1.5: Side product formation from carbenes.[54]

The diazirine group itself is small, but the commonly used aryl diazirines are relatively bulky. These however can be incorporated into molecules with a structure similar to naturally occurring compounds with ease.[54] A particularly attractive feature of diazirines is their high stability towards many conditions such as strongly acidic, strongly basic, oxidising and reducing agents. However, the main drawback of diazirines is their complex and long synthetic routes compared with azides and benzophenones. The considerable amounts of diazo species formed and the reactivity of the singlet carbene with O-H bonds leading to the scavenging of reactive species by water, lowers the crosslinking yields.[50, 54] Conversely, the reactive carbene intermediate is significantly more reactive than the nitrene or diradical, with a shorter half-life and potentially rapid rates for the formation of covalent crosslinks to the target receptor.[50, 51]

There are two categories of diazirines, aliphatic and aromatic. Aliphatic diazirines are smaller in size and recently there has been a steady increase in their use, however aromatic diazirines possess better photochemistry properties.[56] It has been shown that aromatic diazirines generate less of the diazoisomer side-products than aliphatic diazirines upon irradiation with UV light. As an example, chloro-methylchlorodiazirine **1.29** produced carbenes in 36% yield when activated,[69] however phenylchlorodiazirine **1.30** produced carbenes in 99% yield.[56, 70] Nevertheless, many aliphatic diazirine analogues, including alcohols, sugars and amino acids, have been used to determine the binding sites of membrane-bound proteins.[56] A range of residues have been labelled and identified using aliphatic diazirines as biological probes although the most commonly labelled residues were glutamic acid, tyrosine and aspartic acid.

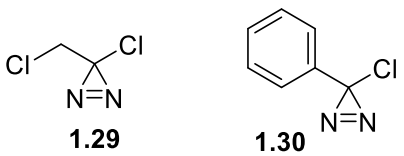

1.29 **1.30**

Figure 1.11: Structure of chloro-methylchlorodiazirine **1.29** and phenylchlorodiazirine **1.30**

Diazirine analogues of amino acids have been incorporated into peptides to study protein-protein, and protein-peptide interactions. The diazirine analogue of methionine, termed Photo-Met **1.31** (**Figure 1.12**) and first synthesised by Thiele

et al.,[71] was prepared and shown to be compatible with SPPS.[72] Muir *et al*, created a semi-synthetic protein using expressed protein ligation with the incorporation of Photo-Met.[72] Using this they were able to capture the interaction between two signalling proteins. Photo-Leu **1.32** (**Figure 1.12**), the diazirine analogue of leucine, was also first synthesised by Thiele *et al.*[71] and has been attached to a photoaffinity probe and used for the crosslinking of proteins in native conditions.[73] The diazirine side chain was found to be stable in ambient light, and in the acidic and basic conditions needed for the peptide synthesis of the probe.[73]

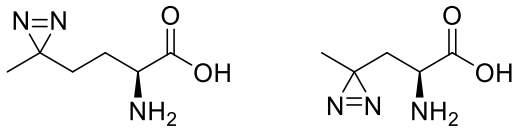

1.31 **1.32**

Figure 1.12: Structures of Photo-Met **1.31** and Photo-Leu **1.32**.

Until recently it was thought that diazirines reacted in an unbiased manner via the carbene produced upon UV irradiation. However, it has now been shown that they have a preference for acidic residues (**Scheme 1.6**).[74, 75] When irradiated with UV light diazirines can form a carbene or isomerise into a linear diazo compound **1.33/1.34**. In 2018, Iacobucci *et al.* noticed a mass shift of −28 Da (corresponding to a loss of N_2) for peptides crosslinked to photo-Met.[74] The only explanation for this was the formation of labile mass-spectrometry-cleavable esters during crosslinking to carboxylic acids. Iacobucci *et al.* found that 75% of photo-Met labelling was to acidic residues, the same percentage of diazirines that photoisomerise into diazo compounds.[74] Just earlier this year, West *et al.* performed a more in-depth study of the labelling preferences of diazirines, comparing alkyl and aryl diazirines.[75] The authors found that alkyl diazirines preferentially react with acidic residues, showing high labelling at lower pH and for probes with a net positive charge.[75] Conversely, aryl diazirines were found to crosslink to all amino acids, were pH independent and readily quenched by water.[75]

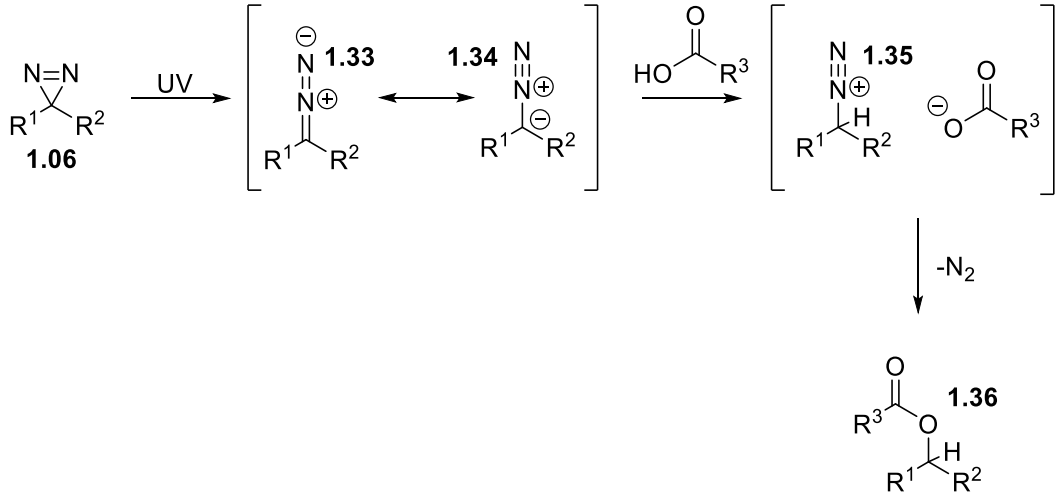

Scheme 1.6: Reactivity of diazo compound **1.33/1.34**, formed upon UV irradiation of diazirine, with carboxylic acid to form ester **1.36**.

1.5.1.1.4 Tetrazoles

The photoreactive tetrazole was first reported in 2007 by Lin *et al.* as a starting material for conveniently synthesising pyrazolines.[76] It was not until a year later that it was presented as a possible bioorthogonal photoreactive group.[77] Under UV irradiation a nitrile imine dipole is formed that is very reactive towards alkenes and carboxylic acids. Although the reactivity is higher for alkenes, carboxylic acids are found in proteins and can therefore be targeted. The reaction of nitrile imine dipoles (formed from UV irradiation of tetrazoles) with carboxylic acids was shown in organic solvent in 1985 by Meier and Heimgartner, though it was only shown to work in physiological conditions in 2016.[59]

Tetrazoles have a unique photolabeling mechanism compared to the other three photoreactive groups mentioned. They show specific reactivity to Asp and Glu residues with reduced non-specific labelling.[58, 61] These decreased background reactions mean that tetrazoles show higher photo crosslinking yields.[58, 60]

Herne *et al.* and Guo *et al.* have both used 2-aryl-5-carboxytetrazole (ACT) in photoreactive probes.[58, 60] Herne *et al.* designed probes based on two drugs profiled extensively in the literature:[58] Dasatinib, an inhibitor of Bruton's tyrosine kinase (BTK) and JQ-1, an inhibitor of bromodomain proteins (**Figure 1.13**). The probes showed similar inhibitory activities as their parent compounds and

achieved 60% and 95% crosslink yield for the Dasatinib **1.37** and JQ-1 probe **1.38** respectively (measured by LC-MS). The Dasatinib probe was crosslinked to BTK, digested with trypsin and analysed by LC-MS/MS. A tripeptide was found linked to the probe via residue Glu-488, the only peptide labelled despite the protein containing 25 Glu and 14 Asp residues. Guo *et al.* designed a probe based on the natural product betulinic acid **1.39** (**Figure 1.13**) that shows a broad spectrum of biological activities but whose cellular targets are unknown. Using the ACT probe, the authors managed to find 9 protein targets of betulinic acid.

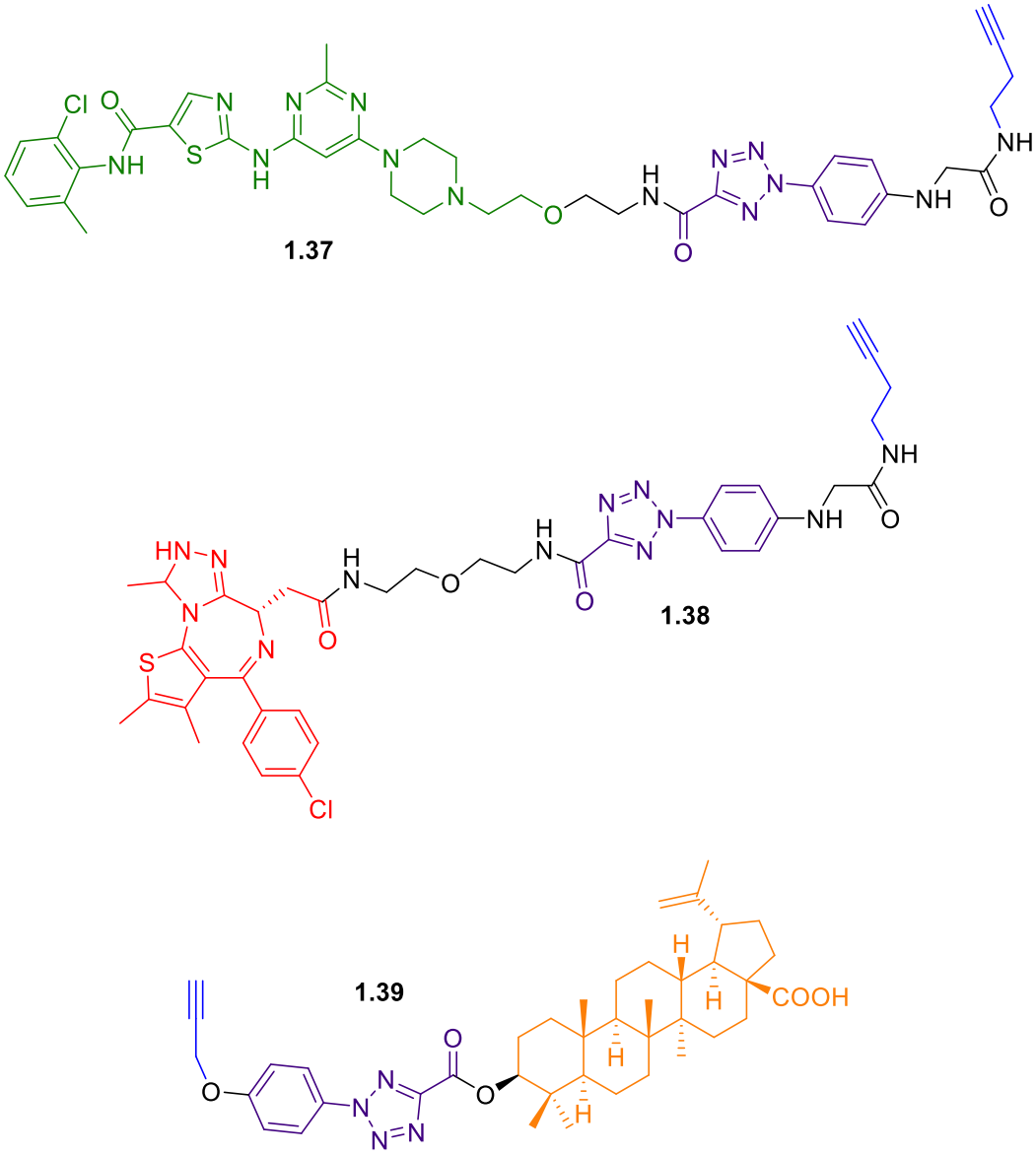

Figure 1.13: Structure of Dasatinib (green) probe **1.37**, JQ-1 (red) probe **1.38** and betulinic acid (orange) probe **1.39**; ACT (purple), alkyne tag (blue).

Cheng *et al.* have shown that substituents other than the phenyl ring on the tetrazole have slower rates of photolysis (analysed by LC-MS) and significantly weaker labelling (tested on bovine serum albumin).[61] Bach *et al.* have used tetrazoles to target Asp and Glu residues in the bacterial proteome, which make up ~12% of all residues.[62] Currently most of the covalent inhibitors used to target bacteria are cysteine-directed, a problem because of the low prevalence of Cys residues (0.6% of all residues in *Staphylococcus aureus*) meaning many binding pockets will not be detected. The authors synthesise a tetrazole probe to target living *Staphylococcus aureus* cells and are able to monitor ~4000 Asp and Glu residues.[62] This is the first time this has been performed in living bacterial cells and the authors hope that this will help the design of new covalent inhibitors for antibiotics.

1.5.2 Click Chemistry

One way to visualise how a probe is binding to a protein is to attach a detectable tag to the probe. This is sometimes installed following binding of the probe to the target protein, employing a bioorthogonal tag, for example an alkyne tag, in a bioorthogonal reaction.

Selective chemical reactions that elicit no change to the functionality of biological systems are termed bioorthogonal reactions.[78, 79] These particular reactions have become significant in chemical biology and proceed without interfering/interacting with biological systems, whilst being stable under normal biological conditions.[80, 81] With the development of bioorthogonal reactions, tagging methods have allowed the attachment of functional groups (FGs) to proteins and the facilitation of selective incorporation of unnatural amino acids (containing bioorthogonal FGs) into proteins in bacteria.[79] Therefore, despite the challenging requirements, a number of reactions have been developed that show biocompatibility and selectivity in biological systems: click chemistry is an important group of these reactions.

Click chemistry was first described by Kolb, Finn and Sharpless in 2001; and is defined as the generation of a substance by the joining of two small building

blocks together with heteroatom links.[82, 83] For a reaction to be termed as click chemistry, as defined by Sharpless *et al.*, it must meet several criteria: the reaction must be tolerant of different FG, it must produce stereospecific products in high yields and generate only harmless by-products.[83] The reactions have simple conditions and require no solvent or an inert solvent. The starting materials and reagents must be readily available and the final product should be easily isolated. Click chemistry reactions often achieve these criteria through high thermodynamic driving forces, and therefore rapidly produce the product.

1.5.2.1 Cu^{I}-Catalysed Azide/Alkyne Cycloaddition

The Cu^{I}-catalysed azide/alkyne cycloaddition (CuAAC) is the most widely used click reaction.[83] In 2002, the Fokin,[84] Sharpless[85] and Meldal[86] research groups all individually reported the efficient Cu^{I} catalysis of azide/alkyne cycloadditions.[79, 82] The non-catalysed azide/alkyne cycloaddition, first discovered by Michael in the 1890's but studied in detail by Huisgen in the late 1900's, is known as the Huisgen 1,3-dipolar cycloaddition.[80, 82] This non-catalysed reaction produces a mixture of 1,5- **1.40** and 1,4-disubstitution **1.41** products, and requires high temperatures and pressures not compatible with biological systems (**Scheme 1.7, A**).[82] The introduction of a copper catalyst forms the 1,4-isomer **1.41** selectively, can be accomplished at atmospheric pressure and does not require high temperatures (**Scheme 1.7, B**).

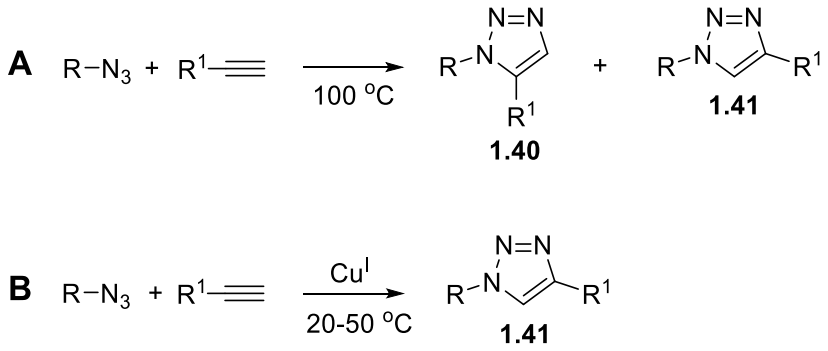

Scheme 1.7: Huisgen cycloaddition (A) and CuAAC (B).

Following this, the CuAAC reaction became very popular as a widely applicable reaction that is easy to carry out. It has been shown to be unaffected by a range

of FGs and solvents, and has been achieved with many different Cu^{I} catalysts.[82] The copper catalyst lowers the activation barrier for the cycloaddition by changing its mechanism, and greatly increases the rate of the transformation.[80] The copper catalysis increases the rate by seven orders of magnitude compared with the Huisgen reaction[79] and is also faster than the Staudinger ligation.[81]

A wide range of copper catalysts can be used for the CuAAC reaction, with the requirement that Cu^{I} species are produced.[82] The mechanism of the CuAAC reaction has been investigated by Finn *et al.* extensively using kinetic studies and DFT calculations.[87] A mechanism in which both the azide and alkyne are coordinated to the same copper centre, with the alkyne also coordinated to a second **1.43**, has been proposed most recently (**Scheme 1.8**).[88]

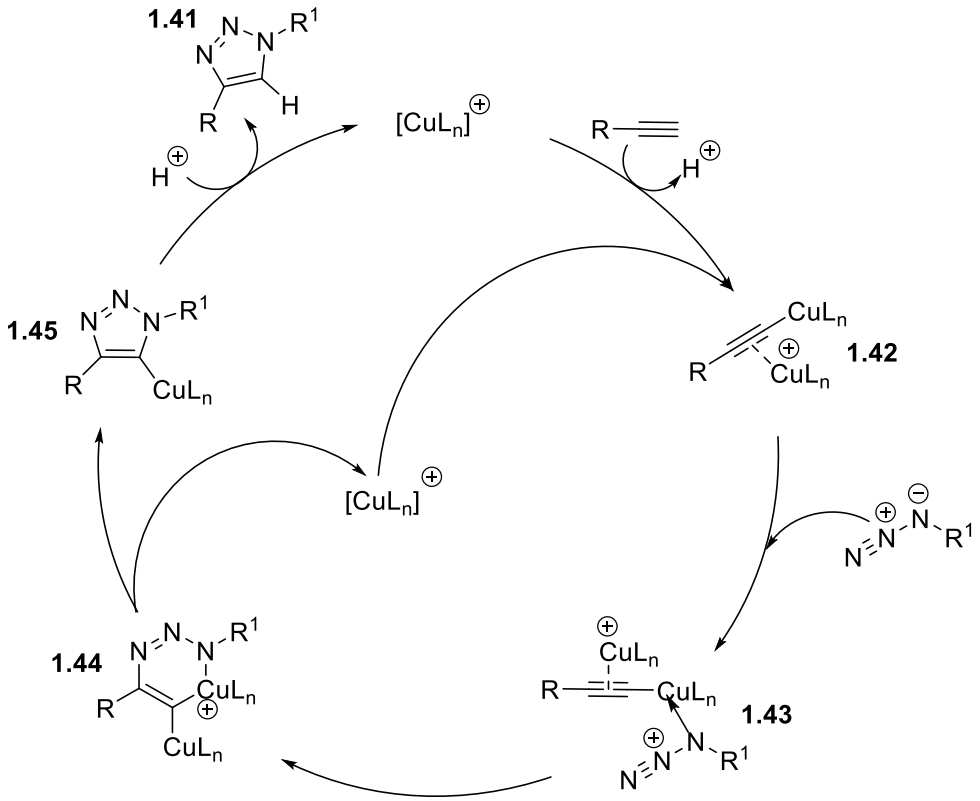

Scheme 1.8: Catalytic mechanism for CuAAC[41].

It has been shown that the success of the CuAAC reaction is linked to the solubility of substrates.[82] Nevertheless, a variety of solvents can be used for the reaction. The CuAAC is successful in non-coordinating, weakly coordinating, polar and aqueous solvents. Indeed, it seems that the CuAAC is solvent

independent. The CuAAC reaction is employed in many fields of study, including chemical biology, polymer chemistry, organic synthesis and materials.[82]

However, despite the many advantages of the elegant CuAAC, it cannot strictly be termed a true bioorthogonal reaction due to the presence of the cytotoxic Cu^{I} catalyst.[78-81]

1.5.3 Mass Spectrometry for Proteomics

Mass spectrometry is an integral part of proteomics. For this reason the technological advances have been huge, including the development of high-resolution mass spectrometry.

There are two main strategies for mass spectrometry for proteomics: top-down and bottom-up (**Figure 1.14**). Top-down proteomics is the analysis of the whole protein, whilst bottom-up proteomics is the analysis of peptides produced from the enzymatic/chemical fragmentation of the protein.[89, 90] In top-down proteomics, the protein of interest is isolated by most commonly 2D SDS-PAGE. The proteins are first separated by isoelectric point and then by their molecular mass. Although 2D SDS-PAGE has excellent resolving power, it has low sensitivity and accuracy causing more groups to change to using HPLC. The isolated protein is then ionised by electrospray ionisation (ESI) and subsequently fragmented in the mass spectrometer. This top-down approach can allow a complete characterisation of protein isoforms and post-translational modifications.[89, 90]

Bottom-up proteomics is more popular than top-down proteomics and can be used for the identification of proteins. There are two work-flows used for bottom-up proteomics: the “sort-then-break” approach first isolates the protein of interest, before digesting into peptide fragments.[90] These peptide fragments can then be analysed by “peptide mass fingerprinting”. The “break-then-sort” approach digests the mixture of proteins without any separation.[90] The mixture of peptides is than separated by multi-dimensional chromatography and analysed by tandem mass spectrometry. For both these approaches, the peptides are ionised by either ESI or matrix-assisted laser desorption/ionisation (MALDI). Trypsin is the most common proteolytic enzyme for digestion in bottom-up proteomics.

However, digestion with trypsin can be poor for hydrophobic regions, especially transmembrane proteins, and often not all tryptic peptides are detected by the mass spectrometer. The “break-then-sort” approach is often known as shotgun proteomics and is very popular. It has been used to analyse cell lysates and tissues extracts.[90] However, due to the complex mixture of peptides generated, high sensitivity and effective separation are needed and often even with this, peptides in low abundance are not detected.

In addition to the two main strategies for mass spectrometry for proteomics, a third has emerged known as middle-down proteomics.[90, 91] In this approach the protein of interest is isolated from the protein mixture and partially digested. This results in peptides longer than 20-25 amino acids (bottom-up results in peptides 7-20 amino acids long) leading to fewer peptides in the sample and less complexity.[91] This can enhance sequence coverage of the protein as there is a higher probability of detecting unique peptides.

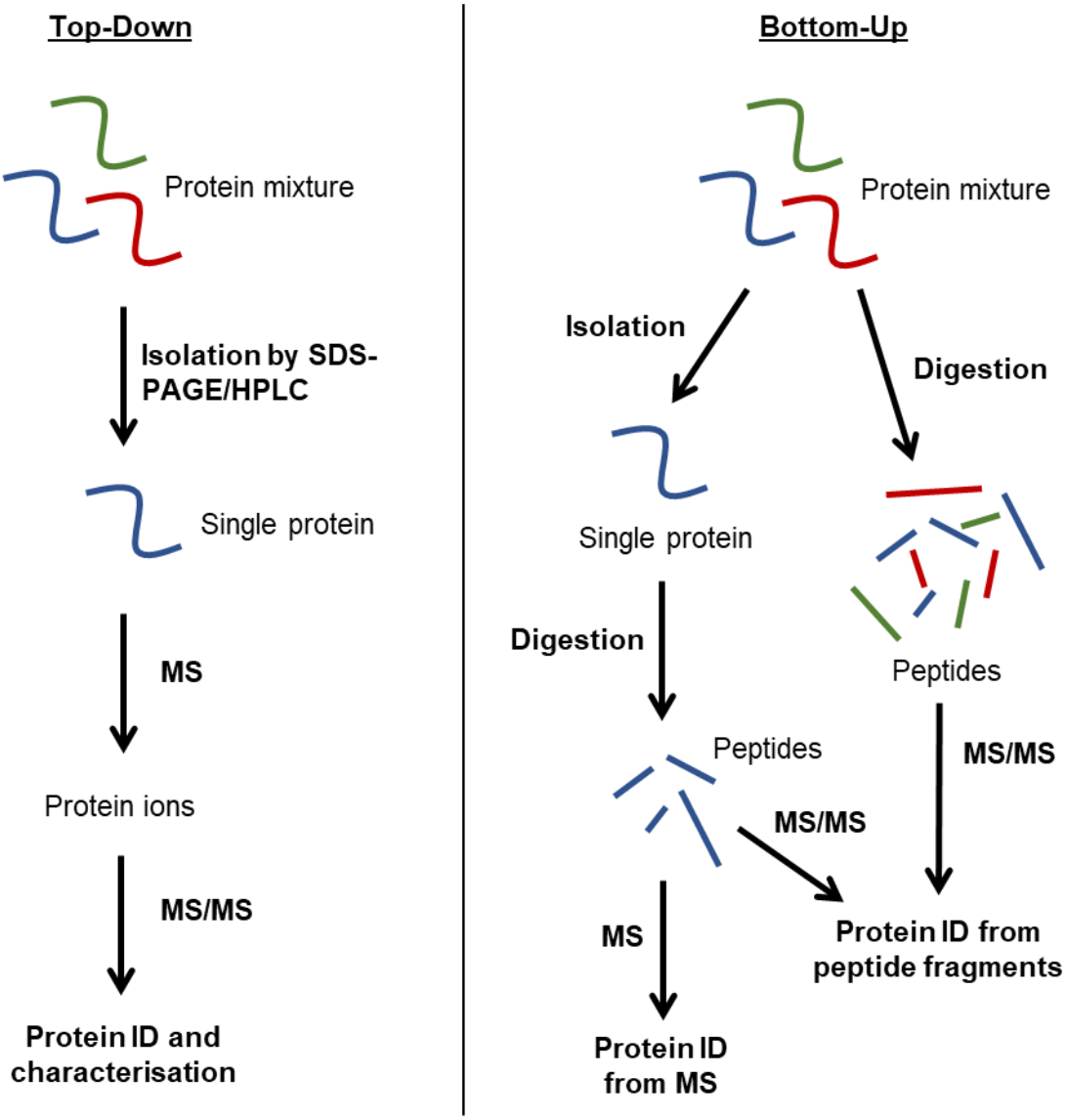

Figure 1.14: Top-down and bottom-up proteomics

1.6 Photoaffinity Probes for GPCRs

1.6.1 Photoaffinity Labelling to Target the Formyl Peptide Receptor

During the 1980's and 1990's several research groups targeted the formyl peptide receptor using photoaffinity labelling.[92-106] The three different formyl peptide receptors are not referred to in these papers; it is unclear whether they are all targeting FPR1 or a mixture of the three FPRs. Niedel *et al.* were the first to attempt the photoaffinity labelling of FPR using a synthetic formyl peptide

containing an azido nitrophenyl as the photoreactive crosslinker **1.46** (**Figure 1.15**).[92] The peptide also contained iodine-125 for detection. Using membranes from human neutrophils the authors were able to crosslink to a protein appearing as a broad band between 55-70 kDa on SDS-PAGE. The chemical nature of this band was unknown, and it was believed to be FPR. Following from this publication there was a series of reports performing photoaffinity labelling to FPR with the hope of interpreting the structure, the precise molecular weight and the formyl peptide binding site. Through the 1980's FPR is continuously described as a 55-70 kDa polypeptide with few discoveries about its structure and function. In 1983 Dolmatch *et al.* perform digestion experiments on FPR to predict that the receptor spans the membrane,[96] and in 1984 Anderson *et al.* expanded on this to present the internalisation of FPR following formyl peptide binding.[97] In 1986 Allen *et al.* performed studies on small peptides, concluding that FPR interacted with ligands similar in size to tetrapeptides.[94] By the end of the 1980's, a deglycosylated form of the receptor with a molecular weight of 38 kDa had been shown to bind to formyl peptides,[98] and from experiments with GTPγS it was thought that FPR resulted from association with G-proteins.[99] There was little change to the structure of photoreactive probes, with the photoreactive group always incorporated into the probe structure via a lysine residue side chain (**Figure 1.15**). The probe designed and synthesised in 1986 by Allen *et al.* with the structure fMLFK(SASD)[94] **1.48** was continually used through to the late 1990's after it was seen to have higher crosslinking efficiency.

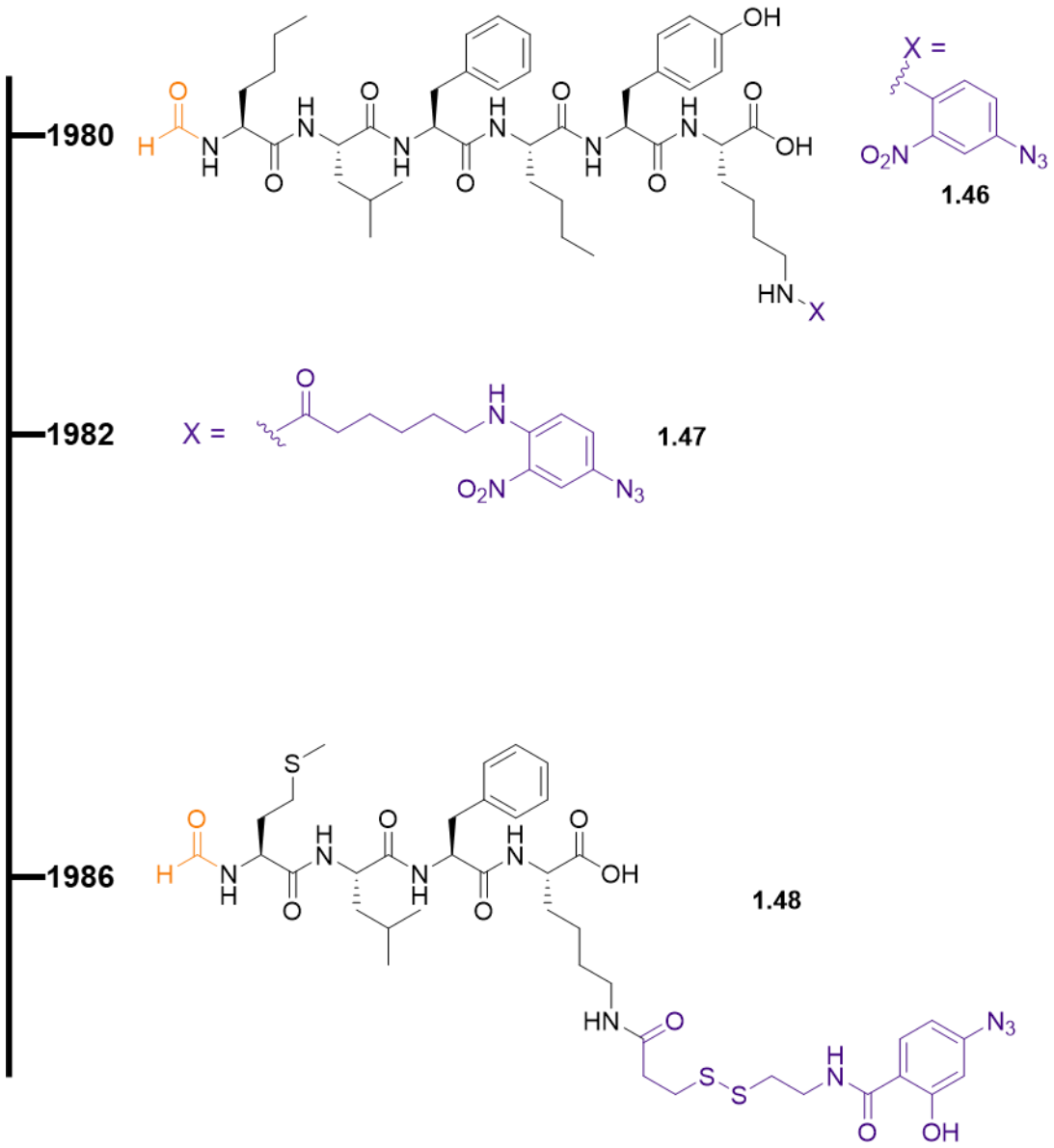

Figure 1.15: Timeline of photoaffinity probe structure used to target FPR

As the 1990's began the photoaffinity labelling of FPR became focused on researching the two affinity states seemingly exhibited by FPR, that were first described by Jesaitis *et al.* in 1989.[99] FPR was found to have two forms with different sedimentation coefficients, and the proportion of these forms could be influenced with the presence of G proteins.[101, 102] The form with a higher sedimentation coefficient was thought to be the complex of FPR with G protein that exhibited a higher binding affinity towards formyl peptides. The second form was a lower affinity state. Although substantial research was undertaken about the forms of FPR no solid conclusion was reached about why they are observed

and the significance behind this, and no further papers were published exploring this work. In 1998, Vilven *et al.* performed extensive research into the diversity of formyl peptides binding FPR.[104] They tested the binding of a range of peptides (varying length and position of photoreactive group) (**Figure 1.16**) with isolated human neutrophils using flow cytometry. The research showed that a fluorescent group placed 2-7 amino acids away from the formyl group was well tolerated and affinity of the peptide improved if the lysine residue was placed further away from the formyl group.[104] Hydrophobic alterations were well tolerated and photoreactive groups could be incorporated. Vilven *et al.* were also the first group to place a photoreactive group (benzophenone) as an unnatural amino acid and show successful labelling of FPR, with similar activity observed as the aryl azide probes.[104]

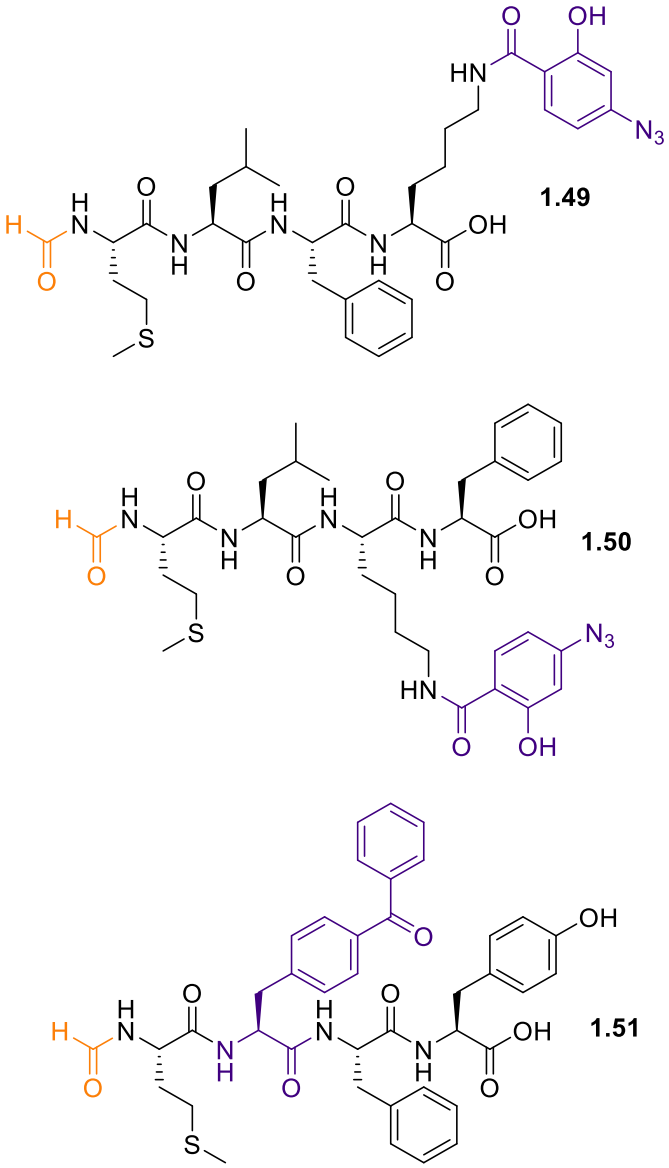

Figure 1.16: Structures of photoreactive formyl peptides to target FPR published by Vilven *et al.*[104]

To conclude the FPR photoaffinity journey a paper was published identifying the ligand binding site of FPR using site-specific photoaffinity labelling.[105] Mills *et al.* synthesised a novel formyl peptide **1.52** to target FPR, containing the photoreactive benzophenone and the fluorescent group fluorescein (**Figure 1.17**). **1.52** showed higher activation of FPR than fMLF, showing enhanced GTPγS binding to FPR-expressing CHO cells and a calculated EC_{50} of 3 nM compared to 6 nM for fMLF in the same assay.[105] Upon UV irradiation, **1.52** specifically crosslinked to the receptor.[105] The crosslinking was performed on CHO membranes with expressed FPR, with the receptor cleaved using cyanogen

bromide (which hydrolyses at the C-terminus of methionine residues) following irradiation. From the limited mass spectrometry experiments they performed; they present that **1.52** is crosslinked to residues 83-85 and using this they model the binding of the probe to an FPR model generated from a rhodopsin template.[105] However, FPR has a low sequence similarity to the rhodopsin receptor (20%)[23] meaning the accuracy of the modelling is questionable. Following this paper, no further work was published on identifying the binding site of FPR and there has been no additional research using photoreactive probes to label FPR.

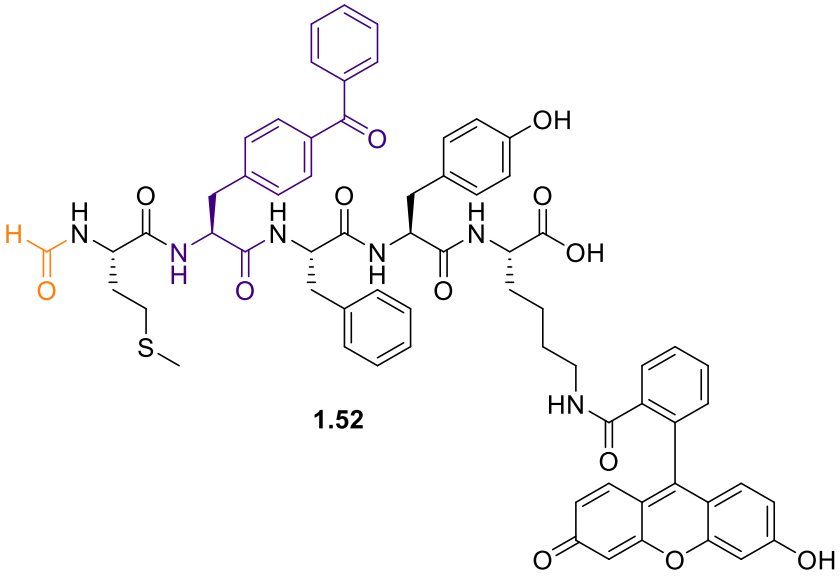

1.52

Figure 1.17: Structure of 1998 FPR probe containing benzophenone and fluorescein[105]

1.6.2 Recent Literature Reports of Diazirine Probes to Target GPCRs

In the past five years there has been a wide range of research on the photoaffinity labelling of GPCRs, with many publications presenting photoreactive probes to target the receptors. In 2017, Muranaka *et al.* released a paper utilising a probe containing the trifluoromethylphenyl diazirine photoreactive group **1.53** (**Figure 1.18**)[107] for the human A_{2A} adenosine receptor, whose antagonism has shown to be a promising treatment for neurodegenerative conditions.[107] Small molecule antagonists of the A_{2A} adenosine receptor were developed into photoaffinity probes. The authors were able to crosslink to their target receptor and locate the position of the crosslink using tandem mass spectrometry of the digested

receptor. Muranaka *et al.* found that **1.53** was most likely crosslinked to tyrosine271 in the 7th transmembrane domain. In addition to this, they performed docking studies which showed the diazirine group in close proximity to tyrosine271.[107] This is the first photoaffinity labelling performed on the A_{2A} adenosine receptor to locate the crosslinked amino acid by mass spectrometry (performed with isolated receptor, not on live cells).

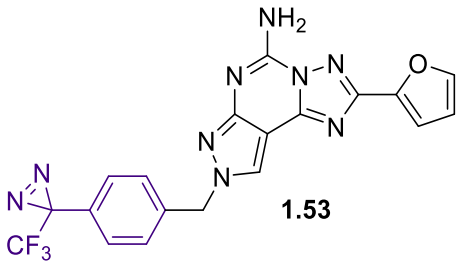

1.53

Figure 1.18: Structure of photoaffinity probe to target the A_{2A} adenosine receptor.[107]

Soethoudt *et al.* studied the type 2 cannabinoid receptor (CB_2R) which plays an important role in the migration and immunosuppression of our cells.[108] In order to develop drugs that target this receptor, its molecular and cellular mechanism needs to be understood. This can be hard for GPCRs given the low levels of expression in cells. Therefore, the authors developed a small molecule probe (LEI121) **1.54** containing a trifluoromethylphenyl diazirine and alkyne tag (**Figure 1.19**).[108] The affinity of LEI121 was determined in a competition experiment with a known ligand using membrane fractions over-expressing CB_2R. Soethoudt *et al.* reported a pK_i of 7.2 for LEI121 and also defined the probe as an inverse agonist to CB_2R.[108] The authors performed 2-step A*f*BPP with LEI121 using click chemistry to introduce Cy5-N3 as the fluorescent azide for in-gel fluorescence analysis, or AlexaFluor647-N3 for flow cytometry analysis. This was performed on the membrane fractions (HL-60 cells were used for flow cytometry to study binding to endogenous CB_2R) and they observed two major labelled bands with SDS-PAGE corresponding to different glycosylated forms of the receptor. Further to this, in-gel digestion was performed followed by mass spectrometry analysis to confirm the glycosylation.[108] Interestingly, the authors also performed crosslinking with two additional probes, containing the diazirine in different locations. These probes showed significantly less labelling, displaying the importance of diazirine positioning in probes.

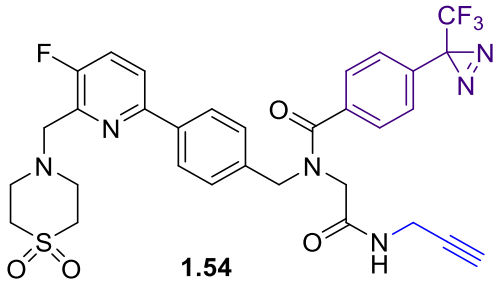

Figure 1.19: Structure of LEI121 photoaffinity probe to target CB_2R.

The increased research into photoaffinity labelling and A*f*BPP has led to groups investigating multifunctional probes. Müskens *et al.* designed a probe based on a trifunctional scaffold **1.55** (**Figure 1.20**) that could be used to target any GPCR.[109] **1.55** incorporates an NHS ester to allow attachment of the probe to a ligand, a diazirine group and a biotin tag for detection. To assess this trifunctional probe, they utilised the NK_1 receptor and its ligand substance P. **1.55** was coupled to the lysine residue in substance P and retained specific binding to NK_1 in live cells that was reduced 4- to 8-fold.[109] Müskens *et al.* used confocal microscopy to image NK_1, and use this to view binding of the probe with fluorescent streptavidin. Crosslinking of the probe to NK_1 is confirmed with a competition experiment and analysed by confocal microscopy and Western Blotting.[109] In addition to this, the group also achieved purification of the crosslinked receptor, and were able to show that only peptides present in NK_1 were crosslinked, confirming the specificity of **1.55**.

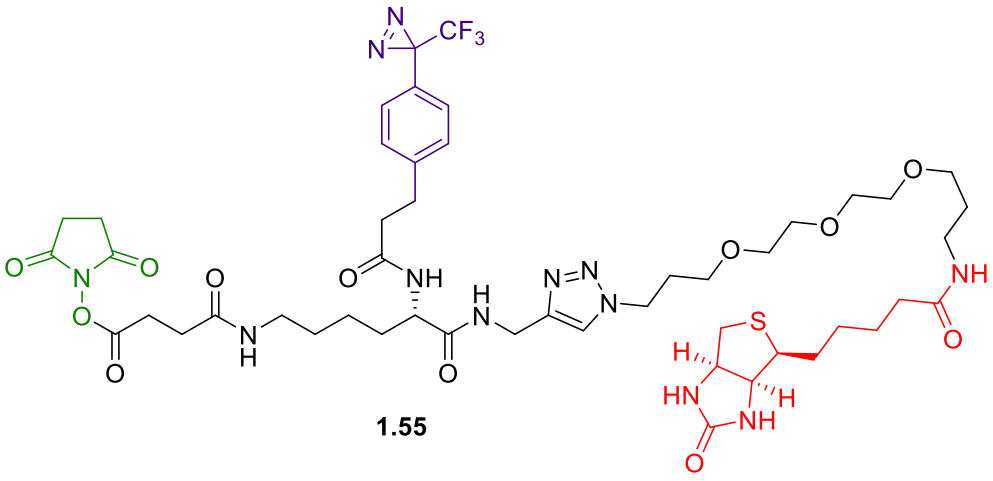

Figure 1.20: Structure of trifunctional scaffold for GPCR photoaffinity probe containing a 3-aryl-3-(trifluoromethyl)diazirine moiety (purple), an NHS ester (green) and a biotin tag (red).[109]

In 2020, Miyajima *et al.* created a tetrafunctional probe consisting of a ligand, the photoreactive group, a hydrazine cleavable linker and a biotin tag.[110] This probe utilised 2-aryl-5-carboxytetrazole (ACT) as the photoreactive group, though the group also designed two trifunctional probes containing diazirines **1.56** and **1.57** (**Figure 1.21**). Miyajima *et al.* were targeting the dopamine receptor D2 (DRD2) as a model receptor. The trifunctional probes contained a photoreactive group linked to a known DRD2 ligand and biotin tag. The authors successfully labelled DRD2 with this reagent, enriched the crosslinked complex using streptavidin beads and performed tandem mass spectrometry to identify crosslinked peptides.[110] This work was completed with seven trifunctional probes containing different photoreactive groups. The labelling efficiency of the diazirine probes was comparable to that of the ACT probes, though the ACT photoreactive group was taken forward due to lower off-target labelling.

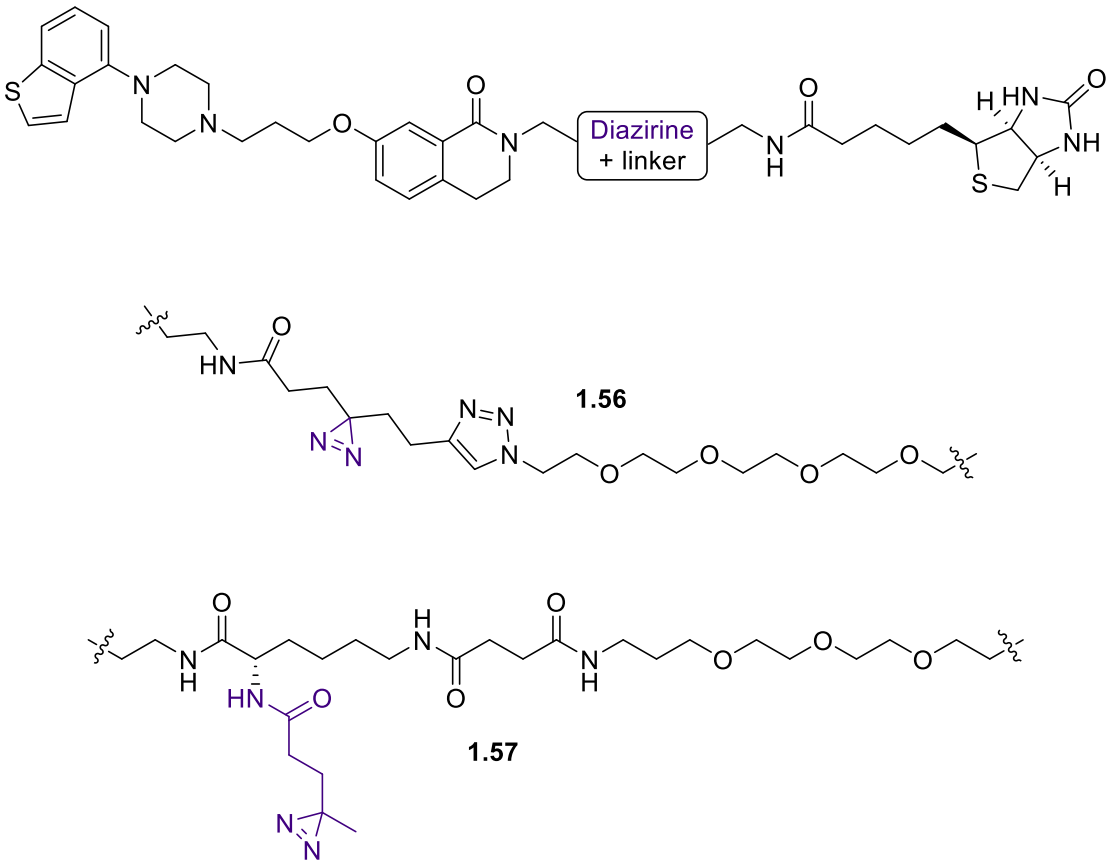

Figure 1.21: Structure of two trifunctional scaffolds synthesised by Miyajima *et al*.[110]

1.6.3 Conclusion

All published work on the PAL of FPR has utilised the benzophenone or phenylazide photoreactive group. In addition to this, most probes (all but one published by Vilven *et al.*) have had the photoreactive group installed on the side chain of an amino acid rather than incorporating an unnatural amino acid into the probe. This means there is a gap in the literature to explore photoreactive probes incorporating diazirines to label FPR. The PAL work published on FPR was mostly performed early-on in the FPR discovery and was used to identify the receptor and answer questions such as; was it a membrane protein, was is glycosylated, what was its molecular weight and what was its affinity state? Only one paper has performed A*f*BPP to locate the crosslink site and learn more about the FPR binding site.

The majority of recent reports of diazirine probes to label GPCRs have been small molecule probes or multi-functional probes. Compared with the PAL performed on FPR in the 80's and 90's, the crosslinking has improved and a lot more papers perform full A*f*BPP with MS of their target protein.

1.7 Project Aims

The overall aim of this project is to develop chemical probes which mimic the actions of bacterial formyl peptides that bind to FPR1 in order to study the interaction in cells and develop new tools to gain a greater understanding of FPR biology. A*f*BPP has become a popular strategy in chemical biology and can be very helpful with increasing our knowledge of protein binding sites, particularly when crystal structures are not available and the protein is difficult to crystalise (for example transmembrane proteins). At the start of this project there were no crystal structures published of any of the human FPRs and although there were many characterised ligands for FPR1 and FPR2, the exact mode of binding and key interactions were not known.

The project has three main aims:

- Design and synthesis of photoaffinity probes based on formyl peptide FPR1 ligands.
- Application of the probes to bind and label FPR1 in live cells.
- The use of proteomics to identify the crosslink site within the binding site of FPR1.

The following will give a brief description of the contents of each chapter.

Chapter 2: Synthesis of photoreactive groups. This chapter discusses the synthesis of three photoreactive diazirines.

Chapter 3: Preparation and use of first-generation photoreactive probes. This chapter presents the design and synthesis of the first-generation probes, incorporating photoreactive diazirines synthesised in chapter 2. The binding of these probes to FPR1 expressed on mammalian cells is tested using flow cytometry.

Chapter 4: Preparation and use of photoreactive probes containing detectable tags. This chapter explores the second-generation of probes to label FPR1, whose structure is based on the well-known fluorescent tracer that shows high binding affinity towards FPR1. The binding of these probes is investigated using a range of flow cytometry assays and the labelling of FPR1 is analysed using SDS-PAGE and Western Blotting.

Chapter 5: Immunoprecipitation and proteomics. This chapter builds on the previous chapter, whereby FPR1-probe complexes are isolated from cell lysate and proteomics of these complexes is attempted.

Chapter 2 Synthesis of Photoreactive Diazirines

2.1 Introduction

Photoreactive diazirines are typically used in crosslinking reactions to form a covalent bond to a protein of interest. Diazirines have been employed in this research due to their high stability towards many conditions,[53] and their highly reactive carbene intermediate which has a shorter half-life than the nitrene and diradical produced by phenylazides and benzophenones respectively.[50] This chapter outlines the different photoreactive diazirines that will be used to crosslink to FPR1 and their syntheses. 4,4-Azo-pentanoic acid **2.01** (to form photo-AcLys **2.02**), photo-Met **2.03** and photo-Leu **2.04** (**Figure 2.1**) were synthesised using methods published in literature.[111, 112] Photo-Met and photo-Leu were synthesised for incorporation into a chemical probe during solid-phase peptide synthesis (SPPS) using coupling conditions analogous to natural amino acids. 4,4-Azo-pentanoic acid was coupled to a lysine residue present in the peptide during SPPS.

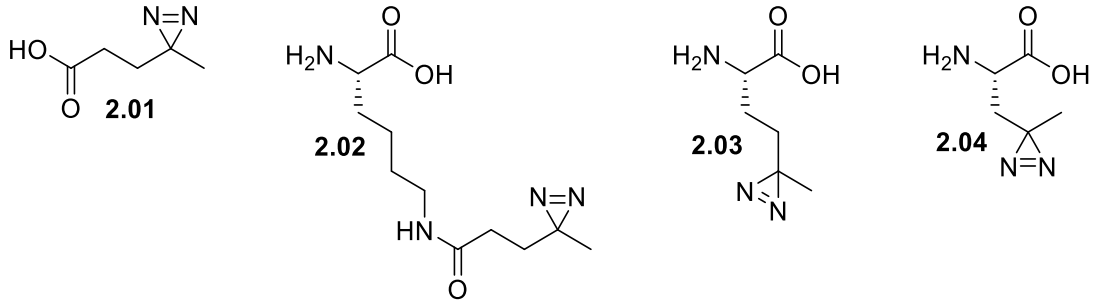

Figure 2.1: Structure of 4,4-Azo-pentanoic acid **2.01**,photo-AcLys **2.02**, photo-Met **2.03** and photo-Leu **2.04**.

2.2 Photoreactive Unnatural Amino Acids

Unnatural amino acids are non-proteinogenic amino acids and are sometimes chemically synthesised. Photo-Met and photo-Leu were designed in 2005 by

Thiele *et al.* and closely resemble the natural amino acids methionine and leucine respectively.[71] 4,4-Azo-pentanoic acid does not resemble an amino acid, but when coupled to a lysine residue becomes photo-AcLys which resembles an acetylated lysine. The incorporation of photo-Met or photo-Leu, instead of small aliphatic amino acids, keeps the structure of the peptide almost unaltered. The diazirines are stable to Fmoc peptide synthesis and cleavage from resin.[112] The following sections describe the synthesis of these photoreactive groups.

2.3 Synthesis of Photoreactive Groups

2.3.1 Synthesis of 4,4-Azo-pentanoic Acid

The formation of 4,4-azo-pentanoic acid was achieved in one synthetic step from the commercially available levulinic acid **2.05** (**Scheme 2.1**). The ketone is converted into a diaziridine **2.06** which is immediately oxidised to a diazirine **2.01**. Formation of the diaziridine moiety is challenging and yields are not consistent, therefore several synthetic methods were attempted using levulinic acid to optimise this reaction.[111, 112]

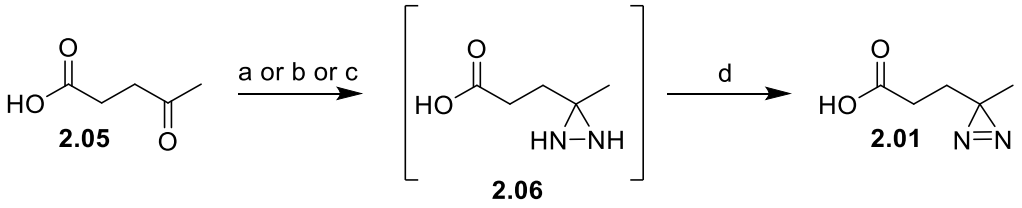

Reagents and conditions: *(a) MeOH, 7N methanolic ammonia, hydroxylamine-O-sulfonic acid, −10 °C;* ***<20%****; (b) MeOH, 7N methanolic ammonia, hydroxylamine-O-sulfonic acid, −10 °C, balloon of gaseous ammonia;* ***28%****; (c) liquid ammonia, hydroxylamine-O-sulfonic acid; (d) MeOH,* Et_3N*, iodine, 0 °C;* ***43%****.*

Scheme 2.1: Formation of 4,4-azo-pentanoic acid **2.01**

Method (a), using 7N methanolic ammonia to form the diaziridine was attempted first.[111] However, this gave yields of less than 20%. It was hypothesised that this was due to the ammonia environment not being maintained. Therefore, this method was repeated with the addition of a balloon filled with ammonia gas (method (b)). This gave a slight increase in yield to 28%. Finally, method (c) was explored in which the levulinic acid was dissolved directly in liquid ammonia,

condensed from ammonia gas using a dry-ice and acetone condenser.[112] A 10% sodium thiosulphate wash was also included in the work-up after reaction completion – this removed any iodine from the crude product. This method gave the highest yield of 43% and was therefore used for all future diazirine formations.

2.3.2 Synthesis of Fmoc-photo-Met

In order to incorporate photo-Met into a peptide Fmoc-photo-Met was synthesised. The synthetic route starting from commercially available L-glutamic acid has been previously published.[112]

2.3.2.1 Synthesis of Boc-Glu(OH)-O^{t}Bu

The first four steps in the synthetic route to Fmoc-photo-Met involved manipulation of protecting groups (**Scheme 2.2**). The first step, selective methylation of one carboxylic acid functional group using trimethylsilyl chloride (TMSCl) in methanol, proceeded as the literature suggested and generated the first product in 98% yield. Following the formation of **2.08**, the primary amine was protected using a *tert*-butyloxycarbonyl (Boc) group. This was achieved using Boc anhydride and sodium hydrogen carbonate, a common strategy for a Boc protection which can be performed in either aqueous or anhydrous conditions. This gave an efficient conversion to **2.09** in 76%. The Boc group is orthogonal to the methyl ester and therefore is not hydrolysed under basic conditions.

The second acid moiety was protected with a ^{t}Bu group, also orthogonal to the methyl ester. This protection was achieved using the Steglich Esterification, a reaction designed by Steglich and Neises involving the addition of DMAP to catalyse the reaction.[113] The Steglich Esterification is performed under mild conditions and at room temperature, providing a facile reaction. After purification Boc-Glu(OMe)-O^{t}Bu **2.10** was afforded in 76% yield.

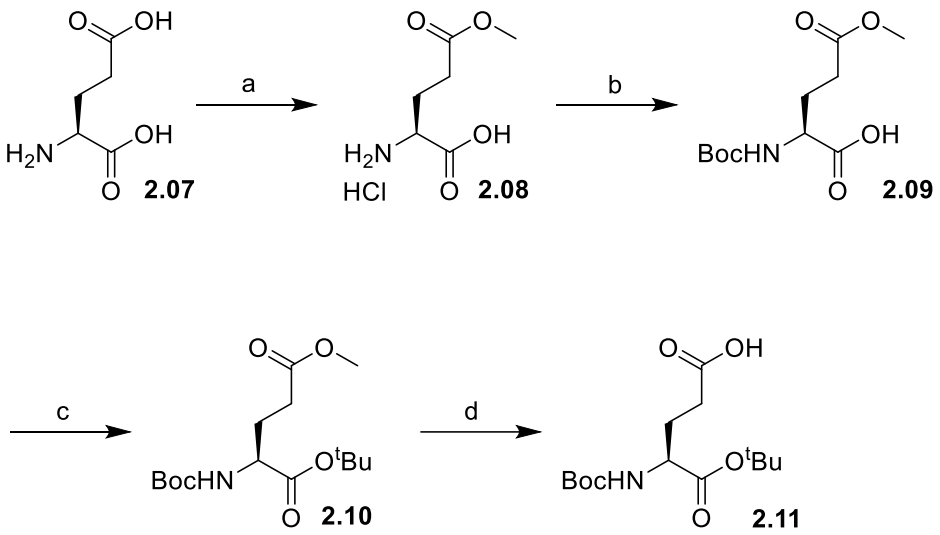

Reagents and conditions: *(a) TMSCl, MeOH,* ***98%****; (b)* Boc_2O*,* $NaHCO_3$*, dioxane:water (2:1), 0 °C,* ***76%****; (c) DCC, DMAP,* ^tBuOH*, DCM,* ***76%****; (d)* $LiOH_{(aq)}$*, THF,* ***96%****.*

Scheme 2.2: Synthesis of Boc-Glu(OH)-O^{t}Bu

The ester hydrolysis to form **2.11** was performed overnight and appeared pure via ^{1}H and ^{13}C NMR spectroscopy, High Resolution Mass Spectrometry (HRMS) and Infrared (IR) spectroscopy without the need for purification. However, failure to achieve a yield above 20% in the following synthetic step - preparation of the Weinreb amide **2.12** - through multiple conditions, suggested the product was not pure. Analysis of a spectrum obtained from Liquid Chromatography-Mass Spectrometry (LC-MS) revealed that during the reaction there had also been partial cleavage of the ^{t}Bu group. This by-product was removed by column chromatography and following this, the Weinreb amide was isolated in 84% yield. It was hypothesised that the cleavage of the ^{t}Bu group could be occurring during the work-up of the reaction in which 0.1 M HCl is used to acidify the solution to pH 3. Therefore, the work-up method was altered to acidify the solution to pH 5. Following this Boc-Glu(OH)-O^{t}Bu **2.11** was isolated in 96% yield and purification via column chromatography was not necessary.

2.3.2.2 Synthesis of Ketone via Weinreb Amide

The ketone precursor **2.13** to the diazirine was synthesised via the Weinreb Amide **2.12** (**Scheme 2.3**). In 1981, Weinreb and Nahm discovered that converting the carboxylic acid derivative to an *N*-methoxy-*N*-methylamide, now known as a

Weinreb Amide, allowed efficient formation of the ketone equivalent.[114] The formation of **2.12** using isobutyl chloroformate and *N*-methylmorpholine proceeded in 84% yield. **2.13** was subsequently formed in a facile Grignard reaction, achieving 64% yield.

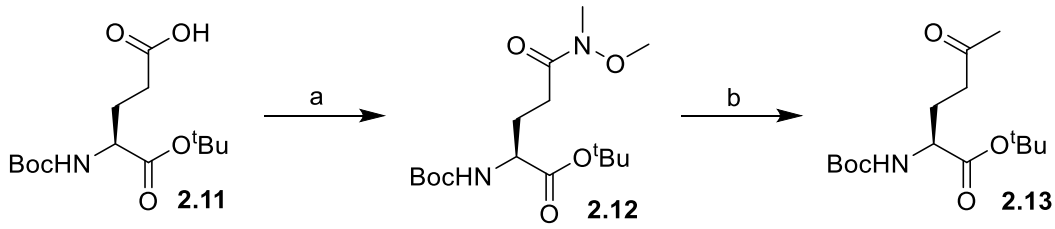

Reagents and conditions: *(a) i) N-methylmorpholine, isobutyl chloroformate, DCM, 0 °C; ii) N,O-dimethylhydroxylamine hydrochloride, DCM, 0 °C,* ***84%****; (b) 3M MeMgBr, toluene, −78 °C,* ***64%****.*

Scheme 2.3: Formation of ketone via Weinreb amide

2.3.2.3 Diazirine Formation and Fmoc-protection

The optimised protocol outlined in section 2.3.1 was used to synthesise the diazirine **2.14** in a 94% yield (**Scheme 2.4**), whereas using the solution of 7N ammonia in methanol gave a yield of 23%. The use of liquid ammonia and the addition of a 10% sodium thiosulphate wash during the work-up yielded a sufficiently pure product (determine using NMR spectroscopy and mass spectrometry) and no further purification was required.

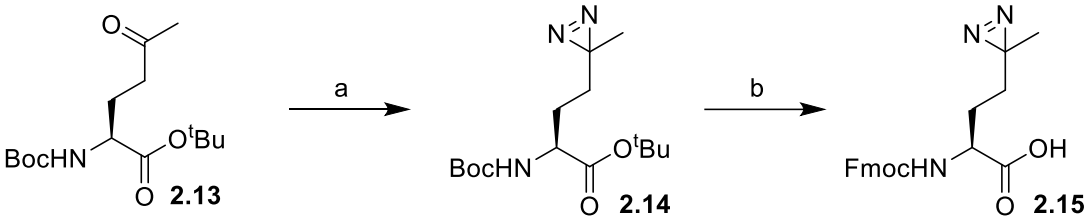

Reagents and conditions: *(a) i) liquid ammonia, hydroxylamine-O-sulfonic acid; ii) MeOH, Et_3N, iodine, 0 °C,* ***94%****; (b) i) THF:4M HCl (1:1); ii) FmocOSu, $NaHCO_3$, water:dioxane (1:1),* ***73%*** *over 2 steps.*

Scheme 2.4: Formation of diazirine and conversion of PGs to yield Fmoc-photoMet

Deprotection of the Boc and ^{t}Bu protecting groups can be achieved using 4M HCl. Following evaporation of the solvent *in vacuo* the amine was immediately protected with an Fmoc group using basic conditions. A higher equivalence of

base was required than recommended in literature due to remaining HCl. The product was obtained in 73% yield as a white solid after purification by column chromatography. This Fmoc-photo-Met **2.15** can be incorporated into a peptide using solid-phase peptide synthesis.

2.3.3 Synthesis of Fmoc-photo-Leu

The synthesis of Fmoc-photo-Leu has been published and begins from the commercially available malonic acid and *N*-Boc-L-aspartic acid methyl ester. [112] Initially this route was attempted, but problems were encountered with the diazirine synthesis.

2.3.3.1 Initial Synthetic Route to Fmoc-photo-Leu

The synthesis of photo-Leu begins differently to photo-Met with a single benzyl protection of malonic acid **2.16** (**Scheme 2.5**). This was achieved using one equivalent of benzylbromide to produce monobenzyl malonate **2.17** in 56% yield, without the need for purification. Following benzyl protection, **2.17** was coupled to *N*-Boc-L-aspartic acid methyl ester. Both reactants were first activated separately before being coupled. *N*-Boc-L-aspartic acid methyl ester was activated with CDI forming an acylimidazole. Monobenzyl malonate was reacted with isopropylmagnesium chloride, creating a reactive enolate. The two activated components were then coupled together in a C-C bond forming reaction to prepare **2.18**. This reaction proceeded as described in literature,[112] providing a yield of 60%. A palladium catalysed hydrogenolysis was subsequently employed to remove the benzyl protecting group, followed with a decarboxylation using triethylamine to give **2.19** in 73% yield.

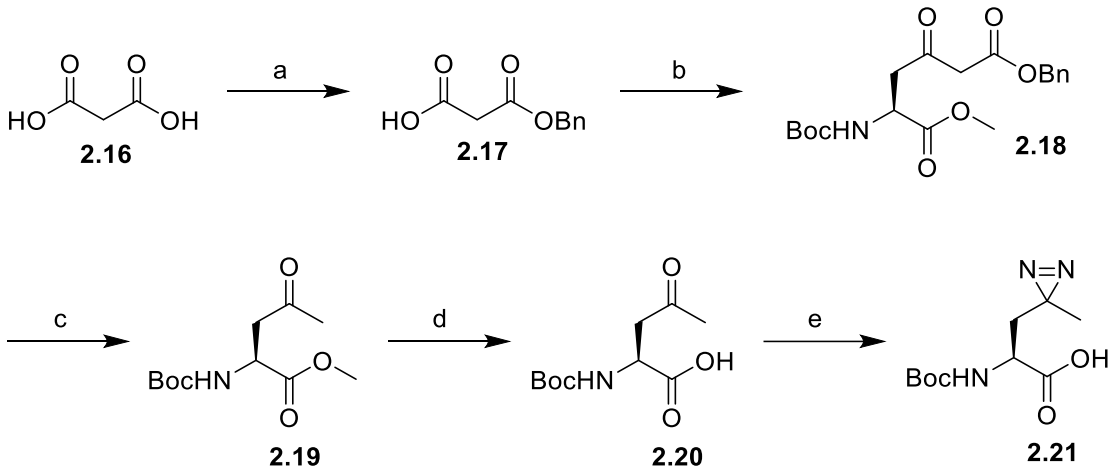

Reagents and conditions: *(a) BnBr, NEt_3, MeCN,* ***56%****; (b) i) isopropylmagnesium chloride, THF, 0 °C; ii) N-Boc-L-aspartic acid methyl ester, CDI, THF; iii) 0 °C;* ***60%****; (c) i) Pd/C, H_2, MeOH; ii) NEt_3, MeOH, reflux, 3 hr;* ***73%****; (d) 1M LiOH, THF,* ***90%****; (e) i) NH_3, hydroxylamine-O-sulfonic acid, –10 °C; ii) MeOH, Et_3N, iodine, 0 °C,* ***<5%****.*

Scheme 2.5: Initial synthetic route to Boc-photo-Leu **2.21**

The final synthetic steps are identical to those in the Fmoc-photo-Met synthesis, starting with the methyl ester hydrolysis in basic conditions. No problems were met with this reaction and **2.20** was formed in 90% yield without the need for further purification. However, all three methods used for the optimisation of the diazirine synthesis were unsuccessful, generating an impure product and a yield of <5% after purification.

2.3.3.2 A Solution to Improve the Diazirine Formation

As a high yield had been obtained for the diazirine synthesis in the route to Fmoc-photo-Met, it was hypothesised that the unprotected carboxylic acid was hindering the diazirine formation in the photo-Leu synthesis. To investigate this, the acid was protected using a ^{t}Bu moiety as outlined in the synthesis of Fmoc-photo-Met (**Scheme 2.6**).

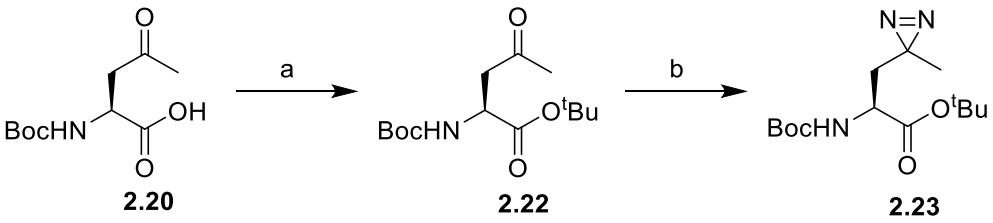

Reagents and conditions: *(a) DCC, DMAP, ^{t}BuOH, DCM, 0 °C,* ***43%****; (b) i) NH_3, hydroxylamine-O-sulfonic acid, –10 °C; ii) MeOH, Et_3N, iodine, 0 °C;* ***42%****.*

Scheme 2.6: *t*-Bu Protection to improve Fmoc-photo-Leu synthesis

Following the protection of the carboxylic acid, the synthesis of the diazirine **2.23** was repeated. Purification of **2.23** was still required, but the yield increased to 42%. Yuichi *et al.* have also previously used **2.22** as the ketone precursor for the diazirine reaction reporting a similar yield of 35%.[115] The addition of the ^{t}Bu protecting group decreased the polarity of the product making the silica column purification more facile as it was eluted first. Therefore, an alternative synthetic route to Fmoc-photo-Leu was proposed, coupling the commercially available *N*-Boc-L-aspartic acid *tert*-butyl ester instead of the methyl ester to the monobenzyl malonic acid.

2.3.3.3 New Synthetic Route to Fmoc-photo-Leu

The synthesis of Fmoc-photo-Leu was completed using the same methods as previously, with the commercially available starting material *N*-Boc-L-aspartic acid tert-butyl ester **2.24** (**Scheme 2.7**). The coupling reaction and palladium hydrogenolysis were not affected by the alternative starting material, and in fact higher yields were achieved for these reactions than before. The Boc and ^{t}Bu deprotection was achieved using 80% TFA in DCM and the amine was re-protected with Fmoc using the same conditions as for Fmoc-photo-Met. Similar to Fmoc-photo-Met, a greater base equivalence was required for the Fmoc protection due to the presence of residual TFA. Fmoc-photo-Leu **2.26** was produced in 59% yield as a white solid.

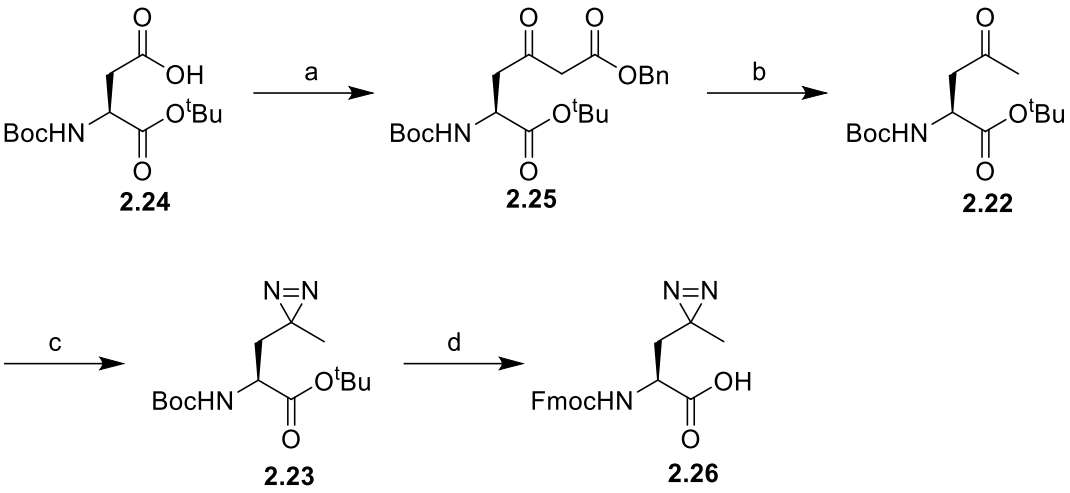

Reagents and conditions: *(a) i) CDI, THF; ii) monobenzyl malonate, isopropylmagnesium chloride, THF, 0 °C; iii) 0 °C;* ***61%****; (b) i) Pd/C, H_2, MeOH; ii) NEt_3, MeOH, reflux, 3 hr;* ***83%****; (c) i) NH_3, hydroxylamine-O-sulfonic acid, –10 °C; ii) MeOH, Et_3N, iodine, 0 °C;* ***42%****; (d) i) 80% TFA in DCM (1:1); ii) FmocOSu, $NaHCO_3$, water:dioxane (1:1),* ***59%*** *over 2 steps.*

Scheme 2.7: Alternative synthetic route to Fmoc-photo-Leu **2.26**

2.4 Conclusion

In this chapter the syntheses of 4,4-azo-pentanoic acid, Fmoc-photo-Met and Fmoc-photo-Leu have been discussed. Optimisation of the diazirine formation for 4,4-azo-pentanoic acid, Fmoc-photo-Met and Fmoc-photo-Leu was accomplished, utilising the condensation of ammonia gas directly onto the ketone starting materials. The highest yield for the synthesis of 4,4-azo-pentanoic acid was 43% using this improved method. The overall yield for the synthesis of Fmoc-photo-Met was 20% and the overall yield for the synthesis of Fmoc-photo-Leu was 7%. The full characterisation of these compounds and their synthetic intermediates is presented in Chapter 7. The incorporation of these photoreactive groups into peptidic probes to target the formyl peptide binding site of FPR1 is described in Chapters 3 and 4.

Chapter 3 Preparation and Use of First-Generation Photoreactive Probes

Photoaffinity labelling is a technique used to study the interaction between a receptor and its ligand.[50] A chemically synthesised probe containing a photoreactive group binds non-covalently to the target receptor. Upon UV activation the photoreactive group forms a covalent bond to the receptor. To study the formyl peptide binding site on FPR1 a series of photoreactive probes mimicking formyl peptides were synthesised. The photoreactive groups 4,4-azo-pentanoic acid, Fmoc-photo-Met and Fmoc-photo-Leu, synthesised in chapter 2 were incorporated into peptides to produce the first generation of probes to target FPR1. This chapter investigates the binding and crosslinking of these probes to FPR1 expressed on the surface of HEK293T mammalian cells. A combination of analytical techniques (SDS-PAGE, Western Blot and flow cytometry) was used to study these probes.

3.1 Photoreactive Chemical Probe Design

Three photoreactive chemical probes were designed, each with the structure: fMLFKXY-OH (**Figure 3.1**), where X is a photoreactive unnatural amino acid and Y is propargyl glycine.

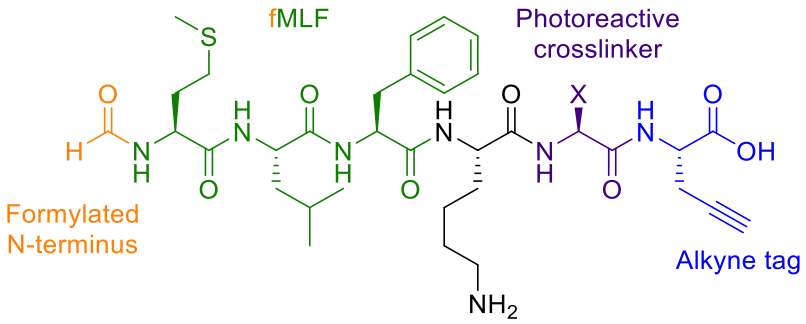

Figure 3.1: Generation 1.0 probe structure

Bacteria incorporate a formyl-methionine at the N-terminus of proteins and therefore it is important to include this for FPR1 recognition.[3, 23] Bufe *et al.* detected a 770-fold reduction in activation of FPR1 for MGFFIS compared with fMGFFIS.[116] The N-terminus of the probes matches the structure of the bacterial peptide fMLF. fMLF has been shown to have a high binding affinity for FPR1 and this motif exists at the N-terminus of several hundred bacterial signal peptides.[116] It has also been published that peptides with fMLF at their N-terminus bind with a higher affinity to FPR1 compared to those without.[3] These three amino acids are all hydrophobic; it has been proposed that it is beneficial for the second and third amino acid to have hydrophobic side chains.[3] This is to allow van der Waals interactions to FPR1 residues.[116] It is suggested that the first three hydrophobic residues can form an α-helical turn in the peptide and this confirmation appears to be a core motif for FPR1 agonist binding.[116] Following from fMLF, many different residues appear to be tolerated from position four.[3, 23, 116] Therefore, because of the high hydrophobicity of the N-terminus, a lysine was incorporated at position four to improve solubility of the probe. The photoreactive group and alkyne tag (incorporated to attach a biotin or fluorescent group to the probe via click chemistry after crosslinking to aid subsequent analysis) were installed at the C-terminus to ensure the fMLF interactions were not hindered. The probes were kept short (six amino acids long) as it has been suggested that FPR1 has a shallower binding pocket compared to FPR2.[23]

3.2 Optimisation of *N*-formylation Reaction

To mimic a bacterial peptide, the chemical probes needed to contain a formyl group at the N-terminus. To achieve this, an *N*-formylation was to be performed at the end of SPPS whilst the peptide was attached to the solid support. Three different methods for *N*-formylation were tested using a simple tripeptide: Met-Leu-Lys(Boc)-NH_2 (**Figure 3.2**) to optimise the protocol.

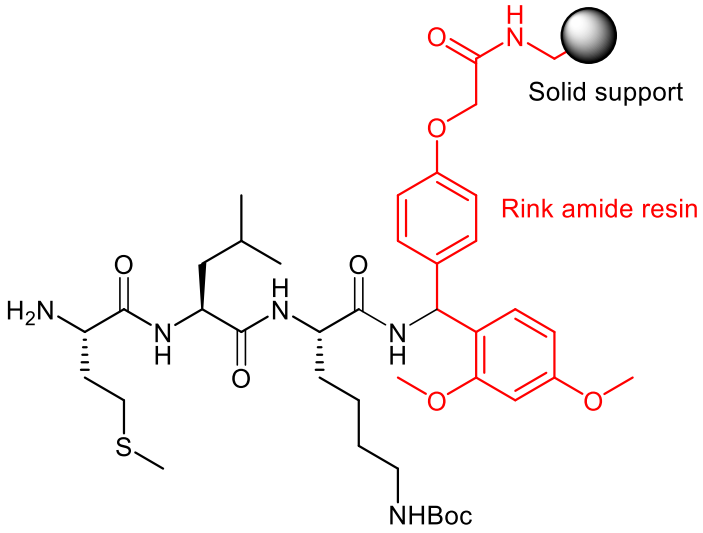

Figure 3.2: Test peptide structure for *N*-formylation optimisation

3.2.1 Formic Acid and Isobutyl Chloroformate

The synthesised tripeptide was used to optimise the *N*-formylation. The activation of formic acid with isobutyl chloroformate was attempted by a previous MChem student, Vikki Clayton, in the group. However, this resulted in poor conversion with the non-formylated peptide still detected by LC-MS. This method was repeated and two additional methods were found in the literature which reported better yields.[117-119] The reaction methods were analysed by mini cleavage of the peptide and LC-MS of the mixture. The first method tested involved the generation of a formylating agent **3.03** *in situ* using formic acid **3.01**, isobutyl chloroformate **3.02** and *N*-methylmorpholine (NMM) (**Scheme 3.1**).[117] All reagents were added to the peptide and the reaction vessel was rotated for two hours at

room temperature. This method was unsuccessful, and no product was seen via LC-MS.

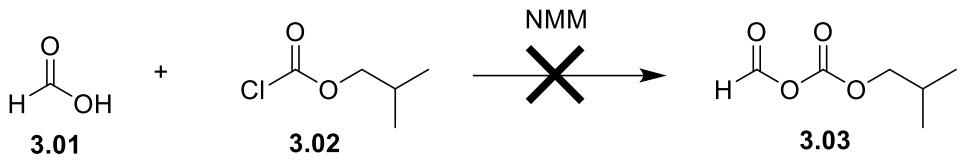

Scheme 3.1: Formation of active species from formic acid **3.01** and isobutyl chloroformate **3.02**

3.2.2 Formic Acid and DCC

The second method involved the activation of formic acid **3.01** using DCC **3.04**.[118] The DCU produced during this reaction was filtered off and the solution concentrated to give the formylating agent (**Scheme 3.2**).[118] This was added to the resin and turned overnight at 4 °C. The temperature was kept low to avoid the decomposition of formic acid. The LC-MS spectra showed only product was present and no starting material. This result was positive, but the reaction required separate formation of the formylating agent and had to be kept cold overnight.

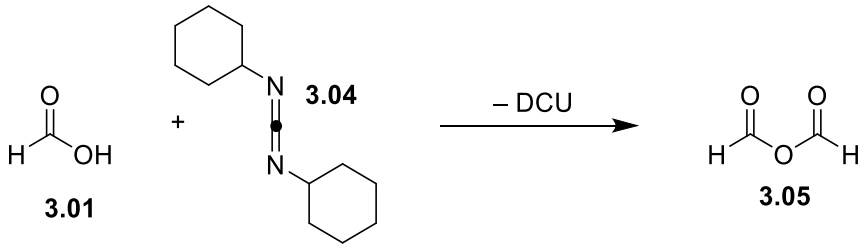

Scheme 3.2: Formation of active species from formic acid **3.01** and DCC **3.04**

3.2.3 *p*-Nitrophenyl Formate

In 2017 Christensen *et al.* published a study reviewing on-resin *N*-formylation methods.[119] The study investigated several well-known formylating agents and highlighted the commercially available *p*-nitrophenyl formate **3.06** (**Figure 3.3**) as the most versatile, with most reaction yields above 90%. Therefore, the final *N*-formylation tested was the addition of **3.06** to the resin with DIPEA in DCM. [119]

The reaction was performed at room temperature and rotated overnight. In this reaction **3.06** is already activated. Analysis via LC-MS showed that the reaction had gone to completion with no starting material present.

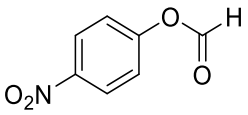

3.06

Figure 3.3: *p*-Nitrophenyl formate **3.06** active species

From these results it was decided that the *N*-formylation reaction using *p*-nitrophenyl formate would be used to formylate the N-termini of the chemical probes due to high yields and operational simplicity.

3.3 Synthesis of Photoreactive Chemical Probes

The synthesis of the photoreactive chemical probes was accomplished using SPPS (**Scheme 3.3**). 2-Chlorotrityl chloride resin was used to generate a free carboxylic acid at the C-terminus upon cleavage. This resin was loaded with Fmoc-propargyl glycine using DIPEA and the percentage of loading was calculated by utilising the UV absorption of dibenzofulvene – the product from Fmoc deprotection using DBU.[120] The combination of Oxyma pure and DIC was used to couple subsequent amino acids, and 20% piperidine in DMF was used for the Fmoc deprotection steps. Cleavage of the peptides was achieved using 2.5% EDT, 2.5% water, 1% TIS in TFA. The addition of EDT is necessary to stop the alkylation of methionine by cations.[121]

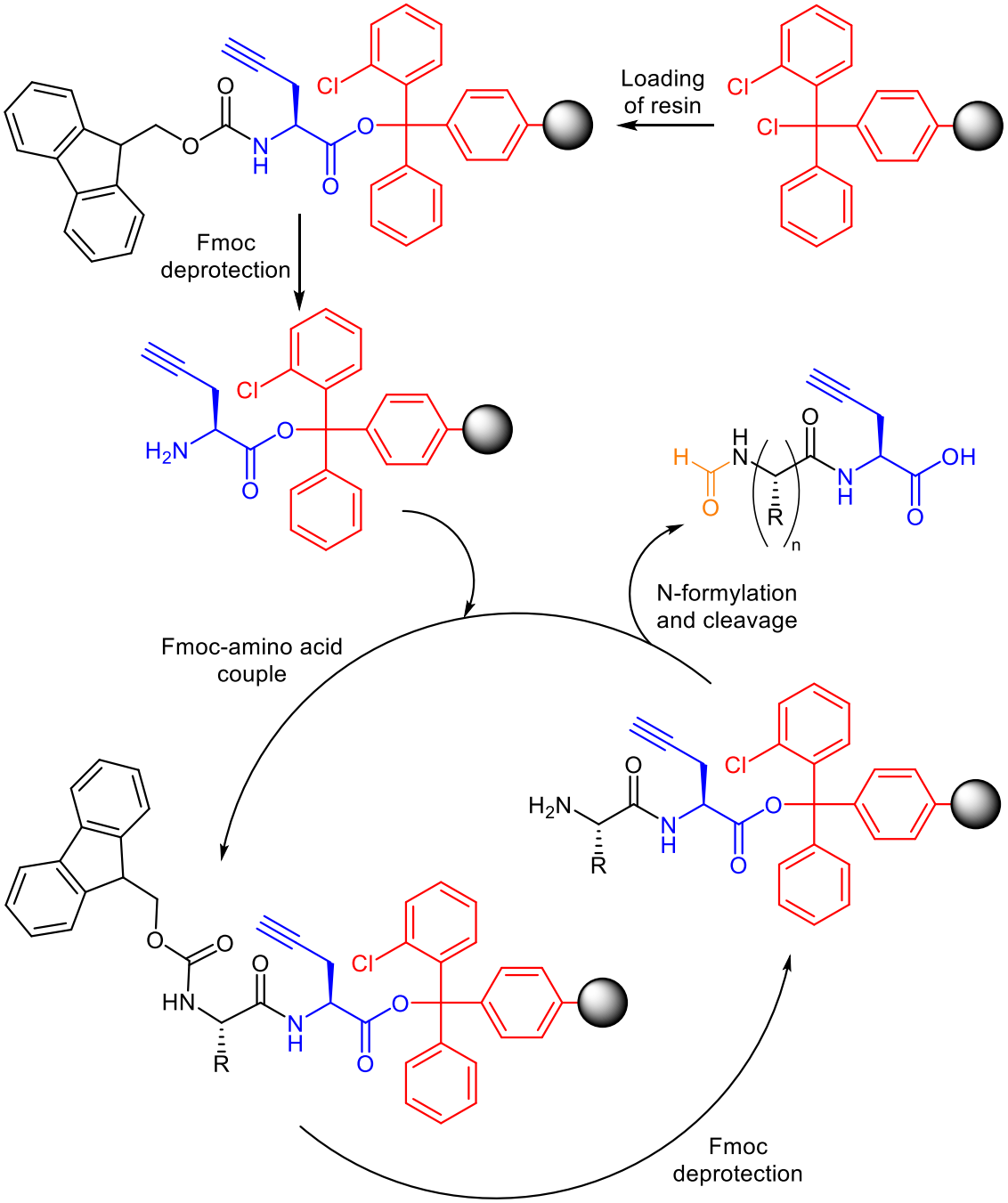

Scheme 3.3: SPPS of chemical probes using chlorotrityl resin (in red attached to black sphere) loaded with propargyl glycine (in blue).

3.3.1 Photoreactive Probe Incorporating 4,4-Azo-pentanoic Acid

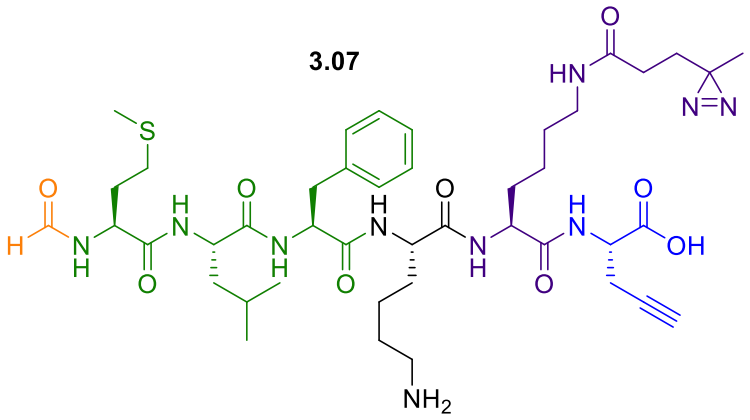

Figure 3.4: Structure of Probe1.0AcLys.

Formyl-Met-Leu-Phe-Lys-photoAcLys-propargyl glycine-OH (Probe1.0AcLys **3.07**) contains 4,4-azo-pentanoic acid attached to the sidechain of a lysine residue via acylation (**Figure 3.4**). This reaction was performed on-resin after the synthesis of the peptide and the *N*-formylation of the methionine residue. The lysine was incorporated as a building block bearing a Dde protecting group that is stable in basic conditions, and therefore unaffected during the Fmoc deprotection steps of SPPS. Following the *N*-formylation, the Dde PG was removed using 2% hydrazine in DMF. The 4,4-azo-pentanoic acid was then coupled to the free amine **3.09** using the same coupling conditions as for the other amino acids (**Scheme 3.4**).

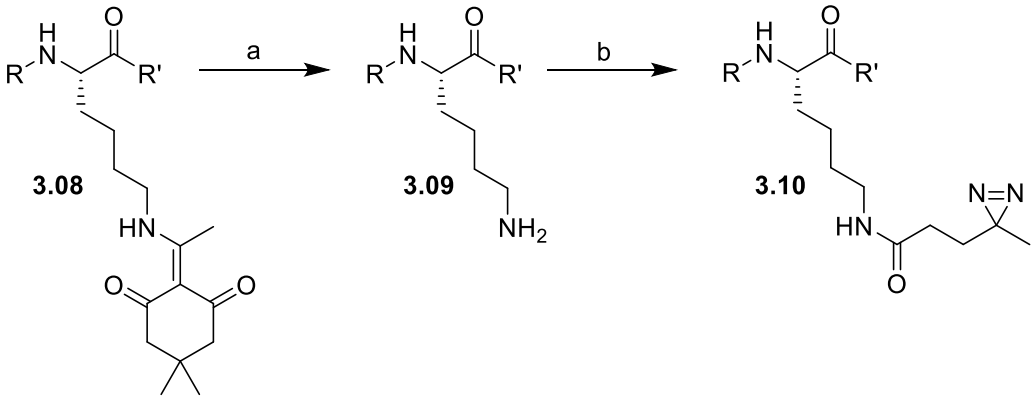

Reagents and conditions: *(a) 2% hydrazine in DMF; (b) oxyma pure, DIC, 4,4-azo-pentanoic acid, DMF.*

Scheme 3.4: Formation of photo-AcLys in peptide chain.

The peptide was subsequently cleaved from the resin and purified using UV-directed HPLC. Probe1.0AcLys was isolated in >99% purity and 68% yield (HPLC shown in section 9.1.2.1).

3.3.2 Photoreactive Probes Incorporating photo-Met and photo-Leu

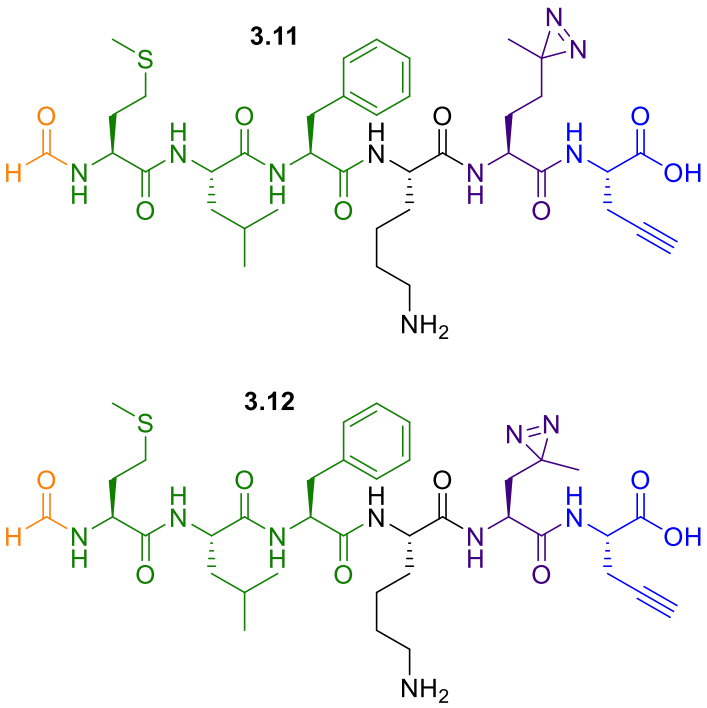

Figure 3.5: Structures of Probe1.0Met **3.11** and Probe1.0Leu **3.12**.

Fmoc-photo-Met and Fmoc-photo-Leu were coupled using the same conditions as for natural amino acids. Formyl-Met-Leu-Phe-Lys-photoMet-propargyl glycine-OH (Probe1.0Met **3.11**) (**Figure 3.5**) was cleaved from the resin and purified using UV-directed HPLC. Probe1.0Met was isolated in >99% purity and 66% yield (HPLC shown in section 9.1.2.2).

Following cleavage of formyl-Met-Leu-Phe-Lys-photoLeu-propargyl glycine-OH (Probe1.0Leu **3.12**) (**Figure 3.5**) LC-MS analysis indicated a mass of 661.43 Da, which was 125 Da less than the expected mass (**Figure 3.6**).

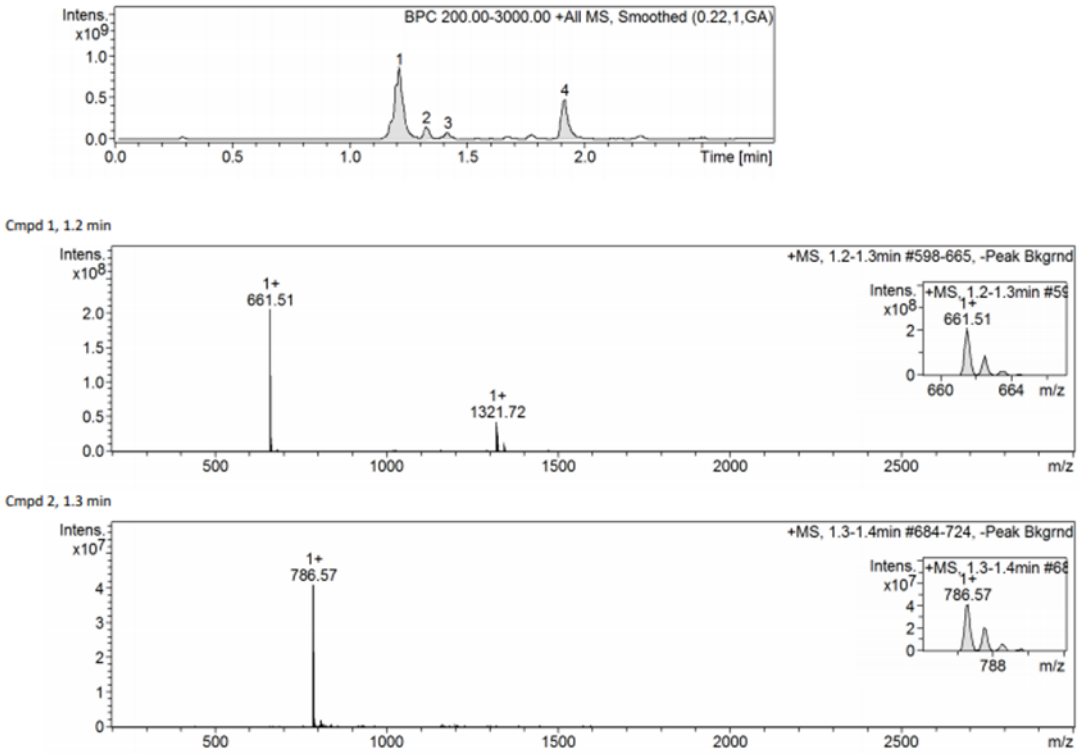

Figure 3.6: LC-MS of Probe1.0Leu following cleavage (before HPLC purification); peak 1 is the main peak and shows a mass 125 Da less than expected; peak 2 is the correct mass of Probe1.0Leu.

The synthesis of the peptide was repeated, performing LC-MS analyses at each amino acid addition. The impurity was detected after the addition of the lysine residue, therefore the synthesis was restarted with a new batch of Fmoc-Lys(Boc). However, this did not resolve the issue. It was hypothesised that during cleavage a cyclisation had occurred between the diazirine and a backbone amide group to give **3.21** (**Scheme 3.5**). To investigate whether the cyclisation was catalysed by heat produced in the cleavage a sample of resin was cleaved at 0 °C. However, this still gave the same mass suggesting the cyclisation was catalysed by TFA during cleavage. The synthesis of the proposed probe was not pursued further. It was first proposed that the cyclisation was initiated with the acid catalysed hydrolysis of the amide bond between photo-Leu and propargyl glycine. However, this side-product was not detected during the synthesis of Probe1.0Met. Therefore, it is more probable that the acid catalyses a ring-formation made favourable by the 5-carbon photo-Leu (**Scheme 3.5**).

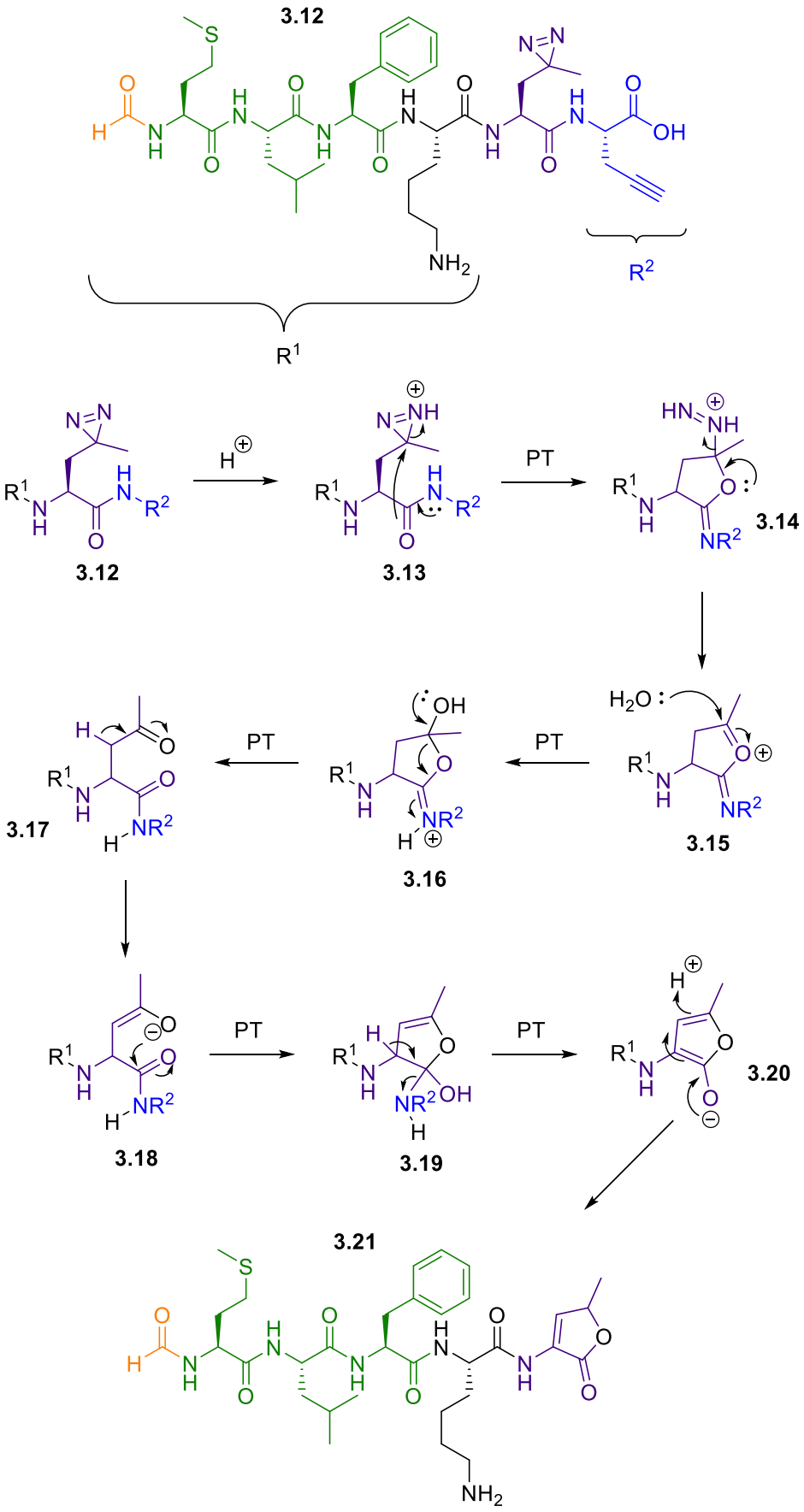

Scheme 3.5: Predicted cyclisation of Probe1.0Leu.

3.4 Establishing the HEK293T Cell Line

To investigate the binding and crosslinking of the photoreactive probes with FPR1 a mammalian cell line expressing FPR1 was established. HEK293T cells (*Homo sapiens* embryonic kidney) are a derivative of HEK293 cells and are highly transfectable (**Figure 3.7**). HEK293T cells were created by introducing the viral SV40 large T antigen into HEK293 cells.[122] Therefore, plasmids that have the SV40 origin of replication undergo replication with a high copy number maintained. For this reason, the cell line is commonly used in biological experiments requiring transient transfection. HEK293T cells are adherent, growing attached to the surface of a culture flask. FPR1 is not produced by HEK293T cells (The Human Protein Atlas)[123] and therefore it was necessary to perform expression through transient transfection.

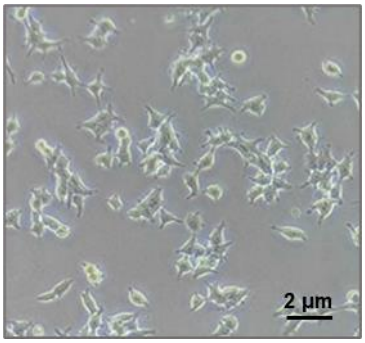

Figure 3.7: Microscope image of HEK293T cells cultured during the project.

3.4.1 Transient Transfection of HEK293T Cells

The commercially available FPR1 cDNA ORF clone (FPR1 plasmid) (GenScript) was transformed into *E. coli* competent cells which were grown and the plasmid extracted. The transfection reagent Turbofect (Thermo Scientific) was used to transfect the HEK293T cells with the FPR1 plasmid. This transient transfection was optimised and FPR1 expression was evaluated by Western Blot (WB) analysis – using recognition of the FLAG-tag (DYKDDDDK) at the C-terminus of the expressed FPR1. It was found that a ratio of 1 µg of plasmid to 3 µL of Turbofect with an incubation time of 24 hours were the optimum transfection conditions (**Figure 3.8**). The samples from the transfection experiments were used

to optimise the conditions for the WB analysis as well. FPR1 is observed as a smear in the WB because it is glycosylated, resulting in multiple migration bands.[124]

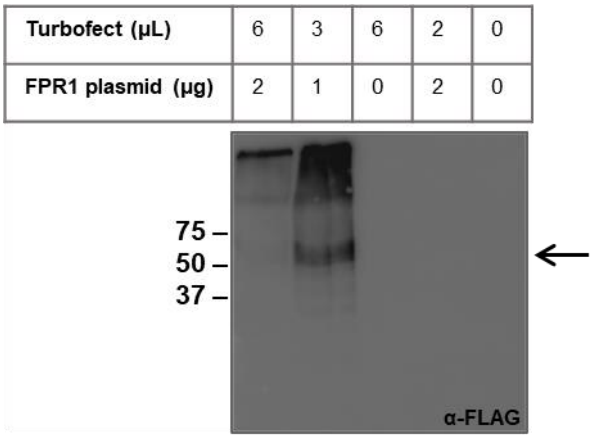

Figure 3.8: Anti-FLAG Western Blot showing optimised conditions of transient transfection of HEK293T cells with FPR1 plasmid, arrow indicates FPR1.

3.4.1.1 Deglycosylation of FPR1

FPR1 expressed on the surface of mammalian cells is naturally glycosylated, increasing its mass from 38 kDa to 50-75 kDa.[47, 125] FPR1 possesses two potential N-glycosylation sites in the N-terminus, Asn4 and Asn10, and one in the second extracellular loop, Asn179.[125] Deglycosylation of FPR1 was conducted on lysed transfected cells to confirm the expression of FPR1. In preparation for deglycosylation, cell lysate samples are generally boiled at 100 °C to denature the protein. However, it was shown that heating at high temperatures caused aggregation of FPR1 (**Figure 3.9**). This is known as thermal aggregation and has been observed with other membrane proteins and GPCRs.[124, 126, 127]

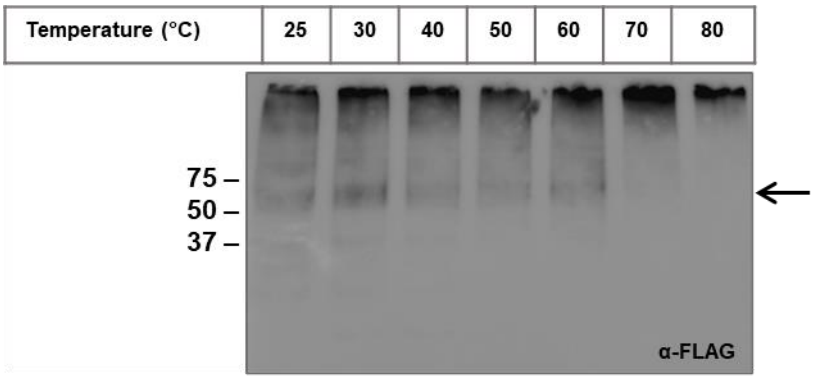

Figure 3.9: Temperature experiment on FPR1 expressed on HEK293T cells; cell lysate samples heated at given temperature for 10 min in sample loading buffer, samples analysed by an anti-FLAG Western Blot.

To denature FPR1 at room temperature, the detergent NP-40 was added to the cell lysate which was subsequently agitated for 30 min. The sample was then incubated with the enzyme peptide-N-glycosydase F (PNGaseF) (Promega), commonly used for deglycosylations of glycoproteins/glycopeptides, for two hours.[128] Deglycosylation was observed, but glycosylated FPR1 was also present. Increasing the incubation time to 24 hours gave the same result, suggesting that the PNGaseF was denaturating. Therefore, the protocol was adapted to include two sequential additions of PNGaseF, each incubated for one hour resulting in near complete deglycosylation (**Figure 3.10**).

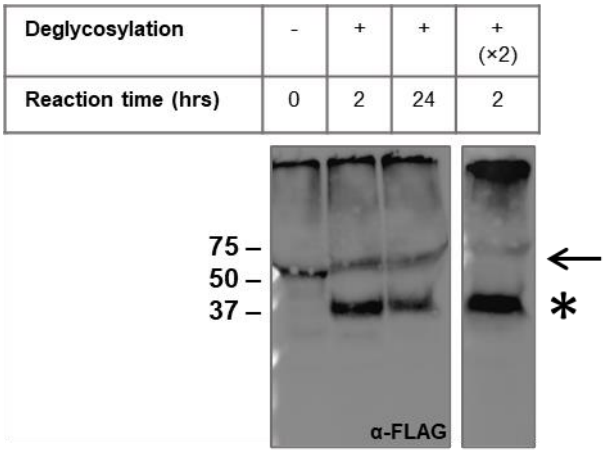

Figure 3.10: Anti-FLAG Western Blot showing deglycosylation of FPR1, glycosylated FPR1 indicated by arrow, deglycosylated FPR1 indicated by star.

3.5 Binding, Crosslinking and Click Reaction of Photoreactive Probes

The binding and crosslinking of the probe was conducted on transfected HEK293T cells prior to lysis (**Scheme 3.6**). To analyse the outcome of this experiment, a copper(I)-catalysed azide-alkyne cycloaddition (CuAAC) was performed on the cell lysate, attaching a TAMRA fluorophore to the probe. The presence of this fluorophore would be analysed using in-gel fluorescence during SDS-PAGE analysis. The FLAG-tag present on FPR1 would allow purification of the FPR1-probe complex from the cell lysate.

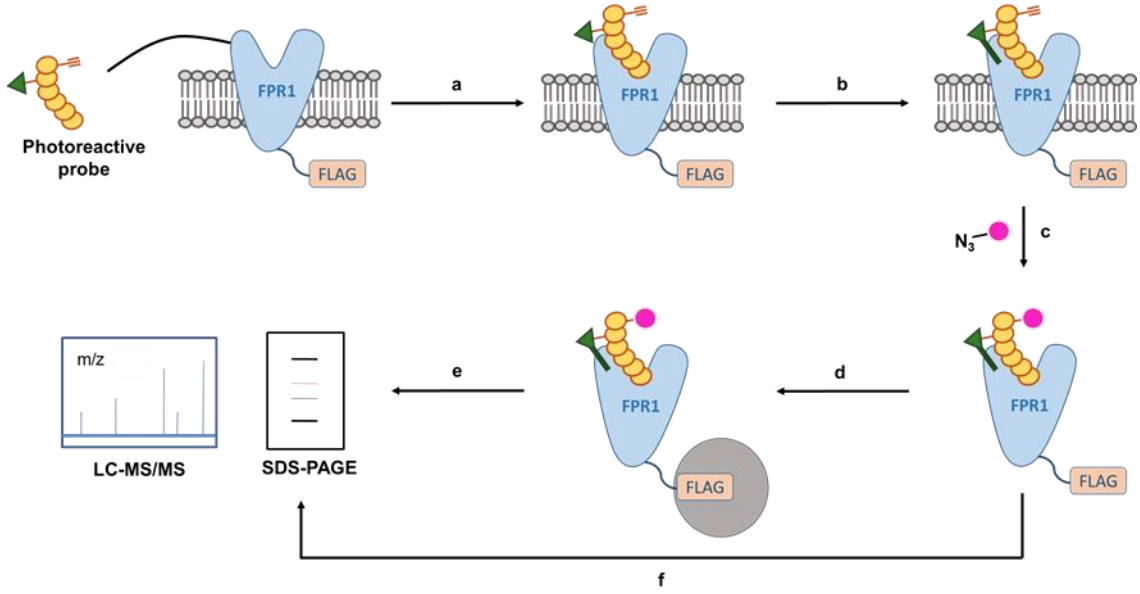

Scheme 3.6: Work-flow of binding and crosslinking of generation 1.0 probes to FPR1 expressed on the surface of HEK293T cells; a) binding of probe to FPR1; b) photo-crosslinking of probe to FPR1 by irradiation of UV light at 365 nm; c) lysis of the cells and CuAAC between the alkyne tag present on the probe and azide-fluor 545; d) affinity pull-down of FPR1-probe complex from cell lysate to anti-FLAG resin using the FLAG-tag present at the C-terminus of FPR1; e) elution of FPR1-probe complex from anti-FLAG resin and analysis by SDS-PAGE or LC-MS/MS; f) analysis of cell lysate by SDS-PAGE.

3.5.1 Binding and Crosslinking of Probe1.0Met to FPR1

The transfected HEK293T cells were washed with PBS and incubated with Probe1.0Met in PBS (1 mL, 1 µM) for 30 mins at 37 °C. After incubation the cells

were irradiated with UV light (365 nm) for 5 mins using a UVP crosslinker (analytic jena AG). Following this the cells were lysed, and the resulting protein concentration determined using a DC protein assay (Bio-Rad). A CuAAC reaction was then performed on the cell lysate with 5-Carboxytetramethylrhodamine-azide (azide-fluor 545). The sample was then analysed by SDS-PAGE using in-gel fluorescence at 550 nm (**Figure 3.11**). The gel was then stained using Coomassie Blue to image the overall protein within the sample.

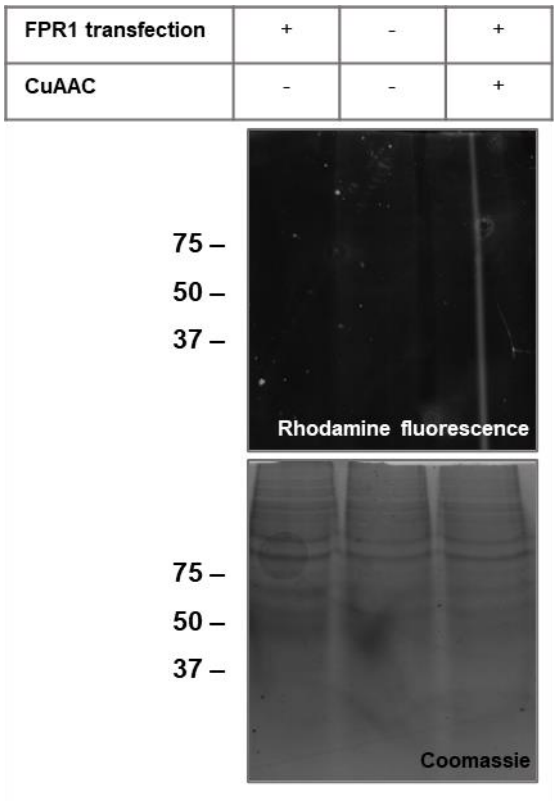

Figure 3.11: SDS-PAGE analysis of Probe1.0Met crosslinking to FPR1

No fluorescence was observed but it was unclear which step in the experiment was unsuccessful: the binding of the probe, the crosslinking of the probe or the CuAAC reaction. Thus, this was investigated further.

3.5.2 Investigation of CuAAC Reaction Conditions

To explore the reason for the unsuccessful binding and crosslinking of Probe1.0Met, the experiment was repeated using three different conditions for the CuAAC reaction:

1) Deglycosylating the sample prior to the CuAAC reaction. Glycopeptides present on the surface of FPR1 could block the alkyne tag on the chemical probe. Deglycosylating the sample first provides the azide-fluor 545 with a less crowded route.
2) Performing the reaction in PBS instead of TBS. It has been suggested in literature that PBS is a better solvent for CuAAC reactions as Tris present in TBS is a competitive ligand for copper and can therefore inhibit the reaction.[129]
3) Increasing the concentration of the click reagents. The protocol used for the CuAAC reaction had been previously employed on a range of cell lysates by Megan Wright and is well established.[130] However, an increased concentration of click reagents could force the CuAAC reaction to completion.

In all cases no in-gel fluorescence was observed during analysis using SDS-PAGE (not shown).

3.5.3 Cold Incubation of Probe1.0Met

The formyl peptide receptors are GPCRs and therefore when an agonist binds to them, they internalise to prevent over-activation.[41] Therefore, incubation with Probe1.0Met at 37 °C for 30 mins could result in internalisation of FPR1. The crosslinking experiment was repeated with incubation of Probe1.0Met at 0 °C. Once again no in-gel fluorescence was detected by SDS-PAGE (not shown).

3.5.4 Testing Probe Binding with Flow Cytometry

Following the unsuccessful crosslinking experiments, it was hypothesised that Probe1.0Met was not binding to FPR1. To test this, flow cytometry was employed. Flow cytometry measures chemical and physical characteristics of individual cells in a sample. The cells are flowed single file through a beam of light which is scattered producing physical characteristic data. A larger degree of forward and side light scattering is indicative of a larger cell or cluster of cells. Flow cytometers

are also equipped with lasers at different wavelengths of light to detect fluorophores.

3.5.4.1 FPR1 Fluorescent Tracer

An appropriate method for quantitatively analysing the binding of chemical probes is through the use of a competitive binding assay. For this method a probe known to bind to FPR1 strongly, was synthesised. Formyl-NLe-Leu-Phe-NLe-Tyr-Lys(FITC)-OH (**Figure 3.12**) has been extensively reported as a strong binder to FPR1 and is therefore often used in competitive binding assays.[131, 132] fNLFNYK-Fl has a K_d value of 2.7 ± 0.3 nM for FPR1 expressed on HEK293T cells.[47] This fluorescent tracer (TracerFITC **3.22**) was synthesised using similar methods as the previous peptides. The lysine side chain was protected with a Dde PG that was removed using 4% hydrazine in DMF following *N*-formylation. 2% Hydrazine in DMF was not strong enough to remove the Dde PG, possibly because the lysine residue was in close proximity to the resin. The FITC tag was coupled to the free amine using DIPEA overnight (in darkness). The peptide was cleaved from the resin using 2.5% TIS, 2.5% water and 95% TFA. After purification using UV directed HPLC, TracerFITC was isolated in 95% purity and 28% yield (Section 9.1.2.3).

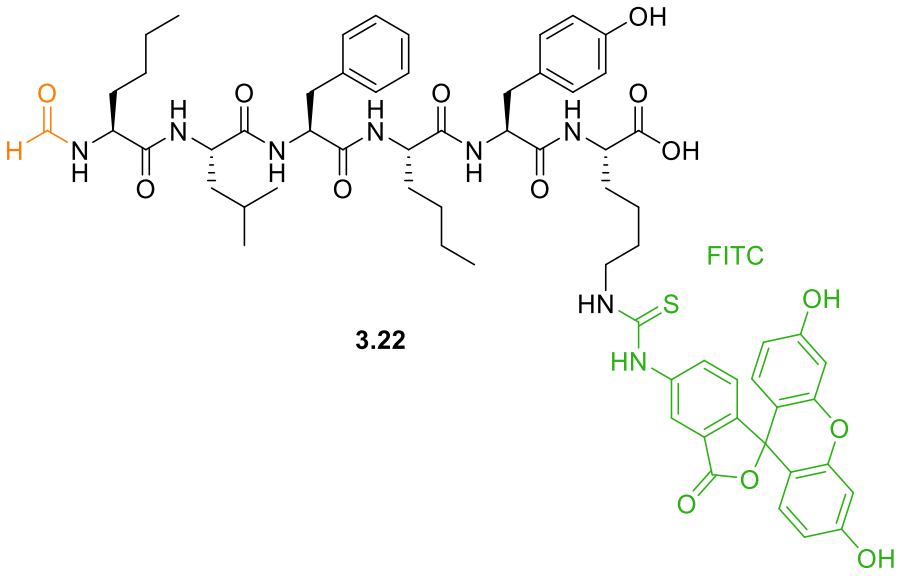

3.22

Figure 3.12: Fluorescent tracer **3.22** to target FPR1

3.5.4.2 Suspension of HEK293T Cells

Flow cytometry requires the sample of cells to be suspended. Therefore, to test the binding of Probe1.0Met to FPR1, the adherent HEK293T cells would need to be suspended after transfection. Four different methods were tested to suspend the cells: trypsin, accutase, PBS with EDTA and PBS with the addition of scraping the surface of cells (**Figure 3.13**). Subsequently the cells were lysed, deglycosylated and the expressed FPR1 was analysed by Western Blot. The expression of FPR1 for the samples suspended with trypsin and accutase was low (**Figure 3.13**). However, expression of FPR1 for the other two samples was as expected. For future experiments the HEK293T cells would be suspended using PBS with EDTA. This is a milder and more reproducible method than scraping the cells. EDTA is also known to assist in reducing cell clumping.

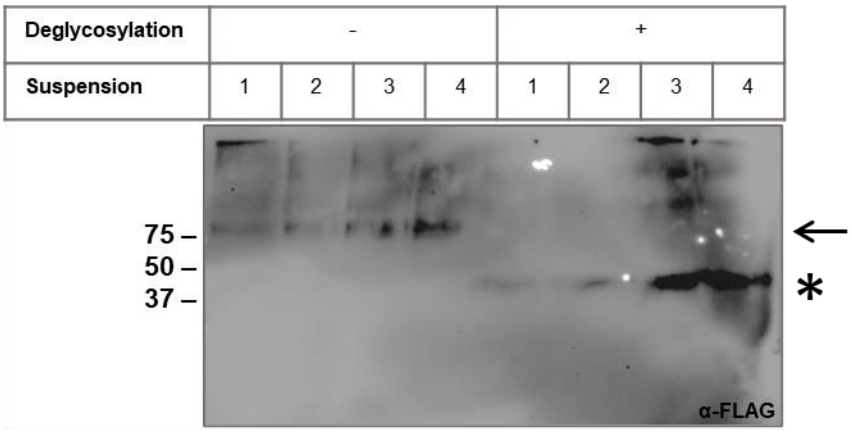

Figure 3.13: Anti-FLAG Western Blot to analyse the suspension methods of transfected HEK293T cells; 1) trypsin; 2) accutase; 3) PBS with EDTA; 4) PBS with scraping of cells; glycosylated FPR1 indicated by arrow, deglycosylated FPR1 indicated by star.

3.5.4.3 Flow Cytometry to Test the Binding of TracerFITC

The synthesised TracerFITC was incubated with HEK293T cells expressing FPR1, and HEK293T cells not expressing FPR1. The fluorescence of these samples was analysed with a CytoFLEX S 4-laser flow cytometer to examine the specific binding of TracerFITC to FPR1. For each sample, the fluorescence of 10,000 cells was read at 525 nm. The data for the samples is presented as a

histogram. The y-axis shows the number of the cells and the x-axis shows the fluorescence intensity at the given wavelength. Therefore, a shift in the peak of the histogram to the right represents an increase in fluorescence at the given wavelength. As expected, TracerFITC bound to the expressed FPR1, and showed no limited non-specific binding as measured by the fluorescence intensity during flow cytometry (**Figure 3.14**).

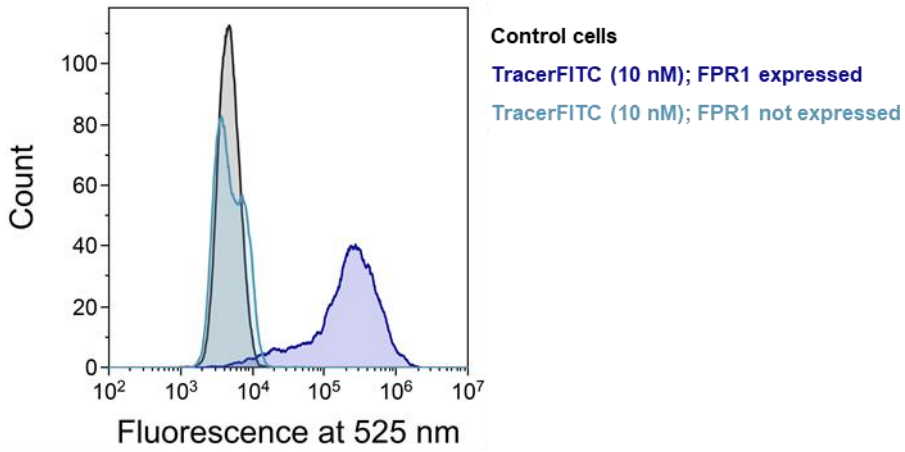

Figure 3.14: Histogram showing the fluorescence at 525 nm of HEK293T cells incubated with TracerFITC; 10,000 cells per sample measured

3.5.4.4 Competitive Binding of Generation 1.0 probes to FPR1

The binding of both probes; Probe1.0Met and Probe1.0AcLys to FPR1 was tested through competitive binding with the TracerFITC. The HEK293T cells expressing FPR1 were incubated with a solution containing the TracerFITC (10 nM) and Probe1.0Met or Probe1.0Aclys (1 µM). Again, the fluorescence of the samples at 525 nm was measured on 10,000 cells. Both probes showed no binding to FPR1, with the fluorescence of the cells not being decreased (**Figure 3.15**).

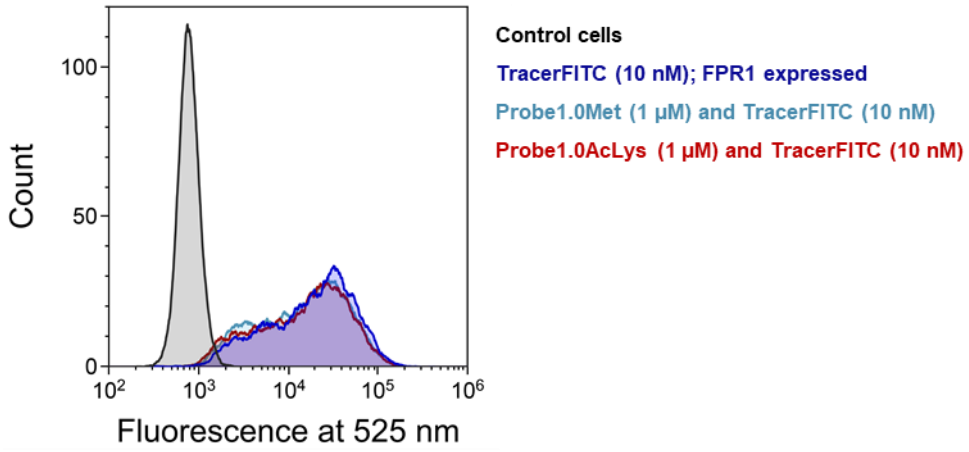

Figure 3.15: Histogram showing the fluorescence at 525 nm of HEK293T cells incubated with TracerFITC, Probe1.0Met and Probe1.0AcLys; 10,000 cells per sample measured.

3.6 Conclusion

The work discussed in this chapter has investigated the binding and crosslinking of the first generation of FPR1 synthetic probes. Two photoreactive probes were synthesised, incorporating photo-AcLys and photo-Met. Unfortunately, both Probe1.0Met and Probe1.0AcLys were unsuccessful in binding to FPR1. The reasons why these probes did not bind will be discussed in chapter 4. However, TracerFITC was shown to bind specifically to FPR1.

In addition to this, much of the methodology for the project was established for the synthesis and evaluation of FPR1 probes. The conditions for the transient transfection of HEK293T cells with FPR1 were optimised, including the technique for the anti-FLAG Western Blot used for analysis. A deglycosylation reaction performed at room temperature was found and optimised for FPR1. Finally, the procedure for binding and crosslinking to FPR1 on the surface of HEK293T cells was developed. These methodologies were implemented in the study of second-generation probes in chapter 4.

Chapter 4 Preparation and Use of Photoreactive Probes Containing Detectable Tags

In Chapter 3 the first-generation of photoreactive probes to target FPR1 were designed and synthesised, incorporating the photoreactive diazirine photo-Met and photo-AcLys. These probes were unfortunately unsuccessful, showing no detectable binding to FPR1. However, a fluorescent tracer (TracerFITC) known to have a high binding affinity for FPR1[131, 132] was synthesised and its specific binding to FPR1 was confirmed using flow cytometry. In addition to this, the transient transfection expression system with HEK293T cells and the flow cytometry assay were established. Given the success of TracerFITC, a new generation of probes was designed based on its structure. The binding and crosslinking of these new probes to FPR1 was evaluated using flow cytometry, confocal microscopy, SDS-PAGE and Western Blotting.

4.1 Generation 2.0 Probe Design and Synthesis

A new photoreactive chemical probe was designed, based on the structure of the well-known fluorescent tracer (**Figure 3.12**),[131, 132] with the structure formyl-photoMet-Leu-Phe-Nle-Tyr-Lys(TAMRA)-OH **4.01** (Probe2.0TAMRA) (**Figure 4.1**).

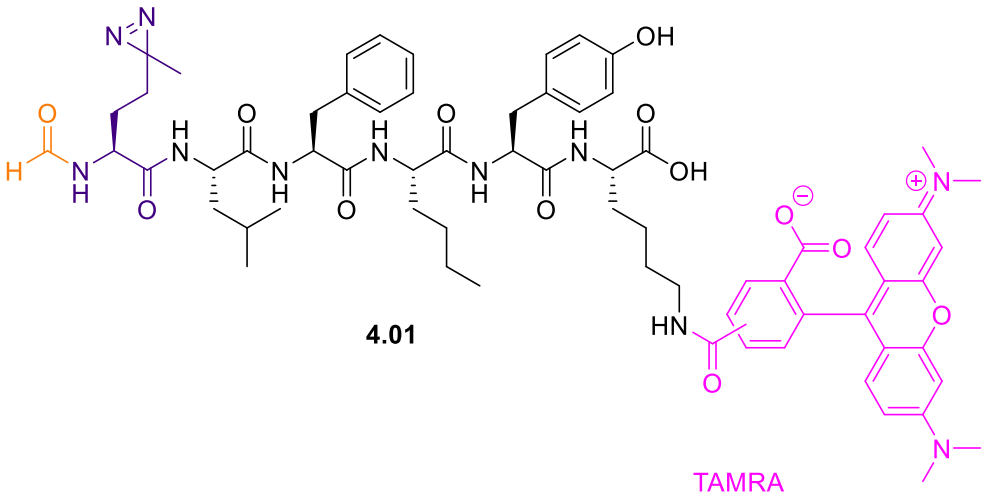

Figure 4.1: Structure of generation 2.0 probe (Probe2.0TAMRA).

Probe2.0TAMRA contains the photoreactive group photo-Met synthesised in Chapter 2 and the TAMRA fluorophore. The addition of a fluorophore in place of an alkyne tag allows for visualisation of the probe through flow cytometry and SDS-PAGE without the need to perform a CuAAC. The TAMRA fluorophore was chosen as it fluoresces at a different wavelength (Em λ_{max} = 578 nm, Ex λ_{max} = 552 nm) to FITC (Em λ_{max} = 525 nm, Ex λ_{max} = 490 nm), therefore Probe2.0TAMRA and TracerFITC can be imaged simultaneously (**Figure 4.2**). However, there is a small amount of bleed-through from the TAMRA fluorescence when imaging FITC fluorescence. The TAMRA moiety is known to be compatible with binding as a similar rhodamine tracer (tetramethylrhodamine labelled N-formyl-Nle-Leu-Phe-Nle-Tyr-Lys) (TMR-peptide) has previously been shown to bind to FPR1.[41]

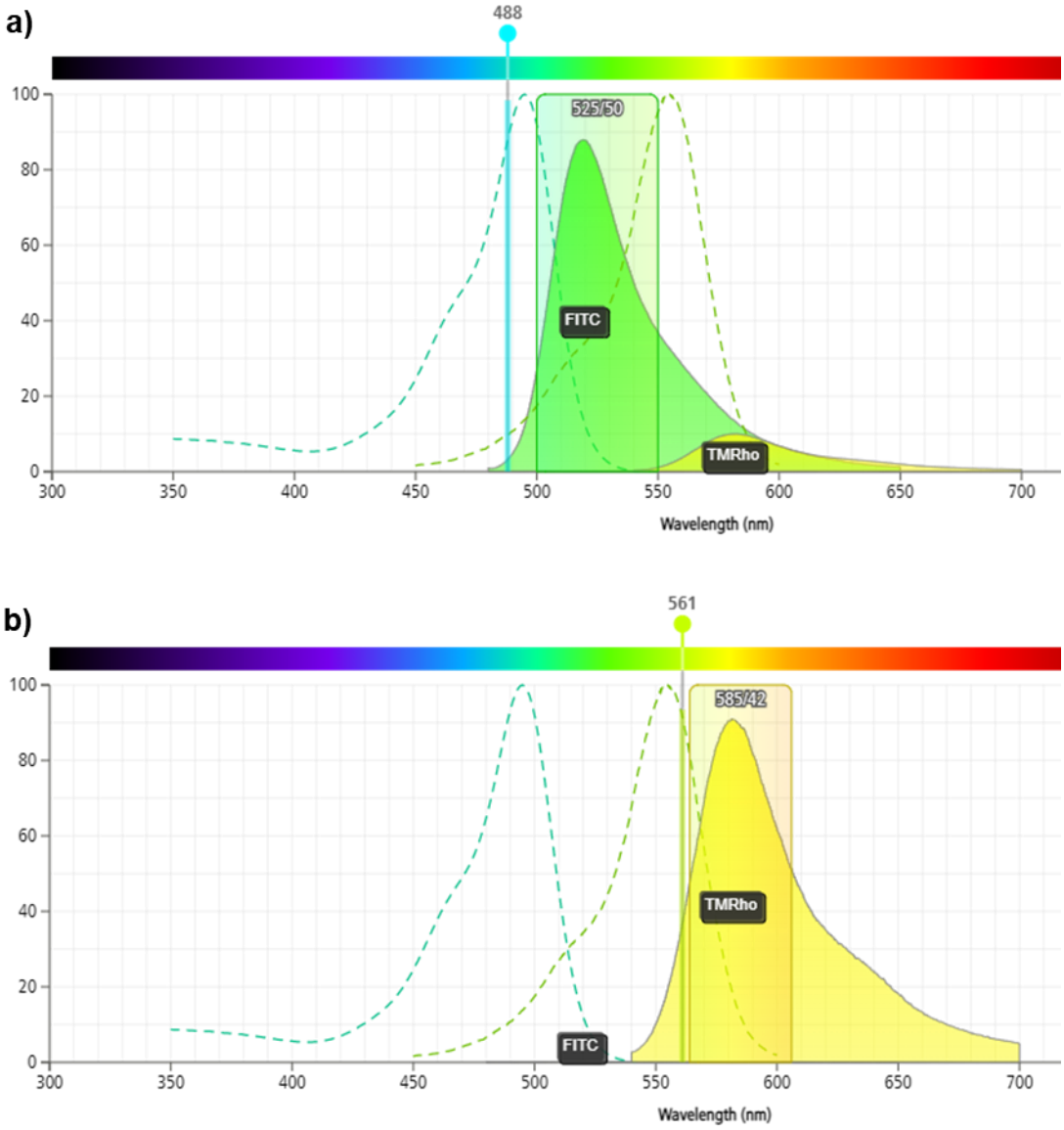

Figure 4.2: Excitation and emission spectra of FITC and TAMRA (Biosciences spectrum viewer); a) 488 nm laser and 525/50 filter used for viewing FITC fluorescence; b) 561 nm laser and 585/42 filter for viewing TAMRA fluorescence.

Probe2.0TAMRA was synthesised using similar methods as the previous peptides outlined in Chapter 3. The lysine side chain was protected with a Dde protecting group that was removed using 4% hydrazine in DMF following *N*-formylation. The TAMRA fluorophore was coupled using the same conditions as for natural amino acids, with the tube kept in darkness. After cleavage and purification using UV directed HPLC, Probe2.0TAMRA was isolated in 98% purity as determined by analytical HPLC and 16% yield (HPLC shown in section 9.1.2.4).

4.2 Flow Cytometry Experiments to Analyse Probe2.0TAMRA Binding to FPR1

A series of experiments employing flow cytometry were used to evaluate the binding of Probe2.0TAMRA to FPR1. With the addition of the TAMRA fluorophore in Probe2.0TAMRA, the specific binding of the probe could be tested using the same procedure as for TracerFITC (Section 3.5.4.3). The difference in fluorescence wavelengths of FITC and TAMRA also allowed for competitive binding experiments.

4.2.1 Specific Binding of Probe2.0TAMRA

The synthesised Probe2.0TAMRA was incubated with HEK293T cells transiently expressing FPR1, and HEK293T cells not expressing FPR1. The fluorescence of these samples was then analysed with a CytoFLEX S 4-laser flow cytometer to examine the specific binding of Probe2.0TAMRA to FPR1. Excitingly, Probe2.0TAMRA showed binding to FPR1 with limited non-specific binding as evaluated with flow cytometry (fluorescence intensity for no FPR1 expression sample scarcely increases compared to the control cells), being consistent throughout repeated experiments (**Figure 4.3**). A small hump is visible to the right of the main peak for no FPR1 expression, indicating off-target binding.

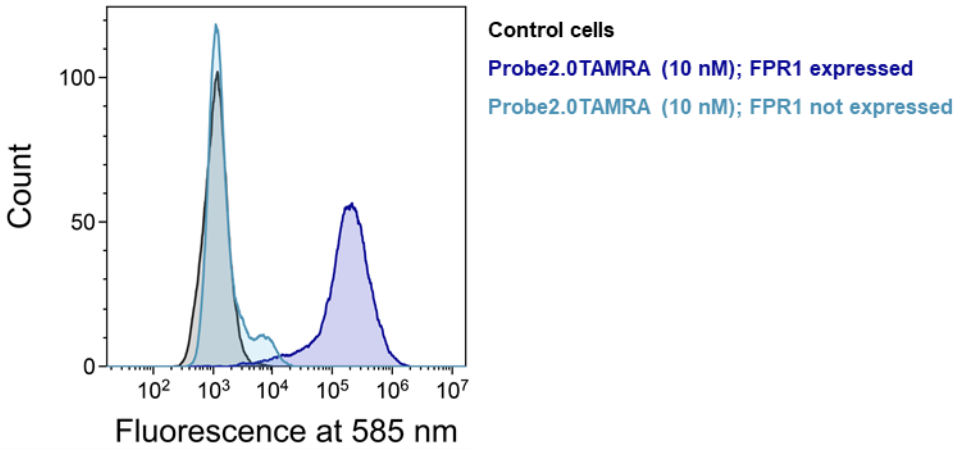

Figure 4.3: Histogram showing the fluorescence at 585 nm of HEK293T cells incubated with Probe2.0TAMRA; 10,000 cells per sample measured.

4.2.2 Concentration Range of Probe2.0TAMRA

To investigate the binding of Probe2.0TAMRA to FPR1 further, the concentration required for maximum specific binding was analysed. Therefore, HEK293T cells expressing FPR1 and HEK293T cells not expressing FPR1 were incubated with Probe2.0TAMRA at concentrations from 0 to 200 nM. The fluorescence of the cells was analysed using flow cytometry. Plotting the difference between the mean fluorescence of cells expressing FPR1 and those not expressing FPR1 for each concentration gave the specific binding curve of Probe2.0TAMRA (**Figure 4.4**).

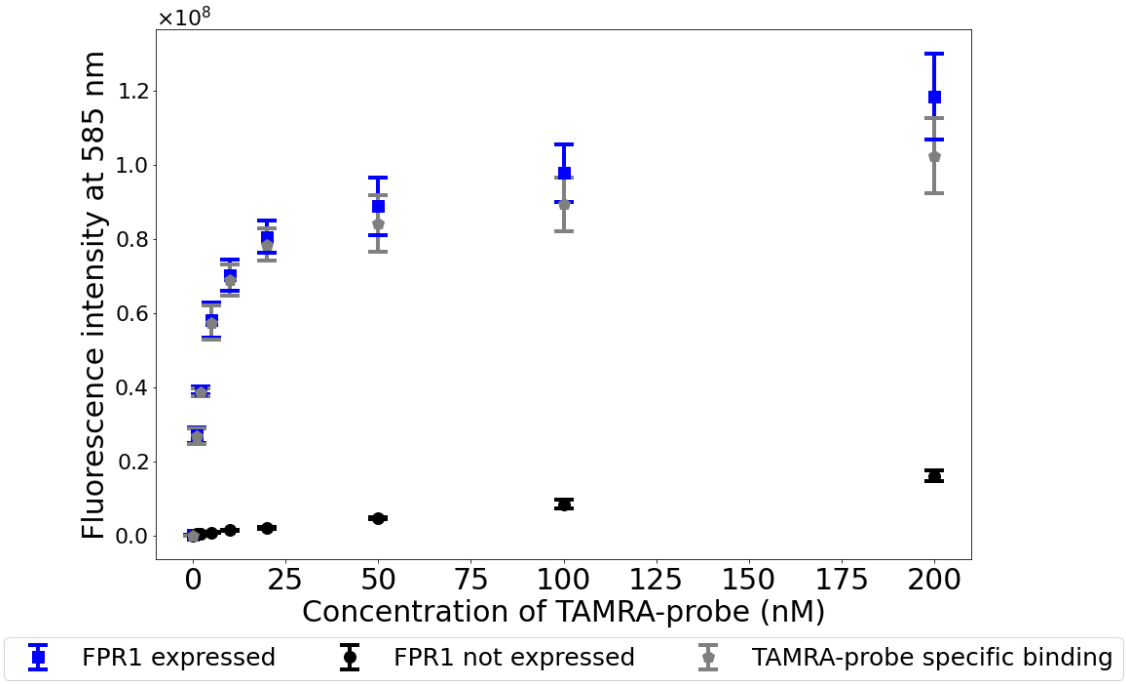

Figure 4.4: Specific binding curve of Probe2.0TAMRA calculated from flow cytometry; three biological replicates performed with bars representing standard error; grey values representing specific binding are the result of subtracting the black values from the blue values.

The specific binding curve of Probe2.0TAMRA is analogous in shape to that of fNLFNYK-Fl (FPR1 expressed on HEK293 cells) published in the literature.[47] Both binding curves begin to plateau at approximately 25 nM and the non-specific binding curves steadily increase with concentration of probe. However, the non-specific binding of fNLFNYK-Fl appears to be a higher proportion of binding than for Probe2.0TAMRA. The non-specific binding of fNLFNYK-Fl never exceeded 30% of total binding, showing approximately 20% non-specific at 100 nM.[47] The

non-specific binding of Probe2.0TAMRA never exceeded 15% of total binding, showing 9% non-specific at 100 nM. Low non-specific binding is essential because it will result in fewer off-target crosslinks. If maximum binding is assumed at 200 nM, then a K_d of approximately 4 nM can be calculated for Probe2.0TAMRA. This K_d is similar in value to that reported for fNLFNYK-Fl (K_d = 3.2 nM),[47] suggesting the peptides have comparable affinities for FPR1. With the binding plateauing by 50 nM and the non-specific binding still low at this concentration (5%), it was decided that a concentration of 50 nM of Probe2.0TAMRA would be used for crosslinking and immunoprecipitation experiments.

4.2.3 Competitive Binding Between TracerFITC and Probe2.0TAMRA

To further confirm the binding of Probe2.0TAMRA to FPR1 a competitive binding experiment was performed between the probe and TracerFITC. As for the competitive binding of generation 1.0 probes the HEK293T cells expressing FPR1 were incubated with a solution containing both TracerFITC (10 nM) and Probe2.0TAMRA (10 nM). An increase of fluorescence at both 525 and 585 nm was observed for transfected cells and the fluorescence for both Probe2.0TAMRA and TracerFITC was also decreased compared to with no competition (**Figure 4.5**). This shows that the two peptides are likely competing for the same binding site on FPR1.

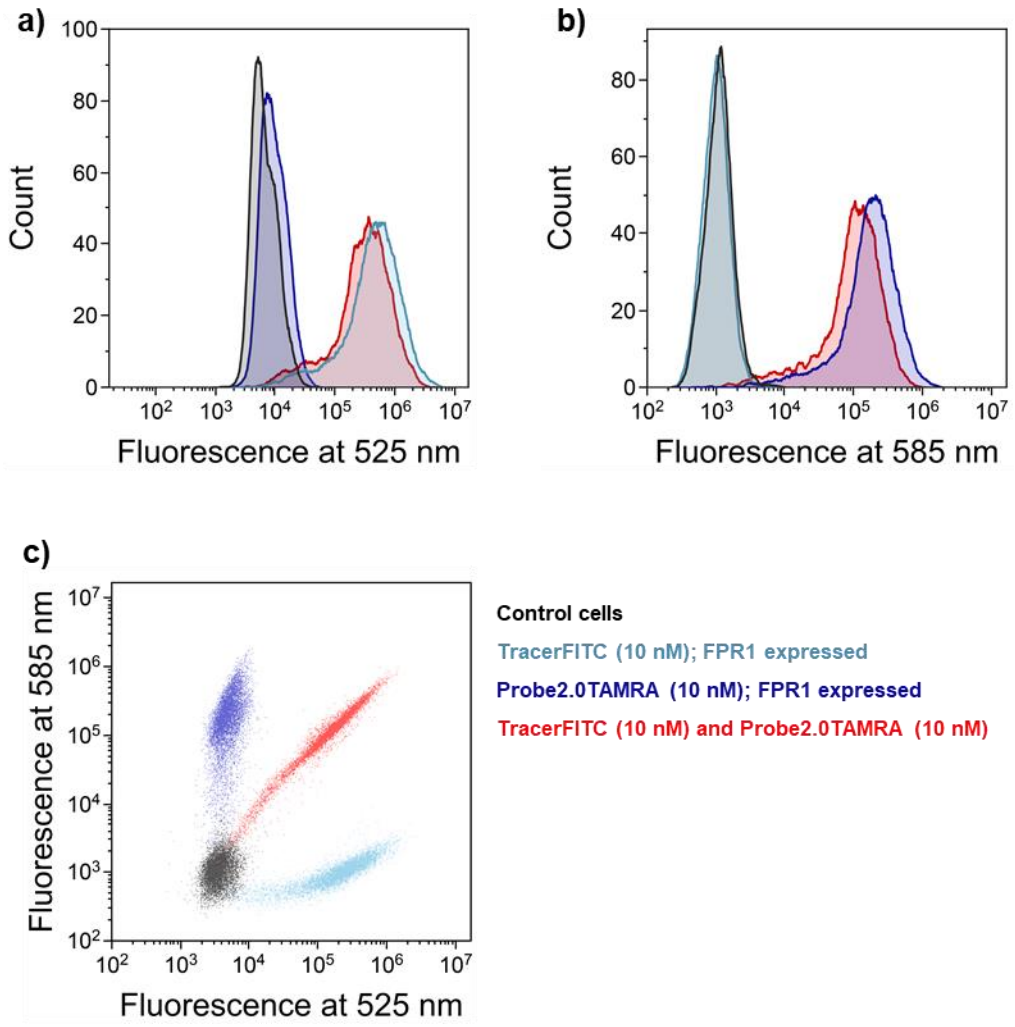

Figure 4.5: Competition between TracerFITC and Probe2.0TAMRA; a) histogram of TracerFITC fluorescence at 525 nm in the presence (red) and absence (grey-blue) of Probe2.0TAMRA; b) histogram of Probe2.0TAMRA fluorescence at 585 nm in the presence (red) and absence (blue) of TracerFITC; c) dot plot showing fluorescence at 525 and 585 nm when TracerFITC and Probe2.0TAMRA incubated separately and simultaneously with FPR1-expressing cells.

The competition between the two peptides was further explored by increasing the concentration of Probe2.0TAMRA from 1 to 200 nM but holding the concentration of TracerFITC constant at 10 nM. With each increase in Probe2.0TAMRA concentration, the fluorescence at 525 nm decreased, showing less binding of TracerFITC (**Figure 4.6**). The fluorescence at 585 nm increased concurrently with probe concentration as more Probe2.0TAMRA became bound to FPR1.

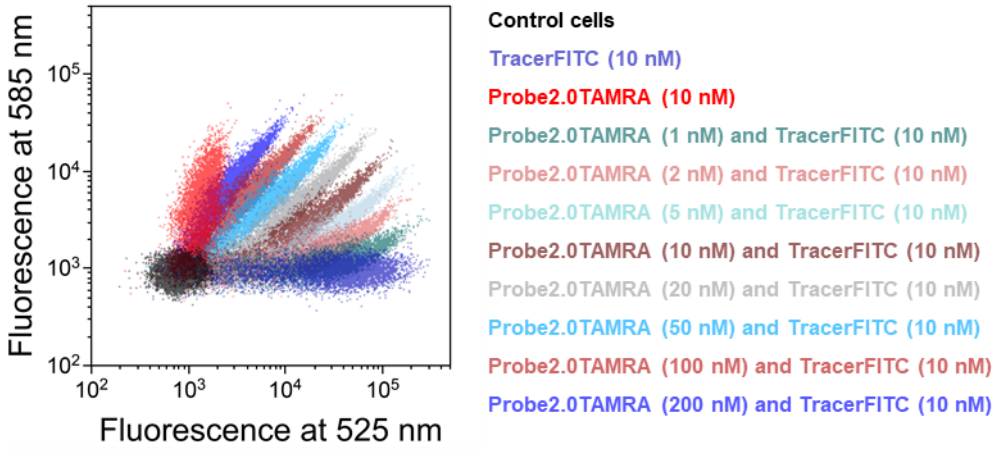

Figure 4.6: Competition between TracerFITC and Probe2.0TAMRA with increasing concentrations of Probe2.0TAMRA; dot plot showing shift of fluorescence from 525 to 585 nm with increasing concentration of Probe2.0TAMRA.

Furthermore, the total FITC and TAMRA fluorescence was calculated for each concentration of Probe2.0TAMRA and the percentage of the maximum fluorescence was plotted against the concentration of Probe2.0TAMRA (**Figure 4.7**). The two fluorescence curves in **Figure 4.7** intersect at 11.2 nM. This shows that the two peptides have similar binding affinities for FPR1, and that the presence of TAMRA and photo-Met in Probe2.0TAMRA does not compromise the binding.

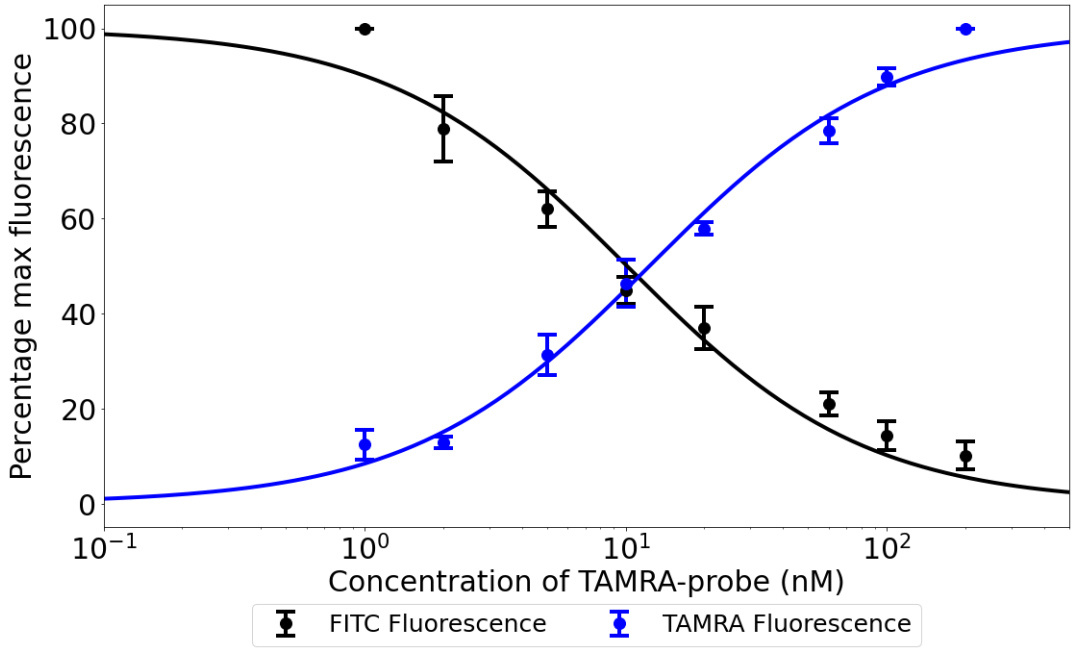

Figure 4.7: Percentage max fluorescence of TracerFITC and Probe2.0TAMRA in competition experiment calculated from flow cytometry; three biological replicates performed with bars representing standard error.

4.2.4 Competitive Binding Between Probe2.0TAMRA and Known Agonist fMLF and Antagonist Boc-MLF

As discussed in Chapter 1, fMLF is a known agonist of FPR1 and binds strongly with an IC_{50} reported in the nanomolar range (L *et al.* reported an IC_{50} of 0.1-1 nM measured from a Ca^{2+} mobilisation assay).[10] Substituting the N-terminal formyl group with a Boc protecting group (Boc-MLF), results in a peptide with antagonistic properties towards FPR1.[8, 23] Higher concentrations of Boc-MLF are predicted to be required to block the binding of Probe2.0TAMRA, with concentrations in the micromolar range (10-50 µM) being previously reported.[133, 134] There has been concern reported that these higher concentrations remove the specificity of Boc-MLF for FPR1 over FPR2.[8, 27] Fortunately, FPR2 is not expressed in HEK293T cells (The Human Protein Atlas).[123]

The competition between Probe2.0TAMRA and fMLF/Boc-MLF was tested using a similar method as for the competition with TracerFITC. HEK293T cells expressing FPR1 were incubated with Probe2.0TAMRA (50 nM) and either fMLF (50 nM) or Boc-MLF (10 µM). The fluorescence of the cells was measured at 585

nm and the intensity compared to that of cells incubated with Probe2.0TAMRA alone. Unfortunately, no decrease in fluorescence was observed for the competition with fMLF, and only a small decrease for the competition with Boc-MLF (**Figure 4.8**).

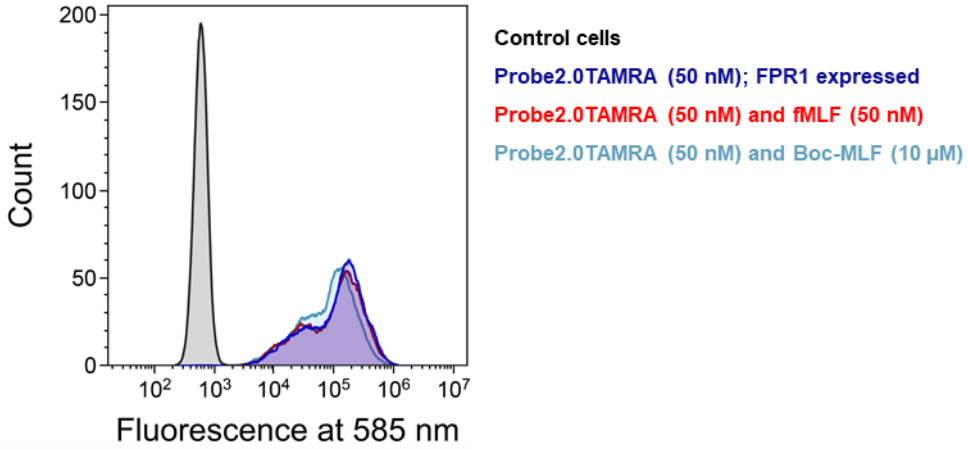

Figure 4.8: Histogram showing the competition between Probe2.0TAMRA and fMLF or Boc-MLF.

Decreasing the concentration of Probe2.0TAMRA to 10 nM and testing higher concentrations of Boc-MLF (20 and 50 µM), revealed clear competition between the two peptides (**Figure 4.9**).

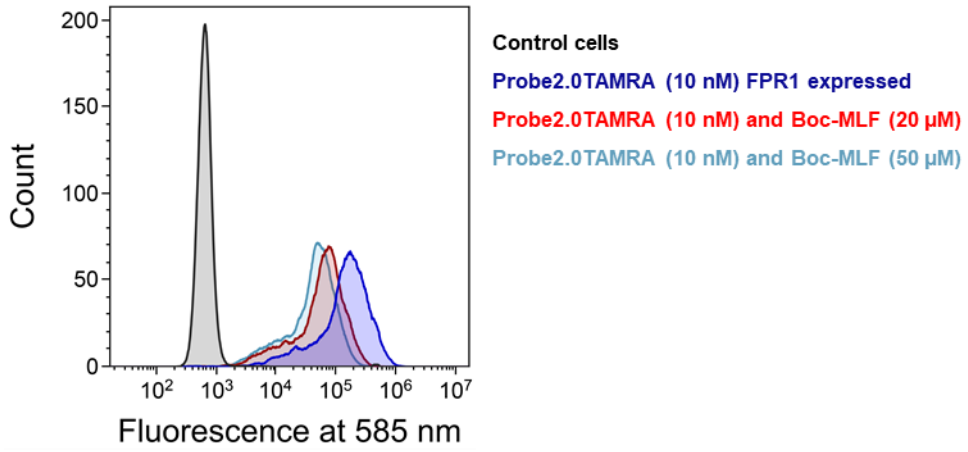

Figure 4.9: Histogram showing the competition between Probe2.0TAMRA and Boc-MLF

Decreasing the concentration of Probe2.0TAMRA to 10 nM and testing three concentrations of fMLF (50, 100 and 200 nM), still produced almost no reduction in fluorescence intensity. This was a very strange result to encounter, given the

supposed nanomolar binding of fMLF to FPR1 and the approximate calculation of a 4 nM K_d for Probe2.0TAMRA. Increasing the concentration of fMLF to a higher range (50 nM – 20 µM) showed competition between the peptides from an fMLF concentration of 1 µM (**Figure 4.10**). Interestingly, other groups have reported the use of fMLF at higher concentrations to achieve competition with other peptidic ligands.[22, 46, 48] Liu *et al.* report the use of fMLF at 10 µM to inhibit fNLFNYK at 2 nM.[46] He *et al.* has reported the competition of fMLF with WK(FITC)MMVm (2.5 nM) and fMLFIIK(FITC) (50 nM) on human and mouse FPR1 respectively. Significant competition was not observed until ~100 nM with WK(FITC)MMVm and 1-10 µM for fMLFIIK(FITC).[22, 48]

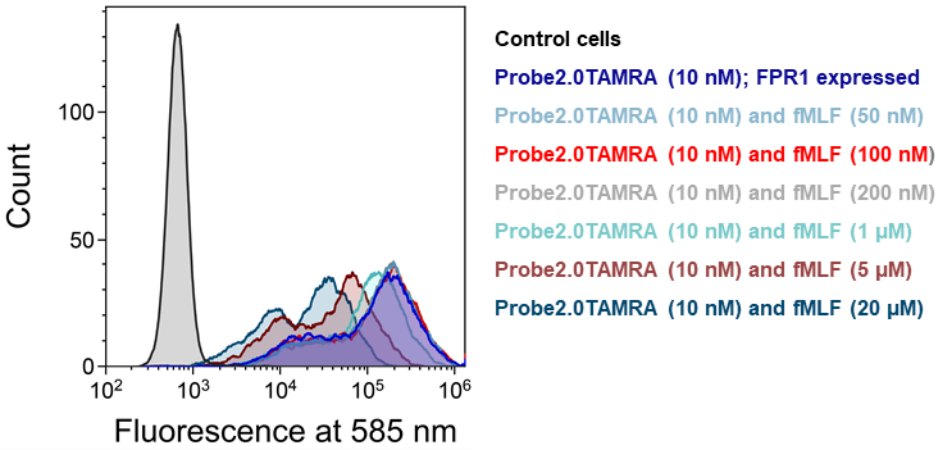

Figure 4.10: Histogram showing the competition between Probe2.0TAMRA and fMLF at a range of concentrations (50 nM – 20 µM).

4.2.5 Binding of Probe2.0TAMRA to Endogenously Expressed FPR1

To assess the binding of Probe2.0TAMRA with endogenously expressed FPR1, the GMS-10 cell line (supplied by DSMZ) was used. GMS-10 cells are derived from brain cancer and show high expression of FPR1.[135] As FPR1 transfection was not necessary, once seeded the cells were left to grow for 48 hrs at 37 °C. Following suspension, the cells were incubated with Probe2.0TAMRA (50 nM) and the fluorescence of the cells measured with flow cytometry. Excitingly, an increase in fluorescence intensity was observed compared with control GMS-10 cells (**Figure 4.11**).

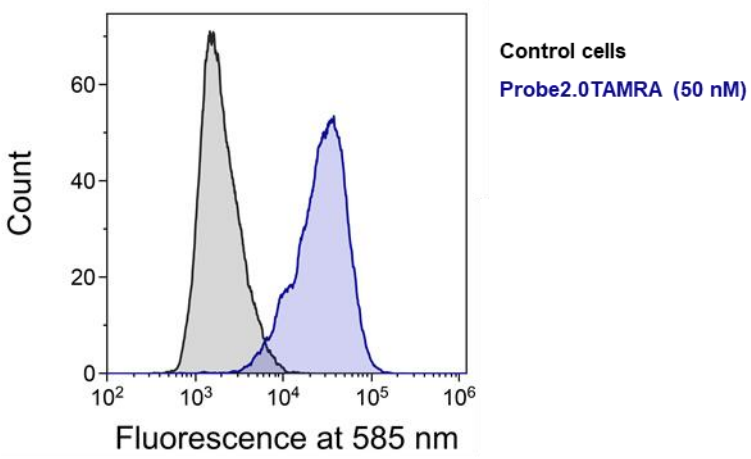

Figure 4.11: Histogram showing the binding of Probe2.0TAMRA to FPR1 expressed on GMS-10 cells.

The shift in fluorescence intensity appears less than for the binding experiment performed with HEK293T cells. This is partially due to the increased background fluorescence of GMS-10 cells (mean fluorescence intensity = 2340) compared with HEK293T cells (mean fluorescence intensity = 940). However, the mean fluorescence intensity observed when Probe2.0TAMRA is bound is also less than for HEK293T cells (mean fluorescence intensities: HEK293T = 240,080; GMS-10 = 32,470). This is expected because the endogenous expression of FPR1 on GMS-10 cells is likely to be a lot lower than with the transient transfection of HEK293T cells.

4.3 Confocal Microscopy to Image the Internalisation of FPR1

It is well-known that upon agonist binding, GPCRs internalise following activation of G protein subunits. The internalisation results in receptor desensitisation, preventing over-activation of the receptor.[9] Formyl peptides act as agonists towards FPR1.[10] The binding of TMR-peptide to FPR1 and the internalisation of the ligand-receptor complex has been previously imaged using confocal microscopy.[41] This experiment was conducted with Probe2.0TAMRA to confirm its agonistic binding to FPR1. A glass bottom culture dish was used to grow and transfect the HEK293T cells, from which the cells could be imaged without fixing. The cells were incubated with Probe2.0TAMRA (10 nM) on ice for 30 mins and

subsequently washed with PBS to remove any unbound probe. The plate was then imaged using a confocal microscope. The transfected cells incubated with Probe2.0TAMRA displayed fluorescence at 561 nm on the membranes of the cells (**Figure 4.12**). This shows the probe binds to FPR1 expressed on the cell membrane and does not enter the cell under these conditions. The control samples showed no fluorescence, further demonstrating the specificity of Probe2.0TAMRA.

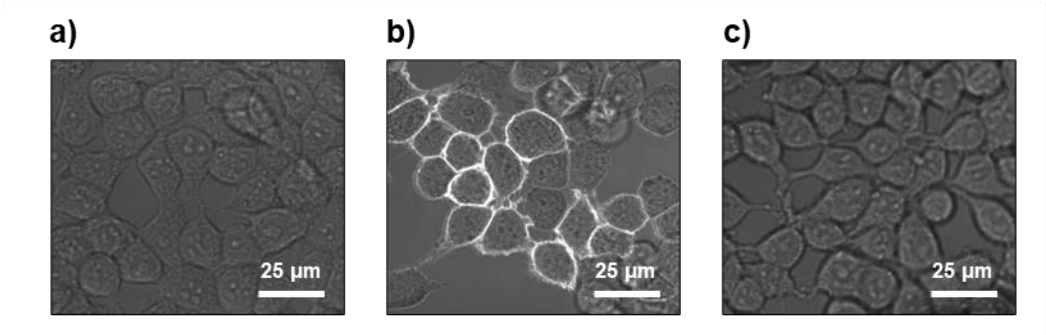

Figure 4.12: Confocal microscopy images of HEK293T cells incubated with Probe2.0TAMRA on ice; a) FPR1 expressed with no Probe2.0TAMRA; b) FPR1 expressed and cells incubated with Probe2.0TAMRA; c) FPR1 not expressed and incubated with Probe2.0TAMRA; images are the overlay of brightfield and fluorescence at 561 nm.

To image the internalisation of FPR1 through the binding of Probe2.0TAMRA, the cells were heated to 37 °C and viewed for 16 min. The fluorescent material was seen to transfer from the cell membrane to the cytosol (**Figure 4.13**), showing that Probe2.0TAMRA is causing internalisation of FPR1.

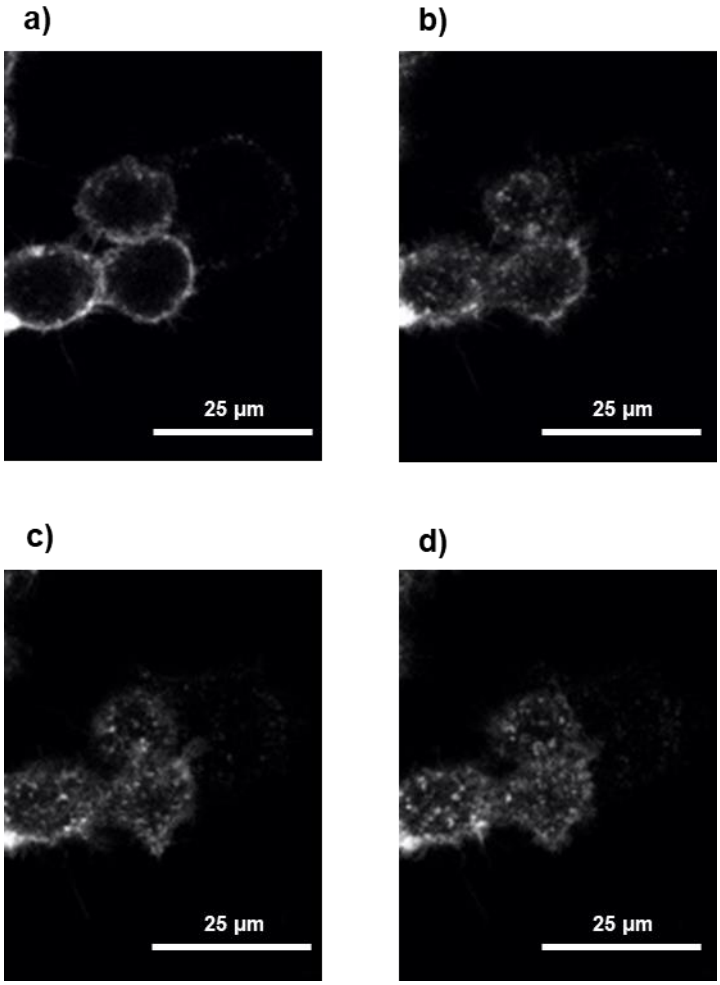

Figure 4.13: Time course of internalisation of probe-FPR1 complex; HEK293T cells transfected overnight at 37 °C, incubated with 10 nM Probe2.0TAMRA at 0 °C for 30 min; fluorescence imaged at 561 nm with confocal microscope for approximately 16 mins after cells were warmed to 37 °C; a) t = 0 mins, b) t = 5 mins, c) t = 12 mins, d) t = 16 mins.

Given the similarity between Probe2.0TAMRA and TMR-peptide, this internalisation was expected and confirms that the replacement of norleucine in position two with photo-Met does not affect the binding to FPR1. The internalisation of Probe2.0TAMRA and TMR-peptide follow a comparable pattern, beginning with the appearance of fluorescent aggregates on and near the cell membrane (**Figure 4.13, b**). The fluorescent aggregates near the cell membrane then form vesicles in the cytoplasm and the clear outline of the cell is lost (**Figure 4.13, c**). These vesicles then merge into bigger vesicles, which fluoresce more on the confocal image (**Figure 4.13, d**). All human neutrophils internalised TMR-peptide at the same rate and to the same extent.[41] This was not the case for

Probe2.0TAMRA with FPR1 expressed on HEK293T cells. Not all cells had fluorescent material on the surface, and those that did showed different rates of internalisation. This may be because the expression of FPR1 is not homogeneous due to transient transfection. However, both TMR-peptide and Probe2.0TAMRA showed no internalisation below 10 °C.

4.4 Binding and Crosslinking of Probe2.0TAMRA to FPR1

The binding and crosslinking of Probe2.0TAMRA to FPR1 expressed on HEK293T cells was achieved using an alternative method to the generation 1.0 probes (**Scheme 4.1**). The transient transfection was performed using the same process as for the generation 1.0 probes. However, instead of incubating the cells with Probe2.0TAMRA in the culture wells, the cells were suspended in PBS and transferred to tubes. The incubation with Probe2.0TAMRA was then performed using the same method as for flow cytometry. The cells were then illuminated with UV light using a UV LED device constructed by Horne *et al.* for diazirine crosslinking.[136] This UV LED device can hold 1.5 mL tubes and irradiates the sample with 365 nm light for 30 s. Horne *et al.* showed that the UV LED device achieved maximal crosslinking yields for an aliphatic diazirine in 10 seconds with less than 2 °C sample heating. Comparatively, when a 6W Hg-Xe lamp was used, crosslinking took 20 minutes with 10 °C sample heating. The UV LED device showed a 130-fold improvement in crosslinking rate and a 6-fold decrease in sample heating.[136] Following crosslinking of Probe2.0TAMRA, the cells were lysed, and their protein concentrations measured using a DC protein assay (Biorad) as before. The TAMRA fluorophore incorporated in Probe2.0TAMRA instead of the alkyne tag used in the generation 1.0 probes removed the need for a CuAAC reaction. Following cell lysis, the samples could be immediately imaged using SDS-PAGE.

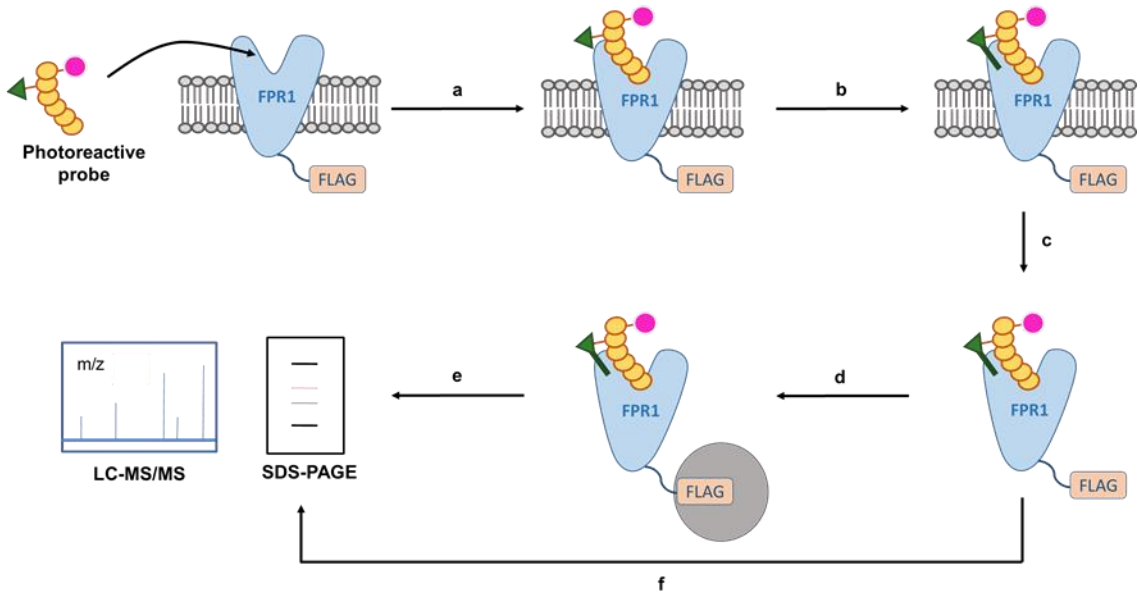

Scheme 4.1: Work-flow of binding and crosslinking of generation 2.0 probes to FPR1 expressed on the surface of HEK293T cells; a) binding of probe to FPR1; b) photo-crosslinking of probe to FPR1 by irradiation of UV light at 365 nm; c) lysis of the cells; d) immunoprecipitation of FPR1-probe complex from cell lysate to anti-FLAG resin using the FLAG-tag present at the C-terminus of FPR1; e) elution of FPR1-probe complex from anti-FLAG resin and analysis by SDS-PAGE or LC-MS/MS; f) analysis of cell lysate by SDS-PAGE.

To test the crosslinking of Probe2.0TAMRA to FPR1, transfected and non-transfected cells were incubated with the probe (1 mL PBS, 10 nM, 30 mins) and irradiated with UV light (365 nm). Following cell lysis, in-gel fluorescence at 550 nm was used to identify crosslinking to FPR1. In the sample with transfected HEK293T cells, a single fluorescent band was observed between 75 and 50 kDa, at the expected molecular weight for glycosylated FPR1, which matched the FPR1 band present in the anti-FLAG Western Blot (**Figure 4.14**). This suggested that Probe2.0TAMRA had crosslinked to FPR1.

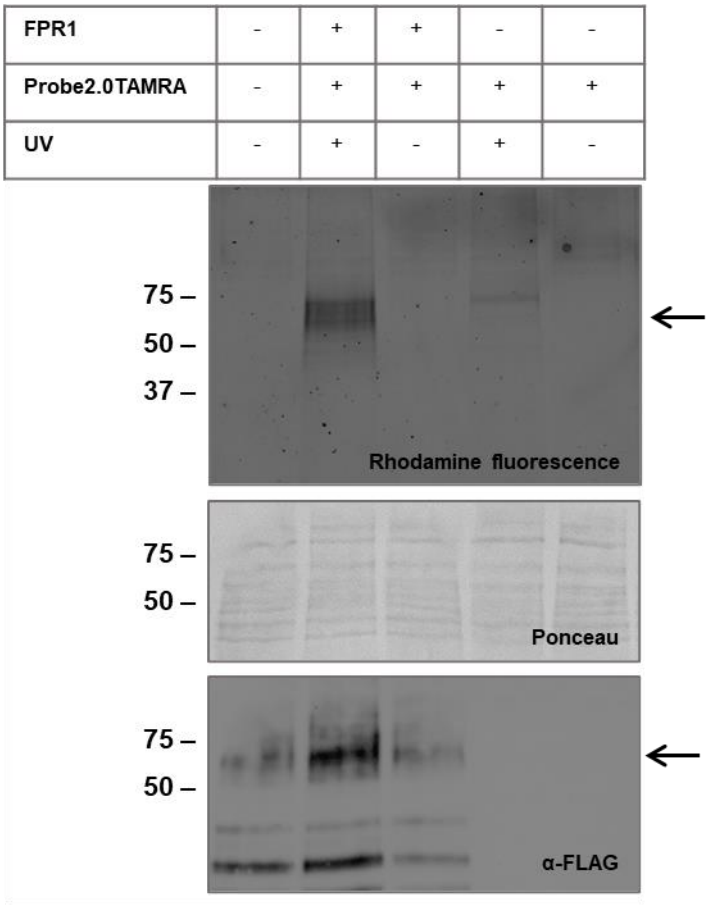

Figure 4.14: SDS-PAGE and Western Blot analysis of crosslinking experiment for Probe2.0TAMRA; transfected HEK293T cells were suspended, incubated with Probe2.0TAMRA and irradiated with UV light (365 nm), following cell lysis SDS-PAGE analysis was performed including in-gel fluorescence at 550 nm and anti-FLAG Western Blotting; Ponceau staining of the Western Blot was also performed to indicate the total protein concentration in each sample, FPR1 indicated with arrow.

A weak signal at 75 kDa was detected in the sample with no FPR1 expression suggesting that non-specific crosslinking is occurring. It is likely that this corresponds to the small hump observed in flow cytometry when FPR1 was not expressed (**Figure 4.3**). This off-target band is not observed in the FPR1+ lane, most likely due to the bright FPR1-Probe2.0TAMRA band. No fluorescence was observed in the samples that were not irradiated with UV light, proving UV-dependent labelling. An additional sample was incubated with Probe2.0TAMRA at room temperature versus 0 °C, to investigate whether this would improve binding/crosslinking. However, this did not appear to have a significant effect

(data not shown). Therefore, future crosslinking experiments were performed at 0 °C to ensure no internalisation occurred.

4.4.1 Experimentation of Repeated Crosslinking

The crosslinking was also analysed using flow cytometry. The cells were incubated and irradiated with Probe2.0TAMRA. Following irradiation, the solution containing Probe2.0TAMRA was removed and the cells were washed with PBS. The cells were then incubated with TracerFITC and the fluorescence measured with flow cytometry. A decrease in fluorescence at 525 nm was observed compared with no competition (**Figure 4.15**). However, the decrease was less significant than for direct competition between Probe2.0TAMRA and Tracer-FITC, suggesting that not all bound Probe2.0TAMRA successfully crosslinked to FPR1. The experiment was repeated, with the addition of two incubations and irradiations with Probe2.0TAMRA. An increase in the amount of receptor crosslinked was signified by a larger decrease in fluorescence intensity at 525 nm (**Figure 4.15**).

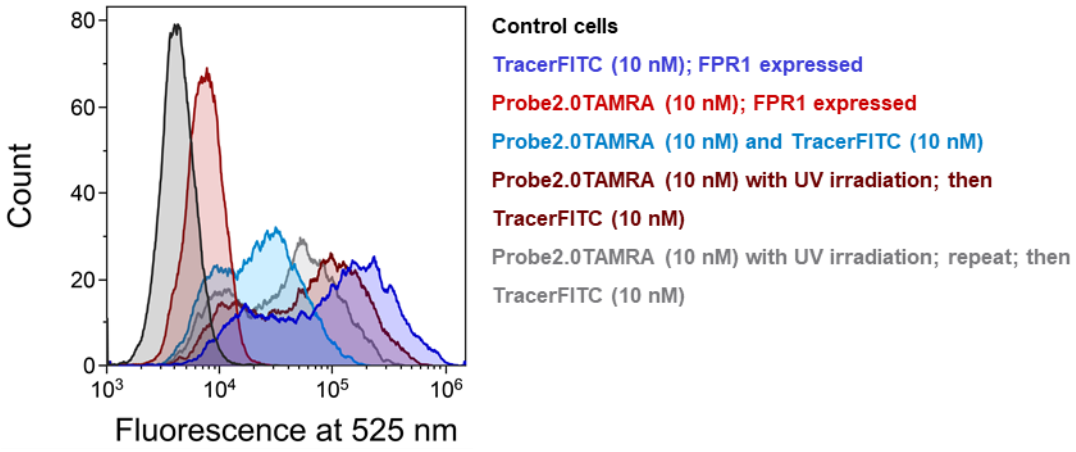

Figure 4.15: Histogram showing the fluorescence at 525 nm of HEK293T cells crosslinked with Probe2.0TAMRA and subsequently incubated with TracerFITC; 10,000 cells per sample measured.

The dual crosslinking of Probe2.0TAMRA was repeated with SDS-PAGE analysis, to examine the effects on non-specific labelling (**Figure 4.16**). Increased crosslinking was observed when two irradiations were performed. However, from

SDS-PAGE analysis it is difficult to determine the significance of three irradiations and the increase of the non-specific binding.

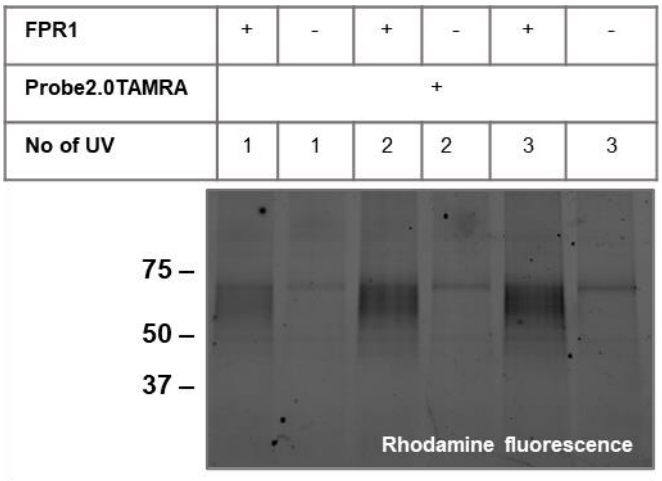

Figure 4.16: In-gel fluorescence analysis of repetitive crosslinking of Probe2.0TAMRA to FPR1.

ImageJ was used to quantify the intensity of the bands detected during in-gel fluorescence. This analysis revealed that crosslinking almost doubles when the sample is incubated with Probe2.0TAMRA and irradiated a second time (**Figure 4.17**). However, the increase with a third crosslinking is much less significant. This result is the same for the off-target band observed when FPR1 is not expressed. Additionally, the protein concentration for the cell lysis samples irradiated three times was lower suggesting there was an increased loss in cells with more transfer of solutions. Therefore, to increase crosslinking the incubation of Probe2.0TAMRA and irradiation of cells can be performed twice.

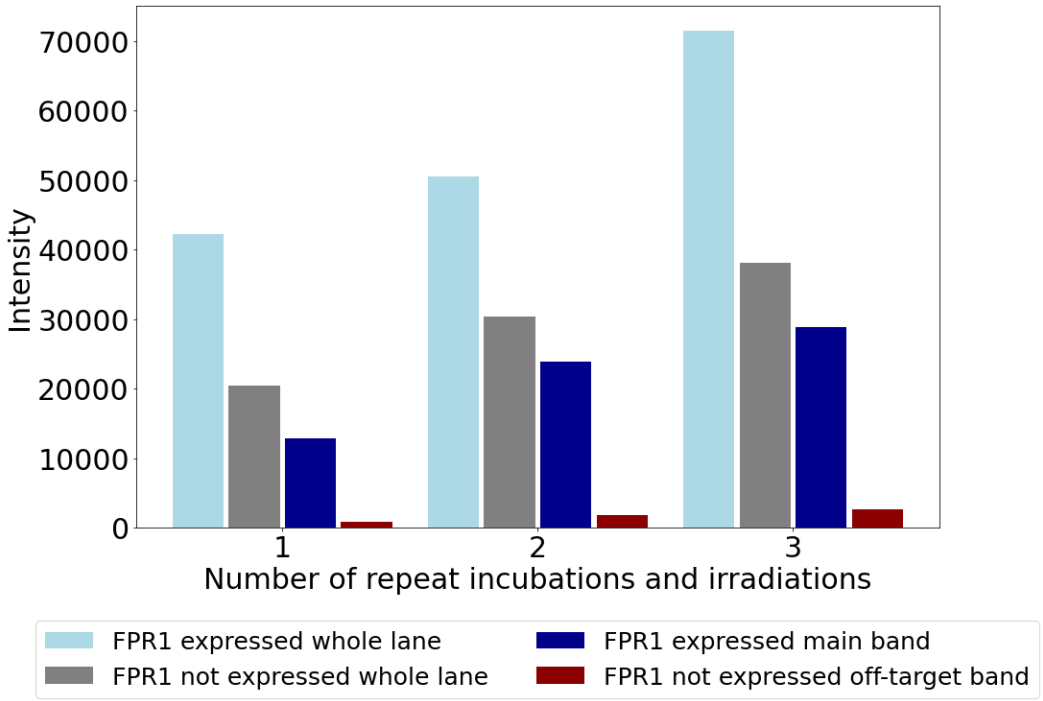

Figure 4.17: Quantification of band intensity for repetitive crosslinking of Probe2.0TAMRA to FPR1, performed with ImageJ.

4.5 Generation 2.1

4.5.1 Generation 2.1 Probe Design and Synthesis

The specific binding and crosslinking of Probe2.0TAMRA to FPR1 was successful. As an alternative structure, this probe was synthesised again, replacing the TAMRA fluorophore with a desthiobiotin tag (**Figure 4.18**). To identify the crosslink site, the probe-receptor complex must be purified from the cell lysate. Incorporating a desthiobiotin tag in the probe allows enrichment of this complex via the probe. Therefore, only crosslinked FPR1 would be enriched. The high affinity binding between streptavidin and biotin is well-known as the strongest biological covalent bond and for that reason it is commonly utilised in chemical biology experiments.[137] Target peptides and proteins are often biotinylated so their purification can be achieved through the use of a streptavidin pull-down. However, due to the strong streptavidin-biotin bond, elution requires harsh conditions such as high temperatures which would aggregate FPR1.

Desthiobiotin is a biotin analogue that doesn't contain sulphur atoms and binds less strongly to streptavidin (by several orders of magnitude).[137] It can therefore be eluted from streptavidin with mild conditions such as a biotin solution.

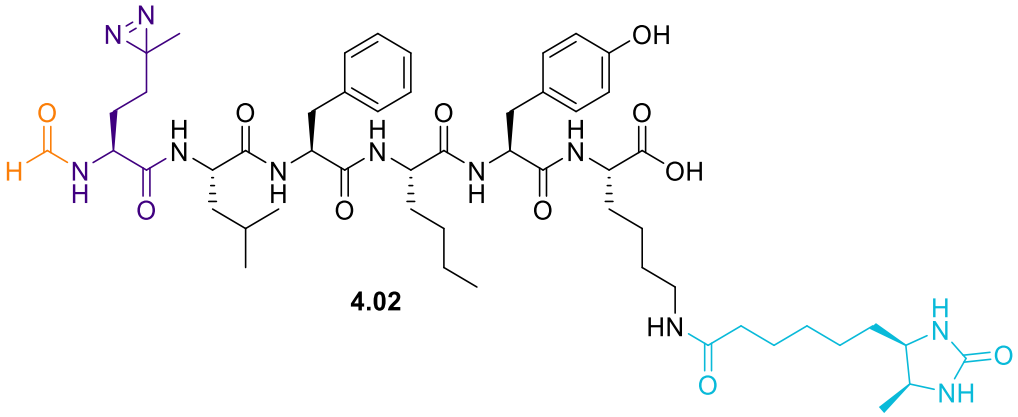

Figure 4.18: Structure of generation 2.1 probe (Probe2.1Desthio).

Probe2.1Desthio was synthesised using similar methods as the previous peptides, using instead a preloaded Fmoc-Lys(*iv*Dde) Wang resin. The *iv*Dde protecting group on the lysine side chain was removed using 8% hydrazine in DMF following *N*-formylation. The desthiobiotin was coupled using HCTU and DIPEA, as coupling was unsuccessful when performed using Oxymapure and DIC. After cleavage and purification using mass-directed HPLC, Probe2.1Desthio was isolated in >99% purity determined via analytical HPLC and 11% yield (HPLC shown in section 9.1.2.5).

4.5.2 Flow Cytometry to Test the Binding of Probe2.1Desthio

The binding of Probe2.1Desthio to FPR1 was tested through competitive binding with TracerFITC, using a similar method as the first-generation probes. The concentration of TracerFITC was kept constant and four different concentrations of Probe2.1Desthio were tested and monitored for a change in fluorescence intensity. HEK293T cells expressing FPR1 were incubated with TracerFITC (10 nM) and Probe2.1Desthio (10-1000 nM). The fluorescence of the cells incubated with both peptides was indeed lower than when incubated with just TracerFITC (**Figure 4.19**). The fluorescence also decreased further as the concentration of Probe2.1Desthio increased. This shows that the two peptides compete for the

same binding site on FPR1 and that Probe2.1Desthio binds to the formyl peptide binding site.

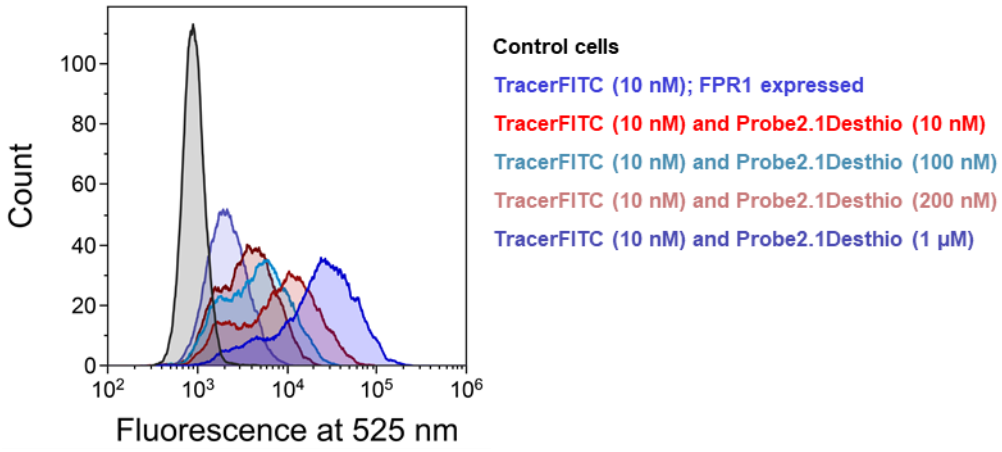

Figure 4.19: Competitive binding between TracerFITC and Probe2.1Desthio to FPR1; both peptides incubated with HEK293T cells expressing FPR1 simultaneously.

4.5.3 Binding and Crosslinking of Probe2.1Desthio

To test the crosslinking of Probe2.1Desthio to FPR1, transfected and non-transfected cells were incubated with the probe (1 mL, 50 nM) and irradiated with UV light (365 nm), using a method analogous to that used for Probe2.0TAMRA. Following cell lysis, a Streptavidin-HRP Western Blot was used to assess crosslinking to FPR1. Unfortunately, no signal was observed (not shown), suggesting that Probe2.1Desthio was not crosslinking to FPR1. A streptavidin and anti-FLAG pull-down were performed, to determine if the signal detection on the Western Blot was the problem. However, there was still no signal detected. A comparison of the binding (analysed by competition with TracerFITC in flow cytometry) between Probe2.1Desthio and Probe2.0TAMRA (**Figure 4.20**) shows that Probe2.1Desthio has a lower binding affinity for FPR1. However, this does not appear significant enough to completely hinder crosslinking.

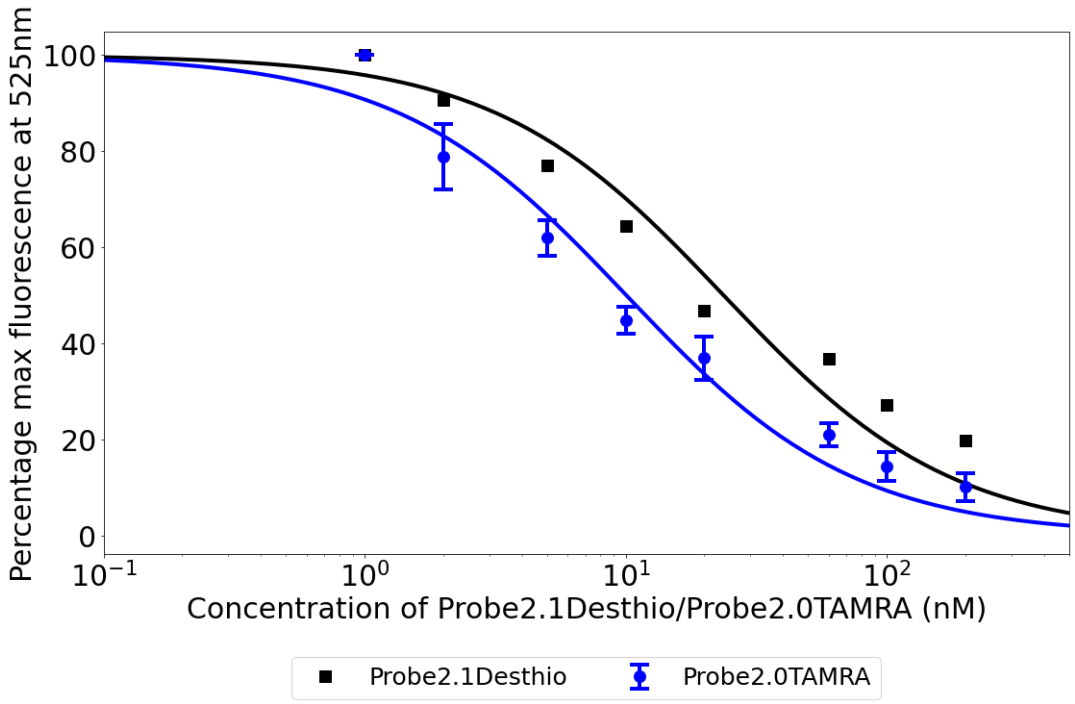

Figure 4.20: Competition between TracerFITC and Probe2.1Desthio/Probe2.0TAMRA

Comparing Probe2.0TAMRA and Probe2.1Desthio, the bigger, bulkier TAMRA fluorophore is likely to be less buried in the FPR1 binding pocket and therefore more easily accessible to an antibody for Western Blot analysis. The fluorescence of the TAMRA group is also observable during in-gel fluorescence allowing for simpler analysis. It is possible that the smaller desthiobiotin tag is buried in the binding pocket and not available to the streptavidin-HRP antibody. A possible solution to this would be to install a linker between the lysine residue and the desthiobiotin tag. However, the crosslinking was first analysed using flow cytometry (**Figure 4.21**). Following incubation and irradiation with Probe2.1Desthio, the cells were incubated with Probe2.0TAMRA. Unfortunately, no decrease in fluorescence was observed compared with Probe2.0TAMRA alone. This supports the hypothesis that Probe2.1Desthio is not crosslinking to FPR1 with significant yield.

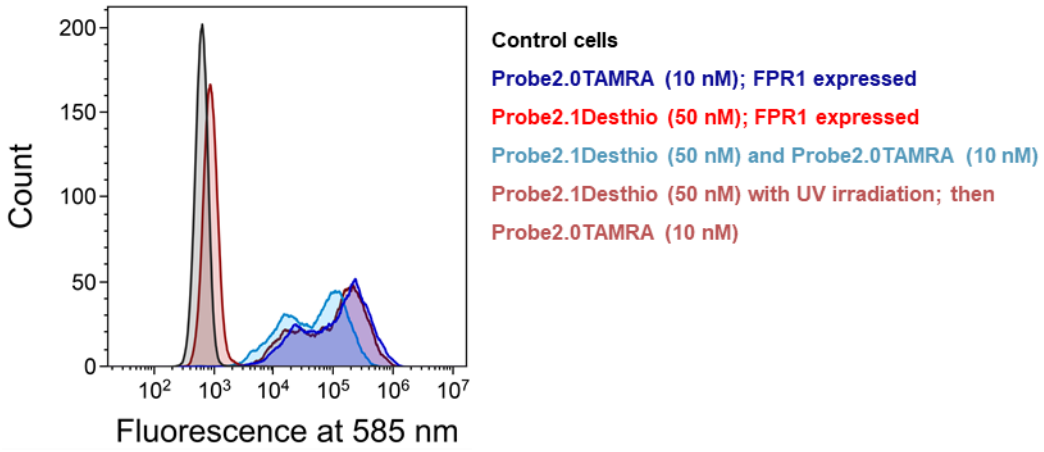

Figure 4.21: Histogram showing the fluorescence at 585 nm of HEK293T cells crosslinked with Probe2.1Desthio and subsequently incubated with Probe2.0TAMRA; 10,000 cells per sample measured.

The data from the flow cytometry experiments suggest that Probe2.1Desthio is binding but not crosslinking. Although Probe2.1Desthio and Probe2.0TAMRA appear to have similar binding affinities to FPR1 (**Figure 4.20**), the on- and off-rates of binding have not been investigated. The TAMRA fluorophore in Probe2.0TAMRA is hydrophobic and though it is neutral in solution it is zwitterionic and possesses a negative and positive charge. These charges can form strong salt bridges with charged residues on the FPR1 binding pocket. The TAMRA fluorophore also contains aromatic rings that can interact with FPR1 through π-stacking. This could contribute to a slower off-rate than Probe2.1Desthio, allowing crosslinking to occur. No further binding or crosslinking was carried out with Probe2.1Desthio.

4.6 Generation 2.2 Probes

Given the success of Probe2.0TAMRA but the failure to identify crosslinking of Probe2.1Desthio, an additional generation of probe was designed exploring an alternative diazirine (**Figure 4.22**). For the identification of the crosslink site, the added mass of the probe is searched amongst the peptide products from protein digestion. However, the probe can be digested itself, and may also fragment during mass spectrometry, making it difficult to predict the added mass.

Cleavable probes can be used to provide a “dead end” with a definitive mass addition. Employing cleavable linkers in photoaffinity probes is becoming more popular for the study of biological molecules.[138] These cleavable linkers are advantageous for the purification of the crosslinked target receptor and for identification in mass spectrometry.[136, 138] A cleavable linker is defined as a molecule with two separate functional heads connected by a cleavable bond. There are several types of cleavable linkers including nucleophile/base sensitive linkers, photocleavable linkers, enzymatically cleavable linkers and reduction sensitive linkers.

Disulphides linkers are a reduction sensitive cleavable bond that are efficiently and rapidly cleaved by mild reducing agents. Disulphide linkers were first applied to crosslinking and proteomics in 1973 by Traut *et al.* using mercaptobutyrimidate.[139]

4.6.1 Generation 2.2 Probe Design and Synthesis

MTS-diazirine **4.05** and MTS-alkynyldiazirine **4.06** (**Figure 4.23**) were incorporated into the peptide in the position of the second norleucine at position four of Probe2.0TAMRA.

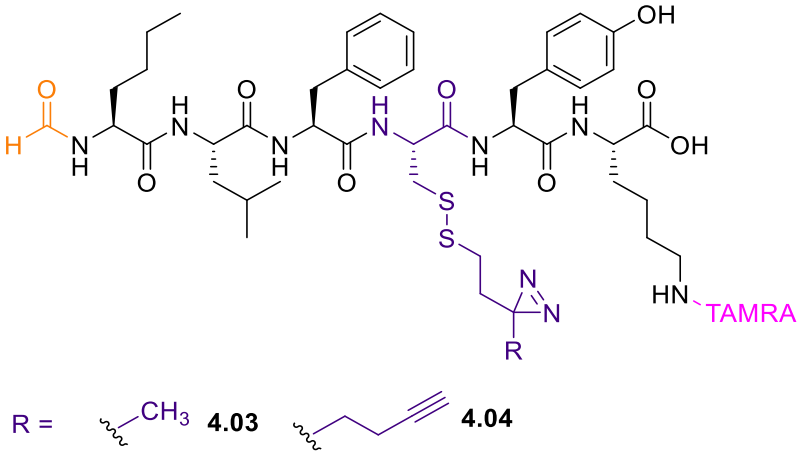

Figure 4.22: Structure of generation 2.2 probes (Probe2.2SDi **4.03** and Probe2.2SDiAlk **4.04**) synthesised by Mehreen Khan.

The disulphide linked diazirines installed in the generation 2.2 probes were inspired by the work of Horne *et al.*[136] and Walko *et al.*[140] Incorporating a

disulphide link between the peptide backbone and the diazirine allows cleavage of the peptide backbone following crosslinking and immunoprecipitation (**Scheme 4.2**). This leaves a thiol "dead-end" crosslinked to the target protein that is more easily located during tandem mass spectrometry. These alternative diazirines have been placed at residue four in the probe, to allow an alternative crosslink location to FPR1 than Probe2.0TAMRA.

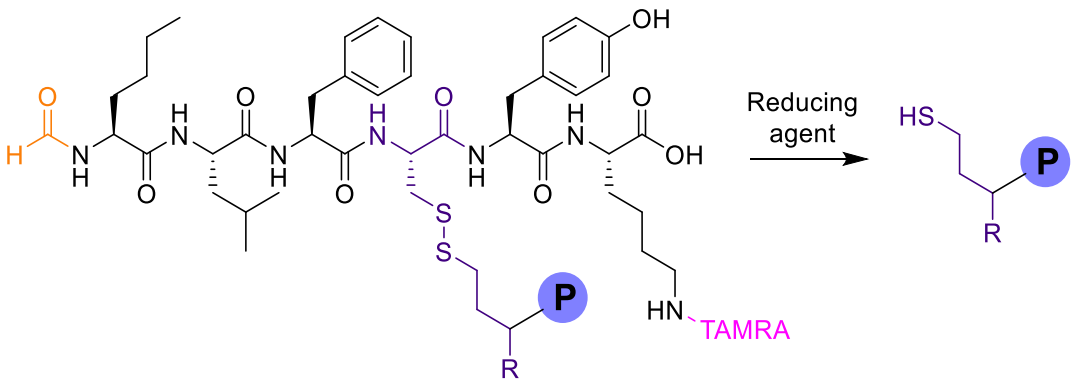

Scheme 4.2: Reductive cleavage of disulphide bond in Probe2.2SDi/SDiAlk crosslinked to protein target (P).

Probe2.2SDi and Probe2.2SDiAlk were synthesised using similar methods as the previous peptides, using a preloaded Fmoc-Lys(*iv*Dde) Wang resin, by Mehreen Khan (MChem student under my supervision). A cysteine residue was coupled at position four for installation of the disulphide linked diazirines following cleavage from the resin. Formylation of the N-terminus, coupling of the TAMRA fluorophore and cleavage from the resin were all performed as before.

MTS-diazirine **4.05** (**Figure 4.23**) can be prepared in three steps from 4-hydroxybutan-2-one[136] and MTS-alkynyldiazirine **4.06** (**Figure 4.23**) can be prepared in seven steps from ethyl acetoacetate.[140] The MTS-diazirine and MTS-alkynyldiazirine were synthesised and provided by Martin Walko.

Figure 4.23: Structure of MTS-diazirine and MTS-alkynyldiazirine synthesised by Martin Walko

After cleavage from the resin, the MTS-diazirine/MTS-alkynyldiazirine were dissolved in minimal methanol and added to the peptide (**Scheme 4.3**). The solution was left in darkness for 30 min before being purified using mass-directed HPLC. Probe2.2SDi was isolated in 89% purity determined via analytical HPLC and 10% yield (HPLC shown in section 9.1.2.6). Probe2.2SDiAlk was isolated in 86% purity determined via analytical HPLC and 10% yield (HPLC shown in section 9.1.2.7).

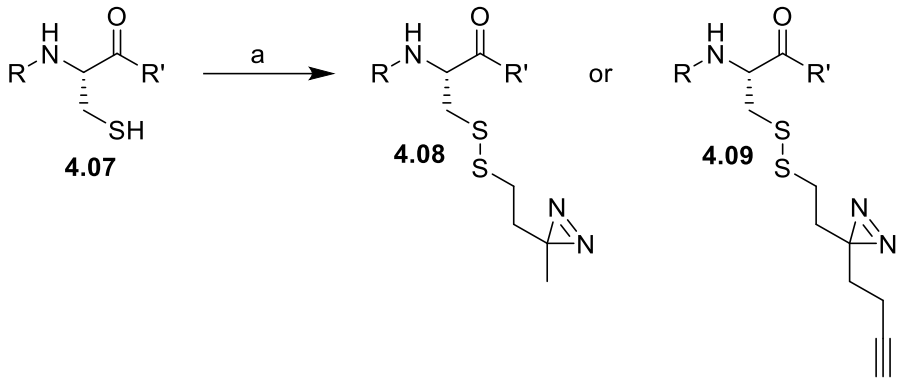

Reagents and conditions: *(a) MTS-diazirine/MTS-alkynyldiazirine, MeOH*

Scheme 4.3: Coupling of MTS-diazirine/MTS-alkynyldiazirine to cysteine residue in peptide

4.6.2 Flow Cytometry to Test the Binding of Probe2.2SDi and Probe2.2SDiAlk

4.6.2.1 Specific Binding of Probe2.2SDi and Probe2.2SDiAlk

The synthesised Probe2.2SDi and Probe2.2SDiAlk were incubated with HEK293T cells expressing FPR1, and HEK293T cells not expressing FPR1. The fluorescence of these samples was then analysed using flow cytometry, as with Probe2.0TAMRA, to examine the specific binding to FPR1. Both Probe2.2SDi and Probe2.2SDiAlk showed binding to FPR1 with limited non-specific binding (**Figure 4.24**). However, the shift in fluorescence is significantly lower (mean fluorescence intensities: Probe2.0TAMRA = 240,080; Probe2.2SDi = 3680; Probe2.2SDiAlk = 3260) than for Probe2.0TAMRA, suggesting that Probe2.2SDi and Probe2.2SDiAlk have lower binding affinities for FPR1. This indicates that the change in diazirine and location of that diazirine on the probe have affected binding. The histograms for the binding of Probe2.2SDi/Probe2.2SDiAlk to FPR1 contain two peaks. The lower intensity peaks occur at the same intensity as the

histogram peak for the control cells, suggesting a population of cells where no probe has bound. This further supports a lower binding affinity for Probe2.2SDi/Probe2.2SDiAlk than Probe2.0TAMRA.

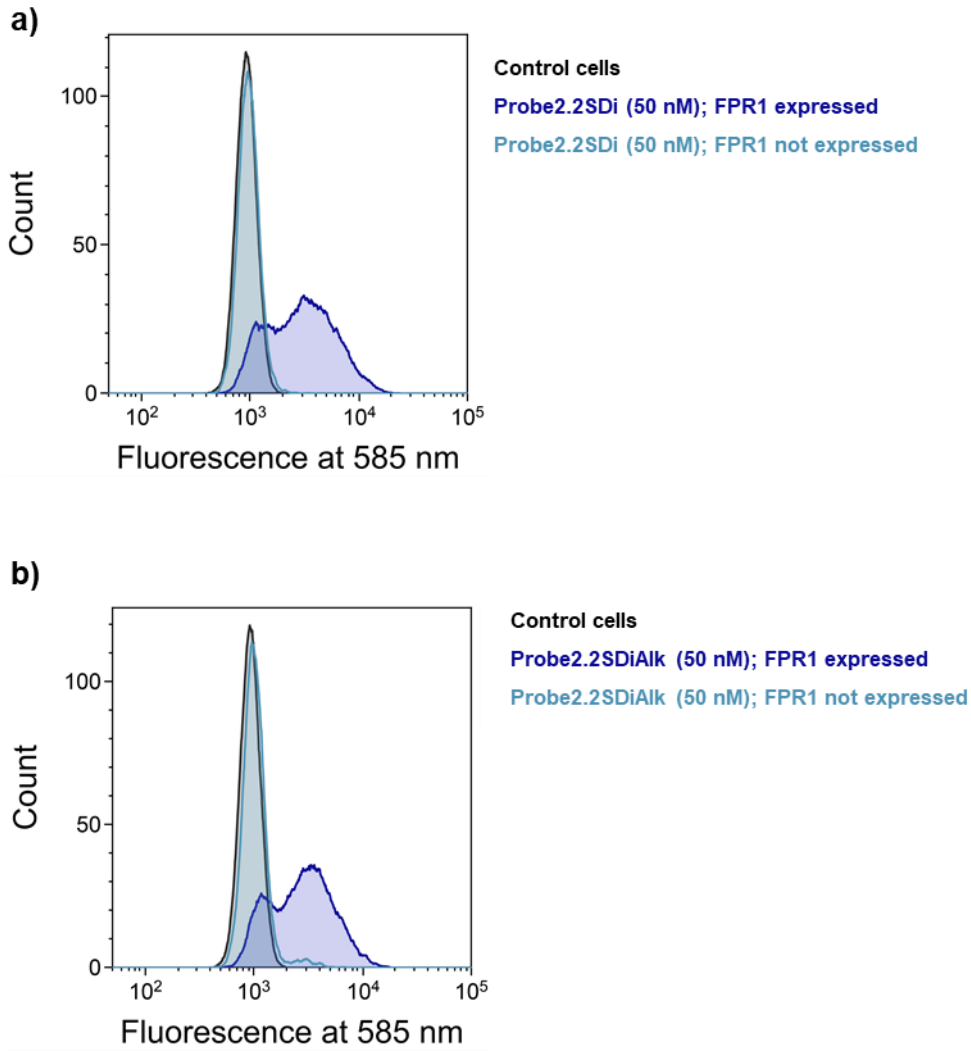

Figure 4.24: Histograms showing the fluorescence at 585 nm of HEK293T cells incubated with Probe2.2SDi (a) and Probe2.2SDiAlk(b); 10,000 cells per sample measured.

4.6.2.2 Competitive Binding Between TracerFITC and Probe2.2SDi/SDiAlk

The binding of Probe2.2SDi/SDiAlk was explored further with a competitive binding experiment between the probe and TracerFITC. This was completed using the same method as before. However, the concentration of Probe2.2SDi/SDiAlk was kept at a higher 50 nM due to the weaker binding. The fluorescence intensity at 525 and 585 nm decreases when compared to TracerFITC and Probe2.2SDi/SDiAlk alone respectively (**Figure 4.25**). This shows

that the two disulphide probes are competing for the same binding site on FPR1 as TracerFITC.

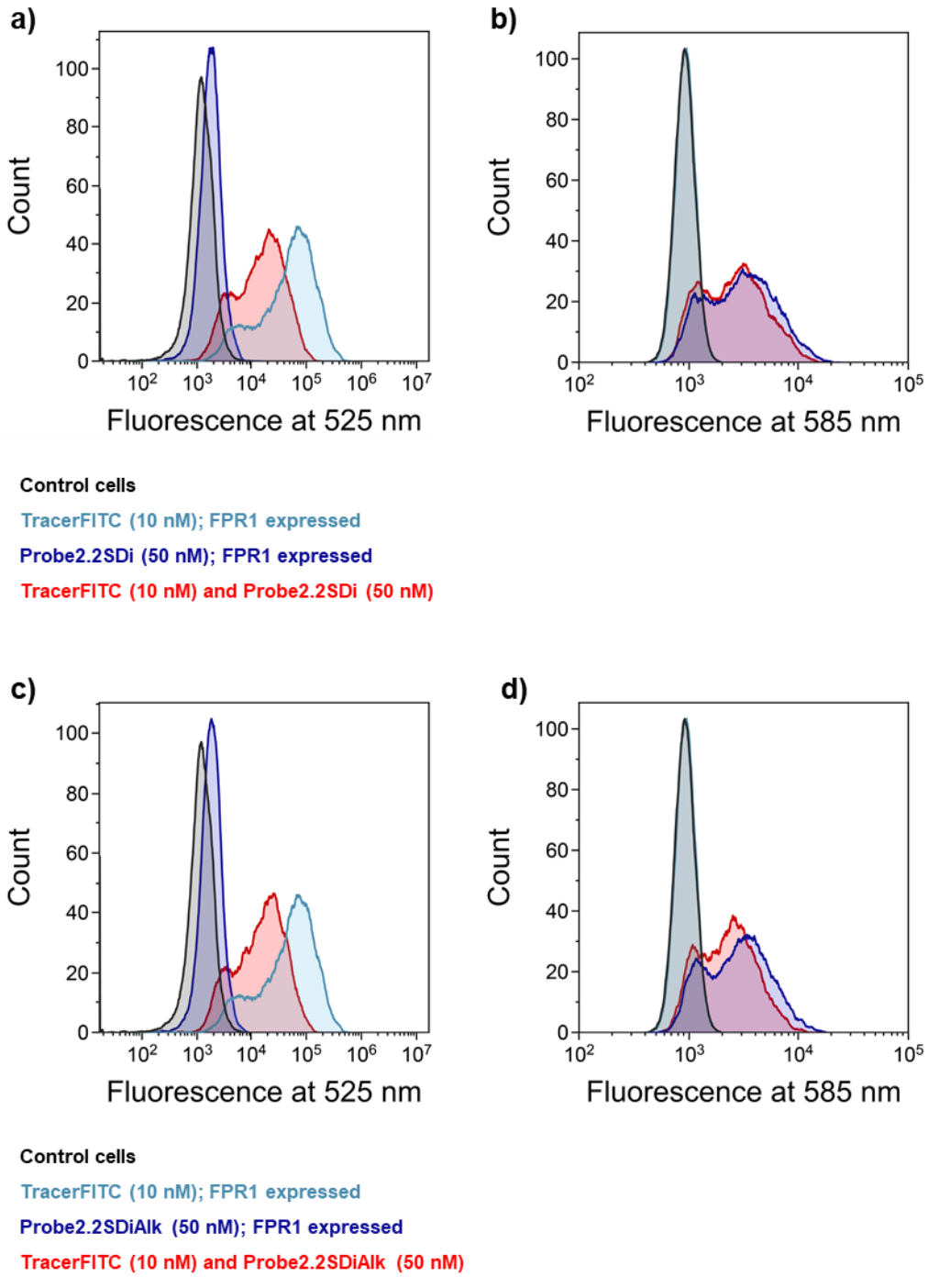

Figure 4.25: Competition between TracerFITC and Probe2.2SDi/SDIALK; a) histogram showing shift in fluorescence of TracerFITC at 525 nm when in competition with Probe2.2SDi; b) histogram showing shift in fluorescence of Probe2.2SDi at 585 nm when in competition with TracerFITC; c) histogram showing shift in fluorescence of TracerFITC at 525 nm when in competition with Probe2.2SDiAlk; d) histogram showing shift in fluorescence of Probe2.2SDiAlk at 585 nm when in competition with TracerFITC.

4.6.3 Binding and Crosslinking of Probe2.2SDi/SDiAlk

To test the crosslinking of Probe2.2SDi/SDiAlk to FPR1, transfected and non-transfected cells were incubated with the probe (1 mL, 50 nM) and irradiated with UV light (365 nm), using the method described for Probe2.0TAMRA. Following cell lysis, in-gel fluorescence at 550 nm was used to identify crosslinking to FPR1. To investigate the cleavable probes, sample loading buffer was used with and without DTT for SDS-PAGE analysis. As a result of the absence of DTT, there is more background fluorescence and laddering observed during in-gel fluorescence. The SDS in the sample loading buffer denatures and unfolds the proteins in the cell lysate, exposing thiols. These free thiols can form disulphide bonds with other thiols that will not be broken in the absence of DTT. This can cause partial folding or aggregation of the protein and is likely to create hydrophobic pockets that the greasy TAMRA fluorophore may stick to, thereby producing laddering during in-gel fluorescence.

A fluorescent band is present between 75 and 50kDa, for Probe2.2SDi crosslinking to FPR1 (**Figure 4.26**), which matches the FPR1 band in the anti-FLAG Western Blot. A fluorescent band is visible in the sample not exposed to UV irradiation at approximately 50 kDa. This suggests that Probe2.2SDi binds to an off-target protein either strongly or covalently. This protein band is also seen when FPR1 is not expressed, in addition to a band at approximately 75 kDa. This shows there is a small level of non-specific binding and crosslinking, as with Probe2.0TAMRA.

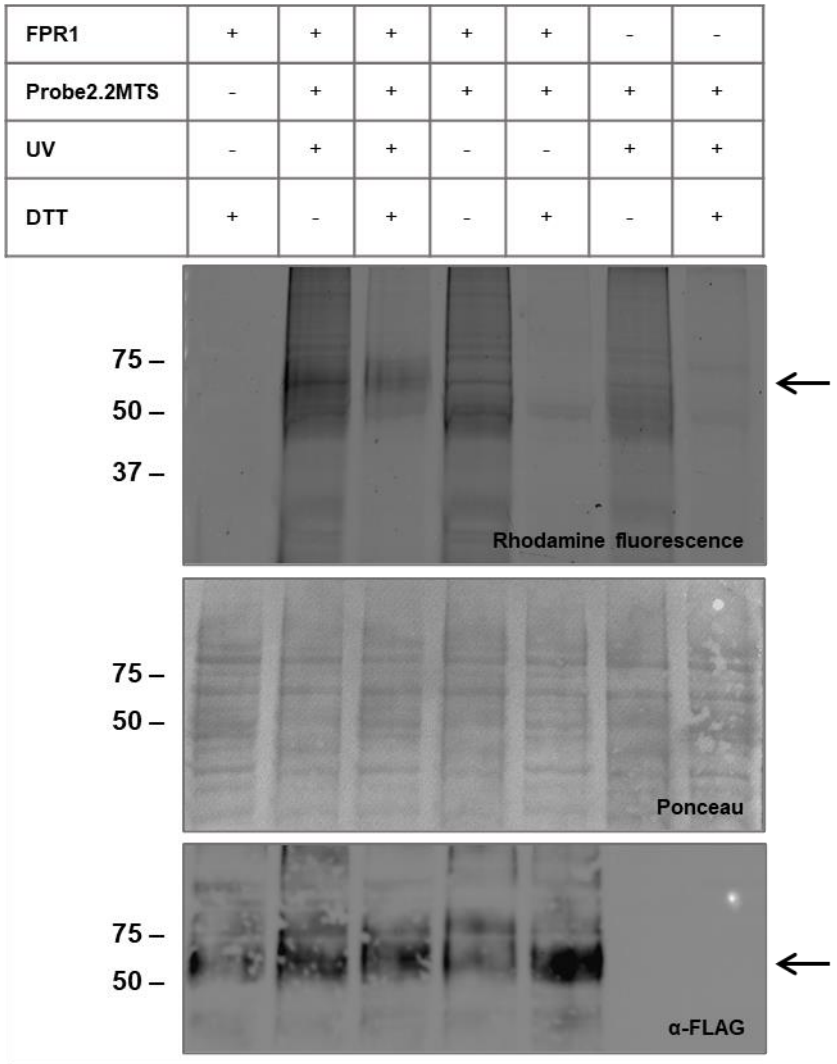

Figure 4.26: SDS-PAGE and Western Blot analysis of crosslinking experiment for Probe2.2SDi; transfected HEK293T cells were suspended, incubated with Probe2.2SDi and irradiated with UV light (365 nm), following cell lysis SDS-PAGE analysis was performed including in-gel fluorescence at 550 nm and anti-FLAG Western Blotting; Ponceau staining of the Western Blot was performed to show the total protein concentration, FPR1 indicated by arrow.

The addition of DTT to the sample loading buffer should remove the fluorescent band of the crosslinked Probe2.2SDi to FPR1 observed in-gel. However, a faint band at the weight of glycosylated FPR1 is still visible (**Figure 4.26**). This is also observed for Probe2.2SDiAlk (**Figure 4.27**). This is likely due to the short incubation time of the cell lysate with the DTT (15 min) and the absence of heating, compared with in literature.[136] It is also probable that FPR1 is not fully denatured, due to the absence of heating, implying that the probe could be buried in a

hydrophobic pocket and less accessible. It has been previously reported that SDS binding is decreased for glycosylated proteins.[127]

Crosslinking is also observed for Probe2.2SDiAlk to FPR1, by the fluorescent band detected between 75 and 50 kDa (**Figure 4.27**). The fluorescence appears less intense than for Probe2.2SDi, although this is unsurprising given the lower fluorescence intensity in flow cytometry for the binding to FPR1 (**Figure 4.24**). There does not appear to be strong/covalent binding to any proteins in the absence of UV irradiation as seen with Probe2.2SDi. However, there is non-specific crosslinking observed when FPR1 is not expressed. This non-specific band occurs at the same molecular weight as for Probe2.2SDi.

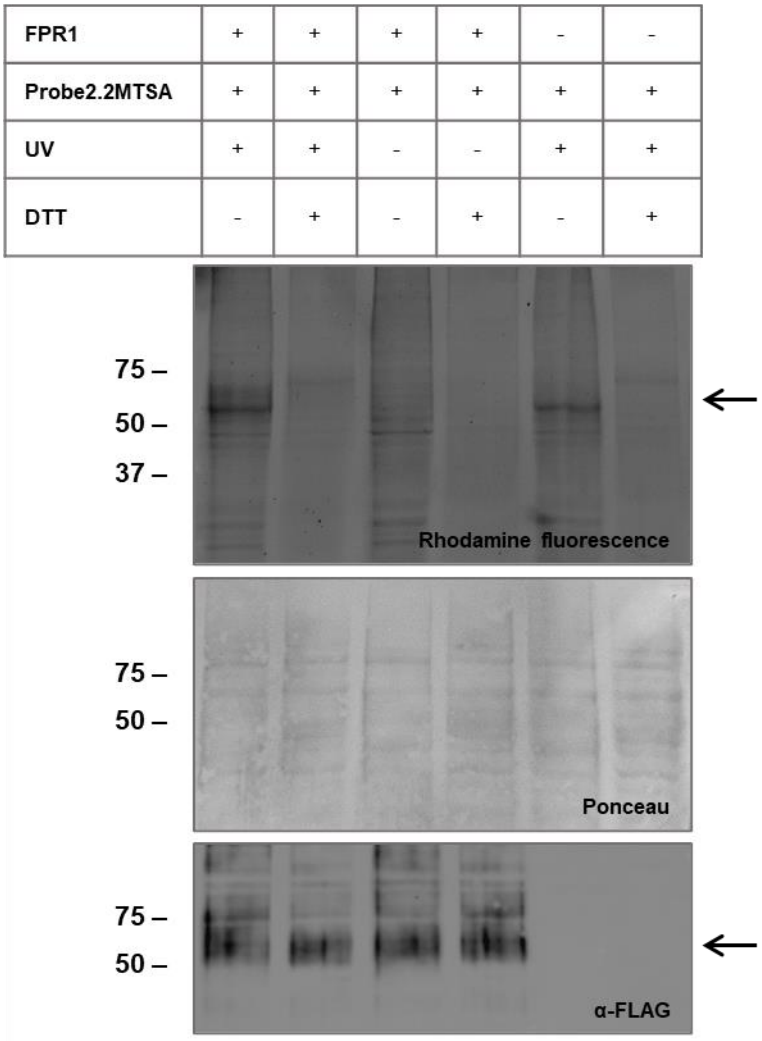

Figure 4.27: SDS-PAGE and Western Blot analysis of crosslinking experiment for Probe2.2SDiAlk; transfected HEK293T cells were suspended, incubated with Probe2.2SDiAlk and irradiated with UV light (365 nm), following cell lysis SDS-PAGE analysis was performed including in-gel fluorescence at 550 nm and anti-FLAG Western Blotting; Ponceau staining of the Western Blot was performed to show the total protein concentration, FPR1 indicated by arrow.

4.7 Conclusion

4.7.1 Structure of Second-Generation Probes

In this chapter the binding and crosslinking to FPR1 of four photoreactive probes have been explored. This second-generation of probes to target FPR1 mainly differ from the previous first-generation by the presence of a detectable tag in the

peptide (**Figure 4.28**). This allows direct observation of the probes and negates the need for a CuAAC. This change was important in identifying and solving problems in the work-flow of this project.

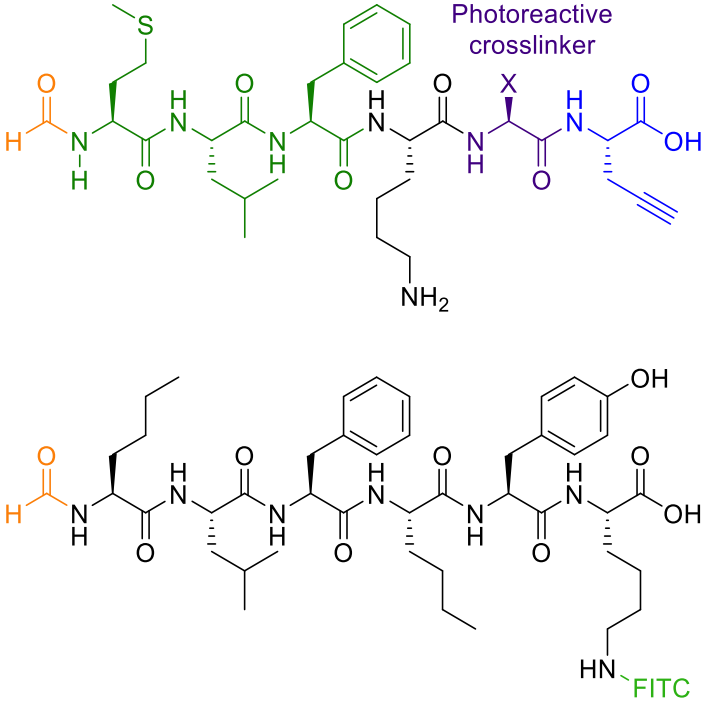

Figure 4.28: Comparison of structure between TracerFITC and Probe1.0

The structure of the probes presented in this chapter were derived from the structure of TracerFITC, known to have a high binding affinity to FPR1. TracerFITC contains a N-formyl norleucine (an isostere for methionine) and Probe1.0 contains a N-formyl methionine, both of which are known to be critical for FPR1 binding.[117] Amino acids two and three are identical for TracerFITC and Probe1.0, forming an fMLF N-terminus structure. Amino acids four and five cause a big difference in structure and the properties of the peptides. In Probe1.0 there is the instalment of a lysine and the photoreactive diazirine, compared with the hydrophobic norleucine and tyrosine respectively in TracerFITC. The lysine residue is positively charged in solution, which will decrease the binding to FPR1 which has a positively charged surface in the binding pocket (**Figure 4.29**).[20] Unfortunately a good homology model was not available when designing the generation 1.0 probes, and other data had suggested that lysine was tolerated.[116] Finally, the Lys(FITC) on TracerFITC compared with the propargyl glycine on Probe1.0 is negatively charged in solution – favourable binding for the positive

surface of FPR1. It is thought that these key differences in the structure are contributing factors to the first-generation probes not binding to FPR1.

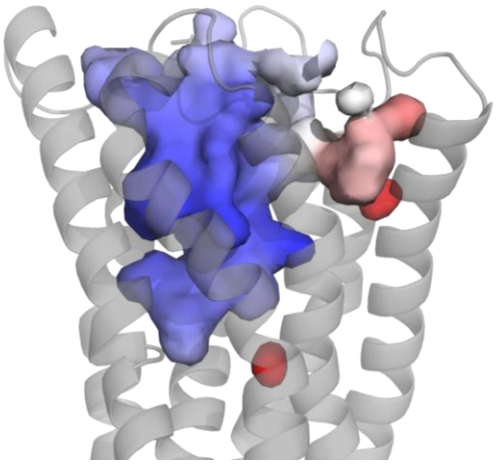

Figure 4.29: Surface FPR1 cavity (from FPR2-based homology model), coloured according to the electrostatic potential from red (negative) to blue (positive), calculated using APBS Electrostatics PDB2PQR.[20, 141]

4.7.2 Probe2.0TAMRA

The success of Probe2.0TAMRA has been outlined in this chapter through a range of different experiments. Probe2.0TAMRA was found to bind to FPR1 specifically with a calculated K_d of ~4 nM. The non-specific binding of Probe2.0TAMRA remains low (<15%) up to a concentration of 200 nM. In addition to this, Probe2.0TAMRA has been shown to compete with TracerFITC, fMLF and Boc-MLF – all known ligands of FPR1. The conservation of binding to FPR1 from changing the N-formyl methionine/norleucine to N-formyl photo-Met is encouraging and shows that the photo-Met can form similar interactions to FPR1. The ligand-induced internalisation of FPR1 by Probe2.0TAMRA was observed, displaying agonistic behaviour of the probe. Probe2.0TAMRA has shown to bind to endogenously expressed FPR1 in glioblastoma cells. This provides confidence that Probe2.0TAMRA could be utilised in primary cells to detect FPR1 expression on different cell types.

The crosslinking of Probe2.0TAMRA to FPR1 was also effective with only small amounts of non-specific crosslinking detected. Further to this, the investigation of

multiple incubations and irradiations with Probe2.0TAMRA proved successful, providing a solution if crosslinking efficiency is low in future experiments. The identity of the off-target band observed from crosslinking during in-gel fluorescence is unknown. However, proteomics could be used to identify the protein. To perform proteomics on the unknown protein, it would need to be enriched from the cell lysate. This would need to be performed via the probe as the protein is not tagged. An anti-TAMRA pull-down was attempted during this project, but proved challenging. Therefore, an alternative probe could be synthesised for the enrichment of this unknown protein.

4.7.3 Probe2.1Desthio

The application of Probe2.1Desthio began positively, showing competition for the formyl peptide binding site with TracerFITC. However, despite showing binding to FPR1, crosslinking experiments analysed by flow cytometry indicate that the probe is not crosslinking. It is unclear why crosslinking was unsuccessful but a faster off-rate could be a contributing factor.

4.7.4 Probe2.2SDi and Probe2.2SDiAlk

Probe2.2SDi and Probe2.2SDiAlk contain a different diazirine group to the previous probes. The MTS-diazirine and MTS-alkynyldiazirine are linked to the peptide backbones via a disulphide bond, which can be cleaved in the presence of a reducing agent. These alternative diazirines have also been inserted at amino acid position four – further from the N-terminus. Probe2.2SDi/SDiAlk both showed specific binding to FPR1 and competed with TracerFITC for the formyl peptide binding site. The probes interact with FPR1 with less affinity than Probe2.0TAMRA. This suggests that the change at residue four from norleucine to the diazirine group is causing the lower binding. Norleucine and the diazirine groups are both non-polar and hydrophobic. However, MTS-diazirine and MTS-alkynyldiazirine are longer and bulkier than norleucine. Therefore, the binding could be hindered sterically. Without a crystal structure of FPR1 this cannot be confirmed, but interestingly there is a lot of different residues reported for position

four of known FPR1 ligands.[116] The scope of residues in a formyl peptide allowed for conservation of binding is something to be explored in the future.

The crosslinking of Probe2.2SDi and Probe2.2SDiAlk to FPR1 was confirmed, showing little non-specific crosslinking. The presence of DTT in the sample loading buffer did not fully cleave the disulphide link between the peptide and FPR1. This may be because the probe is buried and not accessible even in denaturing SDS-PAGE conditions.

Three useful probes have been synthesised and characterised for the labelling of FPR1. The enrichment and proteomics of the complexes formed from the crosslinking of Probe2.0TAMRA and Probe2.2SDi to FPR1 will be explored in Chapter 5.

Chapter 5 Immunoprecipitation and Proteomics

In the previous chapter, the synthesis and use of four photoreactive probes was described. The binding of all four probes was analysed using flow cytometry, showing specific binding for Probe2.0TAMRA, Probe2.2SDi and Probe2.2SDiAlk. Further to this, crosslinking of Probe2.0TAMRA, Probe2.2SDi and Probe2.2SDiAlk to FPR1 was confirmed. The work detailed in this chapter explores the optimisation of the immunoprecipitation of the Probe2.0TAMRA-FPR1 and Probe2.2SDi-FPR1 complexes. Tandem mass spectrometry has also been attempted on these complexes to identify the residues crosslinked to the probe in the FPR1 binding site.

5.1 Anti-FLAG Pull-Down of Probe2.0TAMRA-FPR1 Complex

Immunoprecipitation is a common biochemical technique which isolates a target protein from a mixture of proteins using antibodies attached to solid beads. Using this technique, and the presence of the FLAG tag on the C-terminus of FPR1, the strategy was to isolate the FPR1-Probe2.0TAMRA complex from the cell lysate.

Anti-FLAG magnetic beads (Stratech) are magnetic microspheres covalently coupled to anti-FLAG monoclonal antibodies. Magnetic beads were chosen over agarose beads for this experiment because they do not require centrifugation and fewer beads are lost during handling. The immunoprecipitation was first performed using the manufacturers protocol. The 50% slurry of the magnetic anti-FLAG resin was washed with TBS to remove the glycerol in the solution and equilibrate the beads. The beads were then incubated with the cell lysate (200 µg, 200 µL) at 2 °C for 2 hours. Following incubation, the beads were washed with TBS to remove the unbound protein. To elute FPR1-Probe2.0TAMRA the beads were incubated at 2 °C with 3X FLAG peptide solution (150 ng/µL) for 30 minutes. The immunoprecipitation was then analysed by SDS-PAGE and Western Blot (**Figure 5.1**).

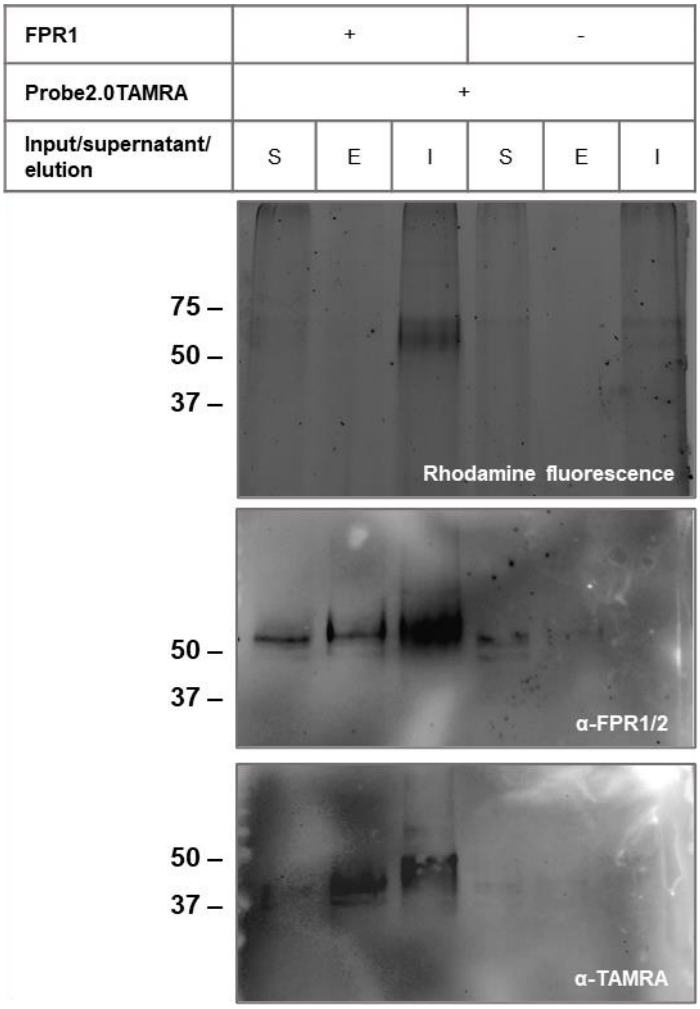

Figure 5.1: SDS-PAGE and Western Blot analysis of anti-FLAG immunoprecipitation of FPR1-Probe2.0TAMRA complex; anti-FPR1/2 Western Blot binds to FPR1; anti-TAMRA binds to the TAMRA fluorophore on Probe2.0TAMRA; input corresponds to sample of cell lysate before immunoprecipitation; 10 µg loaded for input and supernatant samples, 20 µL loaded of the 40 µL elution solution.

Western Blot analysis from the anti-FLAG pull-down experiment gave inconclusive results. There were signals present in the elution sample for both anti-FPR1/2 and anti-TAMRA Western Blots, indicating that some FPR1-Probe2.0TAMRA complexes were being pulled down onto the beads and eluted. However, a signal was also observed in the supernatant samples, suggesting that not all complexes were being pulled down. In addition to this, there was no visible fluorescence at 550 nm for the elution samples, signifying a low concentration of Probe2.0TAMRA in the elution. Therefore, alternative methods adapting the suggested protocol were tested (**Table 5.1**). These included increasing the incubation time, increasing the concentration of the

3X FLAG peptide (Met-[Asp-Tyr-Lys-Xaa-Xaa-Asp]×3-Asp-Tyr-Lys-Asp-Asp-Asp-Asp-Lys) solution for elution and the use of a different, low pH eluting solution.

Incubation Time	Elution solution	FPR1 band present in supernatant		FPR1 band present in elution	
		Fluorescence	WBs	Fluorescence	WBs
2 hrs	3XFLAG (150 ng/µL)	Yes	Yes	No	Yes
12 hrs	3XFLAG (150 ng/µL)	No	No	No	Yes
12 hrs	3XFLAG (300 ng/µL)	Yes	Yes	No	Yes
12 hrs	0.1 M glycine-HCl (pH 3.5)	Yes	Yes	No	No

Table 5.1: Anti-FLAG pull-down conditions and SDS-PAGE/WB analysis outcomes.

The initial increase in incubation time to 12 hours gave promising results. Full pull-down of FPR1-ProbeTAMRA was achieved, with no signal detected in the supernatant sample for in-gel fluorescence or the WBs. However, this was not reproducible. In following experiments, manipulating the elution solution, full pull-down was not accomplished. In addition to this no in-gel fluorescence was detected for the elution sample for any of the experiments. It was evident that the standard protocol was not suitable for the immunoprecipitation of FPR1-Probe2.0TAMRA. Unfortunately, many pull-down procedures currently published involve the heating of samples for elution, which is not possible for FPR1 as discussed in section 3.4.1.1. Nevertheless, another protocol was found, specifically designed for the pull-down of GPCRs.[124]

5.1.1 GPCR-Specific Anti-FLAG Pull-Down

The new pull-down procedure started with a new cell lysis buffer that included cholesterol hemisuccinate (CHS) and *n*-Dodecyl β-D-maltoside (DDM). GPCRs can be unstable in solution due to the removal of membrane lipids during cell lysis,[124] and in order to solubilise a GPCR, detergents need to be added to the lysis buffer. DDM is a mild non-ionic detergent,[142, 143] commonly used to solubilise GPCRs. The addition of lipid-like substances such as CHS can further increases the stability of GPCRs.[142, 143] The combination of DDM and CHS causes the formation of mixed micelles which are similar in structure to the lipid bilayer of the cell membrane. Therefore, this creates a more stabilising environment for the GPCR than regular micelles.

In addition to a new lysis buffer, a new sample loading buffer was also used. This contained urea which is known to reduce aggregation and improve solubility of membrane proteins.[144] Moreover, the urea aids in protein denaturation by breaking hydrogen bonds and hydrophobic interactions, and allowing water to enter the hydrophobic core of the protein.[145]

Following cell lysis with the CHS and DDM containing lysis buffer, the cell lysate was adjusted to 1 µg/ µL as before. The anti-FLAG magnetic beads were washed with TBS three times and subsequently washed once with 0.1 M glycine (pH 3.5). This additional glycine wash removes any unbound FLAG antibody and can greatly improve pull-down efficiency.[124] The glycine was removed from the beads by washing a further three times with TBS and once with the lysis buffer. 200 µg of cell lysate was added to the beads and incubated overnight at 4 °C. After removal of the supernatant, the beads were washed three times with lysis buffer and 40 µL of 1 × urea sample loading buffer was added and incubated for 30 minutes at room temperature. The immunoprecipitation was then analysed by SDS-PAGE and Western Blot (**Figure 5.2**). Excitingly a strong fluorescent band at 50-75 kDa is present during in-gel fluorescence for the elution sample, indicating immunoprecipitation of FPR1-Probe2.0TAMRA.

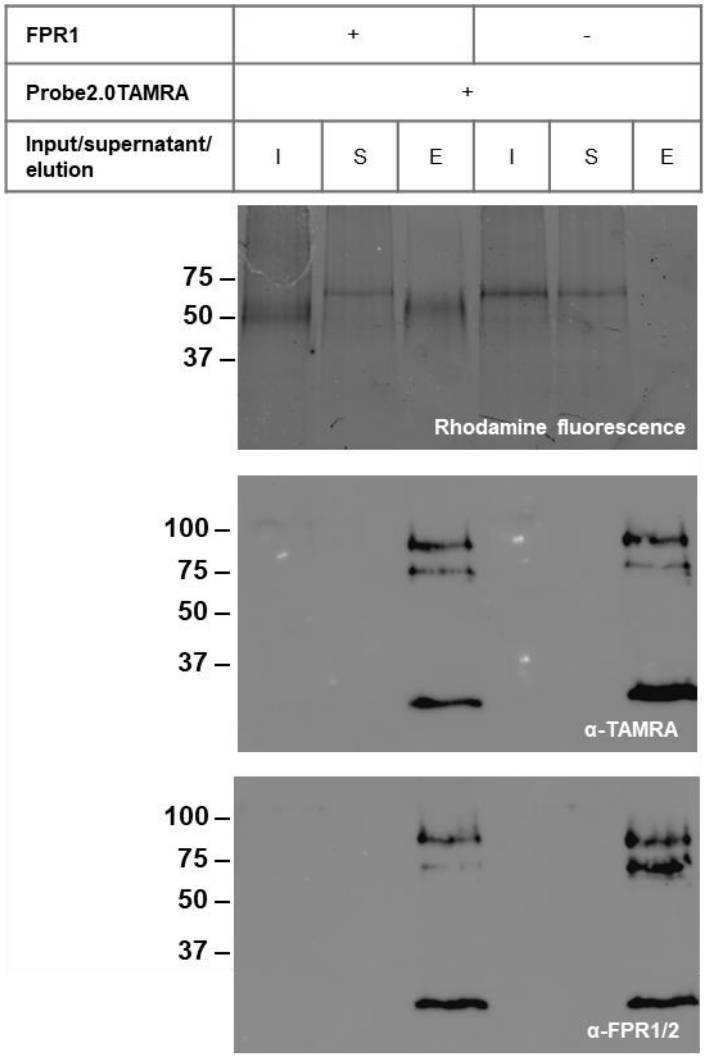

Figure 5.2: SDS-PAGE and Western Blot analysis of GPCR-specific anti-FLAG immunoprecipitation of FPR1-Probe2.0TAMRA complex; 10 µg loaded for input and supernatant samples, 20 µL loaded of the 40 µL elution solution.

The fluorescent FPR1 band is not visible in the supernatant sample, indicating that all FPR1-Probe2.0TAMRA complexes have been pulled down onto the beads. The off-target protein band is present in the supernatant sample providing confidence that it has not been pulled down onto the beads. The same is true for when FPR1 is not expressed, and no fluorescence is observed in the elution. Unfortunately, the only signals detected in both Western Blots were from the elution of the anti-FLAG antibody, likely due to the use of the urea sample loading buffer. The DTT present in the urea sample loading buffer cleaves the link between the FLAG antibody and the magnetic bead. This will cause issues for proteomic analysis as the concentration of FPR1-Probe2.0TAMRA is expected to be low. Therefore, the pull-down was repeated

using the 3X FLAG peptide solution (300 ng/µL) for elution from the beads (**Figure 5.3**). The original lysis buffer without CHS and DDM was also used, as the addition of CHS and DDM made the cell lysate viscous and difficult to work with. Once again there was a clear, strong fluorescent band in the elution sample with FPR1 expression observed during in-gel fluorescence. This shows that the anti-FLAG pull-down works with the original lysis buffer and the 3X FLAG peptide elution.

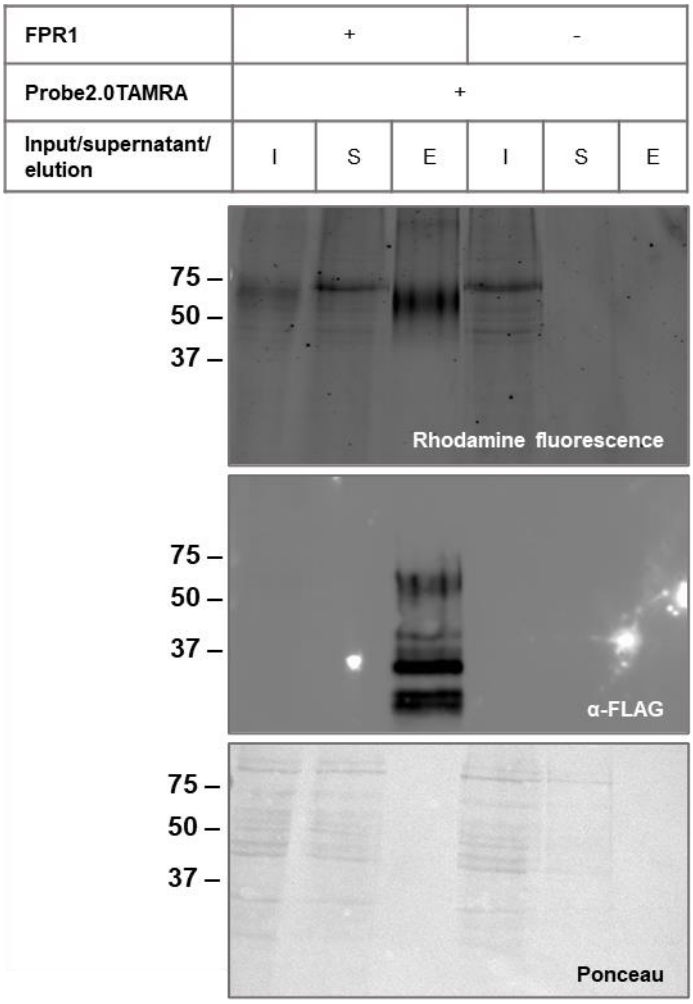

Figure 5.3: SDS-PAGE and Western Blot analysis of GPCR-specific anti-FLAG immunoprecipitation of FPR1-Probe2.0TAMRA complex with original lysis buffer and 3X FLAG solution for elution; 200 µg of cell lysate incubated with beads; 10 µg loaded for input and supernatant samples, 20 µL loaded of the 40 µL elution solution.

The anti-FLAG antibody bands present in the Western Blots in the previous experiment are not visible and they are also not observed in the Ponceau stain. This confirms that the anti-FLAG antibody has not been eluted with FPR1-Probe2.0TAMRA. The FPR1 band in the FPR1+ elution sample was detected in the

anti-FLAG Western Blot, although this was not observed for the input sample. This is likely due to the higher concentration of the elution sample. The ponceau stain shows no bands in the elution sample suggesting that no other proteins were purified with FPR1 at a detectable concentration.

Given the success of this pull-down, it is likely that the main contributing factor for the success of the GPCR-specific pull-down is the addition of the 0.1M glycine (pH 3.5) wash of the beads. This suggests that the anti-FLAG magnetic beads used contained a large proportion of unbound FLAG antibody which was hindering the pull-down.

5.2 First Proteomics Experiment

To determine the crosslink site of Probe2.0TAMRA, bottom-up proteomics was employed, as discussed in section 1.5.3. The anti-FLAG pull-down of FPR1-Probe2.0TAMRA was repeated using 0.5 mg of cell lysate to increase the amount of FPR1-Probe2.0TAMRA in the elution. All proteomics experiments performed were completed by Rachel George in the University of Leeds FBS Mass Spectrometry Facility. In-solution digestion of FPR1 was chosen over in-gel digestion to give higher recovery of peptides because the concentration of FPR1-Probe2.0TAMRA was low and not detectable with Coomassie stain. The suspension trapping (S-Trap) method was used for bottom-up proteomic sample preparation. The S-Trap is a sample preparation tool compatible with low concentration samples, first described by Zougman *et al.*[146] The protein sample is made to 5% SDS and acidified, before being added to methanol; these three steps solubilise and denature the protein. The protein is then reduced and alkylated, before being added to the S-Trap where it binds by weak affinity interactions to the silica. This allows the protein solution to be washed to remove any detergents or salts. Following this the protein is digested and peptide products are eluted because the S-Trap has no affinity for them.

The FPR1-Probe2.0TAMRA sample was denatured and added to the S-Trap micro column. Following washes of the sample, the protein was digested with trypsin and chymotrypsin separately for 15 minutes at 46 °C. Chymotrypsin is often used in addition to trypsin for the digestion of hydrophobic proteins due to the lack of tryptic

cleavage sites in the transmembrane regions. The peptides were collected, and tandem mass spectrometry was performed using an Orbitrap Velos mass spectrometer. A coverage of 35% was achieved from the trypsin digest and 27% from the chymotrypsin digest, with 45% combined coverage of FPR1 from the two (**Figure 5.4**). In this experiment the crosslink location was not identified (the additional mass of the probe following crosslinking was searched for).

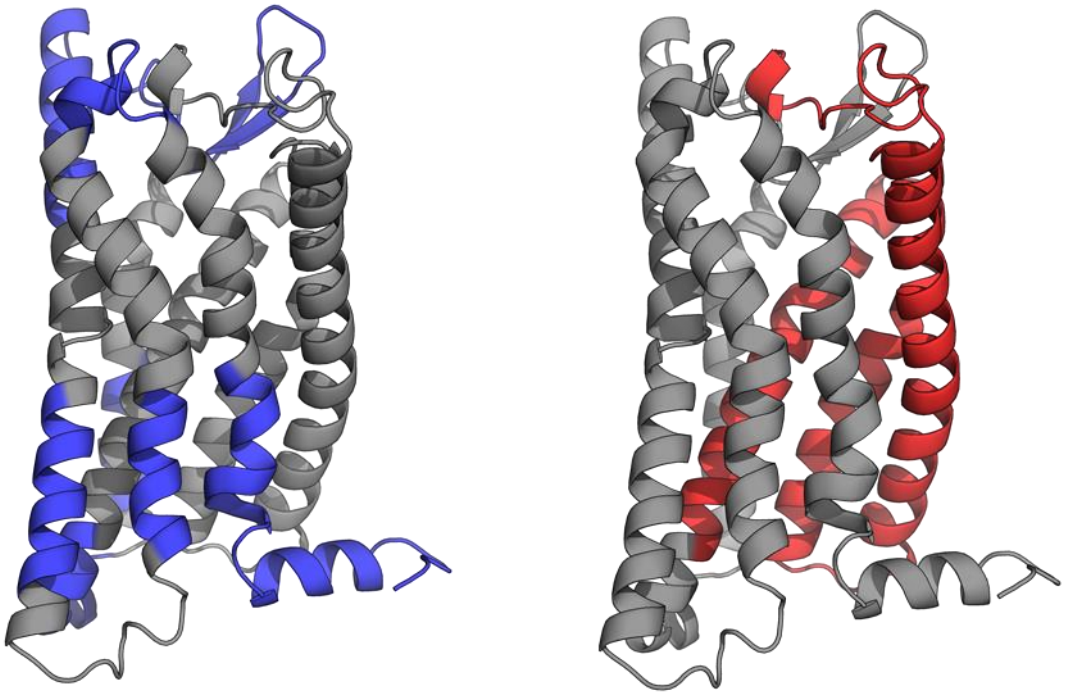

Figure 5.4: Homology model of FPR1 based off the structure of FPR2 showing combined coverage of first proteomics experiment (left), protein coverage in blue; first 123 residues at N-terminus highlighted (right) (red).

From the first proteomics experiment the detection of FPR1 peptides was promising. However, as shown in **Figure 5.4**, the coverage in the top half of the transmembrane helices was poor and there was no coverage for the first 124 residues at the N-terminus. Unfortunately, the coverage for digestion with chymotrypsin was poorer than with trypsin and didn't cover many additional areas in the protein. A possible solution to this poor coverage was to deglycosylate FPR1, so there were no glycans hindering digestion. FPR1 has three potential glycosylation sites; Asn4, Asn10, and Asn179.[125]

5.3 Anti-FLAG Pull-Down with Deglycosylation of FPR1

Tunicamycin can be used to block the glycosylation of proteins in cells. However, it has been shown that tunicamycin negatively affected the binding of high-affinity agonists and that N-terminal glycosylation is crucial for proper FPR1 folding.[125] It was therefore decided that a deglycosylation reaction with PNGaseF, as used in chapter 3, would be employed in conjunction with the anti-FLAG pull-down.

Three different methods were tested for the deglycosylation of FPR1 with the anti-FLAG pull-down:

1. Deglycosylation before incubation with anti-FLAG magnetic beads.
2. Incubation with anti-FLAG magnetic beads followed by deglycosylation on-bead.
3. Deglycosylation after elution from anti-FLAG magnetic beads.

All three methods were successful, showing elution of deglycosylated FPR1 at ~38 kDa (**Figure 5.5**).

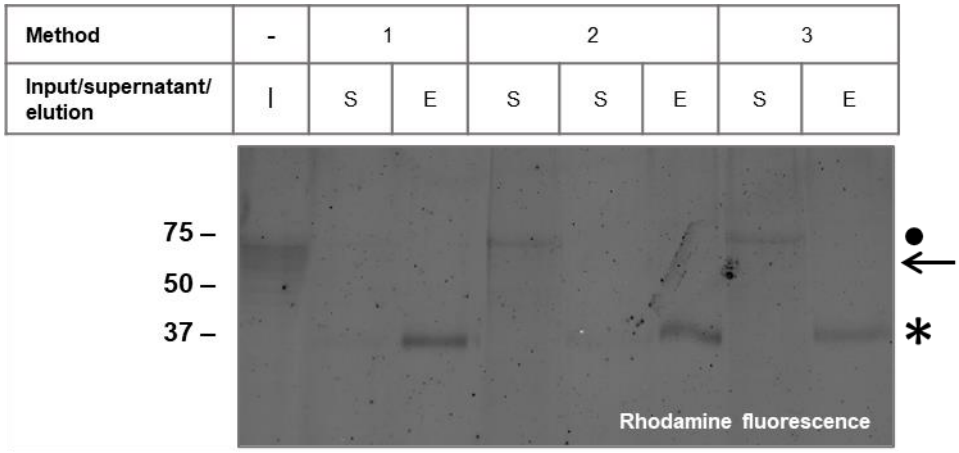

Figure 5.5: In-gel fluorescence analysis of deglycosylation with pull-down methods; arrow indicates glycosylated FPR1, star indicates deglycosylated FPR1, filled circle indicates off-target band; second supernatant for method 2 is after deglycosylation on-bead.

Performing the deglycosylation first did not affect the pull-down. No FPR1 band was present in the supernatant, suggesting full pull-down of FPR1-Probe2.0TAMRA. This was a promising result and showed that the anti-FLAG magnetic beads tolerated the 10% SDS required for deglycosylation. In method 2, the on-bead deglycosylation did not affect the beads, or cause elution of FPR1-Probe2.0TAMRA as seen by the

absence of a detectable band in the supernatant after deglycosylation. The deglycosylation post pull-down was also successful, although the elution band appears fainter than for the other two methods.

Method 1 was chosen for future pull-down immunoprecipitations. Performing the deglycosylation first ensures there is no PNGaseF in the elution that could interfere with the mass spectrometry experiments. The deglycosylation and pull-down were repeated with 0.5 mg cell lysate to confirm the tolerability at higher protein concentrations (**Figure 5.6**). The pull-down was still successful, showing elution of deglycosylated FPR1-Probe2.0TAMRA.

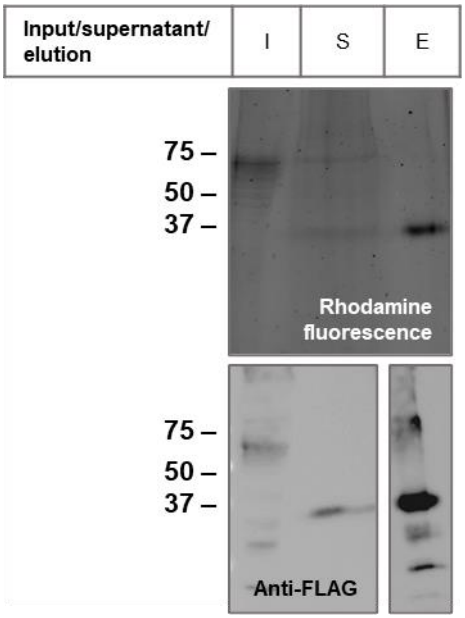

Figure 5.6: SDS-PAGE and WB analysis of deglycosylation followed by anti-FLAG pull-down with 0.5 mg cell lysate; input and supernatant anti-FLAG WB imaged separately to elution due to high intensity of elution.

The FPR1 band in the supernatant was faintly visible during in-gel fluorescence and in the anti-FLAG WB, indicating not all FPR1-Probe2.0TAMRA was pulled down onto the beads. However, this guarantees that the anti-FLAG beads are fully saturated with FPR1-Probe2.0TAMRA and therefore other proteins are less likely to bind.

5.4 Proteomics with Deglycosylated FPR1

RapiGest (**Figure 5.7**) was used to aid reduction, alkylation and the initial digest that occurs prior to adding sample onto the S-Trap micro column. The protein sample was precipated using the chloroform-methanol precipitation and the resulting pellet was dissolved in 0.1% (w/v) RapiGest. Subsequent reduction and alkylation followed the same procedure as the previous experiment. RapiGest was first introduced in 2002 by Waters Corporation to improve protein solubility for proteomic sample preparation.[147] RapiGest significantly accelerates the digestion of proteins by trypsin by exposing proteolytic sites. It has also been shown to improve the solubilisation of hydrophobic membrane proteins and drastically improves their digestion.[147]

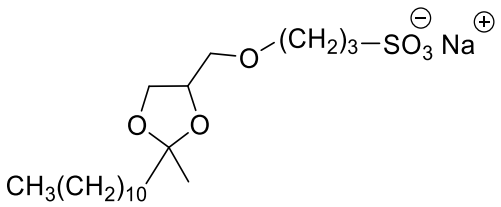

Figure 5.7: Structure of RapiGest

The FPR1-Probe2.0TAMRA sample was digested with RapiGest and trypsin (separately an additional digest with chymotrypsin following the RapiGest and trypsin was performed). Unfortunately, deglycosylation did not improve coverage (41% FPR1 combined coverage) (**Figure 5.8**) and the crosslink location was again not identified.

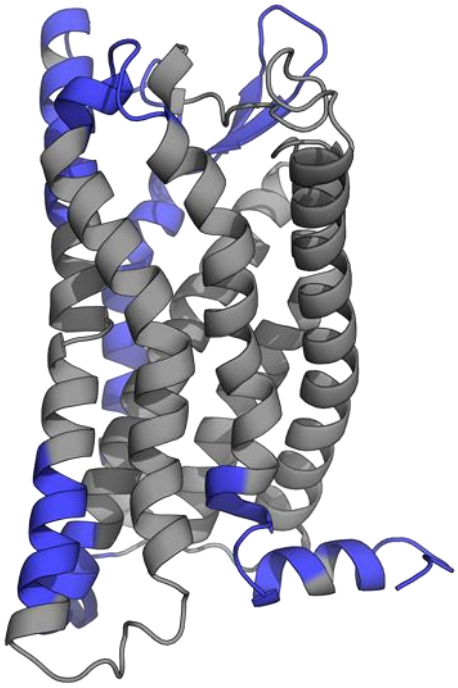

Figure 5.8: Homology model of FPR1 based off the structure of FPR2 showing coverage of proteomics experiment on deglycosylated FPR1; protein coverage in blue.

5.5 Anti-FLAG Pull-Down of FPR1-Probe2.2SDi

As discussed in chapter 4, the use of a cleavable group in a photoaffinity probe can be advantageous for mass spectrometry. Given the unsuccessful proteomics experiments with Probe2.0TAMRA, it was decided that the immunoprecipitation of FPR1-Probe2.2SDi would be attempted. The anti-FLAG pull-down was ineffective without deglycosylation of FPR1, with poor detection of FPR1 in the elution sample (not shown). However, with deglycosylation, good elution of FPR1-Probe2.2SDi was detected (**Figure 5.9**).

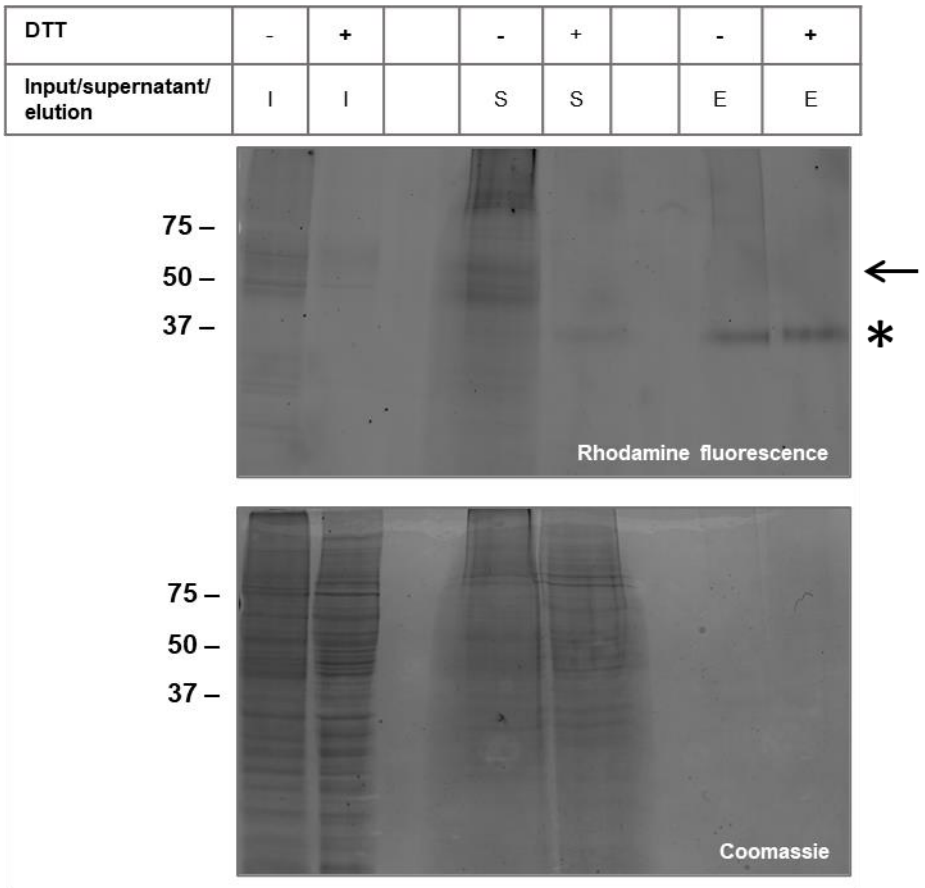

Figure 5.9: Anti-FLAG pull-down with deglycosylation of FPR1-Probe2.2SDi; arrow indicates glycosylated FPR1, star indicates deglycosylated FPR1; 200 µg of cell lysate incubated with beads; 10 µg loaded for input and supernatant samples, 10 µL loaded of the 40 µL elution solution.

As discussed in section 4.6.3, the FPR1 band observed during in-gel fluorescence is not completely removed with the presence of DTT.

5.6 Proteomics with FPR1-Probe2.2SDi

The solubilisation and denaturation of the FPR1-Probe2.2SDi sample was performed as before with trypsin and RapiGest used for digestion. This proteomics experiment gave more promising results, having a coverage of 61% of FPR1 (**Figure 5.10**). Two peptides were picked up in the N-terminal region, though this was still mostly not detected.

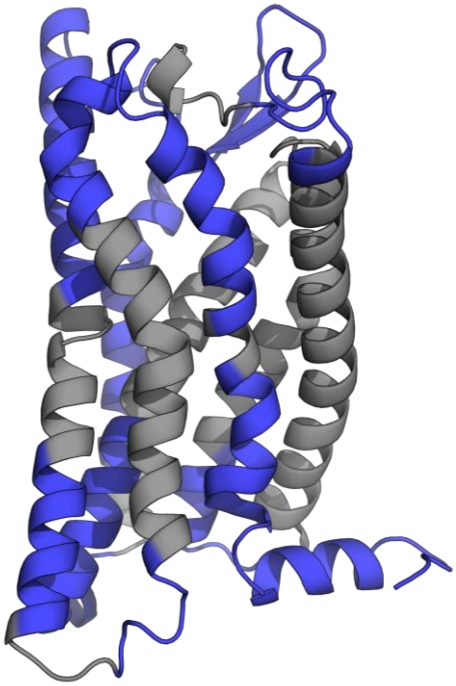

Figure 5.10: Homology model of FPR1 based off the structure of FPR2 showing coverage of proteomics experiment on FPR1-Probe2.2SDi; protein coverage in blue.

The digestion with trypsin requires heating the sample to 95 °C. As issues had been encountered with heating FPR1 previously, it was proposed that the receptor could be aggregating leading to poor digestion and mass spectrometry coverage. Indeed, when studying the formyl peptide binding site in 1998, Mills *et al.* kept their protein sample at 25 °C whilst digesting with trypsin overnight.[105] More recently, when studying the binding site of hedgehog acyltransferase, Lanyon-Hogg *et al.* used urea to solubilise and denature their protein sample which was kept cold throughout digestion.[148] As discussed earlier, it has been shown that urea helps denaturation of GPCRs and limits aggregation. Urea also disrupts intraprotein interactions to improve efficiency of digestion.[149] Therefore, a method for the denaturation and digestion of FPR1 was used inspired by Lanyon-Hogg *et al.*

FPR1-Probe2.2SDi sample was precipitated using the chloroform-methanol precipitation and the resulting pellet was dissolved in ice cold 8 M urea in 100mM Tris, pH 8.5. Reduction and alkylation were performed as before. 100 mM ammonium bicarbonate buffer was added to reduce the concentration of urea before tryptic digest. Unfortunately, this resulted in a combined coverage of only 30% (not shown). Below is a summary table of all proteomics experiments performed on FPR1 (**Table 5.2**).

Probe	Method	Peptides	Coverage
Probe2.0TAMRA	S-Trap Trypsin Chymotrypsin	27	**45%** 35% Trypsin 27% Chymotrypsin
Probe2.0TAMRA	Deglycosylated FPR1 S-Trap RapiGest and trypsin RapiGest and trypsin followed by chymotrypsin	22	**41%** 35% RapiGest trypsin 14% RapiGest trypsin then chymotrypsin
Probe2.2SDi	Deglycosylated FPR1 S-Trap RapiGest and trypsin RapiGest and trypsin followed by chymotrypsin	50	**61%** 41% RapiGest trypsin 48% RapiGest trypsin then chymotrypsin
Probe2.2SDi	Deglycosylated FPR1 Ice-cold urea Trypsin Trypsin then Chymotrypsin	30	**30%** 20% Trypsin 25% Trypsin then chymotrypsin

Table 5.2: Summary of results from proteomics experiments on FPR1.

5.7 Conclusion

The work discussed in this chapter has investigated the immunoprecipitation of two FPR1-probe complexes and preliminary proteomics experiments were performed on these complexes. The use of an anti-FLAG pull-down for the purification of FPR1-Probe2.0TAMRA has been optimised from the standard manufacturing protocol. This involved incorporating a 0.1 M glycine (pH 3.5) wash of the beads prior to incubation with the cell lysate. The extra wash likely removes any unbound FLAG antibody. The fact that this wash step improved the pull-down by such a significant amount suggests

the anti-FLAG beads used contained a lot of unbound FLAG antibody that the FPR1-Probe2.0TAMRA was binding to. The deglycosylation of FPR1 was also performed in conjunction with the pull-down, and it was satisfying to observe that this was successful for all three methods attempted. This anti-FLAG pull-down was also applied to the immunoprecipitation of FPR1-Probe2.2SDi successfully.

Preliminary bottom-up proteomic experiments were then performed on the isolated FPR1-Probe2.0TAMRA and FPR1-Probe2.2SDi. Unfortunately, poor coverage in the N-terminal and transmembrane regions was achieved for both complexes, though this is not unusual for hydrophobic transmembrane proteins. However, the addition of RapiGest to the trypsin digest, and use of urea to denature whilst keeping the sample cold did not improve results. Deglycosylation was also unsuccessful in improving coverage. Two other papers have discussed digestion and mass spectrometry analysis of FPR1.[105, 128] In 1998 Mills *et al.* performed PAL on FPR1, followed by digestion with CNBr and trypsin, and MS to locate the crosslink site.[105] However, they do not discuss the coverage that they achieve with MS, only the probe crosslinked peptide is mentioned. In 2013 Maaty *et al.* investigated C-terminal phosphorylation sites on FPR1, also performing a digest with trypsin followed by MS analysis.[128] The authors show identified peptides from residues 312-350 and 191-201. This is lower coverage than achieved in this project, although with the focus on the C-terminal phosphorylation other peptides may not have been discussed. Docking experiments with Probe2.0TAMRA and the homology model of FPR1 (performed by Tameryn Stringer) revealed that residues interacting with the diazirine were not included in the coverage achieved with the first proteomics experiment (**Figure 5.11**). This further highlights the need for an alternative protocol to digest FPR1.

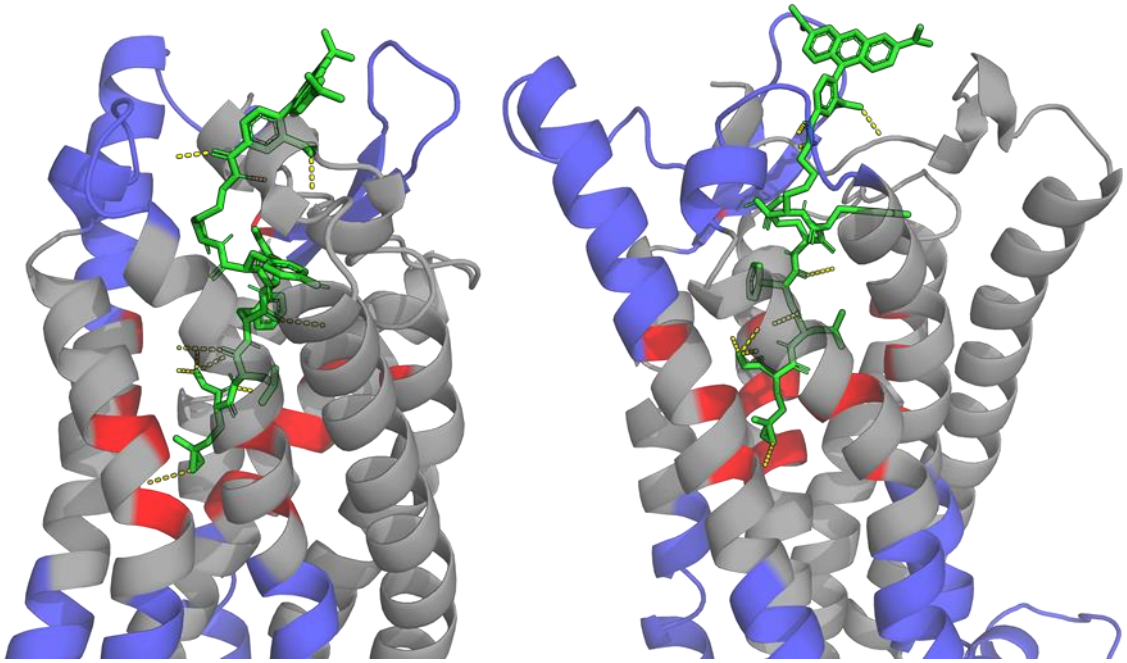

Figure 5.11: Molecular docking of Probe2.0TAMRA to homology model of FPR1 performed by Tameryn Stringer showing front (right) and back (left) view; coverage achieved in first proteomics experiment (blue), interactions between the diazirine and FPR1 residues (red).

In addition to RapiGest, there are other mass spectrometry compatible detergents such as Invitrosol and PPS Silent Surfactant.[149] These both help to solubilise and mildly denature the protein to aid in digestion, without inhibiting proteolytic enzymes or damaging the protein. Higher solubilisation and improved tryptic digestion has been observed when Invitrosol and PPS Silent Surfactant are used.[149] Furthermore, different organic-aqueous solvent systems for the denaturation steps can be used, for example 80% acetonitrile in water has been shown to give good results when used with Invitrosol. Chen *et al.* compared the trypsin digest of the cytoplasmic fraction of mammalian cell lysate with detergents in organic-aqueous systems. When Invitrosol was used with 80% acetonitrile in water 1584 peptides were identified compared with 269 for 80% methanol in water.[149] Waas *et al.* also showed that the number of peptides found with Invitrosol was increased when using acetonitrile, and further increased with guanidine as an additive, especially for hydrophobic peptides.[150] The sequence coverage obtained for FPR1 could benefit from optimisation of detergent and solvent used.

For the digestion of FPR1, the proteolytic enzymes trypsin and chymotrypsin were used. Trypsin is usually the enzyme of choice for mass spectrometry-based proteomics. However, trypsin cleaves after arginine and lysine residues and as these are not hydrophobics residues they are often uncommon in the transmembrane region of GPCRs (**Figure 5.12**).

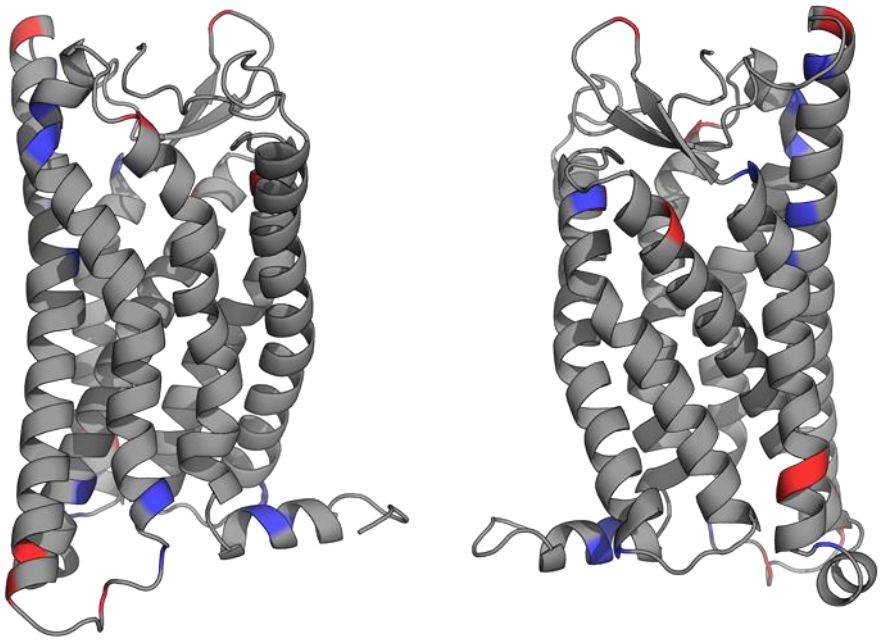

Figure 5.12: Arginine (blue) and lysine (red) residues on FPR1

The additional use of chymotrypsin often aids protein coverage,[151] though this has not been the case for FPR1. Other enzymes, such as proteinase K and elastase, have also been used for the digestion of transmembrane proteins. Elastase has been described as a semi-specific enzyme, cleaving mainly at Ala, Val, Leu, Ile, Ser, and Thr residues (**Figure 5.13**).[152] It shows better transmembrane coverage than trypsin, in a comparison experiment performed by Rietschel *et al.* 20 transmembrane peptides of the bacterial rhodopsin protein were identified with trypsin compared to 174 with elastase.[152] More proteolytic enzymes need to be tested for the digestion of FPR1, and potentially sequential digests experimented with also.

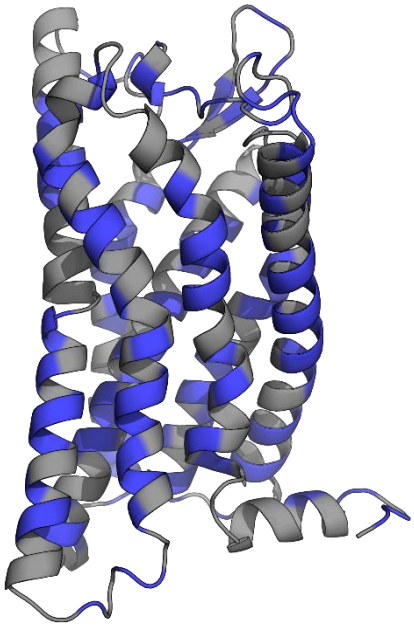

Figure 5.13: Possible cleavage sites of elastase on FPR1 (blue).

Chapter 6 Conclusions and Future Work

The overall aim of this project was to design and develop photoreactive probes that mimic formyl peptides to bind and label FPR1. By labelling FPR1 with a photoreactive probe and performing bottom-up proteomics on the complex, I hoped to gain knowledge of the binding site of FPR1. This chapter will outline the conclusions for this thesis and propose future work for the project. A summary of each chapter will be given with discussion on the work completed. Finally, future avenues of this project, particularly the possible applications of these probes, will be proposed.

6.1 Synthesis of Photoreactive Diazirines

Chapter 2 outlined the synthesis of three known photoreactive groups. 4,4-Azo-pentanoic acid, Fmoc-photo-Met and Fmoc-photo-Leu have all been synthesised previously and their synthetic routes have been published in literature.[71, 112] However, an alternative strategy was required for the Fmoc-photo-Leu synthesis to improve the diazirine forming reaction. The *t*-Bu protected acid **2.22** was used (as for Fmoc-photo-Met) and this greatly increased the diazirine yield. An adapted synthetic route was formed, similar to that reported by Yuichi *et al.*[115] Although the synthesis of Fmoc-photo-Leu from *N*-Boc-L-aspartic acid methyl ester has been previously reported, to our knowledge the synthetic route starting with *N*-Boc-L-aspartic acid tert-butyl ester and proceeding via **2.25** has not been previously published.

6.2 First-Generation Probes

Chapter 3 described the design and synthesis of the first-generation photoreactive probes. Two photoreactive probes were synthesised, incorporating photo-AcLys and

photo-Met. However, neither of the probes showed binding to FPR1 expressed on HEK293T cells. Despite this disappointing result, a lot of methodology was established for the expression of FPR1 in mammalian cells and the work-flow used for testing binding with flow cytometry. In addition to this, the well-known fluorescent tracer was synthesised. Although the first-generation probes were unsuccessful in binding to FPR1 there is the possibility to use them to bind to FPR2. FPR2 binds to a more diverse range of ligands than FPR1, and the lysine residue at position 4 in the first-generation probe structure could increase binding due to the more negatively charged surface of the FPR2 binding pocket.

6.3 Second-Generation Probes

Chapter 4 described the design and synthesis of three types of second-generation probes and their binding and crosslinking to FPR1. The design of this new generation was based on the structure of Tracer-FITC which has a high binding affinity towards FPR1. Probe2.0TAMRA was shown to specifically bind to FPR1, as analysed by flow cytometry, and cause internalisation of FPR1 observed by confocal microscopy. Following from the confocal imaging of Probe2.0TAMRA-induced FPR1 internalisation, I also hoped to image the recycling of FPR1. The heating of HEK293T cells expressing FPR1 and confocal imaging would be performed after incubation and irradiation with Probe2.0TAMRA. With the probe crosslinked to FPR1, more of the desensitisation and internalisation process could be viewed, although there could still be the issue of ligand degradation. Following from this, the probe crosslinked to FPR1 with little off-target crosslinking observed by SDS-PAGE. The off-target crosslinked protein was approximately 75 kDa and unknown. It is possible that the identity of this protein could be discovered by adapting the probe to contain an alkyne tag or an affinity tag to pull it out of the cell lysate. Probe2.0TAMRA was also shown to bind to GMS-10 cells that endogenously express FPR1.

The success of this probe inspired the design of Probe2.1Desthio, bearing a desthiobiotin tag for future purification of the FPR1-probe complex. This probe was also shown to bind to FPR1, through competition with TracerFITC. However, all attempts to crosslink failed. It was proposed that the probe could have a fast off-rate

hindering crosslinking. Following the publication of the FPR2-based homology model of FPR1, docking studies with this probe could help to highlight why it does not crosslink.

Two probes containing a cleavable disulphide bond were also synthesised (Probe2.2SDi and Probe2.2SDiAlk). The crosslink site of these probes could potentially be easier to find in the proteomics experiments, due to the “dead-end” created when the disulphide is cleaved with reducing agent. Probe2.2SDi and Probe2.2SDiAlk both showed binding to FPR1 as analysed by flow cytometry, but at a lower affinity than Probe2.0TAMRA (reduced shift in fluorescence in flow cytometry compared with control cells). Both probes also crosslinked to FPR1 with only small amounts of off-target labelling. The cleavage of the disulphide bonds was not fully achieved as confirmed by bands still visible during in-gel fluorescence. It was proposed that this was due to incomplete denaturation of FPR1. Following investigation for the anti-FLAG pull-downs and proteomic experiments, it is possible that the presence of urea in the sample loading buffer could aid in this.

6.4 Anti-FLAG Pull-Down and Proteomics of FPR1-Probe Complexes

Chapter 5 discussed the immunoprecipitation of FPR1-Probe2.0TAMRA and FPR1-Probe2.2SDi by an anti-FLAG pull-down and the preliminary bottom-up proteomic experiments of these isolated complexes. The anti-FLAG pull-down was optimised and used in combination with the deglycosylation reaction. FPR1-Probe2.0TAMRA and FPR1-Probe2.2SDi were successfully eluted and no other proteins were detected by in-gel fluorescence or Coomassie stain. Several proteomic experiments have been attempted on both FPR1-Probe2.0TAMRA and FPR1-Probe2.2SDi. Poor sequence coverage of FPR1 has been achieved in the transmembrane and N-terminal region and no crosslink sites have been identified. The sample preparation and digestion of the FPR1-probe complexes requires optimisation.

6.5 Work-Flow Establishment for Binding and Crosslinking Studies

As this was a new project in the group, the work-flow used for binding and crosslinking to FPR1 had to established and optimised. The transient transfection conditions for the expression of FPR1 in HEK293T cells were optimised to ensure efficient and correct expression. For the incubation of the cells with probes many approaches were trialled testing temperature, buffer, using adhered cells or suspending them in buffer. Following from this, the irradiation with UV light for crosslinking has been performed with two different UV lamps also testing washing of the cells between incubation with probe and irradiation, and the effect of multiple irradiations on crosslinking efficiency. Finally, the anti-FLAG pull-down for the immunoprecipitation of FPR1-probe complexes has been optimised and shown to work following the delgycosylation of FPR1. This work-flow establishment forms the fundamentals of this project and can be applied to the future photoaffinity labelling of FPR1.

6.6 Future Work

The following section will discuss the future work directly for this project and other possible future avenues.

6.6.1 Bottom-Up Proteomic Experiments on FPR1

The final aim of this project was to perform bottom-up proteomics on FPR1 crosslinked to a photoreactive probe to locate the site of crosslink. With this I hoped to gain knowledge into how the formyl peptides bind to FPR1 and what key residues are interacting. With this information I could better understand what ligands are tolerated by FPR1, how other ligands might bind and propose unknown ligands. Therefore, immediate future work for this project will be to optimise the digestion of FPR1 to achieve better sequence coverage. This will require the testing of different enzymes, solvents and additives, and will be best performed on unlabeled FPR1. When the optimum sequence coverage is achieved for FPR1, the crosslink sites for Probe2.0TAMRA and Probe2.2SDi can be identified. It is expecteed that this may be

difficult for Probe2.0TAMRA due to the possibility of digestion and fragmentation during mass spectrometry. The Probe2.2SDi crosslink site should prove easier to locate as it is a “dead-end” and can be searched for as an artificial post-translational modification. As a group we have also begun modelling of the synthesised probes with the homology model of FPR1. This will hopefully provide further insight to how the probes are binding and may even highlight why Probe2.0TAMRA binds with a higher affinity than Probe2.2SDi/SDiAlk.

Assuming the success of Probe2.2SDi, Probe2.0TAMRA can be synthesised with the MTS-diazirine in place of photo-Met (**Figure 6.1**). Theoretically this should give a different crosslink site than Probe2.2SDi and therefore provide more information on the binding site of FPR1. It was proposed that the decrease in binding affinity for Probe2.2SDi/SDiAlk compared to Probe2.0TAMRA was likely due to a steric issue as the sidechain is longer than norleucine. It is possible that positioning the MTS-diazirine at residue one could affect the binding affinity even further, as it would be deeper in the FPR1 binding pocket. For this reason, modelling of this probe with the homology model of FPR1 would be beneficial prior to its synthesis.

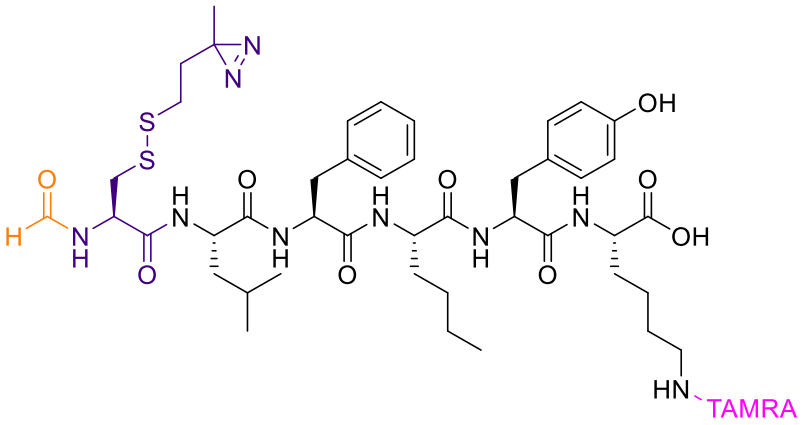

Figure 6.1: Modified structure of Probe2.0TAMRA with disulphide linked diazirine instead of photo-Met.

6.6.2 A New Generation of Probes

To learn more about the binding site of FPR1 and predict what ligands could bind, it is ideal to have multiple probes with different crosslink sites. With a homology model of FPR1 now available, new probes can be modelled to test their binding. To start, the

second-generation structure can be used and additional diazirines employed in various positions. Following from this, new probe structures should be designed to provide alternative binding modes. From flow cytometry analysis of the crosslinking of Probe2.0TAMRA (**Figure 4.1**), it was observed that not all bound probes were crosslinking to FPR1. There could be several reasons for this: crosslinking to solvent, oxidation of the carbene, isomerisation to a diazo compound. Although it has now been published that the diazo compounds react with acidic residues to form crosslinks, the abundance of Asp and Glu residues in FPR1 is very low (<5%). This also indicates that tetrazoles would be a poor photoreactive group for FPR1. However, the use of phenylazides and benzophenones could be utilised in future probes.

6.6.3 The Labelling of Endogenous FPR1 with Probe2.0TAMRA

Given the success of Probe2.0TAMRA binding to endogenously expressed FPR1 on GMS-10 cells – a glioblastoma cell line – the labelling of FPR1 expressed in other cell lines will be experimented. Indeed, this work has already begun in our group, employing Probe2.0TAMRA to label FPR1 expressed on THP-1 and U87 cells. The THP-1 cell line is a monocytic leukemia cell line[153] showing FPR1/2/3 expression[31] and U87 is a glioblastoma cell line, showing FPR1 expression, commonly used for brain cancer research.[34] A discussed in chapter 1, it has been shown that FPR1 expression in THP-1 cells increases when exposed to *Mycobacterium tuberculosis*-specific antigens.[31] Tumours formed from glioblastoma cells retain high FPR1 expression and the response of these FPR1 from mitochondrial peptides can be inhibited with the chemotaxis inhibitory protein of *Staphylococcus aureus.*[34] The labelling of FPR1 in these cell lines could therefore prove pharmacologically relevant. This labelling also provides a stepping stone to employing the use of Probe2.0TAMRA in primary cells. In this way, Probe2.0TAMRA can be used to identify FPR1 expression in cells. An improved understanding of the expression pattern of FPR1 could allow us to learn more about how the receptor works and what factors cause its upregulation. With the presence of the fluorophore, these probes could also be used to identify sites of inflammation and bacterial infection, for example, because cells will be increasing expression of FPR1.

6.6.4 Photoaffinity Labelling to FPR2

The work described in this thesis could be applied to FPR2 (and indeed FPR3). Work was started during this project for the photoaffinity labelling of FPR2; expression of FPR2 in HEK293T cells by transient transfection was optimised and the well-known fluorescent tracer WK(FITC)YMVm for FPR2 was synthesised. However, following the publication of the two papers containing FPR2 structures,[20, 21] efforts were focused on FPR1. Although these structures of FPR2 have been published, there are still many unanswered questions about ligand binding to FPR2. Therefore, the use of photoaffinity labelling could still be valuable. With the structure of FPR2 now published, photoreactive probes for use in PAL on FPR2 can be modelled first to assess binding prior to synthesis.

Chapter 7 Experimental

7.1 Synthesis of small molecules

7.1.1 General experimental

All glassware used was dried in an oven prior to the reaction. Unless otherwise stated all commercial reagents were used as received and reactions were performed in an inert atmosphere using N_2. All reactions were monitored by analytical thin layer chromatography using aluminium TLC plates coated with silica gel $60F_{254}$ purchased from Merck. TLC plates were visualized by UV light (λ=254 nm) and an aqueous potassium permanganate dip.

Flash column chromatography was performed using silica gel (60 Å, 40 – 63 micron) purchased from Merck.

^{1}H NMR and ^{13}C NMR spectra were recorded using a Bruker 400 ultra-shield spectrometer (400 MHz) in $CDCl_3$ (reference of 7.26 for ^{1}H NMR and 77.2 for ^{13}C NMR) and MeOD (reference of 4.78 and 3.31 for ^{1}H NMR, and 49.15 for ^{13}C NMR). All chemical shifts are expressed in parts per million downfield from tetramethylsilane. Peak splittings are noted as singlet (s), doublet (d), triplet (t), quartet (q), pentet (p) and multiple (m) and combinations of the stated J coupling constants are recorded to the nearest 0.5 Hz.

IR spectra were recorded using a Bruker ALPHA spectrometer.

Low resolution electrospray (ES+) ionisation mass spectra were obtained on a Bruker HCTUltra mass spectrometer.

High resolution ES+ mass spectra were obtained on a Bruker Daltonics MicroTOF mass spectrometer.

7.1.2 Synthesis and characterisation

4,4-azo-pentanoic acid 2.01

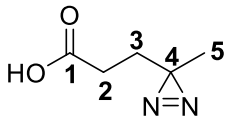

2.01

Levulinic acid (1.0 g, 8.6 mmol) was dissolved in liquid ammonia (30 mL) by the condensing of ammonia gas with an ice-acetone condenser. The solution was stirred for 5 hr with the condenser kept at −78 °C. Hydroxylamine-*O*-sulfonic acid (131 mg, 10.0 mmol) was dissolved in dry MeOH (10 mL) and added dropwise to the reaction solution. The mixture was stirred overnight, being allowed to warm to room temperature. Nitrogen was subsequently blown through the reaction for one hour to remove any ammonia. The solution was then filtered, washed with MeOH (20 mL) and concentrated under reduced pressure. The resulting oil was re-dissolved in dry MeOH (10 mL) and cooled to 0 °C. Et_3N (1.6 mL, 11 mmol) was added dropwise to the solution whilst iodine (2.8 g, 11 mmol) was crushed and dissolved in dry MeOH (20 mL). The iodine solution was then added dropwise to the reaction solution until the colour stayed dark brown. After 1 hour of stirring at 0 °C, EtOAc (10 mL) was added to the reaction mixture. The solution was washed with 1M HCl (10 mL), 10% $Na_2S_2O_3$ (10 mL) and brin (10 mL). The organic solution was dried over $MgSO_4$ and concentrated under reduced pressure to yield the product **2.01** as a pale-yellow oil (470 mg, 3.67 mmol, 43%).

^{1}H NMR (400 MHz, $CDCl_3$) δ 2.23 (2H, t, *J* = 7.5 Hz, C-2), 1.72 (2H, t, *J* = 7.5 Hz, C-3), 1.04 (3H, s, C-5); **^{13}C NMR (100 MHz, $CDCl_3$)** δ 178.1, 29.5, 28.6, 25.2, 20.9, 19.8; **LCMS** (ES+) m/z calculated for $C_5H_9N_2O_2Na$ $[M+H]^+$ 129.07, found 129.07; **R_f** 0.1 (30% ethyl acetate in pentane, 1% acetic acid).

The experimental data are consistent with the literature values.[154, 155]

(S)-2-amino-5-methoxy-5-oxopentanoic acid hydrochloride (H-Glu(OMe)-OH) 2.08

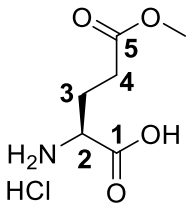

2.08

TMSCl (28.5 mL, 224 mmol) was added dropwise to a suspension of L-glutamic acid (15.0 g, 102 mmol) in dry methanol (150 mL) at room temperature over 5 min. The mixture was stirred for 20 minutes and the solvent removed under reduced pressure to furnish the product **2.08** as a white solid (19.5 g, 98.7 mmol, 98%).

^{1}H NMR (400 MHz, MeOD) δ 3.93 (1H, dt, *J* = 6.5, 2.5 Hz, C-2), 3.56 (3H, s, Me), 2.55-2.35 (2H, m, C-4), 2.17-1.97 (2H, m, C-3); **^{13}C NMR (100 MHz, MeOD)** δ 175.6 (C-5), 171.4 (C-1), 53.8 (C-2), 53.3 (Me), 30.4 (C-3), 26.7 (C-4); **HRMS** (ES+) m/z calculated for $C_6H_{11}NO_4Na$ $[M+Na]^+$ 184.058029, found 184.057657; **R_f** 0.19 (2% ethanol in DCM).

The experimental data are consistent with the literature values.[112, 156]

(S)-2-((*tert*-butoxycarbonyl)amino)-5-methoxy-5-oxopentanoic acid (Boc-Glu(OMe)-OH) 2.09

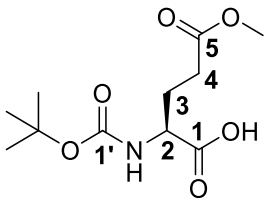

2.09

H-Glu(OMe)-OH (10.0 g, 50.6 mmol) was dissolved in dioxane/water (2:1, 150 mL) and cooled to 0 °C. Boc_2O (13.2 g, 60.7 mmol) and $NaHCO_3$ (10.6 g, 127 mmol) were added and the reaction mixture was warmed up to room temperature, before being stirred for 12 hr. The dioxane was removed under reduced pressure and the aqueous solution was washed with diethyl ether (50 mL). 1M HCl was added to adjust the pH to 3 and the resulting solution was extracted with ethyl acetate (2 × 50 mL). The organic solution was washed with water (50 mL) and brine (50 mL), and dried over anhydrous Na_2SO_4. Removal of the solvent under reduced pressure yielded the product **2.09** as a pale yellow oil (10.0 g, 38.3 mmol, 76%).

^{1}H NMR (400 MHz, $CDCl_3$) δ 5.22 (1H, d, *J* = 8.0 Hz, NH), 4.40-4.29 (1H, m, C-2), 3.68 (3H, s, Me), 2.53-2.38 (2H, m, C-4), 2.27-2.19 (1H, m, C-3), 2.05-1.96 (1H, m, C-3), 1.43 (9H, s, ^{t}Bu); **^{13}C NMR (100 MHz, $CDCl_3$)** δ 176.3, 173.6, 155.5, 52.9, 52.0, 30.3, 28.4, 27.6; **HRMS** (ES+) m/z calculated for $C_{11}H_{19}NO_6Na$ $[M+Na]^+$ 284.110458, found 284.110436; $C_{11}H_{19}NO_6K$ $[M+K]^+$ 300.084395, found 300.0843910; **R_f** 0.33 (40% ethyl acetate in pentane).

The experimental data are consistent with the literature values.[112, 156]

(S)-5-(*tert*-butoxy)-4-((*tert*-butoxycarbonyl)amino)-5-oxopentanoic acid (Boc- Glu(OH)-O*t*-Bu) 2.10

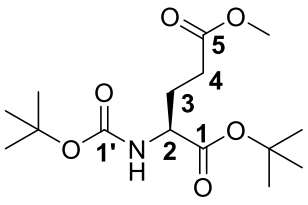

2.10

DCC (9.47 g, 45.9 mmol), DMAP (469 mg, 3.84 mmol) and ^{t}BuOH (36.6 mL, 383 mmol) were added to ice-cold DCM (150 mL). Boc- Glu(OMe)-OH (10.03 g, 38.39 mmol) was dissolved in DCM (100 mL) and added dropwise to the ice-cold mixture. The reaction solution was stirred for one hour at 0 °C and allowed to warm to room temperature over 12 hr with stirring. The DCM was removed under reduced pressure and the resulting white solid was re-dissolved in ethyl acetate (100 mL). The suspension was filtered through celite to remove DCU and the filtrate washed with 0.1 M HCl (100 mL), saturated sodium $NaHCO_3$ (100 mL) and brine (100 mL). The organic solution was dried over anhydrous Na_2SO_4 and concentrated under reduced pressure. The crude product was purified using column chromatography (10% ethyl acetate in pentane) to yield the product **2.10** as a white solid (9.30 g, 29.3 mmol, 76%).

^{1}H NMR (400 MHz, $CDCl_3$) δ 5.07 (1H, d, *J* = 8.5 Hz, NH), 4.19-4.09 (1H, m, C-2), 3.67 (3H, s, Me), 2.46-2.31 (2H, m, C-4), 2.19-2.10 (1H, m, C-3), 1.95-1.86 (1H, m, C-3), 1.46 (9H, s, ^{t}Bu), 1.43 (9H, s, ^{t}Bu); **^{13}C NMR (100 MHz, $CDCl_3$)** δ 173.4, 171.4, 155.5, 82.3, 79.9, 53.3, 51.9, 30.3, 28.5, 28.3, 28.1; **HRMS** (ES+) m/z calculated for $C_{15}H_{27}NO_6Na$ $[M+Na]^+$ 340.173058, found 340.174113; **R_f** 0.30 (30% ethyl acetate in pentane).

The experimental data are consistent with the literature values.[112, 156]

(S)-5-(*tert*-butoxy)-4-((*tert*-butoxycarbonyl)amino)-5-oxopentanoic acid (Boc- Glu(OH)-O*t*-Bu) 2.11

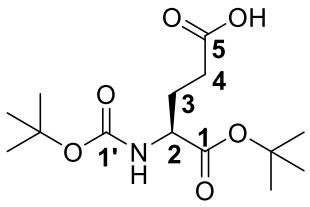

2.11

A 1M LiOH solution (15.8 mL, 15.8 mmol) was added dropwise to a solution of Boc-Glu(OH)-O*t*-Bu (2.5 g, 7.9 mmol) in THF (50 mL) over 30 min. The reaction mixture was left to stir for 2 hr before being cooled to 0 °C. 0.1M HCL was added dropwise to the solution until the pH was 5. The organic layer was extracted with ethyl acetate (2 × 50 mL), washed with brine (50 mL) and dried over anhydrous Na_2SO_4. Concentrating under reduced pressure yielded the product **2.11** as a white solid (2.3 g, 7.6 mmol, 96%).

^{1}H NMR (400 MHz, $CDCl_3$) δ 5.16 (1H, d, *J* = 8.0 Hz, NH), 4.29-4.07 (1H, m, C-2), 2.53-2.37 (2H, m, C-4), 2.23-2.09 (1H, m, C-3), 1.99-1.84 (1H, m, C-3), 1.47 (9H, s, ^{t}Bu), 1.44 (9H, s, ^{t}Bu); **^{13}C NMR (100 MHz, $CDCl_3$)** δ 177.1, 171.0, 155.7, 53.2, 30.2, 28.3, 28.0; **HRMS** (ES+) m/z calculated for $C_{14}H_{25}NO_6Na$ $[M+Na]^+$ 326.157408, found 326.158035; **R_f** 0.44 (30% ethyl acetate in pentane, 1% acetic acid).

The experimental data are consistent with the literature values.[112, 157]

(S)-*tert*-butyl 2-((*tert*-butoxycarbonyl)amino)-5-(methoxy(methyl)amino)-5-oxopentanoate 2.12

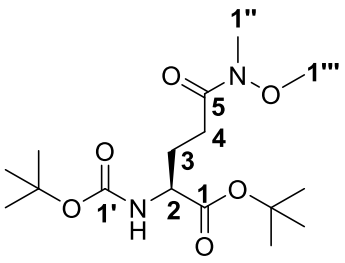

2.12

Boc- Glu(OH)-O*t*-Bu (300 mg, 0.99 mmol) dissolved in DCM (25 mL) and isobutyl chloroformate (0.17 mL, 1.3 mmol) were added to *N*-methylmorpholine (0.27 mL, 2.5 mmol) at 0 °C. The reaction mixture was stirred for one hour at 0 °C before *N*,*O*-dimethylhydroxylamine hydrochloride (116 mg, 1.19 mmol) was added portion-wise. The reaction mixture was stirred for a further 16 hr at room temperature and subsequently quenched with 0.1 M HCl (10 mL). The organics were extracted with DCM (3 × 20 mL), washed with brine (30 mL) and dried over anhydrous Na_2SO_4. The crude product was concentrated under reduced pressure and purified via column chromatography (30% ethyl acetate in pentane) to furnish the product **2.12** as a colourless oil which solidified upon standing (290 mg, 0.84 mmol, 84%).

^{1}H NMR (400 MHz, $CDCl_3$) δ 5.19 (1H, d, *J* = 8.5 Hz, NH), 4.27-4.16 (1H, m, C-2), 3.69 (3H, s, C-1’’’), 3.20 (3H, s, C-1’’), 2.63-2.44 (2H, m, C-4), 2.23-2.12 (1H, m, C-3), 1.99-1.90 (1H, m, C-3), 1.49 (9H, s, ^{t}Bu), 1.46 (9H, s, ^{t}Bu); **^{13}C NMR (100 MHz, $CDCl_3$)** δ 171.6, 155.5, 122.7, 81.9, 79.6, 61.2, 53.8, 32.3, 28.3, 28.0, 27.6; **HRMS** (ES+) m/z calculated for $C_{16}H_{30}N_2O_6Na$ $[M+Na]^+$ 369.199607, found 369.199125; $C_{16}H_{30}N_2O_6K$ $[M+K]^+$ 385.173545, found 385.172647; $C_{32}H_{60}N_4O_{12}Na$ $[2M+Na]^+$ 715.409994, found 715.409804; **R_f** 0.29 (60% ethyl acetate in pentane).

The experimental data are consistent with the literature values.[112, 157]

(S)-*tert*-butyl-2-((*tert*-butoxycarbonyl)amino)-5-oxohexanoate 2.13

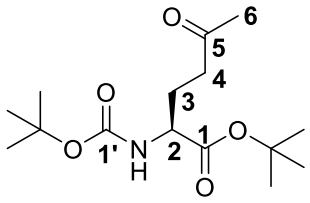

2.13

(S)-*tert*-butyl-2-((*tert*-butoxycarbonyl)amino)-5-(methoxy(methyl)amino)-5-oxopentanoate (1.066 g, 3.08 mmol) was dissolved in toluene (50 mL) and cooled to −78 °C. Methylmagnesium bromide solution 3.0 M (2.11 mL, 6.34 mmol) was added dropwise over 30 minutes, after which the solution was warmed to −5 °C and stirred for three hr. The reaction was quenched with 0.1 M HCl (20 mL) and the organic solution extracted with ethyl acetate (3 × 20 mL). The solution was dried over anhydrous Na_2SO_4 and concentrated under reduced pressure. The crude product was purified via column chromatography (10% ethyl acetate in hexane) to furnish the product **2.13** as a colourless oil (0.555 g, 1.84 mmol, 64%).

^{1}H NMR (400 MHz, $CDCl_3$) δ 5.05 (1H, d, *J* = 6.0 Hz, NH), 4.19-4.09 (1H, m, C-2), 2.63-2.43 (2H, m, C-4), 2.15 (3H, s, Me), 2.13-2.05 (1H, m, C-3), 1.90-1.78 (1H, m, C-3), 1.49 (9H, s, ^{t}Bu), 1.44 (9H, s, ^{t}Bu); **^{13}C NMR (100 MHz, $CDCl_3$)** δ 207.7, 171.6, 155.6, 82.2, 79.9, 53.4, 39.6, 30.1, 28.4, 28.1, 27.0; **HRMS** (ES+) m/z calculated for $C_{15}H_{27}NO_5Na$ $[M+Na]^+$ 324.178144, found 324.178500; $C_{15}H_{27}NO_5K$ $[M+K]^+$ 340.152081, found 340.151683; $C_{30}H_{54}N_2O_{10}Na$ $[2M+Na]^+$ 625.367067, found 625.367033; **R_f** 0.44 (60% ethyl acetate in hexane).

The experimental data are consistent with the literature values.[112, 157]

(S)-tert-butyl 2-((tert-butoxycarbonyl)amino)-4-(3-methyl-3H-diazirin-3-yl)butanoate 2.14

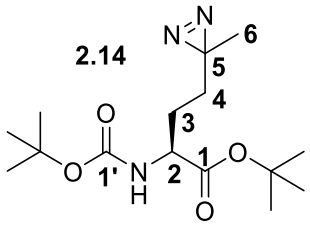

(S)-*tert*-butyl 2-((*tert*-butoxycarbonyl)amino)-5-oxohexanoate (1.0 g, 3.3 mmol) was dissolved in liquid ammonia (30 mL) by the condensing of ammonia gas with an ice-acetone condenser. The solution was stirred for 5 hr with the condenser kept at −78 °C. Hydroxylamine-*O*-sulfonic acid (441 mg, 3.90 mmol) was dissolved in dry MeOH (10 mL) and added dropwise to the reaction solution. The mixture was stirred overnight, being allowed to warm to room temperature. Nitrogen was subsequently blown through the reaction for one hour to remove any ammonia. The solution was then filtered, washed with MeOH (20 mL) and concentrated under reduced pressure. The resulting oil was re-dissolved in dry MeOH (10 mL) and cooled to 0 °C. Et_3N (1.4 mL, 9.9 mmol) was added dropwise to the solution whilst iodine (1.1 g, 4.3 mmol) was crushed and dissolved in dry MeOH (20 mL). The iodine solution was then added dropwise to the reaction solution until the colour stayed dark brown. After 1 hour of stirring at 0 °C, EtOAc (10 mL) was added to the reaction mixture. The solution was washed with 1M HCl (10 mL), 10% $Na_2S_2O_3$ (10 mL) and brine (10 mL). The organic solution was dried over $MgSO_4$ and concentrated under reduced pressure to yield the product **2.14** as a pale yellow oil (940 mg, 3.00 mmol, 94%).

^{1}H NMR (400 MHz, $CDCl_3$) δ 4.99 (1H, d, *J* = 8.0 Hz, NH), 4.18-4.08 (1H, m, C-2), 1.74-1.65 (1H, m, C-3), 1.52-1.40 (2H, m, C-4), 1.37-1.27 (1H, m, C-3), 1.49 (9H, s, ^{t}Bu), 1.44 (9H, s, ^{t}Bu), 1.01 (3H, s, C-6); **^{13}C NMR (100 MHz, $CDCl_3$)** δ 171.5, 155.4, 82.3, 80.0, 53.5, 30.5, 28.5, 28.1, 27.6, 25.5, 19.8; **HRMS** (ES+) m/z calculated for $C_{15}H_{27}N_3O_4Na$ $[M+Na]^+$ 336.189377, found 336.189526; $C_{15}H_{27}N_3O_4K$ $[M+K]^+$ 352.163314, found 352.163238; $C_{30}H_{54}N_6O_8Na$ $[2M+Na]^+$ 649.389533, found 649.389315; **R_f** 0.48 (20% ethyl acid in hexane).

The experimental data are consistent with the literature values.[112, 158]

Fmoc-photo-Met 2.15

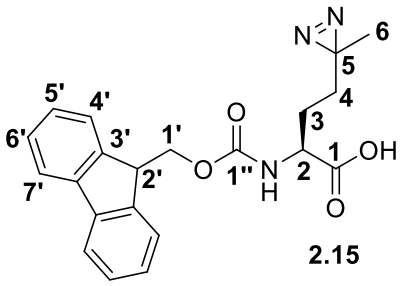

2.15

4M HCl (25 mL) was added to (S)-tert-butyl 2-((tert-butoxycarbonyl)amino)-4-(3-methyl-3H-diazirin-3-yl)butanoate (250 mg, 0.798 mmol) in THF (25 mL) and the solution was stirred at room temperature until the starting material was consumed. The solvent was removed under reduced pressure and the resulting yellow powder re-dissolved in water/dioxane (1:2) (12 mL). $NaHCO_3$ was added to the solution until the pH was basic. FmocOSu (324 mg, 0.960 mmol) was dissolved in dioxane (1 mL) and added dropwise to the reaction, which was then stirred at room temperature for 24 hr. The dioxane was removed under reduced pressure and water (5mL) added to the residue. 1M HCl was added until the pH reached 4 and following this the organic solution was extracted with EtOAc (3 × 10 mL). The combined organics were dried over Na_2SO_4 and concentrated to give the crude product. Purification using column chromatography (20% EtOAc in hexane, 1% TFA) furnished the product **2.15** as a white solid (220 mg, 0.580 mmol, 73%).

^{1}H NMR (400 MHz, $CDCl_3$) δ 7.77 (2H, d, *J* = 7.5 Hz, C-4'), 7.58 (2H, d, *J* = 7.5 Hz, C-7'), 7.41 (2H, t, *J* = 7.5 Hz, C-5'/C-6'), 7.32 (2H, t, *J* = 7.5 Hz, C-5'/C-6'), 5.21 (1H, d, *J* = 8.0 Hz, NH), 4.60-4.49 (1H, m, C-2), 4.44 (1H, d, *J* = 7.0 Hz, C-1'), 4.40-4.32 (1H, m, C-1'), 4.22 (1H, t, *J* = 6.5 Hz, C-2'), 1.88-1.76 (1H, m, C-3), 1.64-1.34 (3H, m, C-3, C-4); **^{13}C NMR (100 MHz, $CDCl_3$)** δ 210.4, 180.2, 177.0, 175.0, 166.5, 164.9, 161.8, 159.0, 157.6, 147.3, 62.9; **HRMS** (ES+) m/z calculated for $C_{21}H_{22}N_3O_4$ $[M+H]^+$ 380.160483, found 380.160801; $C_{21}H_{21}N_3NaO_4$ $[M+Na]^+$ 402.142427, found 402.141935; **R_f** 0.34 (60% ethyl acetate in hexane).

The experimental data are consistent with the literature values.[72, 112]

3-(benzyloxy)-3-oxopropanoic acid 2.17

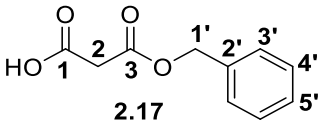

2.17

Et_3N (13.7 mL, 98.3 mmol) and benzylbromide (11.7 mL, 98.3 mmol) were added to a solution of malonic acid (10.2 g, 98.3 mmol) in acetonitrile (150 mL). The resulting solution was refluxed for three hr before being cooled to 0 °C and 1M HCl was added (100 mL). The organic solution was extracted with ethyl acetate (3 × 50 mL) and saturated $NaHCO_3$ (3 × 50 mL), and cooled to 0 °C. 1M HCl was added to the solution until pH 3, and was extracted with toluene (3 × 50 mL). The organic solution was dried over anhydrous Na_2SO_4 and concentrated under reduced pressure to yield a colourless oil. The oil was left at −20 °C to form a white solid (10.67 g, 54.99 mmol, 56%).

^{1}H NMR (400 MHz, $CDCl_3$) δ 11.60 (1H, s, OH), 7.37 (5H, m, C-2', C-3', C-4', C-5'), 5.22 (2H, s, C-1'), 3.49 (2H, s, C-2), **^{13}C NMR (400 MHz, $CDCl_3$)** δ 172.0 (C-1), 166.5 (C-3), 135.1 (C-2'), 128.7 (C-4'), 128.6 (C-5'), 128.4 (C-3'), 67.7 (C-1'), 41.0 (C-2); **HRMS** (ES+) m/z calculated for $C_{10}H_{10}NO_4Na$ $[M+Na]^+$ 217.0471, found 217.0466; **R_f** 0.21 (80% ethyl acetate in hexane).

The experimental data are consistent with the literature values.[112, 159]

(S)-6-benzyl 1-methyl 2-((tert-butoxycarbonyl)amino)-4-oxohexanedioate

2.18

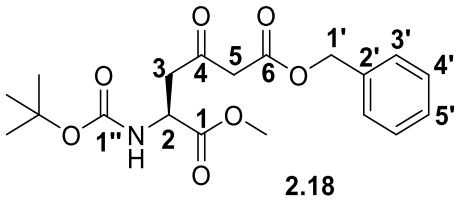

2.18

Solution A: CDI (6.72 g, 37.6 mmol) was added in portions to *N*-Boc-*L*-aspartic acid methyl ester (9.32 g, 37.7 mmol) dissolved in THF (80 mL). The reaction mixture was stirred at room temperature for 3 hr.

Solution B: 3-(Benzyloxy)-3-oxopropanoic acid (7.29 g, 37.6 mmol) was dissolved in THF (60 mL) and cooled to 0 °C. Isopropylmagnesium chloride solution 2.0 M (41 mL, 83 mmol) was added dropwise to the solution that was next stirred at 0 °C for 1 hour, followed by 50 °C for 30 minutes.

Solution B was added to solution A at 0 °C and the reaction mixture was stirred at room temperature for 16 hr. The organic solution was extracted with ethyl acetate (3 × 50 mL), washed with brine (50 mL) and dried over anhydrous Na_2SO_4. The solution was concentrated under reduced pressure and the product purified via column chromatography (30% ethyl acetate in hexane) to yield the product **2.18** as a pale orange oil (10.5 g, 27.7 mmol, 60%).

^{1}H NMR (400 MHz, $CDCl_3$) δ 7.36 (5H, m, C-2', C-3', C-4', C-5'), 5.43 (1H, d, *J* = 9.0 Hz, NH), 5.27 (2H, s, C-1'), 4.52 (1H, dt, *J* = 9.0, 4.5 Hz, C-2), 3.76 (2H, s, C-5), 3.50 (3H, s, Me), 3.25 (1H, dd, *J* = 18.0, 4.0 Hz, C-3), 3.08 (1H, dd, *J* = 18.0, 4.5 Hz, C-3), 1.44 (9H, s, ^{t}Bu); **^{13}C NMR (100 MHz, $CDCl_3$)** δ 200.8, 171.6, 166.5, 155.6, 135.3, 128.8, 128.7, 128.5, 67.5, 52.8, 49.5, 49.2, 45.0, 28.4; **HRMS** (ES+) m/z calculated for $C_{19}H_{25}NO_7Na$ $[M+Na]^+$ 402.152323, found 402.152154; $C_{38}H_{50}N_2O_{14}Na$ $[2M+Na]^+$ 781.315425, found 781.315412; **R_f** 0.10 (50% ethyl acetate in hexane).

The experimental data are consistent with the literature values.[112, 160]

(S)-methyl 2-((tert-butoxycarbonyl)amino)-4-oxopentanoate 2.19

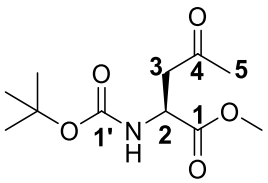

2.19

(S)-6-benzyl 1-methyl 2-((tert-butoxycarbonyl)amino)-4-oxohexanedioate (3.60 g, 9.55 mmol) was dissolved in wet methanol (60 mL) and palladium on carbon (0.10 g, 0.95 mmol) was added. The reaction was stirred for three hr whilst being fed hydrogen from a balloon. Upon completion, the solution was filtered through celite to remove the palladium and the solvent removed under reduced pressure. The oil was redissolved in methanol and reacted with Et_3N (2.66 mL, 19.1 mmol) at reflux for two hr. Purification via column chromatography (50% ethyl acetate in hexane) yielded the product **2.19** as a colourless oil (1.70g, 6.94 mmol, 73%).

^{1}H NMR (400 MHz, $CDCl_3$) δ 5.47 (1H, d, *J* = 8.0 Hz, NH), 4.49 (1H, dt, *J* = 9.0, 4.5 Hz, C-2), 3.72 (3H, s, Me), 3.17 (1H, dd, *J* = 18.0, 4.5 Hz, C-3), 2.99 (1H, dd, *J* = 18.0, 4.5 Hz, C-3), 2.16 (3H, s, C-5), 1.44 (9H, s, ^{t}Bu); **^{13}C NMR (100 MHz, $CDCl_3$)** δ 206.7, 172.0, 155.7, 52.8, 49.6, 45.6, 30.1, 28.5; **HRMS** (ES+) m/z calculated for $C_{11}H_{19}O_5Na$ $[M+Na]^+$ 268.115543, found 268.115818; $C_{11}H_{19}O_5K$ $[M+K]^+$ 284.089481, found 284.088971; $C_{22}H_{38}O_{10}Na$ $[2M+Na]^+$ 513.241866, found 513.241642; **R_f** 0.59 (60% ethyl acetate in hexane).

The experimental data are consistent with the literature values.[161]

(S)-methyl 2-((tert-butoxycarbonyl)amino)-4-oxopentanoate 2.20

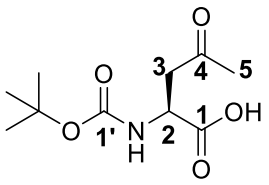

2.20

A 1M LiOH solution (4.0 mL, 4.0 mmol) was added dropwise to a solution of Boc-Glu(OH)-O*t*-Bu (430 mg, 1.75 mmol) in THF (10 mL) over 30 min. The reaction mixture was left to stir for 30 min at room temperature, followed by 1 hr at 0 °C. 0.1M HCL was added dropwise to the solution until the pH was 3/4. The organic layer was extracted with ethyl acetate (3 × 10 mL), washed with brine (20 mL) and dried over anhydrous Na_2SO_4. Concentrating under reduced pressure yielded the product **2.20** as a white solid (364 mg, 1.58 mmol, 90%).

^{1}H NMR (400 MHz, $CDCl_3$) δ 5.54 (1H, d, *J* = 8.5 Hz, NH), 4.59-4.44 (1H, m, C-2), 3.20 (1H, dd, *J* = 18.0, 2.5 Hz, C-3), 2.95 (1H, dd, *J* = 18.0, 4.5 Hz, C-3), 2.19 (3H, s, C-5), 1.44 (9H, s, ^{t}Bu); **^{13}C NMR (100 MHz, $CDCl_3$)** δ 206.9, 175.5, 155.7, 49.6, 45.1, 29.9, 28.3; **HRMS** (ES+) m/z calculated for $C_{10}H_{17}O_5Na$ $[M+Na]^+$ 254.099893, found 254.099529; **R_f** 0.14 (60% ethyl acetate in hexane, 1% acetic acid).

The experimental data are consistent with the literature values.[161]

(S)-*tert*-butyl 2-((*tert*-butoxycarbonyl)amino)-5-oxopentanoate 2.22

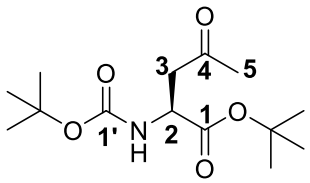

2.22

DCC (0.51 g, 2.6 mmol), DMAP (27 mg, 0.22 mmol) and ^{t}BuOH (2.1 mL, 22 mmol) were added to ice-cold DCM (10 mL). (S)-methyl 2-((*tert*-butoxycarbonyl)amino)-4-oxopentanoate (500 mg, 2.16 mmol) was dissolved in DCM (10 mL) and added dropwise to the ice-cold mixture. The reaction solution was stirred for one hour at 0 °C and allowed to warm to room temperature over 12 hr with stirring. The DCM was removed under reduced pressure and the resulting white solid was re-dissolved in ethyl acetate (10 mL). The suspension was filtered through celite to remove DCU and the filtrate washed with 0.1 M HCl (10 mL), saturated sodium $NaHCO_3$ (10 mL) and brine (10 mL). The organic solution was dried over anhydrous Na_2SO_4 and concentrated under reduced pressure. The crude product was purified using column chromatography (30% ethyl acetate in hexane) to yield the product **2.22** as a white solid (260 mg, 0.910 mmol, 43%).

^{1}H NMR (400 MHz, $CDCl_3$) δ 5.43 (1H, d, *J* = 8.5 Hz, NH), 4.41-4.32 (1H, m, C-2), 3.10 (1H, dd, *J* = 18.0, 4.5 Hz, C-3), 2.89 (1H, dd, *J* = 18.0, 4.5 Hz, C-3), 2.16 (3H, s, C-5), 1.44 (18H, s, ^{t}Bu); **^{13}C NMR (100 MHz, $CDCl_3$)** δ 171.5, 155.4, 82.3, 80.0, 53.5, 30.5, 29.9, 28.5, 28.1, 27.6, 25.5, 19.8; **HRMS** (ES+) m/z calculated for $C_{14}H_{25}NNaO_5$ $[M+Na]^+$ 310.162494, found 310.162892; $C_{14}H_{25}NKO_5$ $[M+K]^+$ 326.136431, found 326.136259; $C_{28}H_{50}N_2NaO_{10}$ $[2M+Na]^+$ 597.335767, found 597.335817; **R_f** 0.24 (20% ethyl acetate in hexane).

The experimental data are consistent with the literature values.[162]

(S)-*tert*-butyl 2-((*tert*-butoxycarbonyl)amino)-4-(3-methyl-3H-diazirin-3-yl)propanoate 2.23

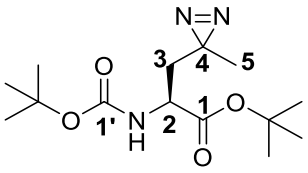

2.23

(S)-*tert*-butyl 2-((*tert*-butoxycarbonyl)amino)-5-oxopentanoate (250 mg, 0.871 mmol) was dissolved in liquid ammonia (10 mL) by the condensing of ammonia gas with an ice-acetone condenser. The solution was stirred for 5 hr with the condenser kept at −78 °C. Hydroxylamine-*O*-sulfonic acid (115 mg, 1.17 mmol) was dissolved in dry MeOH (5 mL) and added dropwise to the reaction solution. The mixture was stirred overnight, being allowed to warm to room temperature. Nitrogen was subsequently blown through the reaction for one hour to remove any ammonia. The solution was then filtered, washed with MeOH (20 mL) and concentrated under reduced pressure. The resulting oil was re-dissolved in dry MeOH (5 mL) and cooled to 0 °C. Et_3N (0.4 mL, 2.6 mmol) was added dropwise to the solution whilst iodine (280 mg, 1.10 mmol) was crushed and dissolved in dry MeOH (10 mL). The iodine solution was then added dropwise to the reaction solution until the colour stayed dark brown. After 1 hour of stirring at 0 °C, EtOAc (5 mL) was added to the reaction mixture. The solution was washed with 1M HCl (5 mL), 10% $Na_2S_2O_3$ (5 mL) and brine (5 mL). The organic solution was dried over $MgSO_4$ and concentrated under reduced pressure to yield the product **2.23** as a pale yellow oil (110 mg, 0.368 mmol, 42%).

^{1}H NMR (400 MHz, $CDCl_3$) δ 5.08 (1H, d, *J* = 9.0 Hz, NH), 4.25 (1H, d, *J* = 7.5 Hz, C-2), 1.82 (1H, dd, *J* = 15.0, 6.0 Hz, C-3), 1.62 (1H, dd, *J* = 15.0, 7.5 Hz, C-3), 1.49 (9H, s, ^{t}Bu), 1.47 (9H, s, ^{t}Bu), 1.09 (3H, s, C-5); **^{13}C NMR (100 MHz, $CDCl_3$)** δ 170.9, 155.3, 82.8, 80.2, 51.1, 38.5, 28.4, 28.1, 20.0; **HRMS** (ES+) m/z calculated for $C_{14}H_{25}N_3NaO_4$ $[M+Na]^+$ 322.173727, found 322.173831; $C_{14}H_{25}N_3KO_4$ $[M+K]^+$ 338.147664, found 338.147319; $C_{28}H_{50}N_6NaO_8$ $[2M+Na]^+$ 621.358233, found 621.358124; **R_f** 0.89 (40% ethyl acetate in hexane).

(S)-6-benzyl 1-*tert*-butyl 2-((*tert*-butoxycarbonyl)amino)-4-oxohexanedioate 2.25

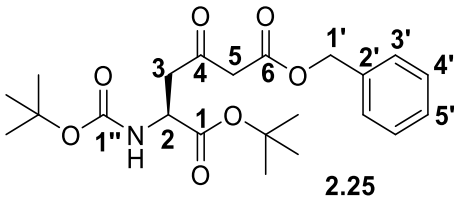

2.25

Solution A: CDI (6.72 g, 37.6 mmol) was added in portions to *N*-Boc-*L*-aspartic acid tert-butyl ester (9.32 g, 37.7 mmol) dissolved in THF (80 mL). The reaction mixture was stirred at room temperature for 3 hr.

Solution B: 3-(Benzyloxy)-3-oxopropanoic acid (7.29 g, 37.6 mmol) was dissolved in THF (60 mL) and cooled to 0 °C. Isopropylmagnesium chloride solution 2.0 M (41 mL, 83 mmol) was added dropwise to the solution that was next stirred at 0 °C for 1 hour, followed by 50 °C for 30 minutes.

Solution B was added to solution A at 0 °C and the reaction mixture was stirred at room temperature for 16 hr. The organic solution was extracted with ethyl acetate (3 × 50 mL), washed with brine (50 mL) and dried over anhydrous Na_2SO_4. The solution was concentrated under reduced pressure and the product purified via column chromatography (30% ethyl acetate in hexane) to yield the product **2.25** as a pale orange oil (3.82 g, 9.07 mmol, 61%).

^{1}H NMR (400 MHz, $CDCl_3$) δ 7.40-7.30 (5H, m, C-2', C-3', C-4', C-5'), 5.40 (1H, d, *J* = 8.5 Hz, NH), 5.17 (2H, d, *J* = 3.0 Hz, C-1'), 4.38 (1H, dt, *J* = 9.0, 4.5 Hz, C-2), 3.50 (2H, d, *J* = 1.5 Hz, C-5), 3.20 (1H, dd, *J* = 18.0, 4.5 Hz, C-3), 3.02 (1H, dd, *J* = 18.0, 4.5 Hz, C-3), 1.43 (9H, s, ^{t}Bu), 1.42 (9H, s, ^{t}Bu); **^{13}C NMR (100 MHz, $CDCl_3$)** δ 200.7, 170.0, 166.6, 155.7, 135.3, 128.8, 128.6, 128.5, 82.5, 80.0, 67.4, 50.2, 49.3, 45.3, 28.5, 28.0; **HRMS** (ES+) m/z calculated for $C_{22}H_{31}NNaO_7$ $[M+Na]^+$ 444.199273, found 444.199314; $C_{44}H_{62}N_2NaO_{14}$ $[2M+Na]^+$ 865.409325, found 865.409437; **R_f** 0.53 (50% ethyl acetate in hexane).

(S)-*tert*-butyl 2-((*tert*-butoxycarbonyl)amino)-4-oxopentanoate 2.22

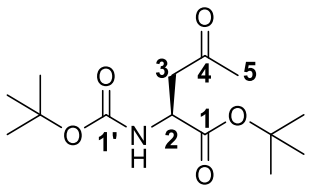

2.22

(S)-6-benzyl 1-*tert*-butyl 2-((*tert*-butoxycarbonyl)amino)-4-oxohexanedioate (3.60 g, 9.55 mmol) was dissolved in wet methanol (60 mL) and palladium on carbon (0.10 g, 0.95 mmol) was added. The reaction was stirred for three hr whilst being fed hydrogen from a balloon. Upon completion, the solution was filtered through celite to remove the palladium and the solvent removed under reduced pressure. The oil was redissolved in methanol and reacted with Et_3N (2.66 mL, 19.1 mmol) at reflux for two hr. Purification via column chromatography (50% ethyl acetate in hexane) yielded the product **2.22** as a colourless oil (2.15 g, 7.48 mmol, 83%).

^{1}H NMR (400 MHz, $CDCl_3$) δ 5.43 (1H, d, *J* = 8.5 Hz, NH), 4.41-4.32 (1H, m, C-2), 3.10 (1H, dd, *J* = 18.0, 4.5 Hz, C-3), 2.89 (1H, dd, *J* = 18.0, 4.5 Hz, C-3), 2.16 (3H, s, C-5), 1.44 (18H, s, ^{t}Bu); **^{13}C NMR (100 MHz, $CDCl_3$)** δ 171.5, 155.4, 82.3, 80.0, 53.5, 30.5, 29.9, 28.5, 28.1, 27.6, 25.5, 19.8; **IR** (neat, cm^{-1}) √ 3466, 3324, 3008, 2980, 2931, 2849, 2049, 1701, 1717, 1625, 1569, 1490, 1455, 1433, 1404, 1393, 1367, 1356, 1218, 1151, 1087, 1055, 1031; **HRMS** (ES+) m/z calculated for $C_{14}H_{25}NNaO_5$ $[M+Na]^+$ 310.162494, found 310.162892; $C_{14}H_{25}NKO_5$ $[M+K]^+$ 326.136431, found 326.136259; $C_{28}H_{50}N_2NaO_{10}$ $[2M+Na]^+$ 597.335767, found 597.335817; **R_f** 0.24 (20% ethyl acetate in hexane).

The experimental data are consistent with the literature values.[162]

Fmoc-photo-Leu 2.26

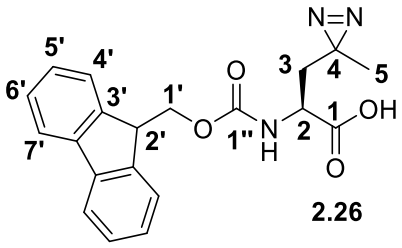

2.26

TFA (9 mL) was added to (S)-tert-butyl 2-((tert-butoxycarbonyl)amino)-4-(3-methyl-3H-diazirin-3-yl)propanoate (70 mg, 0.23 mmol) in DCM (1 mL) and the solution was stirred at room temperature until the protecting groups were removed. The solvent was removed under reduced pressure and the resulting yellow oil re-dissolved in water/dioxane (1:2) (8 mL). $NaHCO_3$ was added to the solution until the pH was basic. FmocOSu (50 mg, 0.57 mmol) was dissolved in dioxane (1 mL) and added dropwise to the reaction, which was then stirred at room temperature for 24 hr. The dioxane was removed under reduced pressure and water (5mL) added to the residue. 1M HCl was added until the pH reached 4 and following this the organic solution was extracted with EtOAc (3 × 5 mL). The combined organics were dried over Na_2SO_4 and concentrated to give the crude product. Purification using column chromatography (20% EtOAc in hexane, 1% TFA) furnished the product **2.26** as a white solid (60 mg, 0.16 mmol, 73%).

^{1}H NMR (400 MHz, MeOD) δ 7.70 (2H, d, *J* = 7.5 Hz, C-4'), 7.62 (2H, d, *J* = 7.5 Hz, C-7'), 7.29 (2H, d, *J* = 7.5 Hz, C-5'/C-6'), 7.21 (2H, d, *J* = 7.5 Hz, C-5'/C-6'), 4.34-4.21 (1H, m, C-1'), 4.17 (1H, t, *J* = 7.0 Hz, C-2'), 4.06-3.98 (1H, m, C-1'), 1.96-1.83 (1H, m, C-3), 1.55 (1H, dd, *J* = 15, 10.5 Hz, C-3), 0.95 (3H, s, C-5); **^{13}C NMR (100 MHz, MeOD)** δ 145.2, 142.6, 128.8, 128.1, 126.3, 120.9, 112.4, 70.0, 68.1; **HRMS** (ES+) m/z calculated for $C_{20}H_{19}N_3NaO_4$ $[M+Na]^+$ 388.126777, found 388.126783; **R_f** 0.11 (60% ethyl acetate in hexane, 1% TFA).

The experimental data are consistent with the literature values.[161]

7.2 Solid Phase Peptide Synthesis

7.2.1 General Reagents and Equipment

All amino acids and other reagents were purchased from Novabiochem and Sigma Aldrich and were used without further purification.

Fritted polypropylene tubes (10 mL) were purchased from Biotage and used as the vessels for peptide synthesis.

Dissolution of reagents and peptides was achieved by agitation through the use of a Stuart rotator.

2-Chlorotrityl chloride resin (loading 1.33 mmol/g) was used as the stationary phase for peptide synthesis.

Analysis of peptides during SPPS was performed using a Thermo Ultimate 3000 UHPLC, Bruker Amazon Speed ion trap mass spec with a Phenomenex Aeris Peptide XB C18 column (100 x 2.1mm, 2.6um particle size). Gradient from 0.1% TFA/ 2% MeCN (v/v) in water to 0.1% TFA/ 98% MeCN (v/v) in water with a flow rate of 0.85ml/min.

Analysis of final peptides was performed using an Agilent 1290 Infinity with Diode Array Detection with an Ascentis Peptide ES C18 column (100 x 2.1mm, 2.7um particle size). Gradient from 0.1% TFA/ 5% MeCN (v/v) in water to 0.1% TFA/ 95% MeCN (v/v) in water with a flow rate of 0.5ml/min.

7.2.2 General Methods for Solid Phase Peptide Synthesis

7.2.2.1 Method 1 – Loading of 2-Chlorotrityl chloride resin

2-Chlorotrityl chloride resin was swollen in DCM for 30 mins. Fmoc-Pra (1 equiv.) and DIPEA (4 equiv.) were dissolved in dry DCM (10 mL per gram of resin). This solution was added to the swollen resin and stirred for 2 hr. Following this, the resin was washed three times with DCM/MeOH/DIPEA (17:2:1), three times with DCM, twice with DMF then twice with DCM. The resin was dried by blowing nitrogen through it for 30 mins. A 5 mg sample of the resin was taken and the loading calculated. 2% DBU in DMF (2 mL) was added to the resin and agitated

for 30 mins. This solution was then diluted with MeCN to 10 mL. 2 mL of this solution was then further diluted with MeCN to 25 mL. A reference solution was made using the same method without the addition of resin. The optical density at 304 nM was then recorded of the sample and reference on a spectrophotometer, and the loading calculated using the following equation:

$$\frac{mmol}{g} = \left(Abs_{sample} - Abs_{ref}\right) \times \frac{16.4}{mg\ of\ resin}$$

7.2.2.2 Method 2 – Deprotection of Fmoc Group

20% piperidine in DMF (2 mL) was added to the resin and stirred for 3 mins. The solution was then filtered and the method repeated twice more. The resin was washed with DMF, followed by DCM and DMF again.

7.2.2.3 Method 3 – Coupling of Fmoc Protected Amino Acid

Fmoc protected amino acid (5 equiv. natural amino acid; 3 equiv. photoreactive amino acid/TAMRA/desthiobiotin), oxyma pure (5 equiv.) and DIC (5 equiv.) were dissolved in minimal amount of DMF. The solution was added to the resin and stirred for 40 mins. The solution was filtered and the resin washed with DMF, followed by DCM and DMF again.

7.2.2.4 Method 4 – Test for Coupling

To test the success of coupling, a small sample of resin was taken and TFA (50 µL) was added. The TFA was evaporated by blowing nitrogen onto the sample. Water (100 µL) and acetonitrile (100 µL) were added, the solution filtered into a vial and an LCMS ran. If coupling was unsuccessful, method 3 was repeated; if coupling was successful methods 2-4 were repeated for each amino acid.

7.2.2.5 Method 5 – *N*-formylation

After the Fmoc deprotection of the final amino acid, the N-terminus was formylated. *p*-Nitrophenyl formate (5 equiv.) and DIPEA (10 equiv.) were dissolved in DCM (2 mL) and added to the resin which was subsequently stirred for 12 hr. The solution was filtered and the resin was washed three times with

DMF, three times with DCM and three times with MeOH. The resin was dried by blowing nitrogen through it for 30 mins.

7.2.2.6 Method 6 – Cleavage from the Resin

A solution of 94% TFA, 2.5% water, 2.5% EDT and 1% TIPS (2 mL) was added to the dried resin and left for 2 hr with occasional swirling. The solution was filtered and the resin washed twice with TFA (1 mL). The filtrates were combined and TFA was removed by blowing nitrogen over the solution. Cold diethyl ether (8-fold volume) was added to the solution which cause the peptide to crash out of solution. The precipitation was pelleted on a centrifuge (4,000 × g, 10 min) and the diethyl ether poured off (this was repeated). The pellet was dissolved in water/dioxane (1:1) and lyophilised.

7.2.3 Synthesised Peptides

Formyl-Met-Leu-Phe-Lys-photoAcLys-Pra-OH 3.07

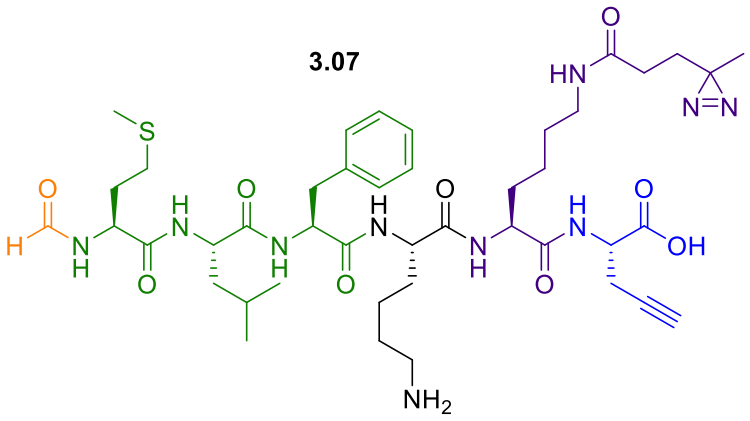

Formyl-Met-Leu-Phe-Lys-photoAcLys-Pra-OH was synthesised on 2-chlorotrityl chloride resin using methods 2-6. Following *N*-formylation the Dde protecting group on the second lysine was removed; 2% hydrazine monohydrate in DMF (1 mL) was added to the resin and turned for 3 mins before being filtered (this was repeated three times). The resin was then washed three times with DMF. 4,4-azo-pentanoic acid was then coupled to the free amine using method 3. The solution was filtered and the resin was washed three times with DMF, three times with DCM and three times with MeOH. The resin was dried by blowing nitrogen through it for 30 mins. The isolated peptide was then purified using UV-directed HPLC. Gradient from 0.1% TFA/ 5% MeCN (v/v) in water to 0.1% TFA/ 95% MeCN (v/v) in water over 15 mins. The peptide was synthesised in 68% yield.

HRMS (ES+) m/z calculated for $C_{43}H_{67}N_{10}O_9S$ $[M+H]^+$ 899.479708, found 899.479708.

Formyl-Met-Leu-Phe-Lys-photoMet-Pra-OH 3.11

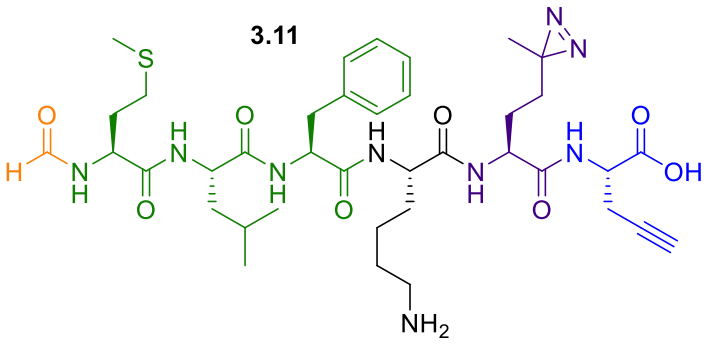

Formyl-Met-Leu-Phe-Lys-photoMet-Pra-OH was synthesised on 2-chlorotrityl chloride resin using methods 2-6. The isolated peptide was then purified using UV-directed HPLC. Gradient from 0.1% TFA/ 5% MeCN (v/v) in water to 0.1% TFA/ 95% MeCN (v/v) in water over 15 mins. The peptide was synthesised in 66% yield.

HRMS (ES+) m/z calculated for $C_{38}H_{58}N_9O_8S$ $[M+H]^+$ 801.414634, found 801.416991.

Formyl-NLe-Leu-Phe-NLe-Tyr-Lys(FITC)-OH 3.22

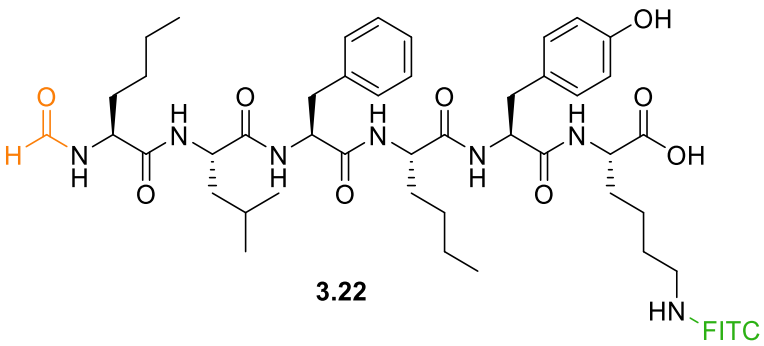

3.22

Formyl-NLe-Leu-Phe-NLe-Tyr-Lys(FITC)-OH was synthesised on 2-chlorotrityl chloride resin using methods 1-5. However, the resin was loaded with Fmoc-Lys(Dde) in place of Fmoc-Pra. Following the *N*-formylation reaction, the Dde was removed from the lysine side chain using 4% hydrazine in DMF. FITC (6 equiv.) was then coupled to the free amine with DIPEA (10 equiv.) overnight in darkness. The peptide was then cleaved from the resin using a different cleavage cocktail of 2.5% TIS, 2.5% water and 95% TFA. The isolated peptide was then purified using UV-directed HPLC. Gradient from 0.1% TFA/ 5% MeCN (v/v) in water to 0.1% TFA/ 95% MeCN (v/v) in water over 15 mins. The peptide was synthesised in 28% yield as a yellow amorphous solid.

HRMS (ES+) m/z calculated for $C_{64}H_{77}N_8O_{14}S$ $[M+H]^{2+}$ 607.269955, found 607.269374.

Formyl-photoMet-Leu-Phe-NLe-Tyr-Lys(TAMRA)-OH 4.01

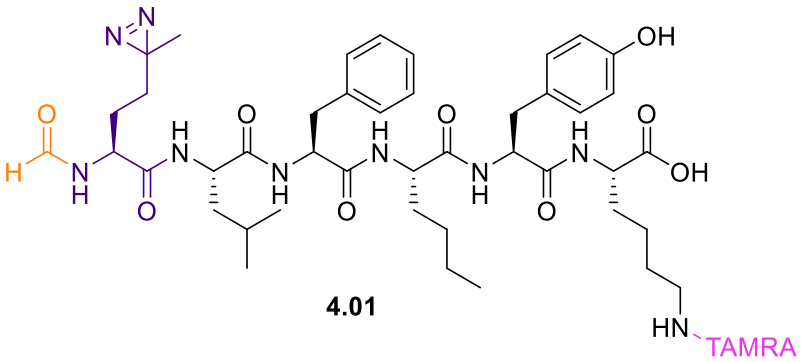

4.01

Formyl-photoMet-Leu-Phe-NLe-Tyr-Lys(TAMRA)-OH was synthesised on 2-chlorotrityl chloride resin using methods 1-5. However, the resin was loaded with Fmoc-Lys(Dde) in place of Fmoc-Pra. Following the *N*-formylation reaction, the Dde was removed from the lysine side chain using 4% hydrazine in DMF and the TAMRA fluorophore was coupled. The peptide was then cleaved from the resin using a different cleavage cocktail of 2.5% TIS, 2.5% water and 95% TFA. The isolated peptide was then purified using UV-directed HPLC. Gradient from 0.1% TFA/ 5% MeCN (v/v) in water to 0.1% TFA/ 95% MeCN (v/v) in water over 15 mins. The peptide was synthesised in 16% yield as a bright pink amorphous solid.

HRMS (ES+) m/z calculated for $C_{68}H_{83}N_{11}O_{13}$ $[M+H]^{2+}$ 632.320275, found 632.320381.

Formyl-photoMet-Leu-Phe-NLe-Tyr-Lys(desthiobiotin)-OH 4.02

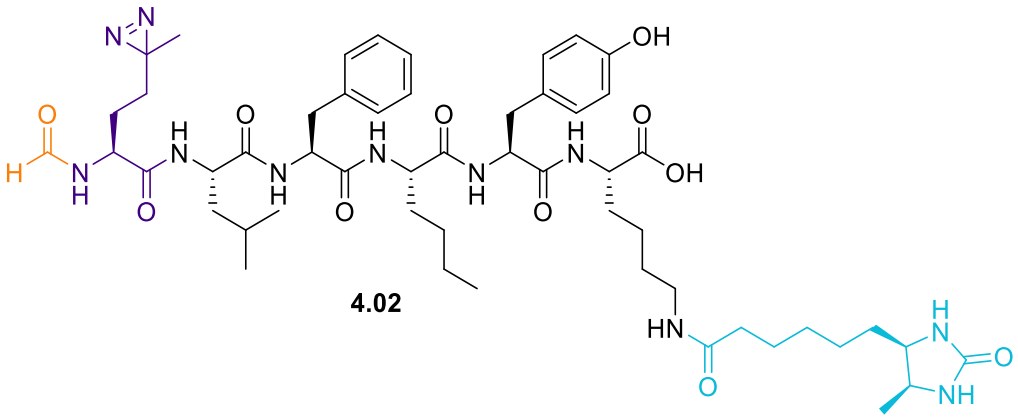

4.02

Formyl-photoMet-Leu-Phe-NLe-Tyr-Lys(desthiobiotin)-OH was synthesised on preloaded Fmoc-Lys(ivDde) Wang resin using methods 2-5. Following the *N*-formylation reaction, the ivDde was removed from the lysine side chain using 4% hydrazine in DMF and the desthiobiotin was coupled using HCTU (5 equiv) and DIPEA (10 equiv). The peptide was then cleaved from the resin using a different cleavage cocktail of 2.5% TIS, 2.5% water and 95% TFA. The isolated peptide was then purified using UV-directed HPLC. Gradient from 0.1% TFA/ 5% MeCN (v/v) in water to 0.1% TFA/ 95% MeCN (v/v) in water over 15 mins. The peptide was synthesised in 11% yield as a white solid.

HRMS (ES+) m/z calculated for $C_{53}H_{79}N_{11}O_{11}$ $[M+H]^+$ 1046.603879, found 1046.611846.

Formyl-NLe-Leu-Phe-Cys(MTS-diazirine)-Tyr-Lys(TAMRA)-OH 4.03

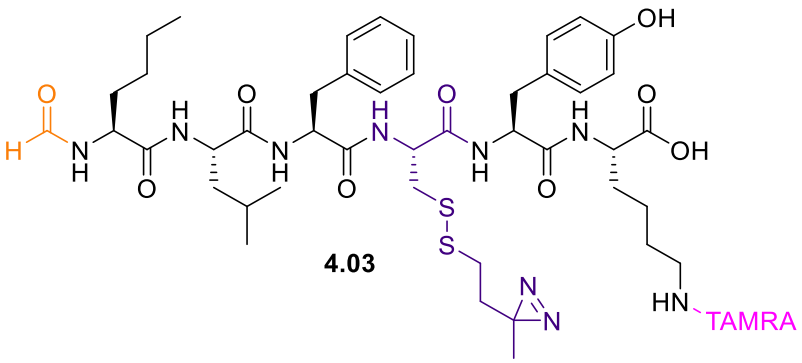

4.03

Formyl-NLe-Leu-Phe-Cys(MTS-diazirine)-Tyr-Lys(TAMRA)-OH was synthesised on preloaded Fmoc-Lys(ivDde) Wang resin using methods 2-5. Following the *N*-formylation reaction, the ivDde was removed from the lysine side chain using 4% hydrazine in DMF and the desthiobiotin was coupled using HCTU (5 equiv) and DIPEA (10 equiv). The peptide was then cleaved from the resin using a different cleavage cocktail of 2.5% TIS, 2.5% water and 95% TFA. MTS-diazirine (3 equiv) was dissolved in minimal amount of methanol, added to the peptide (20mg) and left for 30 minutes. The isolated peptide was purified using mass directed HPLC. Gradient from 5% MeCN (v/v) in water to 95% MeCN (v/v) in water over 20 min. The peptide was synthesised in 10% yield as a bright pink amorphous solid.

HRMS (ES+) m/z calculated for $C_{69}H_{86}N_{11}O_{13}S_2$ $[M+2H]^{2+}$ 670.801363, found 670.801248.

Formyl-NLe-Leu-Phe-Cys(MTS-alkynyldiazirine)-Tyr-Lys(TAMRA)-OH 4.04

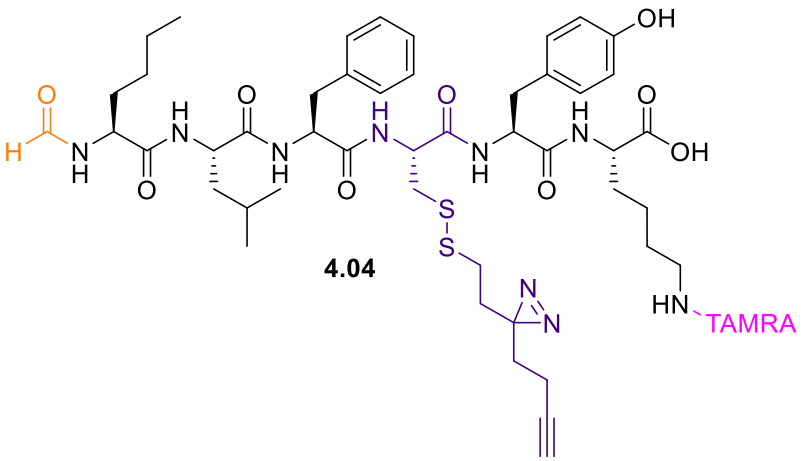

4.04

Formyl-NLe-Leu-Phe-Cys(MTS-alkynyldiazirine)-Tyr-Lys(TAMRA)-OH was synthesised on preloaded Fmoc-Lys(ivDde) Wang resin using methods 2-5. Following the *N*-formylation reaction, the ivDde was removed from the lysine side chain using 4% hydrazine in DMF and the desthiobiotin was coupled using HCTU (5 equiv) and DIPEA (10 equiv). The peptide was then cleaved from the resin using a different cleavage cocktail of 2.5% TIS, 2.5% water and 95% TFA. MTS-alkynyldiazirine (3 equiv) was dissolved in minimal amount of methanol, added to the peptide (20mg) and left for 30 minutes. The isolated peptide was purified using mass directed HPLC. Gradient from 5% MeCN (v/v) in water to 95% MeCN (v/v) in water over 20 min. The peptide was synthesised in 10% yield as a bright pink amorphous solid.

HRMS (ES+) m/z calculated for $C_{72}H_{88}N_{11}O_{13}S_2$ $[M+2H]^{2+}$ 689.809205, found 689.808576.

7.3 Biochemical Methods

7.3.1 General Methods and Equipment

Reagents were supplied from Sigma-Aldrich, Fisher Scientific and VWR International. All recipe components were dissolved in 18.2 MΩ H_2O to the final volume stated. The pH of the solutions was adjusted using 1 M NaOH of 5 M HCl.

Sterilisation of media, buffers and appropriate equipment was performed using a Prestige Medical bench top autoclave. Thermo Electron Corporation Holten LaminAir laminar flow cabinet was used to maintain a sterile environment when necessary. Bacterial cultures were incubated using a Stuart Orbital Incubator and LB-agar plates were incubated in a Binder BD23 incubator. Centrifugation was performed using either a Heraeus multifuge 3 S-R centrifuge or a Heraeus Fresco-17 centrifuge. Spectrophotometric readings were measured using a Thermo Scientific NanoDrop 2000. SDS-PAGE was carried out using a BioRad Mini-PROTEAN Tetra Cell system and a BioRad Power PAC 1000. A BioRad ChemiDoc MP Imaging System was used to image polyacrylamide gels using a combination of UV and white light (DyLight 550 602/50 green epifluorescence, Coomassie Blue 715/30 far red epifluorescence, Chemiluminescent 647SP no light).

7.3.2 Media and buffers

7.3.2.1 Growth media

LB media: 25 g L^{-1} LB freeze-dried powder (Fisher) in H_2O, sterilised in an autoclave for 20 mins at 120 °C.

LB-agar media: 25 g L^{-1} LB freeze-dried powder (Fisher) and 15 g L^{-1} of Agar powder (Fisher) in H_2O, sterilised in an autoclave for 20 mins at 120 °C.

7.3.2.2 Buffers for protein and DNA analysis

Lysis buffer: 0.1% (w/v) SDS, 1% (v/v) Triton X-100, 150 mM NaCl, 50 mM Tris (pH 7.5), 1 × EDTA-free protease inhibitors.

Phosphate-buffered saline (PBS) pH 7.4 (purchased as tablets from Fisher): 0.01 M phosphate buffer, 0.0027 M potassium chloride, 0.137 M NaCl.

SDS-PAGE separating gel buffer: 1.5 M Tris-HCl pH 6.8.

SDS-PAGE stacking gel buffer: 0.5 M Tris-HCl pH 8.8.

SDS-PAGE loading buffer: 62.5 mM Tris-HCl, 5% (w/v) β-mercaptethanol, 10% (w/v) glycerol, 2.5% (w/v) SDS, 0.002% (w/v) bromophenol blue.

SDS-PAGE running buffer (×5): 125 mM Tris-base, 960 mM glycine, 0.5% (w/v) SDS

Western blot transfer buffer: 1.51 g Tris-base, 7.2 g glycine, 100 mL methanol, 400 mL H_2O.

Western blot blocking buffer (3%): 1.50 g fat-free dried milk powder in PBS.

Coomassie stain: Coomassie G-250, 40% (v/v) methanol, 10% (v/v) acetic acid in H_2O.

Coomassie destain: 40% (v/v) methanol, 10% (v/v) acetic acid.

Ponceau Stain: 0.1% w/v Ponceau S in 5% acetic acid.

TBS: 50 mM Tris-HCl, 150 mM NaCl, pH 7.4

Tris-acetate-EDTA (TAE) (×50): 2 M Tris-HCl, 20 mM acetic acid, 1 mM EDTA.

7.3.3 Bacterial Transformation of FPR1 gene cDNA ORF

7.3.3.1 Transformation of *E. coli* Cells

10 µL of *E. coli* competent cells and 2 µg of plasmid containing FPR1 gene (**Figure 7.1**) (GenScript, OHu10847) were mixed together in a sterile Eppendorf tube on ice. The cells were incubated for 25 min to allow diffusion of the plasmid, followed by a heat shock for 30 s at 42 °C and a further incubation on ice for 5 min to allow

uptake of the plasmid. 1 mL of LB media was added to the cells and incubated at 37 °C with shaking (200 rpm) for 1 hr. A 100 µL and concentrated aliquot were used to inoculate sterilised agar plates made using ampicillin (100 µg/mL). The plates were incubated overnight at 37 °C and transferred to the fridge in the morning to halt growth.

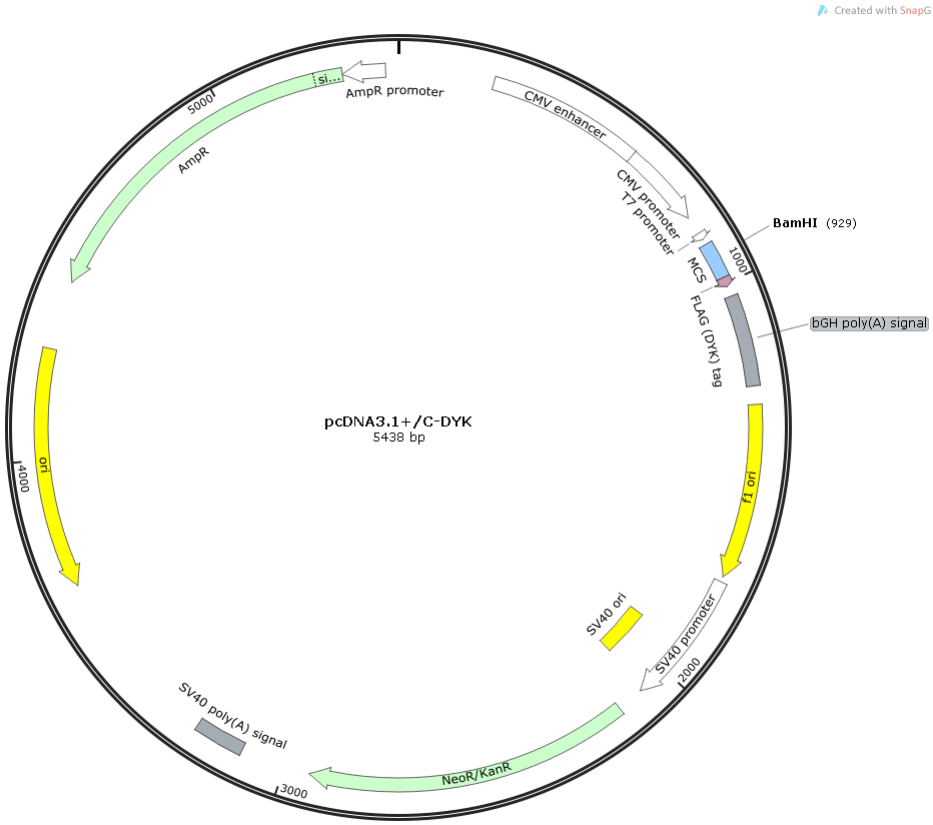

Figure 7.1: Map of plasmid containing FPR1 gene

7.3.3.2 Preparation of Midi-Culture

A single colony from the transformed *E. coli* cells was transferred to 35 mL of LB media containing ampicillin (100 µg/mL) and incubated at 37 °C with shaking overnight. A QIAGEN Plasmid Plus Midi Kit was used to obtain the transformed plasmid.

7.3.3.3 Digestion of Plasmid to Check Purification

300 ng of plasmid was mixed with 1 unit of BamHI and CutSmart buffer (×1), and made to 50 µL with H_2O. The sample was incubated at 37 °C for 40 mins and then stored at –20 °C. Analysis of this digestion was performed with the use of agarose gel electrophoresis.

7.3.3.4 Agarose Gel Electrophoresis

Sample separation by agarose gel electrophoresis was carried out using Tris-acetate gels. 1% w/v agarose was added to 40 mL of Tae buffer and heated for 45 s to near boiling. The solution was allowed to cool and 0.4 µL of SYBR stain was added. The solution was poured into a mould with a comb added and allowed to set. The set gel was placed in a gel tank and DNA samples were loaded in loading buffer. Gels were run with TAE buffer (diluted to ×1) at 400 V for 40 min.

7.3.4 Mammalian Cell Culture

Cell were incubated in a humidified atmosphere at 37 °C containing 5% CO_2.

HEK293T cells were cultured in Dulbecco's Modified Eagle Medium (DMEM, Fisher) supplemented with 1% L-glutamine, 10% v/v fetal bovine serum (FBS) and 1% v/v Pen-Strep. Cells were detached using 1 × trypsin in PBS.

7.3.5 Probe Crosslinking in HEK293T Cells and cell lysis

7.3.5.1 Transient Transfection

HEK293T cells were seeded in a 6-well plate (2×10^5 cells/well) and incubated at 37 °C overnight. The plasmid containing FPR1 gene (0.7 µg/µL stock) and Turbofect (Fisher) were mixed with DMEM and incubated at room temperature for 15 min (1 µg of plasmid and 3 µL of Turbofect in 100 µL of media per well). The solution was added to the plated cells and incubated at 37 °C overnight.

7.3.5.2 Probe Incubation, Crosslinking and lysis of adhered cells

Transfected cells were washed with PBS and incubated with 1 mL of 10 nM probe in PBS at 0 °C for 30 min (6-well plate placed on ice). Following incubation, the cells were washed with PBS (1 mL × 2) and irradiated with UV light (365 nm) for 5 min using a UV LED device.

PBS solution removed from wells. 200 µL of lysis buffer was added and cell lysate scraped and transferred to Eppendorf tubes. The samples were chilled for 15 min. Cell debris was pelleted by centrifugation at 13,300 rpm for 15 min at 4 °C. Protein concentration was determined by the DC protein assay (Bio-Rad) using BSA to generate a standard curve. Lysates were kept at –80 °C until required.

7.3.5.3 Probe Incubation, Crosslinking and lysis of suspended cells

Transfected cells were washed with PBS and incubated in 1 mL of PBS with EDTA (per well) at 37 °C for 3 mins to detach. The cells were then transferred into sterile Eppendorf tubes and centrifuged at 2000 rpm for 3 min at 4 °C to pellet the cells. Subsequently the cells were incubated with 1 mL of 10 nM probe in PBS at 0 °C for 30 min. Following incubation the cells were washed with PBS (1 mL × 2) and irradiated with UV light (365 nm) for 30 s using a UV LED device developed for diazirine crosslinking.[136, 140] Samples were centrifuged at 2000 rpm for 3 min at 4 °C and the PBS solution removed. 200 µL of lysis buffer was added and the lysate chilled for 15 min. Cell debris was pelleted by centrifugation at 13,300 rpm for 15 min at 4 °C. Protein concentration was determined by the DC protein assay (Bio-Rad) using BSA to generate a standard curve. Lysates were kept at –80 °C until required.

7.3.6 Gel-Based Fluorescent Imaging

Crosslinked cell lysate samples were analysed using gel-based fluorescent imaging. Proteins were separated by SDS-PAGE (180 V, 50 min) with 4% stacking gels and 12% resolving gels on a BioRad Mini-PROTEAN Tetra Cell system with 10 µL All blue standards (BioRad). Fluorescence was measured

using a BioRad ChemiDoc MP Imaging System with a Cy3 filter. A Western Blot was subsequently performed of the gel to analyse FPR1 expression.

7.3.7 Western Blot Analysis

For Western blot analysis, samples were separated by SDS-PAGE as above. A PVDF membrane (BioRad) was soaked in MeOH for 1 min, followed by transfer buffer for 1 min. Two squares of extra thick blot paper (BioRad) and the protein gel were soaked in transfer buffer for 2 min. The transfer sandwich was then prepared in a Trans-Blot Semi-Dry Transfer Cell (BioRad) in the following order: blot paper, PVDF membrane, gel, blot paper. The transfer was run using a BioRad Power PAC 1000 at 15 V for 30 min.

The membrane was soaked in 3% blocking buffer for 1 hr at room temperature. Following this the membrane was incubated with the primary antibody in 10 mL blocking buffer for 2 hr at room temperature. The membrane was washed with 0.05% Tween in PBS (3 × 5 min). The membrane was then incubated with the secondary antibody 10 mL blocking buffer for 1 hr at room temperature and washed with 0.05% Tween in PBS (3 × 5 min).

Primary Antibody	Target Species	Conjugate	Working Dilution
FLAG Tag, mAb, mouse (GenScript, A00187-100)	FLAG Tag	-	1:10,000
Anti-FPR1/2, clone NFPR1, mouse (Merck, MABF271)	FPR1/2	-	1:1000
TAMRA, mAB, mouse (ThermoFisher Scientific, MA1-041)	TAMRA	-	1:1000

Secondary Antibody			
Goat anti-Mouse IgG, HRP (ThermoFisher Scientific, 62-6520)	Mouse	HRP	1:10,000

Table 7.1: Antibodies used for Western blotting

A BioRad Clarity ma Western ECL substrate kit was used with a BioRad ChemiDoc MP Imaging System to image the Western blot. The Western blot was then Ponceau stained for 5 min in staining solution followed by destaining in water.

7.3.8 Deglycosylation of FPR1

Cell lysate sample adjusted to 1 µg/ µL (50 µL, 50 µg). K_2HPO_4 was added to 0.1 M, SDS was added to 1% and NP40 was added to 1%. The sample was agitated for 30 min at room temperature. 20 units of PNGase F was added to the sample and agitated for 1 hr at room temperature. A further 20 units of PNGase F was added to the sample and agitated for 1 hr at room temperature. Sample loading buffer was added, and the sample stored at –20 °C. Deglycosylation was analysed by Western blot as above.

7.3.9 Flow Cytometry

Cells were transfected and incubated with the probe as above. The binding of the probes was observed using a CytoFLEX S 4-laser flow cytometer. The cell samples were loaded in a 1.5 mL Eppendorf and 10,000 events were taken per sample at a flow rate of 30 µL/min. For probes containing a FITC group the 488 nm laser with a 525/40 band pass filter was used, for probes containing a TAMRA group the 561 laser with a 585/42 band pass filter was used. The data produced from the flow cytometer was then analysed using Kaluza. For further analysis,

mean fluorescence values were exported from Kaluza and use to plot graphs with Python. In the case for Probe2.0TAMRA, Python was also used to calculate K_d.

7.3.10 Confocal Microscopy

Cells were transfected as above and incubated with the probe adhered to plate (35 mm glass-bottom plate). The cells were incubated with 1 mL of 10 nM probe in PBS at 0 °C for 30 min. The binding and internalisation of the probes was observed using a Zeiss LSM880 + Airyscan inverted confocal microscope. A DPSS 561 nm laser was used to view the TAMRA fluorescence with an objective of 20x. The data produced was then analysed using Zen.

7.3.11 Anti-FLAG Pull-Down

Cell lysate sample adjusted to 1 µg/ µL (200 µL, 200 µg). 50 µL of suspended anti-FLAG M2 magnetic beads (Sigma Aldrich, M8823) were transferred to an Eppendorf and washed three times with TBS, once with 0.1 M glycine (pH 3.5), three times with TBS and once with lysis buffer. The cell lysate sample was added to the beads and incubated overnight with agitation at 4 °C. The supernatant was removed to a new tube and the beads washed three times with lysis buffer. 40 µL of 3X FLAG-peptide (Sigma Aldrich, F4799) in TBS (300 ng/µL) was added to the beads and incubated for 30 min with agitation at room temperature. The elution mixture was removed to a new tube and the sample analysed by Western blot as above.

7.3.11.1 Anti-FLAG Pull-Down for Proteomics

Cell lysate sample adjusted to 1 µg/ µL (500 µL, 500 µg), and deglycosylated as above. 100 µL of suspended anti-FLAG M2 magnetic beads (Sigma Aldrich, M8823) were transferred to an Eppendorf and washed three times with TBS, once with 0.1 M glycine (pH 3.5), three times with TBS and once with lysis buffer. The cell lysate sample was added to the beads and incubated overnight with agitation at 4 °C. The supernatant was removed to a new tube and the beads washed three

times with lysis buffer. 40 µL of 3X FLAG-peptide (Sigma Aldrich, F4799) in TBS (750 ng/µL) was added to the beads and incubated for 30 min with agitation at room temperature. The elution mixture was removed to a new tube and the sample analysed by Western blot as above.

7.3.12 Proteomics

7.3.12.1 S-Trap Method Used For Trypsin, Chymotrypsin and Trypsin+Chymotrypsin

Samples were processed using the S-TRAP Micro column (PROTIFI, NY, USA) following the manufacturer's instructions. Proteins were fully solubilised by adding 20 µL of 10% SDS solution to a 20 µL sample. Reduction and alkylation were then performed: DTT was added to a final concentration of 20 mM before heating to 56 °C for 15 min with shaking, the sample was left to cool and following this iodoacetamide was added to a final concentration of 40 mM, before heating to 20 °C for 15 min with shaking in the dark. Phosphoric acid was added to a final concentration of 1.2% to fully denature the proteins. This step ensures destruction of all enzymatic activity and maximises sensitivity to proteolysis. Samples were then diluted with S-Trap binding buffer (100 mM triethylammonium bicarbonate (TEAB) pH 7.1 in methanol) and 1 µg of protease reconstituted in 50mM TEAB was added before quickly being loaded onto the S-trap column. Proteins were captured within the submicron pores of the three-dimensional trap. Proteins captured within the trap present exceptionally high surface area allowing them to be washed free of contaminants. The S-trap was washed by adding 150 µL binding buffer before being spun at 4000 g for 30 s. 30 µL of 0.02 µg/µL protease was then added to the top of the S-trap. Confinement of the protein and protease within the pores of the trap forces fast digestion as the protease is either digesting the substrate or is reflected off the sidewalls straight back to the protein to digest. Two separate proteases were used at the above concentrations, trypsin (Promega, WI, USA) and chymotrypsin (Promega, WI, USA). S-traps were loosely capped and placed in a 1.5mL eppendorf and heated to 46 °C for 15 min with no shaking. Digested peptides were eluted by first spinning the S-trap at 4000 g for 1 min. Further elutions used 40 µL 50mM TEAB, 40 µL 0.2% formic acid, and 30 µL 50% acetonitrile with 0.2% formic acid prior to centrifugation.

Elutions were combined then dried down prior to resuspension in 0.2% formic acid.

7.3.12.2 Use of RapiGest to Aid Digestion

Proteins were precipitated using the chloroform-methanol method.[163] 20 µL of the sample was combined with 100 µL of methanol, 33 µL of chloroform, and 60µL of HPLC grade H_2O and vortexed gently to ensure complete mixing. Samples were centrifuged for 15 min at 14,000 rpm and 4 °C in an Eppendorf centrifuge (Hamburg, Germany). The top layer of the sample was aspirated carefully to not disturb the precipitated protein located within the organic/aqueous interface. An additional 100 µL of methanol was added to each sample followed by gentle vortexing and 15 min of centrifugation. All of the supernatant was completely removed and the pellet was left to air dry for 30 min. The pellet was dissolved in 0.1% (w/v) RapiGest (Waters, UK). Subsequent reduction and alkylation followed the above S-Trap procedure.

7.3.12.3 Cold Urea Method for Denaturation of Protein

The pellet resulting from chloroform-methanol precipitation (as described above) was dissolved in 20 µL ice cold 8 M urea in 100mM Tris, pH 8.5. Reduction and alkylation were performed according to the S-Trap method, though no shaking was applied. Before tryptic digestion, 100 mM ammonium bicarbonate buffer was added to reduce the concentration of urea. 30 µL of 0.02 µg/µL trypsin was added before an overnight incubation at 37 °C. The digest reaction was stopped by adding 5 µL of 1% TFA. µC18 ZipTips were used to clean the tryptic peptides prior to MS analysis.

7.3.12.4 MS Analysis

3 µL sample were injected onto an in house-packed 20 cm capillary column (inner diameter 75 µm, 3.5 µm Kromasil C18 media). An EasyLC nano liquid chromatography system was used to apply a gradient of 4–40% ACN in 0.1% formic acid over 30 min at a flow rate of 250 nL/min. Total acquisition time was

60 min including column wash and re-equilibration. Separated peptides were eluted directly from the column and sprayed into an Orbitrap Velos Mass Spectrometer (ThermoFisher Scientific, Hemel Hempstead, UK) using an electrospray capillary voltage of 2.7 kV. Precursor ion scans were acquired in the Orbitrap with resolution of 60000. Up to 20 ions per precursor scan were selected for fragmentation in the ion-trap. Dynamic exclusion of 30 s was used.

Peptide MS/MS data were processed with PEAKS Studio X+ (Bioinformatic Solutions Inc, Waterloo, Ontario, Canada) and searched against the FPR1 sequence. Carbamiodomethylation was selected as a fixed modification, variable modifications were set for oxidation of methionine and deamidation of glutamine and asparagine. MS mass tolerance was 15 ppm, and fragment ion mass tolerance was 0.01 Da. The peptide false discovery rate was set to 1%.

Chapter 8 References

1. L. A. M. Carneiro, L. H. Travassos and D. J. Philpott, Innate immune recognition of microbes through Nod1 and Nod2: Implications for disease, *Microbes Infect.*, 2004, **6**, 609-616.
2. L. A. M. Carneiro, L. H. Travassos and S. E. Girardin, Nod-like receptors in innate immunity and inflammatory diseases, *Ann Intern Med*, 2007, **39**, 581-593.
3. D. A. Bloes, D. Kretschmer and A. Peschel, Enemy attraction: Bacterial agonists for leukocyte chemotaxis receptors, *Nat. Rev. Microbiol.*, 2015, **13**, 95-104.
4. M. A. Boudreau, J. F. Fisher and S. Mobashery, Messenger functions of the bacterial cell wall-derived muropeptides, *Biochemistry*, 2012, **51**, 2974-2990.
5. W. U. Medyczny, Molecular mechanisms associated with recognition of pathogens by receptors of innate immunity, *Postepy Hig. Med. Dosw.*, 2009, **63**, 30-38.
6. S. R. El-Zayat, H. Sibaii and F. A. Mannaa, Toll-like receptors activation, signaling, and targeting: an overview, *Bulletin of the National Research Centre*, 2019, **43**.
7. B. Bufe and F. Zufall, The sensing of bacteria: emerging principles for the detection of signal sequences by formyl peptide receptors, *Biomol Concepts*, 2016, **7**, 205-214.
8. C. Dahlgren, M. Gabl, A. Holdfeldt, M. Winther and H. Forsman, Basic characteristics of the neutrophil receptors that recognize formylated peptides, a danger-associated molecular pattern generated by bacteria and mitochondria, *Biochem Pharmacol*, 2016, **114**, 22-39.
9. D. A. Dorward, C. D. Lucas, G. B. Chapman, C. Haslett, K. Dhaliwal and A. G. Rossi, The role of formylated peptides and formyl peptide receptor 1 in governing neutrophil function during acute inflammation, *Am. J. Pathol*, 2015, **185**, 1172-1184.
10. Y. Le, P. M. Murphy and J. M. Wang, Formyl-peptide receptors revisited, *Trends Immunol.*, 2002, **23**, 541-548.
11. I. A. Schepetkin, L. N. Kirpotina, A. I. Khlebnikov, N. Cheng, R. D. Ye and M. T. Quinn, Antagonism of human formyl peptide receptor 1 (FPR1) by chromones and related isoflavones, *Biochem Pharmacol*, 2014, **92**, 627-641.
12. P. M. Murphy, H. L. Tiffany, D. McDermott and S. K. Ahuja, Sequence and organization of the human N-formyl peptide receptorencoding gene, *Gene*, 1993, **133**, 285-290.
13. F. Boulay, M. Tardif, L. Brouchon and P. Vignais, The Human 7V-Formylpeptide Receptor. Characterization of Two cDNA Isolates and Evidence for a New Subfamily of G-Protein-Coupled Receptors, *Biochemistry*, 1990, **29**, 11123-11133.

14. A. Grunbeck and T. P. Sakmar, Probing G protein-coupled receptor - Ligand interactions with targeted photoactivatable cross-linkers, *Biochemistry*, 2013, **52**, 8625-8632.
15. L. Gambardella and S. Vermeren, Molecular players in neutrophil chemotaxis-focus on PI3K and small GTPases, *J. Leukoc. Biol.*, 2013, **94**, 603-612.
16. K. Wenzel-Seifert and R. Seifert, Functional differences between human formyl peptide receptor isoforms 26, 98, and G6, *Naunyn Schmiedebergs Arch. Pharmacol.*, 2003, **367**, 509-515.
17. A. Waller, K. L. Sutton, T. L. Kinzer-Ursem, A. Absood, J. R. Traynor, J. J. Linderman and G. M. Omann, Receptor Binding Kinetics and Cellular Responses of Six N-Formyl Peptide Agonists in Human Neutrophils, *Biochemistry*, 2004, **43**, 8204-8216.
18. M. J. Rabiet, E. Huet and F. Boulay, Human mitochondria-derived N-formylated peptides are novel agonists equally active on FPR and FPRL1, while Listeria monocytogenes-derived peptides preferentially activate FPR, *Eur J Immunol*, 2005, **35**, 2486-2495.
19. R. Tavano, D. Segat, C. Fedeli, G. Malachin, E. Lubian, F. Mancin and E. Papini, Formyl-Peptide Receptor Agonists and Amorphous SiO2-NPs Synergistically and Selectively Increase the Inflammatory Responses of Human Monocytes and PMNs, *Nanobiomedicine (Rij)*, 2016, **3**, 2.
20. T. Chen, M. Xiong, X. Zong, Y. Ge, H. Zhang, M. Wang, G. Won Han, C. Yi, L. Ma, R. D. Ye, Y. Xu, Q. Zhao and B. Wu, Structural basis of ligand binding modes at the human formyl peptide receptor 2, *Nat Commun*, 2020, **11**, 1208.
21. Y. Zhuang, H. Liu, X. Edward Zhou, R. Kumar Verma, P. W. de Waal, W. Jang, T. H. Xu, L. Wang, X. Meng, G. Zhao, Y. Kang, K. Melcher, H. Fan, N. A. Lambert, H. Eric Xu and C. Zhang, Structure of formylpeptide receptor 2-Gi complex reveals insights into ligand recognition and signaling, *Nat Commun*, 2020, **11**, 885.
22. H. Q. He, E. L. Troksa, G. Caltabiano, L. Pardo and R. D. Ye, Structural determinants for the interaction of formyl peptide receptor 2 with peptide ligands, *J Biol Chem*, 2014, **289**, 2295-2306.
23. H.-Q. He and R. Ye, The Formyl Peptide Receptors: Diversity of Ligands and Mechanism for Recognition, *Molecules*, 2017, **22**, 455-455.
24. Y. Le, J. J. Oppenheim and J. M. Wang, Pleiotropic roles of formyl peptide receptors, *Cytokine and Growth Factor Reviews*, 2001, **12**, 91-105.
25. I. Migeotte, D. Communi and M. Parmentier, Formyl peptide receptors: a promiscuous subfamily of G protein-coupled receptors controlling immune responses, *Cytokine Growth Factor Rev*, 2006, **17**, 501-519.
26. R. D. Ye, F. Boulay, J. M. Wang, C. Dahlgren, C. Gerard, M. Parmentier, C. N. Serhan and P. M. Murphy, International Union of Basic and Clinical Pharmacology. LXXIII. Nomenclature for the formyl peptide receptor (FPR) family, *Pharmacol Rev*, 2009, **61**, 119-161.
27. A. L. Stenfeldt, J. Karlsson, C. Wenneras, J. Bylund, H. Fu and C. Dahlgren, Cyclosporin H, Boc-MLF and Boc-FLFLF are antagonists that preferentially inhibit activity triggered through the formyl peptide receptor, *Inflammation*, 2007, **30**, 224-229.

28. K. Wenzel-Seifert and R. Seifert, Cyclosporin H Is a Potent and Selective Formyl Peptide Receptor Antagonist *The journal of immunology*, 1993, **150**, 4591-4599.
29. D. S. Ahmet, H. A. Basheer, A. Salem, D. Lu, A. Aghamohammadi, P. Weyerhauser, A. Bordiga, J. Almeniawi, S. Rashid, P. A. Cooper, S. D. Shnyder, V. Vinader and K. Afarinkia, Application of small molecule FPR1 antagonists in the treatment of cancers, *Sci Rep*, 2020, **10**, 17249.
30. F. Cattaneo, M. Parisi and R. Ammendola, Distinct Signaling Cascades Elicited by Different Formyl Peptide Receptor 2 (FPR2) Agonists, *Int. J. Mol. Sci.*, 2013, **14**, 7193-7230.
31. Y. C. Chen, Y. P. Chang, C. C. Hsiao, C. C. Wu, Y. H. Wang, T. Y. Chao, S. Y. Leung, W. F. Fang, C. P. Lee, T. Y. Wang, P. Y. Hsu and M. C. Lin, Blood M2a monocyte polarization and increased formyl peptide receptor 1 expression are associated with progression from latent tuberculosis infection to active pulmonary tuberculosis disease, *Int J Infect Dis*, 2020, **101**, 210-219.
32. J. Hu, G. Li, Y. Tong, Y. Li, G. Zhou, X. He, P. Xie, J. M. Wang and Q. Sun, Transduction of the gene coding for a human G-protein coupled receptor FPRL1 in mouse tumor cells increases host anti-tumor immunity, *Int Immunopharmacol*, 2005, **5**, 971-980.
33. Y. Zhou, X. Bian, Y. Le, W. Gong, J. Hu, X. Zhang, L. Wang, P. Iribarren, R. Salcedo, O. M. Howard, W. Farrar and J. M. Wang, Formylpeptide receptor FPR and the rapid growth of malignant human gliomas, *J Natl Cancer Inst*, 2005, **97**, 823-835.
34. J. C. Boer, D. M. van Marion, J. V. Joseph, N. M. Kliphuis, H. Timmer-Bosscha, J. A. van Strijp, E. G. de Vries, W. F. den Dunnen, F. A. Kruyt and A. M. Walenkamp, Microenvironment involved in FPR1 expression by human glioblastomas, *J Neurooncol*, 2015, **123**, 53-63.
35. R. Zhang and X. Xie, Tools for GPCR drug discovery, *Acta Pharmacol Sin.*, 2012, **33**, 372-384.
36. R. J. Lefkowitz and J. Roth, Radioreceptor Assay of Adrenocorticotropic Hormone: New Approach to Assay of Polypeptide Hormones in Plasma, *Science*, 1970, **170**, 633-635.
37. D. Harder and D. Fotiadis, Measuring substrate binding and affinity of purified membrane transport proteins using the scintillation proximity assay, *Nat Protoc*, 2012, **7**, 1569-1578.
38. N. Nelson, A Novel Method for the Detection of Receptors and Membrane Proteins by Scintillation Proximity Radioassay, *Analytical Biochemistry* 1987, **165**, 287-293.
39. G. Milligan, Principles: Extending the utility of [35S]GTPgS binding assays, *Trends Pharmacol. Sci.*, 2003, **24**, 87-90.
40. O. Shimomura, S. Inouye, B. Musicki and Y. Kishi, Recombinant aequorin and recombinant semi-synthetic aequorins, *Biochem. J.*, 1990, **270**, 309-312.
41. J. E. Niedel and I. Kahane, Receptor-Mediated Internalisation of Fluorescent Chemotactic Peptide by Human Neutrophils, *Science*, 1979, **205**, 1412-1414.
42. L. M. Luttrell and R. J. Lefkowitz, The role of β-arrestins in the termination and transduction of G-protein-coupled receptor signals, *J. Cell. Sci.*, 2002, **115**, 455-465.

43. A. Waller, P. C. Simons, S. M. Biggs, B. S. Edwards, E. R. Prossnitz and L. A. Sklar, Techniques: GPCR assembly, pharmacology and screening by flow cytometry, *Trends Pharmacol Sci*, 2004, **25**, 663-669.
44. L. A. Sklar, B. S. Edwards, S. W. Graves, J. P. Nolan and E. R. Prossnitz, Flow cytometric analysis of ligand-receptor interactions and molecular assemblies, *Annu Rev Biophys Biomol Struct*, 2002, **31**, 97-119.
45. L. A. Sklar, J. Vilven, E. Lynam, D. Neldon, T. A. Bennett and E. Prossnitz, Solubilization and Display of G Protein-Coupled Receptors on Beads for Real-Time Fluorescence and Flow Cytometric Analysis, *Biotechniques*, 2000, **28**, 976-985.
46. F. C. Liu, H. P. Yu, Y. T. Syu, J. Y. Fang, C. F. Lin, S. H. Chang, Y. T. Lee and T. L. Hwang, Honokiol suppresses formyl peptide-induced human neutrophil activation by blocking formyl peptide receptor 1, *Sci. Rep.*, 2017, **7**, 6718.
47. E. H. Schneider, J. D. Weaver, S. S. Gaur, B. K. Tripathi, A. J. Jesaitis, P. S. Zelenka, J. L. Gao and P. M. Murphy, The leukocyte chemotactic receptor FPR1 is functionally expressed on human lens epithelial cells, *J Biol Chem*, 2012, **287**, 40779-40792.
48. H. Q. He, D. Liao, Z. G. Wang, Z. L. Wang, H. C. Zhou, M. W. Wang and R. D. Ye, Functional characterization of three mouse formyl peptide receptors, *Mol Pharmacol*, 2013, **83**, 389-398.
49. M. H. Wright and S. A. Sieber, Chemical proteomics approaches for identifying the cellular targets of natural products, *Nat Prod Rep*, 2016, **33**, 681-708.
50. E. Smith and I. Collins, Photoaffinity labeling in target- and binding-site identification, *Future Med. Chem.*, 2015, **7**, 159-183.
51. Y. Sadakane and Y. Hatanaka, Photochemical Fishing Approaches for Identifying Target Proteins and Elucidating the Structure of a Ligand-binding Region Using Carbene-generating Photoreactive Probes, *Anal Sci*, 2006, **22**, 209-218.
52. A. Singh, E. R. Thornton and F. H. Westheimer, Photolysis of Diazoacetylchymotrypsin, *J. Biol. Chem.*, 1962, **237**, 3006-3008.
53. D. Lapinsky, Tandem photoaffinity labeling-bioorthogonal conjugation in medicinal chemistry, *Bioorg Med Chem*, 2012, **20**, 6237-6247.
54. P. P. Geurink, L. M. Prely, G. A. van der Marel, R. Bischoff and H. S. Overkleeft, Photoaffinity Labelling in Activity-Based Protein Profiling, *Top. Curr. Chem.*, 2012, **324**, 85-114.
55. J. Shafer, P. Baronowsky, R. Laursen, F. Finn and F. H. Westheimer, Products from the Photolysis of Diazoacetyl Chymotrypsin, *J. Biol. Chem.*, 1966, **241**, 421-427.
56. J. Das, Aliphatic diazirines as photoaffinity probes for proteins: Recent developments, *Chem. Rev.*, 2011, **111**, 4405-4417.
57. Y. Wang and Q. Lin, Synthesis and Evaluation of Photoreactive Tetrazole Amino Acids, *Org. Lett.*, 2009, **11**, 3570-3573.
58. A. Herner, J. Marjanovic, T. M. Lewandowski, V. Marin, M. Patterson, L. Miesbauer, D. Ready, J. Williams, A. Vasudevan and Q. Lin, 2-Aryl-5-carboxytetrazole as a New Photoaffinity Label for Drug Target Identification, *J Am Chem Soc*, 2016, **138**, 14609-14615.
59. S. Zhao, J. Dai, M. Hu, C. Liu, R. Meng, X. Liu, C. Wang and T. Luo, Photo-induced coupling reactions of tetrazoles with carboxylic acids in aqueous

solution: application in protein labelling, *Chem Commun (Camb)*, 2016, **52**, 4702-4705.
60. H. Guo, J. Xu, P. Hao, K. Ding and Z. Li, Competitive affinity-based proteome profiling and imaging to reveal potential cellular targets of betulinic acid, *Chem Commun (Camb)*, 2017, **53**, 9620-9623.
61. K. Cheng, J. S. Lee, P. Hao, S. Q. Yao, K. Ding and Z. Li, Tetrazole-Based Probes for Integrated Phenotypic Screening, Affinity-Based Proteome Profiling, and Sensitive Detection of a Cancer Biomarker, *Angew. Chem. Int. Ed. Engl.*, 2017, **56**, 15044-15048.
62. K. Bach, B. L. H. Beerkens, P. R. A. Zanon and S. M. Hacker, Light-Activatable, 2,5-Disubstituted Tetrazoles for the Proteome-wide Profiling of Aspartates and Glutamates in Living Bacteria, *ACS Cent Sci*, 2020, **6**, 546-554.
63. G. W. J. Fleet, R. R. Porter and J. R. Knowles, Affinity labelling of antibodies with aryl nitrene as reactive group [8], *Nature*, 1969, **224**, 511-512.
64. C. R. Kemnitz, W. L. Karney and W. T. Borden, Why Are Nitrenes More Stable than Carbenes? An Ab Initio Study, *J Am Chem Soc*, 1998, **120**, 3499-3503.
65. Y. Chen and E. M. Topp, Photolytic Labeling and Its Applications in Protein Drug Discovery and Development, *J Pharm Sci*, 2019, **108**, 791-797.
66. R. E. Galardy, L. C. Craig and M. P. Printz, Benzophenone triplet: A new photochemical probe of biological ligand-receptor interactions, *Nature New Biol.*, 1973, **242**, 127-128.
67. A. Wittelsberger, B. E. Thomas, D. F. Mierke and M. Rosenblatt, Methionine acts as a "magnet" in photoaffinity crosslinking experiments, *FEBS Lett*, 2006, **580**, 1872-1876.
68. R. A. G. Smith and J. R. Knowles, Aryldiazirines. Potential Reagents for Photolabeling of Biological Receptor Sites, *J. Am. Chem. Soc.*, 1973, **95**, 5072-5073.
69. T. Wakahara, Y. Niino, T. Kato, Y. Maeda, T. Akasaka, M. T. H. Liu, K. Kobayashi and S. Nagase, A Nonspectroscopic Method To Determine the Photolytic Decomposition Pathways of 3-Chloro-3-alkyldiazirine: Carbene, Diazo and Rearrangement in Excited State, *J. Am. Chem. Soc.*, 2002, **124**, 9465-9468.
70. T. Akasaka, M. T. H. Liu, Y. Niino, Y. Maeda, T. Wakahara, M. Okamura, K. Kobayashi and S. Nagase, Photolysis of Diazirines in the Presence of C60: A Chemical Probe for Carbene/Diazomethane Partitioning, *J. Am. Chem. Soc.*, 2000, **122**, 7134-7135.
71. M. Suchanek, A. Radzikowska and C. Thiele, Photo-leucine and photo-methionine allow identification of protein-protein interactions in living cells, *Nature Methods*, 2005, **2**, 261-268.
72. M. Vila-Perellö, M. R. Pratt, F. Tulin and T. W. Muir, Covalent capture of phospho-dependent protein oligomerization by site-specific incorporation of a diazirine photo-cross-linker, *J. Am. Chem. Soc.*, 2007, **129**, 8068-8069.
73. A. L. MacKinnon, J. L. Garrison, R. S. Hegde and J. Taunton, Photo-leucine incorporation reveals the target of a cyclodepsipeptide inhibitor of cotranslational translocation, *J. Am. Chem. Soc.*, 2007, **129**, 14560-14561.

74. C. Iacobucci, M. Gotze, C. Piotrowski, C. Arlt, A. Rehkamp, C. Ihling, C. Hage and A. Sinz, Carboxyl-Photo-Reactive MS-Cleavable Cross-Linkers: Unveiling a Hidden Aspect of Diazirine-Based Reagents, *Anal Chem*, 2018, **90**, 2805-2809.
75. A. V. West, G. Muncipinto, H. Y. Wu, A. C. Huang, M. T. Labenski, L. H. Jones and C. M. Woo, Labeling Preferences of Diazirines with Protein Biomolecules, *J Am Chem Soc*, 2021, **143**, 6691-6700.
76. Y. Wang, C. I. R. Vera and Q. Lin, Convenient Synthesis of Highly Functionalized Pyrazolines via Mild, Photoactivated 1,3-Dipolar Cycloaddition, *Org. Lett.*, 2007, **9**, 4155-4158.
77. Y. Wang, W. J. Hu, W. Song, R. K. V. Lim and Q. lin, Discovery of Long-Wavelength Photoactivatable Diaryltetrazoles for Bioorthogonal 1,3-Dipolar Cycloaddition Reactions, *Org. Lett.*, 2008, **10**, 3725-3728.
78. N. J. Agard, J. A. Prescher and C. R. Bertozzi, A strain-promoted [3 + 2] azide-alkyne cycloaddition for covalent modification of biomolecules in living systems, *J. Am. Chem. Soc.*, 2004, **126**, 15046-15047.
79. E. M. Sletten and C. R. Bertozzi, Bioorthogonal chemistry: Fishing for selectivity in a sea of functionality, *Angew. Chem. Int. Ed.*, 2009, **48**, 6974-6998.
80. E. M. Sletten and C. R. Bertozzi, From mechanism to mouse: A tale of two bioorthogonal reactions, *Acc. Chem. Res.*, 2011, **44**, 666-676.
81. K. Lang and J. W. Chin, Bioorthogonal reactions for labeling proteins, *ACS Chem Biol.*, 2014, **9**, 16-20.
82. L. Liang and D. Astruc, The copper(I)-catalyzed alkyne-azide cycloaddition (CuAAC) "click" reaction and its applications. An overview, *Coord. Chem. Rev.*, 2011, **255**, 2933-2945.
83. H. C. Kolb, M. G. Finn and K. B. Sharpless, Click Chemistry: Diverse Chemical Function from a Few Good Reactions, *Angew. Chem. Int. Ed.*, 2001, **40**, 2004-2021.
84. V. V. Rostovtsev, L. G. Green, V. V. Fokin and K. B. Sharpless, A stepwise huisgen cycloaddition process: Copper(I)-catalyzed regioselective "ligation" of azides and terminal alkynes, *Angew. Chem. Int. Ed.*, 2002, **41**, 2596-2599.
85. Z. P. Demko and K. B. Sharpless, A click chemistry approach to tetrazoles by huisgen 1,3-dipolar cycloaddition: Synthesis of 5-sulfonyl tetrazoles from azides and sulfonyl cyanides, *Angew. Chem. Int. Ed.*, 2002, **41**, 2110-2113.
86. C. W. Tornøe, C. Christensen and M. Meldal, Peptidotriazoles on solid phase: [1,2,3]-Triazoles by regiospecific copper(I)-catalyzed 1,3-dipolar cycloadditions of terminal alkynes to azides, *J. Org. Chem.*, 2002, **67**, 3057-3064.
87. V. O. Rodionov, S. I. Presolski, D. D. Díaz, V. V. Fokin and M. G. Finn, Ligand-accelerated Cu-catalyzed azide-alkyne cycloaddition: A mechanistic report, *J. Am. Chem. Soc.*, 2007, **129**, 12705-12712.
88. J. Lehmann, M. H. Wright and S. A. Sieber, Making a Long Journey Short: Alkyne Functionalization of Natural Product Scaffolds, *Chem. Eur. J.*, 2016, **22**, 4666-4678.
89. B. T. Chait, Mass Spectrometry: Bottom-Up or Top-Down?, *Science*, 2006, **314**, 65-66.

90. X. Han, A. Aslanian and J. R. Yates, 3rd, Mass spectrometry for proteomics, *Curr Opin Chem Biol*, 2008, **12**, 483-490.
91. P. B. Pandeswari and V. Sabareesh, Middle-down approach: a choice to sequence and characterize proteins/proteomes by mass spectrometry, *RSC Advances*, 2019, **9**, 313-344.
92. J. Niedel, J. Davis and P. Cuatrecasas, Covalent Affinity Labeling of the Formyl Peptide Chemotactic Receptor, *J. Biol. Chem.*, 1980, **255**, 7063-7066.
93. R. G. Painter, M. Schmitt, A. J. Jesaitis, L. A. Sklar, K. Preissner and C. G. Cochrane, Photoaffinity Labeling of the N-Formyl Peptide Receptor of Human Polymorphonuclear Leukocytes, *Journal of Cellular Biochemistry*, 1982, **20**, 203-214.
94. R. A. Allen, J. O. Tolley and A. J. Jesaitis, Preparation and properties of an improved photoaffinity ligand for the N-formyl peptide receptor *Biochimica et Biophysica Acta*, 1986, **882**, 271-280.
95. M. Schmitts, R. G. Painterg, A. J. Jesaitis, K. Preissner, L. A. Sklar and C. G. Cochrane, Photoaffinity Labeling of the N-Formyl Peptide Receptor Binding Site of Intact Human Polymorphonuclear Leukocytes, *J. Biol. Chem.*, 1983, **258**, 649-654.
96. B. Dolmatch and J. Niedel, Formyl Peptide Chemotactic Receptor, *J. Biol. Chem.*, 1983, **258**, 7570-7577.
97. R. Anderson and J. Niedel, Processing of the Formyl Peptide Receptor by HL-60 Cells, *J. Biol. Chem.*, 1984, **259**, 13309-13315.
98. R. A. Allen, R. W. Erickson and A. J. Jesaitis, Identification of a human neutrophil protein of Mr 24000 that binds N-formyl peptides: co-sedimentation with specific granules *Biochimica et Biophysica Acta*, 1989, **991**, 123-133.
99. A. J. Jesaitis, J. O. Tolley, G. M. Bokoch and R. A. Allen, Regulation of Chemoattractant Receptor Interaction with Transducing Proteins by Organizational Control in the Plasma Membrane of Human Neutrophils, *The Journal of Cell Biology*, 1989, **109**, 2783-2790.
100. K. Vosbeck, P. Tobias, H. Mueller, R. A. Allen, K. Arfors, R. J. Ulevitch and L. A. Sklar, Priming of Polymorphonuclear Granulocytes by Lipopolysaccharides and Its Complexes With Lipopolysaccharide Binding Protein and High Density Lipoprotein, journal of leukocyte biology, *J. Leukoc. Biol.*, 1990, **47**, 97-104.
101. R. K. Bommakanti, G. M. Bokoch, J. O. Tolley, R. E. Schreiber, D. W. Siemsen, K. N. Klotz and A. J. Jesaitis, Reconstitution of a Physical Complex between the N-Formyl Chemotactic Peptide Receptor and G Protein, *J. Biol. Chem.*, 1992, **267**, 7576-7581.
102. R. E. Schreiber, E. A. Prossnitz, R. D. Ye, C. G. Cochrane, A. J. Jesaitis and G. M. Bokoch, Reconstitution of recombinant peptide receptor with G protein, *J. Leukoc. Biol.*, 1993, **53**, 470-474.
103. A. J. Jesaitis, R. W. Erickson, K. N. Klotz, R. K. Bommakanti and D. W. Siemsen, Functional Molecular Complexes of Human N-Formyl Chemoattractant Receptors and Actin, *The journal of immunology*, 1993, **151**, 5653-5665.
104. J. C. Vilven, M. Domalewski, E. R. Prossnitz, R. D. Ye, N. Muthukumaraswamy, R. B. Harris, R. J. Freer and L. A. Sklar, Strategies

for positioning fluorescent probes and crosslinkers on formyl peptide ligands, *J Recept Signal Transduct Res*, 1998, **18**, 187-221.
105. J. S. Mills, H. M. Miettinen, D. Barnidge, M. J. Vlases, S. Wimer-Mackin, E. A. Dratz, J. Sunner and A. J. Jesaitis, Identification of a Ligand Binding Site in the Human Neutrophil Formyl Peptide Receptor Using a Site-specific Fluorescent Photoaffinity Label and Mass Spectrometry, *J. Biol. Chem.*, 1998, **273**, 10428-10435.
106. K. N. Klotz, K. L. Krotec, J. Gripentrog and A. J. Jesaitis, Regulatory interaction of N-formyl peptide chemoattractant receptors with the membrane skeleton in human neutrophils, *The journal of immunology*, 1994, **152**, 801-810.
107. H. Muranaka, T. Momose, C. Handa and T. Ozawa, Photoaffinity Labeling of the Human A2A Adenosine Receptor and Cross-link Position Analysis by Mass Spectrometry, *ACS Med Chem Lett*, 2017, **8**, 660-665.
108. M. Soethoudt, S. C. Stolze, M. V. Westphal, L. van Stralen, A. Martella, E. J. van Rooden, W. Guba, Z. V. Varga, H. Deng, S. I. van Kasteren, U. Grether, I. J. AP, P. Pacher, E. M. Carreira, H. S. Overkleeft, A. Ioan-Facsinay, L. H. Heitman and M. van der Stelt, Selective Photoaffinity Probe That Enables Assessment of Cannabinoid CB2 Receptor Expression and Ligand Engagement in Human Cells, *J Am Chem Soc*, 2018, **140**, 6067-6075.
109. F. M. Muskens, R. J. Ward, D. Herkt, H. van de Langemheen, A. B. Tobin, R. M. J. Liskamp and G. Milligan, Design, Synthesis, and Evaluation of a Diazirine Photoaffinity Probe for Ligand-Based Receptor Capture Targeting G Protein-Coupled Receptors, *Mol Pharmacol*, 2019, **95**, 196-209.
110. R. Miyajima, K. Sakai, Y. Otani, T. Wadatsu, Y. Sakata, Y. Nishikawa, M. Tanaka, Y. Yamashita, M. Hayashi, K. Kondo and T. Hayashi, Novel Tetrafunctional Probes Identify Target Receptors and Binding Sites of Small-Molecule Drugs from Living Systems, *ACS Chem Biol*, 2020, **15**, 2364-2373.
111. M. R. Bond, H. Zhang, P. D. Vu and J. J. Kohler, Photocrosslinking of glycoconjugates using metabolically incorporated diazirine-containing sugars, *Nature Protoc.*, 2009, **4**, 1044-1063.
112. T. Yang, Z. Liu and X. D. Li, Developing diazirine-based chemical probes to identify histone modification 'readers' and 'erasers', *Chem. Sci.*, 2015, **6**, 1011-1017.
113. B. Neises and W. Steglich, Simple Method for the Esterification of Carboxylic Acids, *Angew. Chem. Int. Ed.*, 1978, **17**, 522-524.
114. S. Nahm and S. Weinreb, N-methoxy-N-methylamides as effective acylating agents, *Tetrahedron Lett.*, 1981, **22**, 3815-3818.
115. Y. Masuda, K. Aoyama, M. Yoshida, K. Kobayashi, T. Ohshiro, H. Tomoda and T. Doi, Design, Synthesis, and Biological Evaluation of Beauveriolide Analogues Bearing Photoreactive Amino Acids, *Chem. Pharm. Bull.*, 2016, **64**, 754-765.
116. B. Bufe, T. Schumann, R. Kappl, I. Bogeski, C. Kummerow, M. Podgó, S. Smola, M. Hoth and F. Zufall, Recognition of Bacterial Signal Peptides by Mammalian Formyl Peptide Receptors, *J. Biol. Chem.*, 2015, **290**, 7369-7387.

117. Y. Hu, N. Cheng, H. Wu, S. Kang, R. D. Ye and J. Cai, Design, Synthesis and Characterization of fMLF-Mimicking AApeptides, *ChemBioChem*, 2014, **15**, 2420-2426.
118. A. Tornesello, M. Sanseverino and F. Buonaguro, Solid Phase Formylation of N-Terminus Peptides, *Molecules*, 2016, **21**, 736-742.
119. S. B. Christensen, A. M. Hansen and H. Franzyk, On-resin N-formylation of peptides: a head-to-head comparison of reagents in solid-phase synthesis of ligands for formyl peptide receptors, *J. Pept. Sci*, 2017, **23**, 410-415.
120. M. Gude, J. Ryf and P. D. White, An accurate method for the quantitation of Fmoc-derivatized solid phase supports, *Letters in Peptide Science*, 2002, **9**, 203-206.
121. E. Atherton and R. C. Sheppard, *Solid phase peptide synthesis: a practical approach*, IRL Press, Oxford, 1989.
122. R. B. DuBridge, P. Tang, H. C. Hsia, P.-M. Leong, J. H. Miller and M. P. Calos, Analysis of Mutation in Human Cells by Using an Epstein-Barr Virus Shuttle System, *Molecular and Cellular Biology*, 1987, **7**, 379-387.
123. M. Uhlén, L. Fagerberg, B. M. Hallström, C. Lindskog, P. Oksvold, A. Mardinoglu, Å. Sivertsson, C. Kampf, E. Sjöstedt, A. Asplund, I. Olsson, K. Edlund, E. Lundberg, S. Navani, C. A.-K. Szigyarto, J. Odeberg, D. Djureinovic, J. O. Takanen, S. Hober, T. Alm, P.-H. Edqvist, H. Berling, H. Tegel, J. Mulder, J. Rockberg, P. Nilsson, J. M. Schwenk, M. Hamsten, K. von Feilitzen, M. Forsberg, L. Persson, F. Johansson, M. Zwahlen, G. von Heijne, J. Nielsen and F. Pontén, Tissue-based map of the human proteome, 2015, **347**, 1260419.
124. R. Basto and W. F. Marshall, in *Methods in Cilia and Flagella*, Academic Press, 2015, vol. 127, pp. 303-322.
125. K. Wenzel-Seifert and R. Seifert, Critical role of N-terminal N-glycosylation for proper folding of the human formyl peptide receptor, *Biochemical and Biophysical Research Communications*, 2003, **301**, 693-698.
126. M. W. McLane, G. Hatzidimitriou, J. Yuan, U. McCann and G. Ricaurte, Heating induces aggregation and decreases detection of serotonin transporter protein on western blots, *Synapse*, 2007, **61**, 875-876.
127. N. Okada, T. Yamamoto, M. Watanabe, Y. Yoshimura, E. Obana, N. Yamazaki, K. Kawazoe, Y. Shinohara and K. Minakuchi, Identification of TMEM45B as a protein clearly showing thermal aggregation in SDS-PAGE gels and dissection of its amino acid sequence responsible for this aggregation, *Protein Expr Purif*, 2011, **77**, 118-123.
128. W. S. Maaty, C. I. Lord, J. M. Gripentrog, M. Riesselman, G. Keren-Aviram, T. Liu, E. A. Dratz, B. Bothner and A. J. Jesaitis, Identification of C-terminal phosphorylation sites of N-formyl peptide receptor-1 (FPR1) in human blood neutrophils, *J Biol Chem*, 2013, **288**, 27042-27058.
129. V. Hong, S. I. Presolski, C. Ma and M. G. Finn, Analysis and optimization of copper-catalyzed azide-alkyne cycloaddition for bioconjugation, *Angew. Chem. Int. Ed. Engl.*, 2009, **48**, 9879-9883.
130. M. H. Wright, C. Fetzer and S. A. Sieber, Chemical Probes Unravel an Antimicrobial Defense Response Triggered by Binding of the Human Opioid Dynorphin to a Bacterial Sensor Kinase, *J Am Chem Soc*, 2017, **139**, 6152-6159.

131. L. A. Sklar, Z. G. Oades, A. J. Jesaitis, R. G. Painter and C. G. Cochrane, Fluoresceinated Chemotactic Peptide and High-Affinity Antifluorescein Antibody as a Probe of the Temporal Characteristics of Neutrophil Stimulation, *Proc. Natl. Acad. Sci*, 1981, **78**, 7540-7544.
132. J. Niedel, S. Wilkinson and P. Cuatrecasas, Receptor-mediated Uptake and Degredation of 125I-Chemotactic Peptide by Human Neutrophils, *J. Biol. Chem.*, 1979, **254**, 10700-10706.
133. R. Belvedere, V. Bizzarro, A. Popolo, F. D. Piaz, M. Vasaturo, P. Picardi, L. Parente and A. Petrella, Role of intracellular and extracellular annexin A1 in migration and invasion of human pancreatic carcinoma cells, *BMC Cancer*, 2012, **14**.
134. Z. Bao, K. Chen, S. Krepel, P. Tang, W. Gong, M. Zhang, W. Liang, A. Trivett, M. Zhou and J. M. Wang, High Glucose Promotes Human Glioblastoma Cell Growth by Increasing the Expression and Function of Chemoattractant and Growth Factor Receptors, *Transl. Oncol.*, 2019, **12**, 1155-1163.
135. DepMap, 2021: DepMap 21Q2 Public. figshare. Dataset.
136. J. E. Horne, M. Walko, A. N. Calabrese, M. A. Levenstein, D. J. Brockwelll, N. Kapur, A. J. Wilson and S. E. Radford, Rapid Mapping of Protein Interactions Using Tag-Transfer Photocrosslinkers, *Angew Chem Int Ed* 2018, **27**, 16688-16692.
137. J. D. Hirsch, L. Eslamizar, B. J. Filanoski, N. Malekzadeh, R. P. Haugland, J. M. Beechem and R. P. Haugland, Easily reversible desthiobiotin binding to streptavidin, avidin, and other biotin-binding proteins: uses for protein labeling, detection, and isolation, *Analytical Biochemistry*, 2002, **308**, 343-357.
138. G. Leriche, L. Chisholm and A. Wagner, Cleavable linkers in chemical biology, *Bioorg Med Chem*, 2012, **20**, 571-582.
139. R. R. Traut, A. Bollen, T.-T. Sun, J. W. B. Hershey, J. Sundberg and L. R. Pierce, Methyl 4-mercaptobutyrimidate as a cleavable crosslinking reagent and its application to the Escherichia coli 30S ribosome, *Biochemistry*, 1973, **12**, 3266-3273.
140. M. Walko, E. Hewitt, S. E. Radford and A. J. Wilson, Design and synthesis of cysteine-specific labels for photo-crosslinking studies, *RSC Advances*, 2019, **9**, 7610-7614.
141. T. J. Dolinsky, J. E. Nielsen, J. A. McCammon and N. A. Baker, PDB2PQR: an automated pipeline for the setup, execution, and analysis of Poisson-Boltzmann electrostatics calculations, *Nucleic Acids Research*, 2004, **32**, W665-W667.
142. R. Grisshammer, in *Methods in Enzymology*, 2009, vol. 463, pp. 631-645.
143. B. Heim, R. Handrick, M. D. Hartmann and H. Kiefer, Refolding and characterization of two G protein-coupled receptors purified from E. coli inclusion bodies, *PLOS ONE*, 2021, **16**, e0247689.
144. S. Soulie, J. V. Moller, P. Falson and M. l. Maire, Urea Reduces the Aggregation of MembraneProteins on Sodium Dodecyl Sulfate – Polyacrylamide Gel Electrophoresis, *Analytical Biochemistry*, 1996, **236**, 363-364.
145. B. J. Bennion and V. Daggett, The molecular basis for the chemical denaturation of proteins by urea, *PNAS*, 2003, **100**, 5142-5147.

146. A. Zougman, P. J. Selby and R. E. Banks, Suspension trapping (STrap) sample preparation method for bottom-up proteomics analysis, *Proteomics*, 2014, **14**, 1006-1000.
147. Y.-Q. Yu, M. Gilar, P. J. Lee, E. S. P. Bouvier and J. C. Gebler, Enzyme-Friendly, Mass Spectrometry-Compatible Surfactant for In-Solution Enzymatic Digestion of Proteins, *Anal Chem*, 2003, **75**, 6023-6028.
148. T. Lanyon-Hogg, M. Ritzefeld, L. Zhang, S. A. Andrei, B. Pogranyi, M. Mondal, L. Sefer, C. D. Johnston, C. E. Coupland, J. L. Greenfield, J. Newington, M. J. Fuchter, A. I. Magee, C. Siebold and E. W. Tate, Photochemical Probe Identification of a Small-Molecule Inhibitor Binding Site in Hedgehog Acyltransferase (HHAT), *Angew. Chem. Int. Ed. Engl.*, 2021, **60**, 13542-13547.
149. E. I. Chen, D. Cociorva, J. L. Norris and J. R. Yates, 3rd, Optimization of mass spectrometry-compatible surfactants for shotgun proteomics, *J Proteome Res*, 2007, **6**, 2529-2538.
150. M. Waas, S. Bhattacharya, S. Chuppa, X. Wu, D. R. Jensen, U. Omasits, B. Wollscheid, B. F. Volkman, K. R. Noon and R. L. Gundry, Combine and conquer: surfactants, solvents, and chaotropes for robust mass spectrometry based analyses of membrane proteins, *Anal Chem*, 2014, **86**, 1551-1559.
151. L. Tsiatsiani and A. J. Heck, Proteomics beyond trypsin, *FEBS J*, 2015, **282**, 2612-2626.
152. B. Rietschel, T. N. Arrey, B. Meyer, S. Bornemann, M. Schuerken, M. Karas and A. Poetsch, Elastase digests: new ammunition for shotgun membrane proteomics, *Mol Cell Proteomics*, 2009, **8**, 1029-1043.
153. S. Tsuchiya, M. Yamabe, Y. Yamaguchi, Y. Kobayashi, T. Konno and K. Tada, Establishment and characterization of a human acute monocytic leukemia cell line (THP-1), *Int. J. Cancer*, 1980, **26**, 171-176.
154. T. Kambe, B. E. Correia, M. J. Niphakis and B. F. Cravatt, Mapping the protein interaction landscape for fully functionalized small-molecule probes in human cells, *J. Am. Chem. Soc.*, 2014, **136**, 10777-10782.
155. L. Wang, A. Ishida, Y. Hashidoko and M. Hashimoto, Dehydrogenation of the NH−NH Bond Triggered by Potassium tert-Butoxide in Liquid Ammonia, *Angew. Chem. Int. Ed.*, 2017, **56**, 870-873.
156. F. Buckingham, A. K. Kirjavainen, S. Forsback, A. Krzyczmonik, T. Keller, I. M. Newington, M. Glaser, S. K. Luthra, O. Solin and V. r. Gouverneur, Organomediated Enantioselective 18F Fluorination for PET Applications, *Angew. Chem. Int. Ed.*, 2015, **54**, 13366-13369.
157. C. Ducho, R. B. Hamed, E. T. Batchelar, J. L. Sorensen, B. Odell and C. J. Schofield, Synthesis of regio- and stereoselectively deuterium-labelled derivatives of l-glutamate semialdehyde for studies on carbapenem biosynthesis, *Org. Biomol. Chem.*, 2009, **7**, 2770-2770.
158. H. Shi, C.-J. Zhang, G. Y. J. Chen and S. Q. Yao, Cell-Based Proteome Profiling of Potential Dasatinib Targets by Use of Affinity-Based Probes, *J. Am. Chem. Soc.*, 2012, **124**, 3001-3014.
159. Q. Ji, H. J. Williams, C. A. Roessner and A. I. Scott, Biomimetic self-condensation of malonates mediated by nucleosides, *Tetrahedron Lett.*, 2007, **48**, 8026-8028.

160. A. R. Mohite and R. G. Bhat, Enantiopure synthesis of side chain-modified α-amino acids and 5-cis-alkylprolines, *J. Org. Chem.*, 2012, **77**, 5423-5428.
161. C. M. Reid, K. N. Fanning, L. S. Fowler and A. Sutherland, Synthesis and reactivity of 4-oxo-5-trimethylsilanyl derived α-amino acids, *Tetrahedron*, 2015, **71**, 245-251.
162. J. E. Baldwin, R. M. Adlington, A. T. Russell and M. L. Smith, Carbon Based Nucleophilic Ring Opening of Activated Monocyclic β-lactams; Synthesis and stereochemical assignment of the ACE inhibitor WF-10129, *Tetrahedron*, 1995, **51**, 4733-4762.
163. D. P. Donnelly, C. M. Rawlins, C. J. DeHart, L. Fornelli, L. F. Schachner, Z. Lin, J. L. Lippens, K. C. Aluri, R. Sarin, B. Chen, C. Lantz, W. Jung, K. R. Johnson, A. Koller, J. J. Wolff, I. D. G. Campuzano, J. R. Auclair, A. R. Ivanov, J. P. Whitelegge, L. Pasa-Tolic, J. Chamot-Rooke, P. O. Danis, L. M. Smith, Y. O. Tsybin, J. A. Loo, Y. Ge, N. L. Kelleher and J. N. Agar, Best practices and benchmarks for intact protein analysis for top-down mass spectrometry, *Nat Methods*, 2019, **16**, 587-594.

Chapter 9 Appendix

9.1 Analysis of Synthesised Peptides

9.1.1 Mass Spectrometry

Peptide	Chemical Formula	Adduct	Expected Mass (Da)	Mass Found (Da)
3.07	$C_{43}H_{67}N_{10}O_9S$	$[M+H]^+$	899.479708	899.479708
3.11	$C_{38}H_{58}N_9O_8S$	$[M+H]^+$	801.414634	801.416991
3.22	$C_{64}H_{77}N_8O_{14}S$	$[M+H]^{2+}$	607.269955	607.269374
4.01	$C_{68}H_{83}N_{11}O_{13}$	$[M+H]^{2+}$	632.320275	632.320381
4.02	$C_{53}H_{79}N_{11}O_{11}$	$[M+H]^+$	1046.603879	1046.611846
4.03	$C_{69}H_{86}N_{11}O_{13}S_2$	$[M+H]^{2+}$	670.801363	670.801248
4.04	$C_{72}H_{88}N_{11}O_{13}S_2$	$[M+H]^{2+}$	689.809205	689.808576

Table 9.1: Summary of mass spectrometry analysis of synthesised peptides.

9.1.2 Analytical HPLC

9.1.2.1 Formyl-Met-Leu-Phe-Lys-photoAcLys-Pra-OH

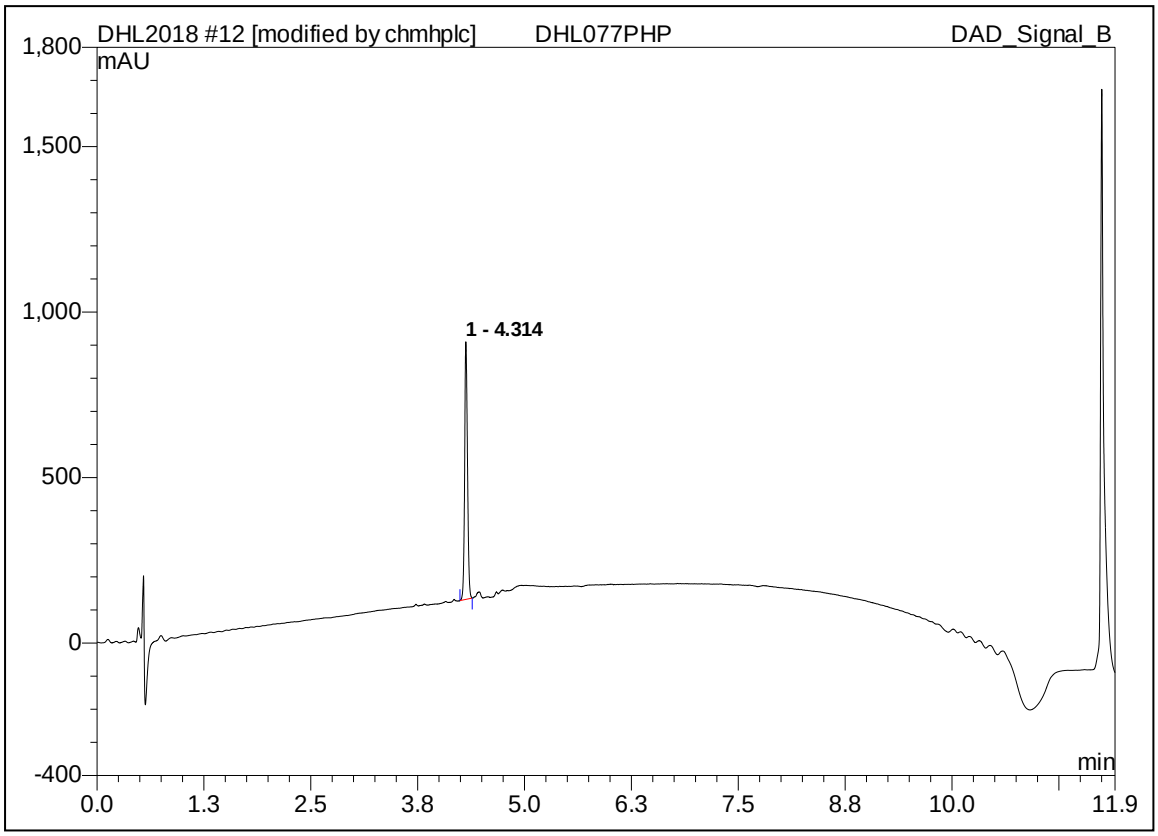

9.1.2.2 Formyl-Met-Leu-Phe-Lys-photoMet-Pra-OH

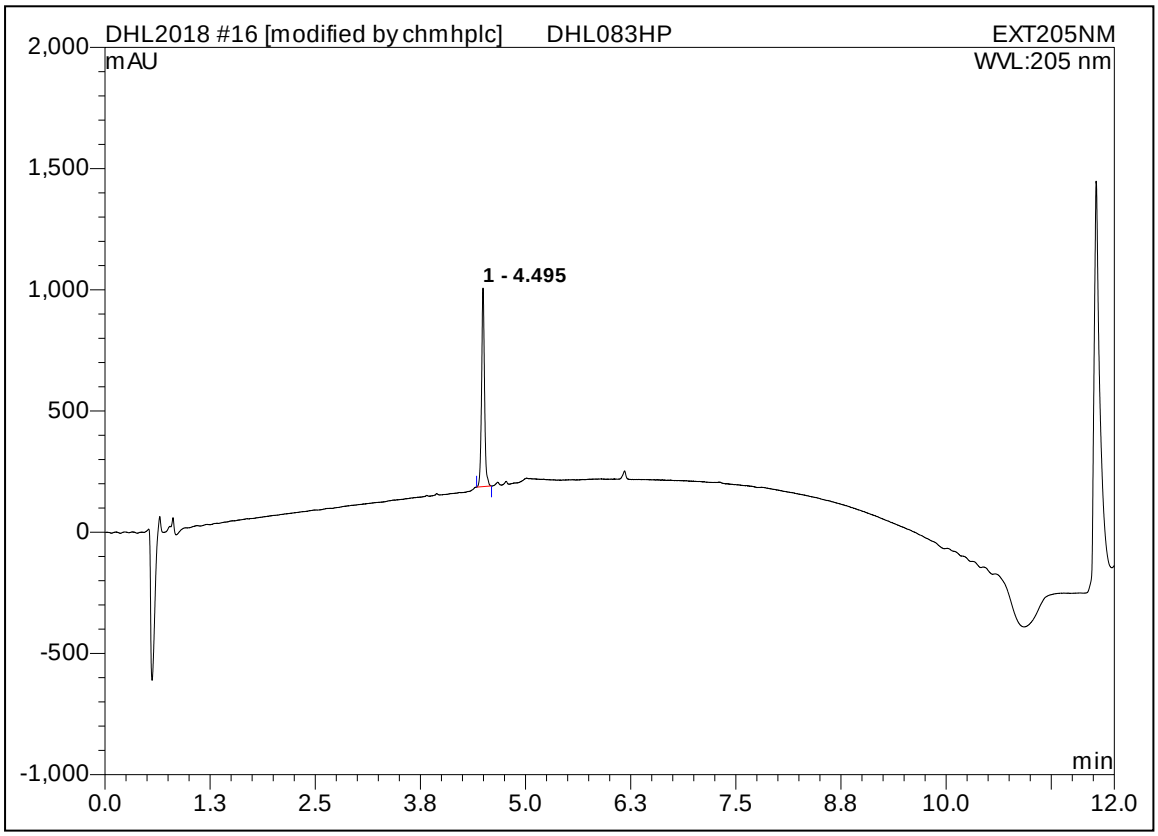

9.1.2.3 Formyl-NLe-Leu-Phe-NLe-Tyr-Lys(FITC)-OH

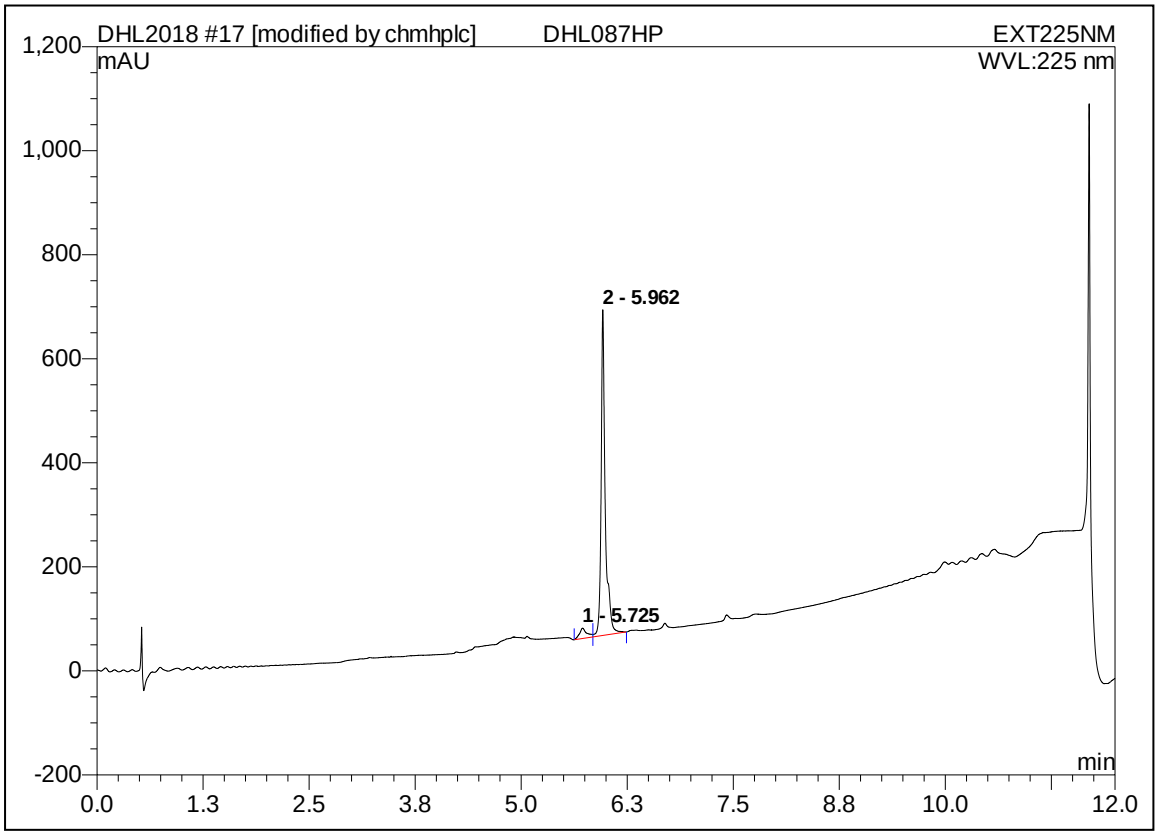

9.1.2.4 Formyl-photoMet-Leu-Phe-NLe-Tyr-Lys(TAMRA)-OH

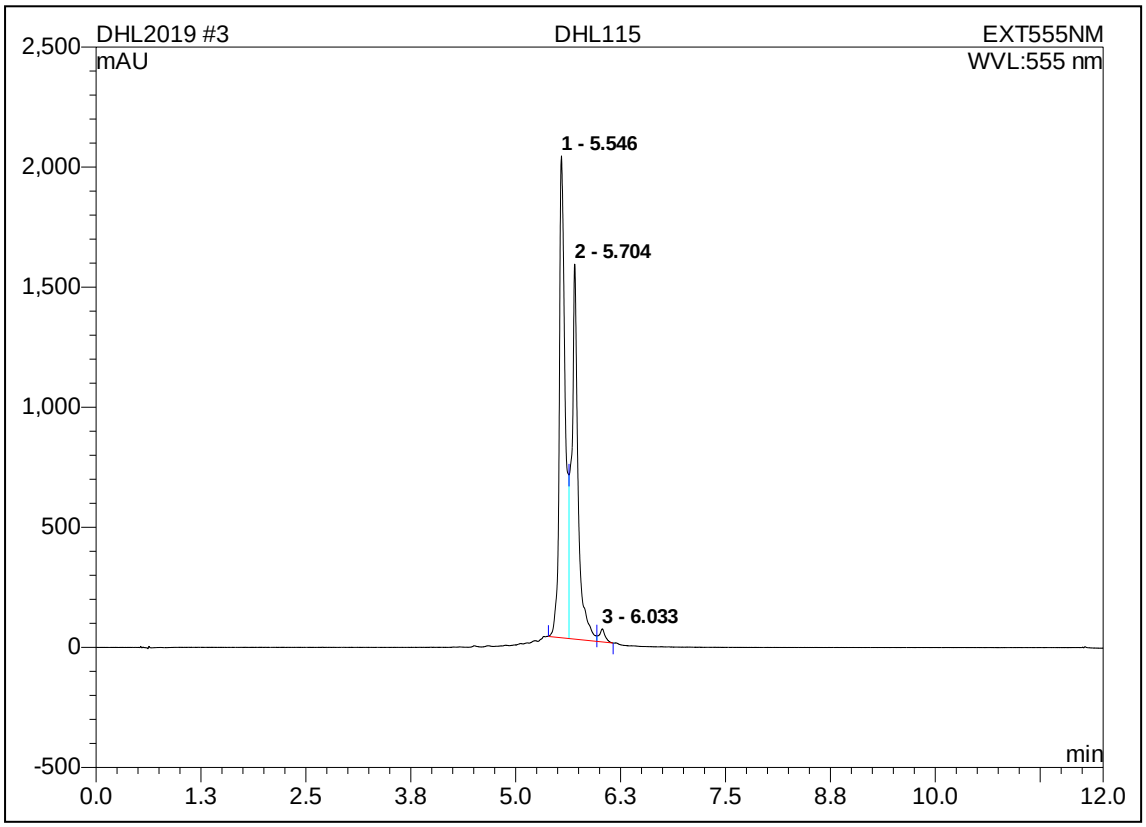

Two peaks are visible in the analytical HPLC, this is due to the presence of both TAMRA isomers.

9.1.2.5 Formyl-photoMet-Leu-Phe-NLe-Tyr-Lys(desthiobiotin)-OH

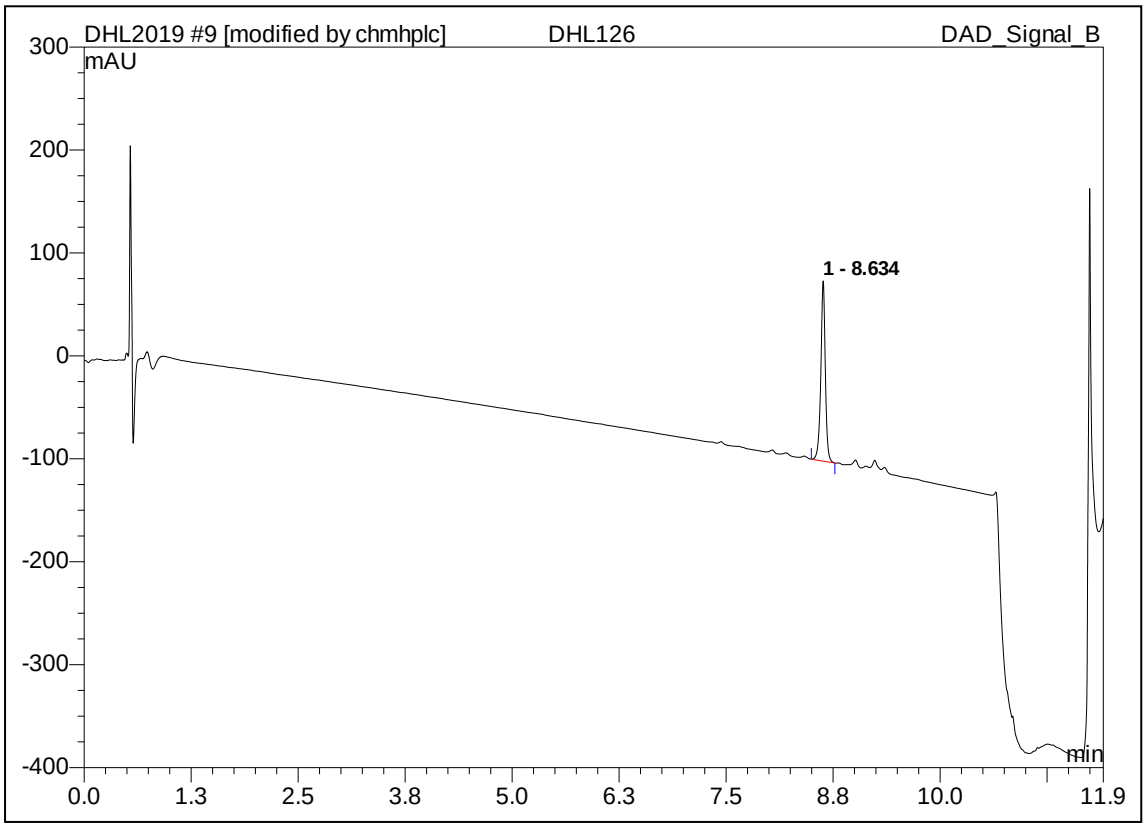

9.1.2.6 Formyl-NLe-Leu-Phe-Cys(MTS-diazirine)-Tyr-Lys(TAMRA)-OH

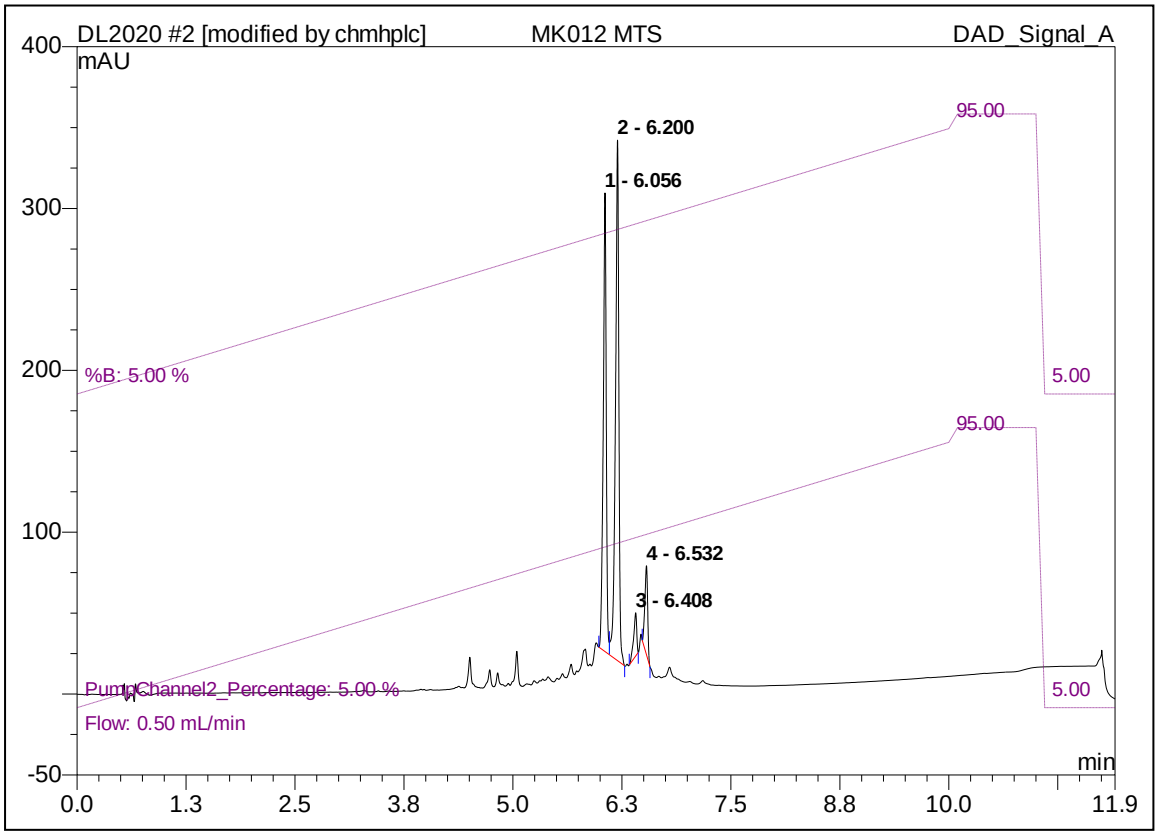

Two main peaks are visible in the analytical HPLC, this is due to the presence of both TAMRA isomers.

9.1.2.7 Formyl-NLe-Leu-Phe-Cys(MTS-alkynyldiazirine)-Tyr-Lys(TAMRA)-OH

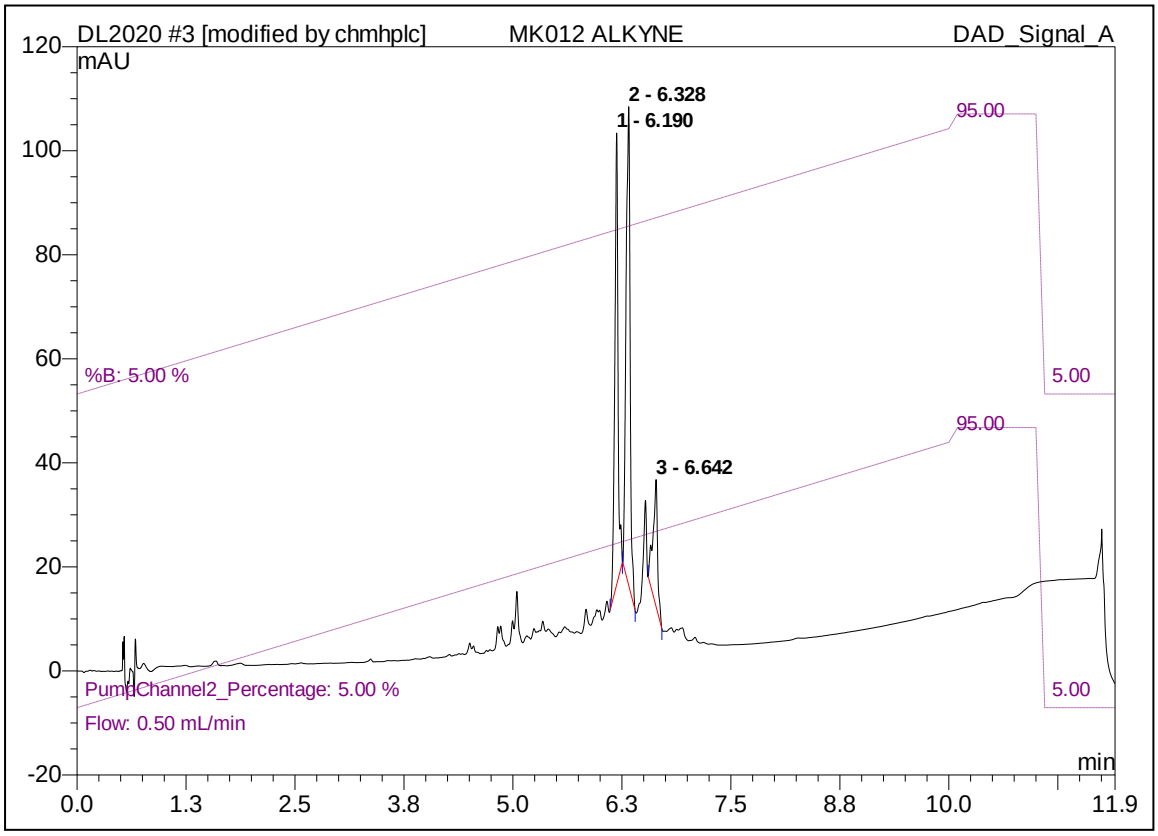

Two main peaks are visible in the analytical HPLC, this is due to the presence of both TAMRA isomers.

9.2 Protein Sequences

9.2.1 FPR1

10	20	30	40	50
M E T N S S L P T N	I S G G T P A V S A	G Y L F L D I I T Y	L V F A V T F V L G	V L G N G L V I W V
60	70	80	90	100
A G F R M T H T V T	T I S Y L N L A V A	D F C F T S T L P F	F M V R K A M G G H	W P F G W F L C K F
110	120	130	140	150

VFTIVDINLF GSVFLIALIA LDRCVCVLHP VWTQNHRTVS LAKKVIIGPW

160 170 180 190 200

VMALLLTLPV IIRVTTVPGK TGTVACTFNF SPWTNDPKER INVAVAMLTV

210 220 230 240 250

RGIIRFIIGF SAPMSIVAVS YGLIATKIHK QGLIKSSRPL RVLSFVAAAF

260 270 280 290 300

FLCWSPYQVV ALIATVRIRE LLQGMYKEIG IAVDVTSALA FFNSCLNPML

310 320 330 340 350

YVFMGQDFRE RLIHALPASL ERALTEDSTQ TSDTATNSTL PSAEVELQAK